Creating additional network capacity on constrained medium voltage networks utilizing distributed generation (specifically PV technology)

Thesis Presented for the Degree of DOCTOR OF PHILOSOPHY in the Department of Electrical Engineering UNIVERSITY OF CAPE TOWN

Candidate: Avinash Ramdhin

Supervisor: Associate Professor Sunetra Chowdhury

Date: 31 October 2023

Declaration

I, **Avinash Ramdhin**, hereby declare that the work on which this thesis is based is my original work (except where acknowledgements indicate otherwise) and that neither the whole work nor any part of it has been, is being, or is to be submitted for another degree in this or any other university. I authorise the University to reproduce for the purpose of research either the whole or any portion of the contents in any manner whatsoever.

Signature: Signed by candidate **Date:** 14 Feb 2024

Abstract

Medium voltage (MV) networks are designed for forward power flow and they radially distribute power to various types of electrical loads. With electrical load growth driven by economic growth, aging networks have limited network capacity to supply the increase in load demand and non-technical losses, such as theft, further exacerbate the problem. This incremental load growth results in the network feeder having unacceptable voltage regulation and/or thermal limitations and such a network is defined as a constrained network where no new load or increase of existing load can be connected. Short-term and long-term mitigation solutions are implemented on these constrained networks to create more electrical capacity to meet the rising load demand. These solutions and investment thereof are also influenced by strategic load forecasting and may include the installation of voltage regulators, shunt compensation, new substations and/or various other network strengthening solutions. Long-term solutions are generally quite costly and the timeline for implementation is extremely long (>3 years). Short-term solutions are limited by equipment ratings and as such the network capacity is improved but by a relatively lower percentage. Due to the fixed and limited output of these devices, an alternate, additional un-constraining mechanism is required. Integrating distributed generation (DG) to medium voltage (MV) networks can improve or worsen the operating level of the network. However, linking this balance of network improvement to the amount of generation would improve the operating level. This research therefore utilizes the integration of DG, specifically solar photovoltaic (PV) installations, as an alternate approach to improve the capacity of constrained electricity networks. Solar PV technology is becoming practically feasible in its installation and cost; and is being supported by industrial and residential load types. The literature review compiled in this thesis highlights the various network improvement solutions utilized to assist MV networks in operating within their grid code regulations. The research then develops a coded method to be utilized for network analysis in DIgSILENT Powerfactory supported by a data analytic interface in Microsoft Excel. This analysis optimally places PV to the network to maximize network capacity and is quantified by defining an objective function that relates network capacity improvement to DG power generation. Technical guides, policies, distribution standards and grid codes that govern the integration of DG to MV and LV (low voltage) networks determine the mathematical constraints of the objective function. The non-linear solutions to the function results in optimizing the amount and allocation of distributed DG along the MV feeder hence creating additional capacity on constrained networks. Particle Swarm Optimization (PSO) was found to be best suited for this research due to its efficiency to solving non-linear optimization problems and is proposed as the appropriate method of optimally integrating DG to un-

constrain MV networks. Suitable applications of the assessment tool are placing microgrids and electric vehicle charging infrastructure.

Two realistic and practical electrical networks (11 kV and 22 kV) supplying rural, commercial and industrial type loads were chosen as test networks. These networks were modelled in DIgSILENT Powerfactory by firstly using the manual method of connecting DG to the network and then secondly by applying the developed DPL script to the same network. Then results were compared to investigate what optimal PV magnitude and point of connection led to what increase in network capacity for both methods. These results are summarized below.

For Network 1, a very interesting relationship was seen when calculating the objective function to achieve the percentage improvement per MW of PV generation added to the network. Different scenarios were used such as, a constrained feeder during a light load scenario was modelled using the above methodology. The network capacity to PV generation ratio (objective function) indicates that the network capacity improvement of 67% could be achieved per MW of generation added. Similarly, for the normal feeder peak load scenario, the objective function (%/MW) was approximated around 40%/MW. The developed tool results correlated closely with the results from the manual method of placing PV on MV networks to maximize network capacity. The applicability of the derived results can be, for example interpreted as such, if one is to install 400 kW of PV on Network 1, the objective function for the peak times is 39%/MW so for 0.4 MW, the network capacity improvement is calculated by 39% x 0.4 = 15.6%.

A similar approach was applied to Network 2 and similar results were derived albeit Network 2 having a voltage regulator as the voltage controlling device on the network. It was concluded from the analysis that there is no linear relationship on the amount of generation and position on a network to which it may be installed. The many tee-off points on the backbone and the variation of load with respect to its location, speaks to the uniqueness of every network and no general rule can be made for PV integration. However, the ratio of the network capacity increase to the amount of generation is more or less consistent for every scenario.

Acknowledgements

I would like to thank the following people for their help, time, support and patience in helping me realise the final goal of completing my thesis:

- *Prof Sunetra Chowdhury* for always being available for queries and help with regard to subject matter and processes undergone throughout the writing of my thesis. Her patience, understanding and invaluable contribution to the essence of this research is much appreciated. The more than adequate support and communication on research matter and thesis checking and compilation has been tremendous which has allowed me to balance my professional work at Eskom as well as ensuring committed time to this research and thesis.
- My employer, Eskom and the EPPEI program for funding my tuition fees and supporting my work to completion (*Prince Moyo, Logan Pillay, Thandiwe Madonda*).
- My Friends and family for assistance in peer reviewing and support to complete this thesis (*Ashwin Ramsoomar, Ravi Moonsamy, Yugan Naidoo, Preshaan Jaglal*).
- My wife, *Dr Sanam Maikoo* and son *Shivansh* for their patience, love, time and support in reaching the conclusion of this work.
- My managers at Eskom who have allowed me to progress with my research as part of Eskom's goals in further pursuing IPP integration research (*Mike Pallett, Nomkhosi Gumede, Kurt Dedekind*).
- My industrial mentor *Dr Clinton Carter Brown*, for the advice, knowledge and guidance in finalizing the proposal of this research.
- My *parents and brother* for their love, time, support and guidance for providing every opportunity they had to enable my ability to pursue further studies.

Table of Contents

List of figures

List of tables

ACRONYMS

ADMD	-	After Diversity Maximum Demand
BESS	-	Battery Energy Storage System
CF	-	Coincidence factor
CAPEX	-	CAPital EXpenditure
DG	-	Distributed generator
DPL	-	DIgSILENT programming language
GIS	-	Geographic information systems
EV	-	Electric vehicle
HV	-	High voltage
kW	-	kilowatt
kV	-	kilovolt
LV	-	Low voltage
LVRT	-	Low voltage ride through
LPF	-	Load power factor
MD	-	Maximum demand
MG	-	Microgrid
MW	-	megawatt
MV	-	medium voltage
NDP	-	Network development plan
PSO	-	Particle Swarm Optimization
PGC	-	Point of generator connection
PUC	-	Point of utility connection
PV	-	Photovoltaic
RVC	-	Rapid voltage change
SSEG	-	Small scale embedded generation
VB	-	Visual Basic

1 Introduction

The growing economy is a direct variable to the load growth on electrical networks. Non-technical losses such as theft, meter tampering etc. also in effect increase network feeder loading. Voltage regulation and conductor thermal limits are the main technical constraints that limit a network's capacity to support the load growth on feeders. In addition, the type of load also affects the network's ability to provide real or active power to new loads. The utility operating these networks have short-term and long-term project plans to mitigate poor network performance or to provide additional electrical capacity to the network. Short-term solutions include using voltage regulators, shunt compensation, smart metering and load shifting to adjacent networks while long-term solutions include building new substations and/or lines in the form of network strengthening projects. South African National Standards (SANS) and regulatory policy (South African Grid Codes) govern the manner in which medium voltage (MV) networks are designed, built and operated. With the installation and control of proposed and/or connected distributed generation (DG) facilities the relevant protection systems, technical system specifications and regulatory documentation are in place to govern its operation. This also includes the relevant guides for the actual installation of the DG facility and its components as well.

In South Africa, Eskom Distribution utility grid networks are transformed to a low voltage level (LV - <1 kV) via step-down medium voltage (MV – 11 kV-22 kV) transformers that have fixed tap settings with a constant percentage increase in LV voltage output. These settings are determined by their locations on the MV network in three derived tap zones and are defined as that part of the network to which the MV voltage is bucked or boosted by the MV/LV transformer. 11 kV reticulation voltages are used in all urban and parts of rural areas. 22 kV reticulation voltages are used in deep rural areas where the establishment of high voltage (HV) infrastructure is generally limited due to terrain, distance and/or environmental constraints. The requirement for long 22 kV feeder networks is to supply the required load with reduced thermal issues as in 11 kV networks. However, at both distribution voltages (11 kV and 22 kV), network constraints are common, and as such have to be mitigated by short-term or long-term solutions as mentioned above.

Currently, three feeder voltage controlling devices affect the voltage profile of an MV network, viz. (1) voltage regulators, (2) capacitor banks and (3) MV/LV tap-changing transformers as explained above. By integrating DGs into the MV network a fourth voltage component would

further determine the resultant MV network voltage profile. The characteristics and effectiveness of this component are determined by the DG's magnitude and location in the tap zones defined above. By knowing which part of the MV network is sensitive to DG injection and what factors determine this sensitivity, a balance of optimizing DG allocation to maximizing network capacity can be achieved.

With the increasing number of DG installations on the MV network, several technical integration issues arise. As a result, the magnitude, location as well as the operating mode of the DG plant are direct variables to the improvement in voltage regulation, thermal limitations and fault level and hence the network capacity. With rooftop PV installations, defined as small scale embedded generation (SSEG < 1MW), various policies and regulations are in now in place to allow export, self-consumption with synchronization and banking of generated power. Similar regulations also apply to larger type PV installations but the scope of work for each connection can be very different.

Capacitor banks raise the network voltage by supplying reactive power to the grid and existing voltage regulators tap the voltage in a unidirectional manner limited by the regulators' current rating. Integrating DG may now start to affect the operation of capacitor banks and voltage regulators commonly used as a temporary fix till long-term solutions are implemented.

The dependency on the utility grid supply is reduced technically due to the load sinking the new DG power with minimum technical integration problems. Such technical problems may be the network feeder overloading due to the additional injected power provided by the DG being less than the load demand on that feeder. However, over the recent years, electrical demand and hence dependence on grid supply has both increased significantly due to economic growth or technological reasons. Typically larger industrial type customers are fed directly from high voltage (HV) systems (customers requiring a bulk supply e.g., for furnaces) and may not function completely on DG due to the high demand of power and fault level. Most industrial establishments have varying load profiles and as such PV outputs may not coincide with the customers' demand; hence an alternate source of energy such as battery storage or even the conventional grid is required. Hybridization of PV and storage offers a more functional system to address the varying feeder loading times with a greater probability of easing stress on the network. Limited capital for new infrastructure, delay in build and installation, and inadequate resources are just some of the driving but delaying solutions to constrained networks and this is where DGs can provide a platform to close this gap. Storage is still currently an expensive addition to the PV mix but with the advent of electric vehicles (EVs), vehicle-to-grid (V2G) support may be a possibility. This research focuses predominantly on assessing PV technology capabilities in providing the capacity required.

1.1 Research problem

MV networks are becoming capacity-constrained resulting in the exceedance of line conductor and equipment thermal and network end of line voltage operating limits. Technical characteristics of a constrained feeder determine the operating level of the network and as such additive power flows become complex with the introduction of voltage devices. Devices for shunt compensation and voltage regulators are employed as short-term solutions to partially mitigate the constraints on MV networks. Inverter-based generation such as solar PV connecting into these MV networks may alleviate these constraints if located appropriately, but determining the magnitude of its penetration and the resultant improvement in network capacity remains a challenge. Large magnitudes of DGs could worsen the connecting MV network due to voltage rise or excessive rapid voltage fluctuation and transmission thermal limit considerations. Determining a voltage operating bandwidth for the feeder network with power flow from the inverter-interfaced DG and local feeder voltage controlling device is of a relatively complex nature and as such the improvement in the network's capacity to the amount of injected power from DG has not been quantified. Utilizing DG as a mechanism to un-constrain MV networks with focus on creating the additional network capacity by optimal allocation using Particle Swarm Optimization (PSO) algorithm, has not been explicitly addressed in previous research of DG integration.

1.2 Research Questions and Objectives

This PhD research aims to address the following research question:

How can integrating inverter-based generation of solar PV systems using optimization techniques be able to un-constrain limited capacity MV feeder networks and what network percentage improvement in this capacity can be achieved?

The following research objectives can be determined as:

1. What short-term and long-term solutions are applied to limited capacity MV networks and what design criteria exist for unidirectional and forward power flow?
2. How can DGs provide additional capacity on constrained MV networks along with existing and/or future installation of voltage regulators and capacitor banks?
3. What objective function best describes the relationship between network capacity and DG integration and how can this be applied to many connecting DG based systems integrating into the same MV network?
4. What optimization algorithm can be used to solve the non-linear function proposed above?
5. How can the results or application be implemented for practical MV networks?

1.3 Proposed Solutions, Scope and Limitations

A comprehensive literature review on the nature of MV networks and technical solutions applied to constrained networks to increase capacity would satisfy the requirements of objective 1. Similarly, the review includes DG in the mix of solutions and motivates the need for the optimization algorithm selected for the study.

To formulate the technical solutions to the stated objectives leading to the development of the objective function, common utility grid networks (with their different components and load characteristics) require steady state modelling incorporating realistic load profiles and load types. Firstly, the conventional modelling of connecting PV systems to the network should be undertaken so that for different scenarios of peak and off-peak loads, voltage, rapid voltage change, thermal and generation values are calculated and stored. This is significant as the results here can act as reference to compare the results derived from the programming script and algorithm. The validation would indicate the accuracy of the script functions considering all input and output variables of the algorithm. The proposed optimization algorithm selected is Particle Swarm Optimization (PSO). Section 2.8 in Chapter 2 discusses the various optimization techniques and compares their validity in selecting PSO. In determining the optimal allocation of PVs, mathematical constraints are derived by the various NERSA regulatory policies (NERSA, “NRS048-4:2009: NRS097-2-3) and technical codes and standards for DG integration at medium voltage level [37] [38]. Network and generator technical operating limitations are to be reviewed to assess if they constrain the DG to achieve its full generating capacity. For example, policy governs reactive power control and as such minimizes possible voltage regulation that can be beneficial to the network constraint issues. Operating modes of the inverter should therefore be looked at as one of solutions to un-constrain MV networks.

MV networks are designed for forward power flow (radial) and as such conductors forming the actual feeder have relatively larger impedances at the beginning of the network than at the end of the network. This is problematic for DG connection to the weaker part of the network as voltage stability becomes an issue. By mathematically defining a mechanism of network improvement percentage (%) per amount of DG penetration, critical points and network paths on MV feeders can be identified leading to the quantification of network upgrades and optimal connecting points for feasible DG project outputs. In most cases, large DGs cannot connect easily to any network point without voltage rise, fault level and a less than 3%-5% voltage variation at the point of connection.

1.4 Proposed Methodology Steps

Step 1: To review all national and international applicable existing reports, guidelines, standards, specifications, grid codes, journals and publications thereby providing a complete review of all subject literature and identifying all the gaps to the proposed objectives. This documentation would outline the gaps of DG integration and limitation to MV networks as well as the problems and mitigation steps associated with constrained MV networks.

Step 2: To build the feeder models for analysis of several utility grid networks, particularly 11 kV and 22 kV networks. These network models consisting of various load types will be built and simulated in DIgSILENT Powerfactory. Static generators representing inverter-based generation of solar PV will be added to several points on the network with each network having different impedance and fault level characteristics.

Step 3: To structure a coded program using DIgSILENT Powerfactory Language (DPL). The program would be able to assess the entire MV network and clean up any duplicate of problematic PV systems before executing further studies. The PSO algorithm would be coded into the program (DPL). Several simulations of different iterations and DG units can then be analysed using the program.

Step 4: To document results of applying the developed program to the network. This is done by the use of matrices to store iteration values where its size is automatically set with the number of iterations and DG units. When applied to the test networks of 11 kV and 22 kV, the applicable standards and regulations will be used to determine the maximum generation on each network and hence the mathematical constraints for the entire DPL code. This would be done by changing each PV output by the number of inverters and output power, keeping its mode of operation constant, and location of the connecting plant to the grid. Three modes of operation of constant power factor control, constant reactive power control and constant voltage control are available but the simulations will use the constant power factor control mode only as per the relevant network and grid codes. By establishing a final bandwidth to which inverter-based generation can connect to different parts of the network, existing constrained network solutions can then be analysed and merged to the final solution for different network models. This would result in the maximum amount of generation that can be distributed along the MV feeder and concurrently creating the improvement in network capacity. The quantification of the magnitude of DG is determined within the resultant operating bandwidth. The objective function is then used to mathematically represent the proposed solution as a result of the above methodology.

Step 5: To view the simulated results of all study cases on a simplistic interface designed and built in Microsoft Excel using Visual Basic programming language. Data collection involving utility grid network data and network component type specifications are from the actual network model built in Powerfactory using data obtained from the utility.

Finding a balance between the maximum amount of DG injection by varying its location optimally may result in a strategy that can remove short-term un-constraining devices on the network implying decommissioning of voltage regulators etc. Data that is required to model both study cases of 11 kV and 22 kV networks consist of:

1. Network data of conductor type, backbone and tee-offs
2. Interconnecting equipment fault level and current ratings
3. Load profile data for different networks
4. Type data of inverter-generator models
5. Type data of MV/LV transformers, voltage regulators and capacitor banks
6. Type data for station controllers for static generators
7. Financial data for MV design configurations

1.5 Contributions of this Research

The research outputs of the above objectives support the ongoing investigations of connecting and assessing distributed generation facilities to utility-grids but specifically focus on MV networks and inverter-based generation of PV technology.

The current problems with existing solutions for un-constraining networks, is that only a certain percentage of improvement in the network's capacity can be achieved. In addition, these solutions are short-term due to their cost effectiveness and ease of installation but will not be able to sustain the networks operating limits due to future network load growth. Integrating DG into this constrained network has its advantages and disadvantages. Generally, the integration of large amounts of DG is more problematic and becomes impractical to connect to MV network feeders. A summary of the contributions of the work derived from this research is documented below:

- This research aims to show that when inverter-based PV generation, is optimally located, operated and managed, the network's capacity (kVA) to accommodate more load is increased with or without network un-constraining devices. A better percentage improvement (difference between source power before and after PV connection) by using inverter-based generation at strategic locations would be seen thus mitigating additional costs.

- By optimally placing DG in the MV network and allowing the utilization of different control modes of operation of the inverter, a greater voltage operating bandwidth can be achieved as well as an improvement in kVA power flow on the network feeders. In the simulations, constant power factor control mode is utilized. Other modes such as voltage control mode is only applicable with mutual agreement with the PV owner as such, as utility voltage on networks cannot be controlled by DG installations. However, this allowance may improve network capacity and improve network performance.
- The proposed strategy and results would suggest where the MV network can be reconfigured, rebuilt or redesigned to maximize the networks performance and maximizing generation integration. This would add to existing design criteria for MV network builds where currently this is not even considered in network planning and design for reverse power flow.
- Internationally, no specific documentation exists that define design criteria for the establishment of upgrade to new MV networks for inverter-based mini grid establishment. The new additional technical design criteria would enable proper planning and utility-grid installation that enables the entire power system to operate with no major constraints.
- Defining a network capacity improvement percentage using DG integration to un-constrain MV networks and using PSO algorithm to achieve this, is the novelty in this research. In addition, its applicability becomes significant in placing microgrids and electric vehicle charging infrastructure. By utilizing the assessment tool, optimal locations of connecting DG that maximizes network capacity and DG magnitude can be found.

1.6 Nature of Outcome and its Benefits

This section briefly presents the nature of the visualization and optimization tool that will be the outcomes of this PhD research. The proposed visualization software tool would analyse a constrained MV network and output the optimal points to which PV should connect to improve network capacity i.e. more power to supply growing or new loads. The optimization tool would require various network parameters to determine an operating magnitude bandwidth. The bandwidth in question would be the upper and lower voltage limits (p.u.) as defined by voltage regulations in the various grid codes. It is proposed that network improvement percentage values can be achieved with the identification of the critical network points. Results from the study performed using DIgSILENT Powerfactory would provide the basis in determining the solutions that the tool would output. The interface would show the maximum distribution of inverter-based generation on the network and network capacity improvement achieved. Also,

tracking the PSO particles in the simulation would show convergence and as such indicate the part of network that is most viable to have as a critical connecting point.

This software tool would contribute significantly to how utilities and end-users (consumers and project developers) approach the conceptualisation and implementation of DG establishments from a technical and financial perspective. Utilities would be able to use the results to create more capacity on constrained networks thus deferring larger Capital Expenditure (CAPEX). The benefits of using the tool would be as follows:

- ✓ Identify critical and optimal connecting points for DG.
- ✓ Identify critical upgrade network paths to un-constrain the network and improve capacity.
- ✓ Determine the maximum DG magnitude per section of feeder.
- ✓ Suggest network improvements that can be made to increase the network's capacity and determine the cost for doing this.
- ✓ Determine the amount of new load that can be connected with optimal allocation of DG
- ✓ Determine the applicability of the tool in connecting microgrids and electric vehicle infrastructure

Utilities, municipalities, project developers and existing consumers would benefit technically and financially from the above analysis. Academics and researchers may use these findings in analysing complex and large-scale projects that will bridge the gap between industry and academic research institutions. PV alone cannot completely un-constrain MV networks and as such additional generation such as storage (including vehicle to grid capabilities) plays a vital role as power is dispatched during peak times when irradiance levels are low. The above benefits are vital in driving sales for the supply authority as a new approach to un-constraining MV networks utilizing DG is proposed. The integration of DG is not new but the above methodology of the hybridization of PV and battery storage to create network capacity improvements opens a new paradigm shift of thinking where current conventional practice is not functioning, especially where non-technical losses dominate.

1.7 Structure of the Thesis

Chapter 1 introduces the research problem, associated solutions and clear objectives of the research goals. Chapter 2 presents the literature review from the nature of MV network characteristics to the applicability of the assessment tool to everyday network analysis. Chapter 3 describes the sequence of events of the coded script presented in DIgSILENT Powerfactory and documents the steps of significant processes through flowcharts. Network characteristics of 11 kV and 22 kV networks utilized in the simulations covered in Chapter 4

are also explained. Chapter 4 presents the simulations of manual integration studies of PV to two networks at 11 kV and 22 kV and thereafter systematically compares the assessment tool results on the same networks and relevant scenarios derived from executing the DPL script. This chapter also provides a discussion on the overall assessment results. Chapter 5 then concludes the research summarizing the significant aspects of all chapters covered in the thesis.

1.8 Conclusion

The analysis proposed in this research would enable a better understanding of the network capability before and after the improvement and is practically most beneficial to developers and electricity distributors as business case models of DG plants and capital investment of infrastructure for upgrade paths becomes more feasible with favourable results. Existing load customers would directly benefit as the network's capacity and reliability increases. Limited investment for strengthening projects complicates the typical trend of planning for future load growth. This growth cannot be halted but encouraged as revenue being the major component in sustaining industry and utilities world-wide. Changing the thinking and approach of providing network capacity, by concurrently supporting the transition of combustion engine vehicles to electric through a positive deployment of charging infrastructure and enabling plug-and-play microgrids, paves the way for a smarter and inexorable technological future. Incorporating this into a strategy tool would undoubtedly expand the knowledge of the propensity of MV networks to DG integration.

2 Literature Review

In order to connect new loads or increase existing load magnitudes on medium voltage (MV) networks, the feeder should have sufficient capacity to cater for this. Voltage regulation and thermal capacities are two defining factors that determine if the network is capable to operate within statutory limits defined by the National Energy Regulator of South Africa (NERSA). Over a period of time electrical load growth driven by economic growth as well as by non-technical losses such as theft etc. pushes the network beyond defined limits; hence capacity of the network becomes constrained resulting in excessive voltage regulation and/or thermal limit contraventions. In the sections that follow, short-term and long-term solutions in un-constraining networks are firstly reviewed. The technical benefits and network improvements are discussed to understand their technical limitations, capabilities and relevant costs. Solar photovoltaic (PV) based distributed Generation (DG) is then proposed as an alternate solution to provide additional network capacity, i.e. to un-constrain the network. Current and legacy methods of improving network capacity involve using voltage control devices such as voltage regulators (VRs), capacitor banks and additional interconnectors or infeeds by changing the X/R ratios. X/R ratio here is defined as the amount of reactance X divided by the amount of resistance R. These methods are further reviewed with the integration of DG. The focus technology and capability of PV in this review and thesis is due to the influx of PV installations and commercial availability as well as the progressive reduction of costs. PV systems have the ability to be used, in addition to much needed generation, in a manner that can provide greater benefits of voltage control via inverter-based systems if these installations can be optimally located on MV networks. Typically, any PV system (>350 kVA as per NERSA guideline, NRS097-2-3), that would synchronize to the grid would require adequate simulation studies to assess the technical feasibility of its integration to the grid. In some cases, the utility may propose the connection point to enable this integration, but in most cases, this is not possible. It therefore becomes imperative to study which part of the network to which DG connects to, can provide the maximum benefit in improving network capacity and reduction of upstream power flow during times of peak distributed generation. Once this is established, the next question is what can be done to improve this capacity with the various solutions mentioned above. Therefore, an algorithm to optimally connect DG installations is required. Particle Swarm Optimization (PSO) algorithm is commonly used in power systems and is used in this thesis for reasons further elaborated in the review, to determine the best integration points to achieve maximum network capacity.

2.1 Distributed Generation (DG)

Utility grids have many challenges on their power system expansion. Electrical demand continues to grow with aging infrastructure, requiring maintenance to extend its life-cycle operation. Projects to provide the necessary strengthening and network refurbishment are greatly staggered due to lack of adequate funding, skilled resources, long lead material timelines and environmental factors. In the United States, investment in the network grid has been falling behind demand growth for a quarter of a century, and investment in increasing generating capacity has been somewhat erratic [3]. In South Africa, over the last few years, generating capacity has gradually increased due to the commissioning of additional coal-fired and renewable energy projects, however the gradual increase in capacity struggles to meet the country's base load and as such, a certain portion of the country's load has to be shed to prevent system collapse. The concern that has also constantly flagged itself during the construction of these plants is the staggering delays in the upgrade or new build of distribution networks due to cost overruns or inadequate resources.

Distribution networks operate at medium voltage (MV, 11 kV up to including 33 kV) and are transformed to low voltage (LV, <=1 kV) for supplying the end-user. Electrical load growth on MV networks over a certain period constrains the network either thermally or results in low end-of-line (EOL) voltages. The network therefore does not operate within regulatory standards, and connecting additional load will either trip the network due to thermal exceedance settings or cause damage to end-user equipment as a result of under voltage [34].

Several mitigating solutions are employed such as splitting the constrained network, increasing backbone conductor size for reducing impedance levels, adding FACT devices such as shunt capacitors or voltage regulators or providing new injections from near-by networks or substations that have the capacity to alleviate the constraint. Each solution offers a certain limitation in improving the network's capacity but may also be not cost-effective. DG integration to the network can un-constrain the feeder by improving the voltage due to voltage rise specially at the point of connection with incremental voltage rise to proximity loads, fault level increase and directly feeding load by the additional power injection thus reducing the upstream demand on the network itself. The most common DG facilities integrated to the MV network level are co-generation plants e.g., sugar mills and solar PV plants or small-scale embedded generation (<1MW) such as rooftop PV (inverter-based generation) and small wind turbines [10].

2.1.1 Load Forecasting and Load Types

This section introduces load forecasting to determine the type and specification of network that is required to be built to supply new electrical loads. The process is relatively sequential and firstly establishes the study area for analysis. This entails gathering information on land use, existing and/or new customers, boundaries etc. A complete analysis of existing loaded networks or technical calculations of new upcoming loads are gathered, modelled and compiled into a complete status quo plan. Individual point loads are summated to produce a feeder loading which should correspond to recorded metering at the source as an accuracy check. Several methods (S-curve, trend etc.) of forecasting can be applied to new point loads or feeder network loads [70]. At this stage common definitions are described, the first being Load Factor (LF) which refers to the average amount of power demand to the peak demand in a specified time period and can be expressed as in equation (2.1) [70]. The hour parameter is based on a typical 30 day billing period.

$$\text{Load Factor (LF)} = \frac{\boldsymbol{Avg\ kWh}}{\boldsymbol{Peak\ kW\ x\ hr}} \qquad (2.1)\ [70]$$

The second is After Diversity Maximum Demand (ADMD), which is defined as the average maximum demand (MD) of a simultaneous group of customers (n) and expressed by equation (2.2) [70].

$$\text{ADMD } (n) = \frac{\sum \boldsymbol{MD(n)}}{\boldsymbol{n}} \qquad (2.2)\ [70]$$

For ADMD calculations using Equation (2.2) [70], the highest consuming month over the design lifespan of the load under consideration should be used based on a 30min demand interval. For example, a group of 100 customers having a total maximum demand of 150 kVA, implies that the ADMD is approximately 150 kVA/100 = 1.5 kVA per household.

Last one is the Coincidence Factor (CF) which plays a major role in the analysis of this research and is described as the ratio of the maximum demand (MD) to the sum of each individual customer maximum demand. This is expressed by equation (2.3) [70].

$$\text{CF} = \frac{\boldsymbol{MD}}{\sum \boldsymbol{MD\ of\ individual\ consumer}} \qquad (2.3)\ [70]$$

Typical forecasting methods include trend forecasting where past load curves are used to predict future load curves and methods such as geo-spatial forecasting, use land-use and customer analytical information to formulate the forecast. In geo-spatial forecasting, load zones are defined per feeder and depending on the land zoning and customer type for that area, a forecast is calculated based on a high, medium and low load growth rate determined

by trend or fixed kVA per hectare value. Figure 2.1 [70] shows different growth rates using the Gompertz curve (S-curve, C = 1 means fast initial growth and C = 10 means slow initial growth, B= No. of years until saturation, A = base load as a fraction of future load between 0 & 1 e.g., 5 MVA/40 MVA = 0.13 or 13%). The curve plots the maximum demand for 1000 customers versus the years of forecasting. Saturation is reached at year 20 where the ADMD is 1.3 kVA (1300 kVA/1000). It can be seen that under or over-estimating the ADMD would result in misinterpreting the year in which to expect a certain load and hence a particular project would not commence at the appropriate time [70].

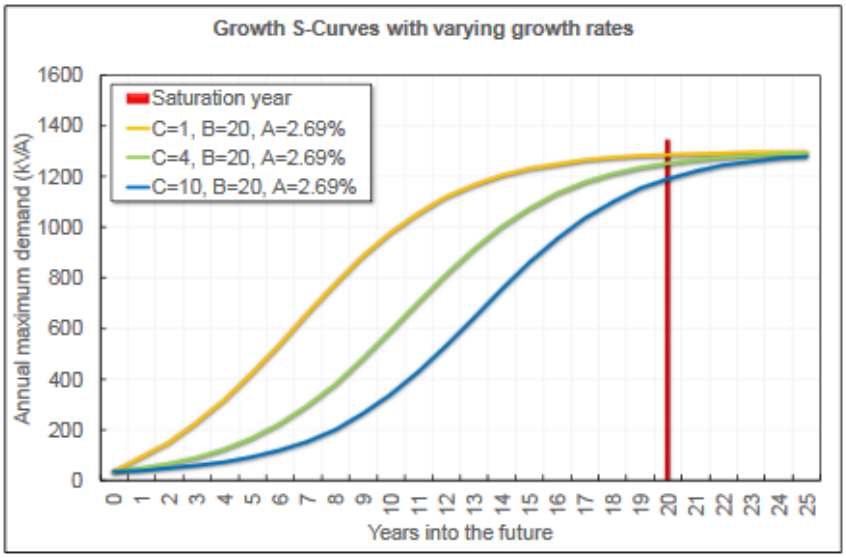

Figure 2.1: Example of an S-curve growth forecast, load saturation is 20 years [70]

Daily load curves as in Figure 2.2 [71] show the variation of load consumed during different hours of the day. The ratio of the area under the curve to the 24-hour period gives the average load (MW) for that day. If the same load data points are plotted in descending order, a load duration curve (LDC) is established [71]. In the LDC the maximum load of a system is represented on the left, whereas decreasing loads of a system are represented on the right in descending order. Therefore, the area under both curves are the same.

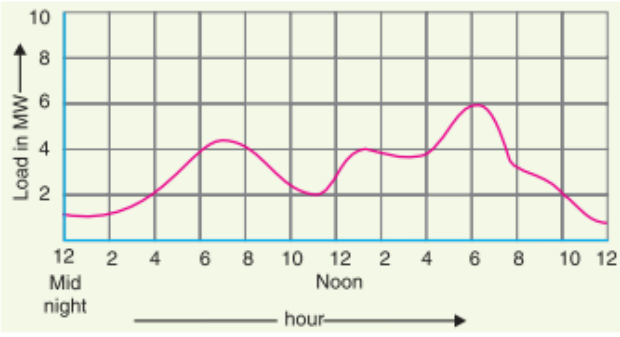

Figure 2.2: Example of a daily load curve [71]

The (LDC) is a much more presentable form of the daily load curve and gives the minimum load present through the time period. Figure 2.3 [72] shows an example of LDC with peak energy shaving and baseload DG. The LDC curve is normalized with respect to the annual load time on the x-axis and normalized peak power with respect to the annual load on the y-axis. The area under the curve shows the energy supplied by the DG and is dependent on the number of operating hours [72].

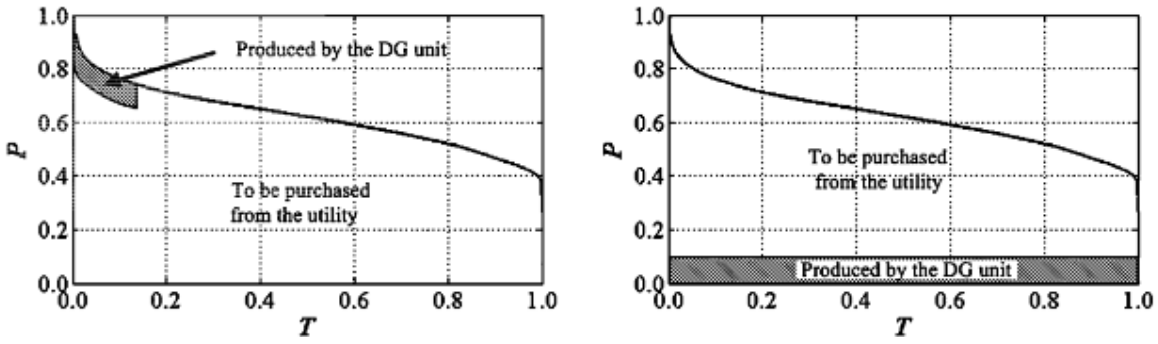

Figure 2.3: Energy associated with DG production mode, Peak shaving (left) and DG baseload (right) effects on the LDC curve [72]

Application of load forecasting is an essential step in the process of infrastructure planning. Once the necessary and relevant information is quantified, the future state of networks is simulated with the new predicted loads and compared to the status quo of networks in the study area. Solutions to address the networks that contravene regulatory standards are then compiled considering investment criteria requirements as per the South African Distribution code: Network code [38]. It is at this stage that short-term and long-term solutions are proposed.

Several types of loads exist. Resistive type loads include lights, heaters etc. and due to its usage have a typical load factor of about 20%. Loads that use magnetic fields for doing work i.e. power to motors have a power factor that is lagging (current lags voltage). Such cases consist of mostly squirrel cage induction machines predominantly used by 70% of industry. Capacitive loads are the third type of load in which the current leads the voltage (leading power factor).

From the analysis, several network issues may arise with the simulation of new cumulative loads i.e. the new loads as well as the increase in supply demand from existing loads. Voltage regulation, thermal limitations and low fault level problems are mitigated by applying voltage regulators, new MV and/or HV injections and build, capacitor banks or re-configuring the existing network. Having adequate fault current/level mitigates voltage instability of the network when a transient event occurs. Also, sufficient fault level enables adequate voltage

when load starts to increase at that particular point. Low impedance HV/MV transformers or new source injections increase the fault level to mitigate the above effects.

2.2 Short term Solutions to Un-constraining Medium Voltage Networks

Short-term solutions are defined as the fastest, cost effective measures to implement when Capital Expenditure (CAPEX) constraints exist and build timelines cannot be met. This would happen when a customer requires a new or increase to his existing supply due to unforeseen network faults of thermal loading or under-voltage. These short-term solutions include installing voltage regulators, capacitor banks or shifting load to adjacent networks. The common characteristic that determines their validity is the limitation on the amount of constraint mitigation the solution offers in terms of limited voltage improvement (p.u) or percentage improvement in thermal capacity.

2.2.1 Short-term Solution Using Capacitor Banks

Capacitor banks provide shunt compensation to parts of the network that require reactive power support due to poor power factors and unacceptable voltage regulation. This raises the voltage within the limitations of the capacitor bank size and ratings. Fixed and switched shunt capacitor banks improve the load power factor and can typically only increase the minimum voltage by 3% to 5% [44]. MV busbar voltages at HV/MV substations are kept relatively constant despite variations in the HV and MV networks by automatic control of HV/MV on-load tap change (OLTC) transformers [44].

Capacitors are connected in parallel to increase the reactive power rating of the capacitor bank and are connected in series to obtain the required voltage of the bank. MV capacitors are located as close as possible to the reactive load to be compensated. MV network capacity is therefore increased as the line loading is decreased and the MV voltage is increased at the point of connection which is defined as that point to which the actual PV system connects to the distribution network. A common location for the placement of an MV capacitor bank is approximately 67% from the MV source for maximum benefit or in the case of multiple capacitor banks, at any point such that 50% of the reactive power flows to the MV source and the other 50% to distributed loads connected below the capacitor bank [75].

The maximum voltage change during capacitor bank switching is given by equation (2.4) [75].

$$\% \text{ Voltage change} = \frac{\boldsymbol{MVAR_{Cap\ switched}}}{\boldsymbol{MVA_{3\ phfault\ level}}} \times 100\% \qquad (2.4)\ [75]$$

where $\boldsymbol{MVAR_{Cap\ switched}}$ is the rating of the capacitor being switched (MVAR)

and $MVA_{3\,phfault\,level}$ is the network grid fault level (A-B-C fault) at the installed point of the capacitor (MVA).

The X/R ratio calculated from the source to the load has a large impact on voltage drop and hence the way in which shunt compensation operates.

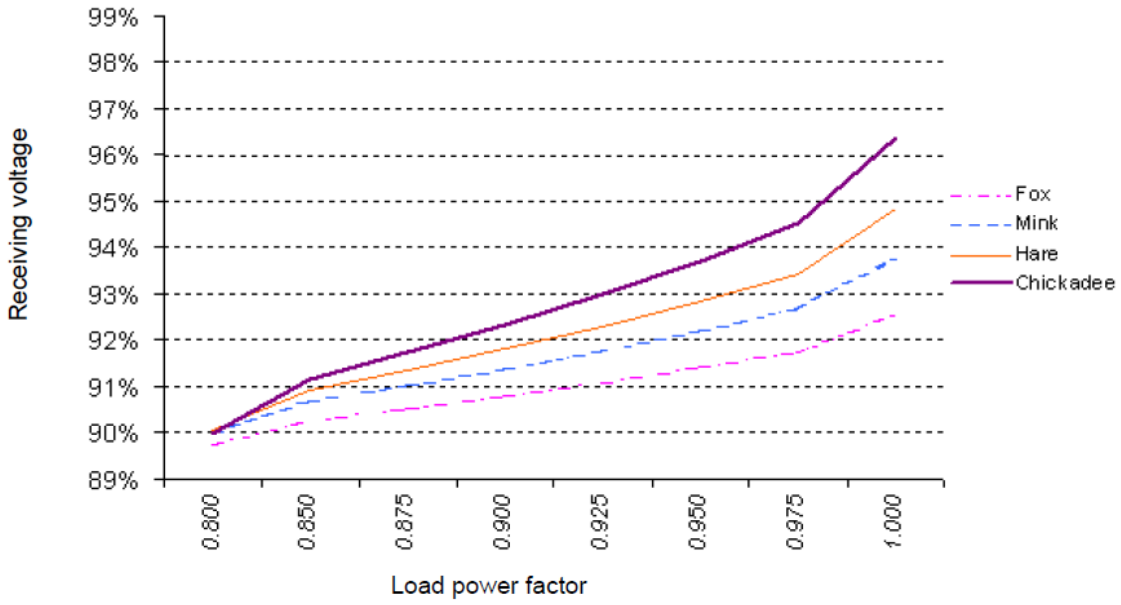

Figure 2.4: Load power factor (LPF) and voltage improvement for different conductor types [75]

In Figure 2.4 [75], the more the compensation to move the load power factor (LPF) towards unity, the greater is the improvement in voltage seen as conductor size is increased (from high impedance Fox conductor to lower impedance Chickadee conductor i.e. as there is a move towards a higher X/R ratios) where the distances remain constant. Mention may be made that Fox, Mink, Hare and Chickadee are different types of line conductors and details on conductor types are explained in section 2.3.1. Fixed capacitor banks are installed halfway down the feeder with switched capacitor banks installed two thirds down the feeder [75]. In [61]and [62] it is shown using Particle Swarm Optimization (PSO) search method that a single DG installation with a single shunt capacitor results in the least investment costs as shown in Figure 2.5 [61][62]. Feeder loading at peak times shows that the network loading of main feeder sections decreases from 70% to 40% with DG and compensation compared to not having either.

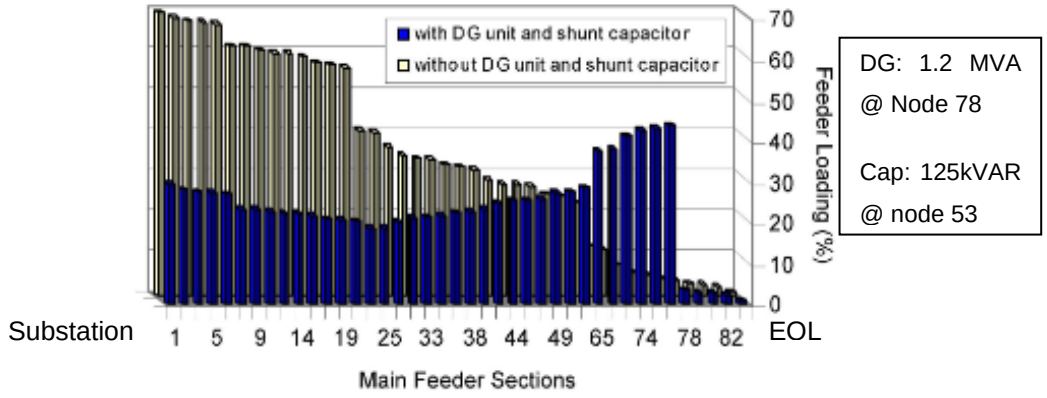

Figure 2.5: Feeder loading with and without DG and shunt compensation [61]

When power factor is improved, the current in the existing system will be reduced, and additional loads can be connected to the same network. This means an increase in the system capacity and less constraint. Figure 2.6 [64] can be used to determine the amount of additional system capacity obtained after a certain power factor correction [64]. To determine the capacity released, one must read the curve in Figure 2.6 with the current power factor of the load/network and then follow the curve to the point to which the capacitor bank will improve the power factor. The vertical distance between the two power factor points measured along the Y-axis will indicate the additional system capacity in p.u. For example, in improving a network power factor from 0.9 to 1.0 (shown by dashed line in Figure 2.6), 0.1 p.u. of system capacity is released. If the system loading is 500 kW and with a 0.1 p.u. improvement implies that 50 kW of network capacity is available to supply additional loads.

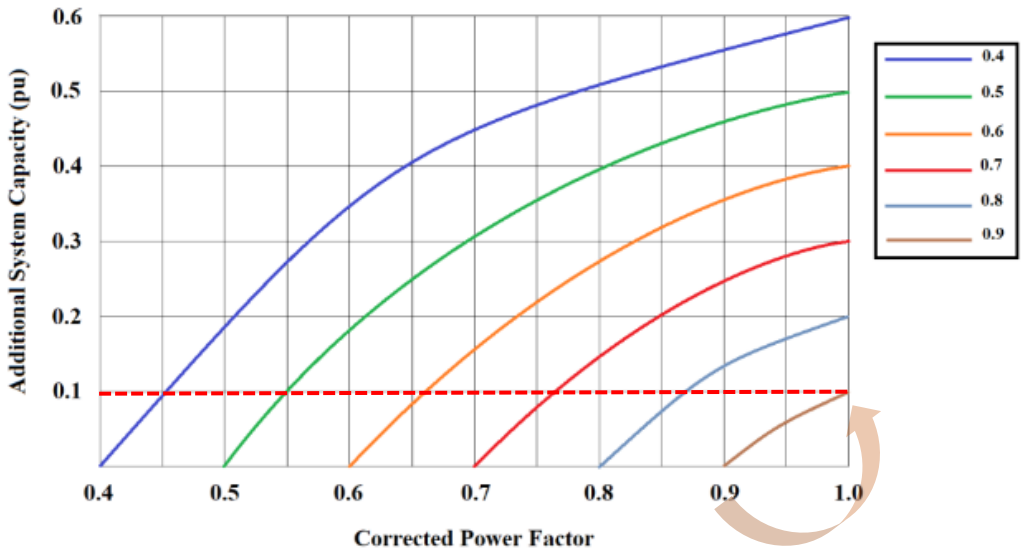

Figure 2.6: Corrected power factor improvement increases system capacity [64]

In [65], a cuckoo search algorithm is used to determine optimal sizes and placements of shunt compensation and DG by also measuring power losses and voltage stability. IEEE 33 and 69 bus systems were used for the analysis. Active power and reactive power loss results for the aforesaid study are shown in Figure 2.7(a) [65] and Figure 2.7(b) [65] respectively for the base case (no compensation or DG) for the 33-bus system and the combination [65]. Figure 2.8 [65] shows the improvement in voltage with the same combination as well. A voltage profile shows the degradation of voltage from the source to the last network node or feeder length and the stability profile shows the voltage profile fluctuation upon a network disturbance.

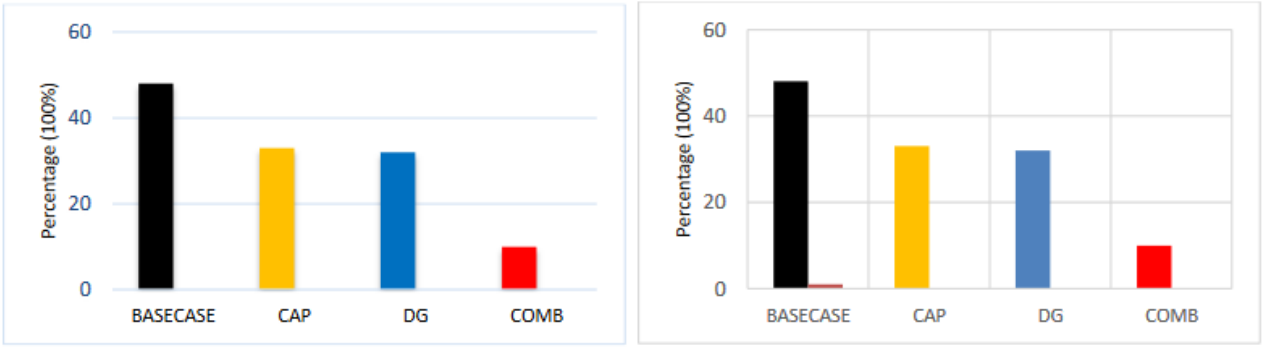

Figure 2.7: (a) Active power loss reduction, (b) Reactive power loss reduction (33-bus system) [65]

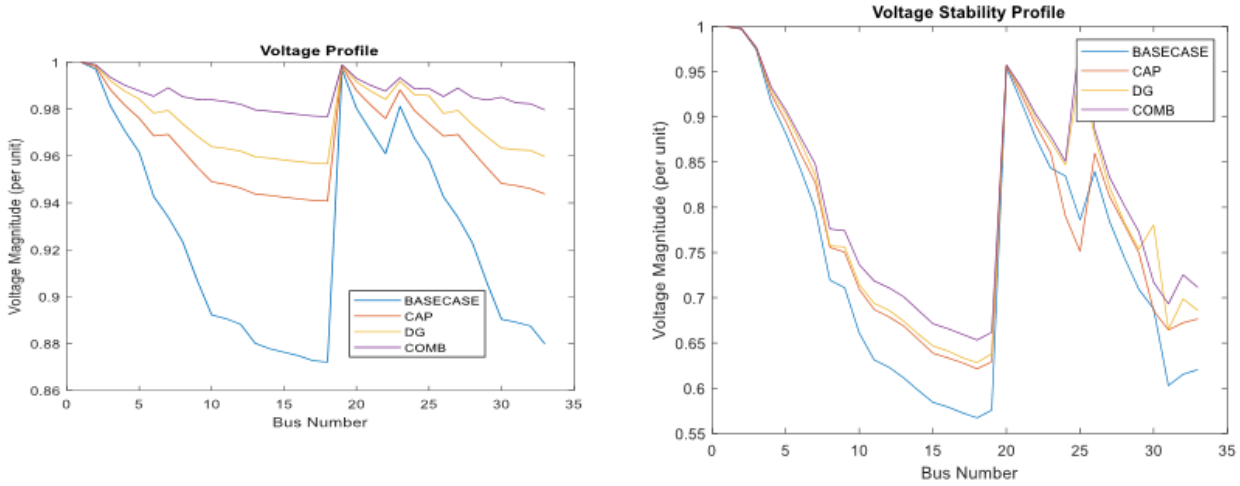

Figure 2.8: Corresponding voltage improvement (33-bus system) with the same combination as Figure 2.7 [65]

Simulations in [65] using the cuckoo search algorithm concludes that a combination of DG integration and capacitor banks offers a better loss reduction and voltage improvement than if they are installed in isolation. In [66], PSO algorithm also shows that the combination of both technologies reduces losses and voltage and as a result, network capacity considerably. In [68], Genetic Algorithm (GA) used on IEEE 33-bus system produces similar results for different DG types.

2.2.2 Short term Solution Using Voltage Regulators

A step-type voltage regulator is essentially an autotransformer and is used to compensate for unacceptably large voltage drop along a feeder in a network. They do not reduce reactive power demand or losses (as shunt capacitor banks do) but can usually vary the voltage over a range of 10 to 15%. In star-connected systems three single-phase regulators (cans) can be connected between phase and neutral to regulate each phase individually. The units must be rated for full load current, and phase-to-ground voltage and can be connected at any point on the MV line to where the regulation is required. In delta-connected networks, three single-phase regulators can be connected between the phases in a closed delta configuration (no ground connection other than for safety and protection purposes) to provide full three-phase voltage regulation. By using two single-phase regulators, an open-delta regulator installation may also be established. Open-delta regulators are generally preferred for long rural feeders (>100 km) as although closed-delta regulators offer more regulation, the installation cost and additional regulator can cost make them less favourable [67]. The industry standard specification for single-phase regulators is ±10% voltage regulation range in 32 steps (16 up and 16 down) which equates to a 0.625% step size. Internal losses and maximum load current of a particular regulator is a function of its tap position. If tap limit settings are set to +/-5% the maximum load current can be increased to 160% but if set to +/-10% then the maximum load current is 100% [76]. This is a characteristic referred to by manufacturers as the “vari-amp” capability [76].

Regulators do not tap fast enough and do not increase fault level, and as a result do not assist in fast network responses during transient operating states. Network losses are higher when compared to utilizing other voltage regulating devices. Capacitor banks should be installed on the load side of the regulator as the reactive power support is dependent on the supply voltage, i.e. the reactive power magnitude is directly proportional to the square of the supply voltage [93].

The presence of solar PV on distribution feeders will lead to increased number of voltage regulator (VR) operations [63]. When a voltage regulator is installed between a PV system and the source substation and if the PV operates at unity power factor, reverse power flow will occur through the VR and will result in the VR trying to control the voltage on the substation side. On the other hand, if the substation is the stronger source, i.e. the source has a strong fault level (kA), the VR fails to set the required voltage set point and reaches its maximum or minimum tap position; the VR moves into a runaway condition [63]. The VR is then ineffective in controlling the voltage of the feeder and a serious over-voltage or under-voltage may occur along the feeder. Until the set point changes, the VR will continue into runaway condition.

However, if the VR operating modes are configured in a bi-directional mode or the controller enables forward or reverse bias depending on the power flow direction, the runaway condition can be mitigated. Also, this condition can be avoided if the PV provides reactive power support instead by importing reactive power (VARS) and thereby reducing the voltage at the point of connection establishing a valid set point for the regulator [63].

The key difference between capacitor banks and voltage regulators is that capacitor banks reduce the losses along the length of the feeder and voltage regulators only improve the voltage at a particular point. Voltage control devices of OLTCs and VRs operate autonomously in a non-coordinated approach. Having PV on distribution feeders and especially with the increase of penetration levels, increase the number of OLTC and VR operations and hence wear and tear of the devices [63] [68]. In order to install more than two PV systems on the same distribution feeder it is required to utilize a voltage regulation mechanism to maintain acceptable voltage levels since automatic voltage regulation is not an available option at the local distribution transformer [69].

2.3 Long-term Solutions to Un-constrain Medium Voltage Networks

2.3.1 MV Network Design Characteristics and Conductor Upgrades

This section looks at network design characteristics and the physical attributes of MV networks. It is also important to understand that when proposing conductor upgrades the CAPEX involved may not be cost-effective for minimal benefit. Standards are in place to ensure that MV networks be designed to the utility's requirements and that safety and efficient operation are prioritized. Typical 11 kV and 22 kV MV networks consist of wood-pole structures designed to physically withstand conductor weight while maintaining adequate ground clearance (sag) as per safety regulations. Table 2.1 [77] lists various conductor types that are utilized depending on the proposed load to be connected and the fault level required. MV lines are generally designed at a temperature of 75ºC with older lines still operating at 50ºC. When line temperature increases due to an increase in line current, the safety distance increases between the ground and sag of line is compromised. In order to mitigate this in addition to providing more network capacity, intermediate conductors and structures are built to tension the sag to the required limit. This process is referred to as *templating* which is also a cost-effective solution for mitigating thermal limitations on MV and HV lines and hence increasing network capacity [92].

Table 2.1: Conductor types, voltages and current ratings per templating temperature [77]

SHORT DESCRIPTION	Current (A) - 50ºC[1]	Current (A) - 70ºC[2]	3-ph fault current Ikss (kA)
COND,AAAC OAK 13.95D 11 kV D3136	312	443	9.64
COND,AAAC OAK 13.95D 22 kV D3136	312	443	9.64
COND,ACSR CHICADEE 18.87D 11 kV	433	625	10
COND,ACSR CHICADEE 18.87D 22 kV	433	625	10
COND,ACSR FOX 8.37D 11 kV D3136	148	210	3.13
COND,ACSR FOX 8.37D 22 kV D3136	148	210	3.13
COND,ACSR HARE 14.16D 11 kV D3136	292	408	8,96
COND,ACSR HARE 14.16D 22 kV D3136	292	408	8.96
COND,ACSR MINK 10.98D 11 kV D3136	292	297	5.39
COND,ACSR MINK 10.98D 22 kV D3136	292	297	5.39

Note: 1 and 2 refer to conductor current rating where the line is designed and built at 50 or 70 degrees Celsius

All MV networks in Eskom utility are built to 22 kV standards utilizing investment criteria determined by the South African grid code advocating a least life-cycle cost approach. In addition, feeder operating parameters such as voltage limitations are governed by the regulations stated in NRS048 [34].

To design an MV line, a bottom up-approach is generally used for new loads. The network loading is determined by applying the coincidence factor (CF) to the network installed capacity. CF is calculated earlier by using equation (2.3). For rural areas the CF is approximately 25-35% and for industrial customers, 65-75%. Once this is determined, the backbone conductor rating can be calculated. In Figure 2.9 [95] an aerial view picture captures proposed customer households with numbers, with aerial bundle LV type conductor connecting each household with LV airdac type cable. Airdac cable is a copper phase conductor, XLPE insulated (cross-linked polyethylene whose material is resistant to heat, moisture, and chemicals) with bare earth conductors typically used for household connections. Digital aerial photographs referred to as rasters are used as a reference layer to create preliminary design of network equipment to be used as depicted in Figure 2.9. Fault level typically decreases with an increase in impedance along a radial network and as such the conductor types used are in addition selected not just for current ratings but fault level as well. Larger to smaller conductors are connected radially and this has been the design philosophy thus far. DG increases the fault level at the point of common coupling (PCC) and point of connection (POC) and hence the conductor size may be inadequate. New design principles therefore need to be relooked at especially with the integration of DG and more specifically PV systems. Once this preliminary design is completed, a single line diagram, as shown in Figure 2.10 [96], is built automatically

(depending on the simulation package e.g. Bentley Microstation, Reticmaster and DIgSILENT Powerfactory) for modelling purposes, to determine if the design meets the regulatory and design criteria. The simulation tool connects the conductors and loads that are geographically placed such that a radial circuit is formed with the MV/LV transformer point as source [95]. The tool (commonly used – Bentley Microstation) enables connectivity to the power systems analysis package where load flow and short circuit studies are executed determining the required voltage drops and three-phase and single-phase fault levels. Design criteria that are defined in the NERSA standards (NRS048) and design parameters are set in the tool and the simulation would therefore highlight the results that do not meet the set criteria. Adjustments to the design are then made and the process is repeated until the simulation produces satisfactory results [94].

Figure 2.9: Example view of MV design extracted from Microstation design tool [95]

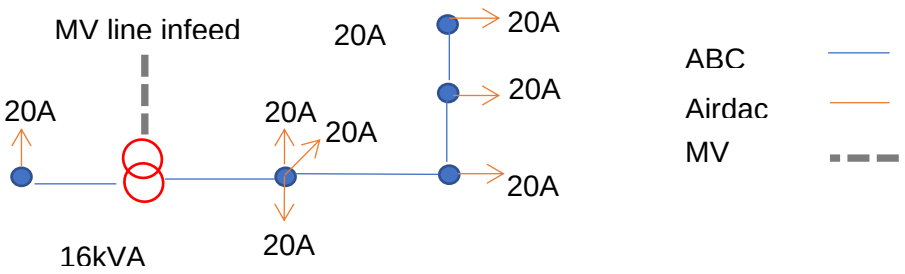

Figure 2.10: Single line diagram for MV design [96]

The iterative process as explained above results in a complete geographic MV network as shown in Figure 2.11 [40]. In this example, two networks are shown emanating from a single source substation (S) with a connecting open point between them. When a complete load flow study is performed, a voltage profile of feeder 1 is shown in Figure 2.11. It can be seen that the voltage reduces towards the end of the line. High impedance conductors will have relatively steeper curves. Tee-off parts of the network are also shown 2.11

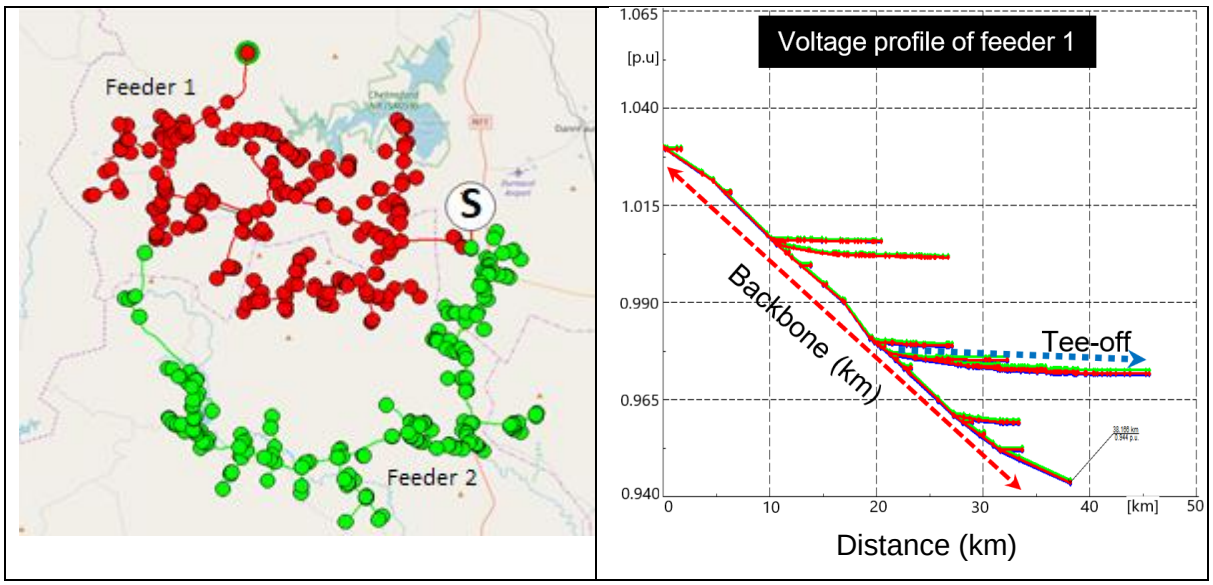

Figure 2.11: Example of MV networks and corresponding voltage profile [40]

MV and LV technologies include three-phase, phase-phase, single-phase and neutral, dual-phase, and single wire earth return (SWER). In Figure 2.10, 16 kVA transformers are single-phase and the capacity to connect all 20A customers must not exceed the transformer rating, the Aerial Bundle Conductor (ABC) thermal rating and the MV line infeed thermal rating. MV feeders are constrained based on two criteria, one being low voltage regulation and the other being conductor thermal exceedances. Networks having voltages <93% (of the substation /nominal voltage) are generally regarded as constrained and networks with thermal loading >85%(of the line/equipment current rating) are also regarded as constrained [94].

Long-term solutions using practical injection points of additional power into constrained networks points can be MV interconnectors from adjacent networks or new feeder bays from existing or new substations. In each approach, reduced impedances result in higher fault levels and hence improved voltages and line capacities. In transmission systems, the X/R ratio is high and in distribution systems the same is low as the line conductor resistance must be taken into account. X/R ratios can only be changed with re-configuration or new injections to networks. Inappropriate X/R ratios can increase the need for reactive power compensation resulting in PCC voltage drops [73]. Hence appropriate X/R ratios for reactive power

injections from DG plants can be used to effectively control voltage for providing network capacity to growing load.

PV installations on residential feeders can be considered a critical case with overvoltage where network feeder impedance plays an important role to determine the voltage rise in the feeder [46]. This is also seen in long radial distribution networks with low X/R ratios in network impedance. Radial networks have characteristics of decreasing voltage with line length and load as well as decreasing fault level only due to line length.

Feeder injections from existing substations are more cost-effective than new substations and can be built in a relatively shorter period of time. However, these long-term solutions are derived from a detailed analysis of the study area, load forecasting and load flow simulation results, and would therefore determine the type of conductor to be used. Existing MV feeder bays cost between R1.5 million to R2 million and new substations with feeder bays are in excess of R70 million due to unforeseen environmental or servitude issues. Re-configuring networks or building interconnectors also directly adjust the impedance and hence provide, if modelled for that purpose, the required additional capacity [94].

2.4 Standards and Guidelines of Medium and Low Voltage Grid Integration

The South African Grid and Distribution codes [38] explain the minimum technical requirements for all grid-connected generators. The South African utility, Eskom, specifies the control mode and power factor of the generator within its physical capability [33]. Generators operating at lagging PF inject reactive power into the grid thereby increasing the voltage at the POC and depending on the magnitude, the connected MV points' voltage will also increase. Similarly, generators operating at leading PF absorb reactive power from the distribution network thereby reducing the voltage at the POC and lowering RVC if problematic at this point. The following sections briefly outline the limitations and constraints that govern the solutions to the optimization problem identified for this research.

2.4.1 Medium Voltage Regulations

The Grid Code for renewable power plants in South Africa [37] specifies the minimum technical and design grid code connection requirements for renewable plants that may connect to the utility grid. LV generators are referred to as Category A in the code up to 1MVA. Up to 100 kVA connected generation, due to sudden voltage drops and peaks on the macro or main grid, the LV generator must be able to continuously operate. As per Figure 2.12 [37], if the voltage dip of the grid drops to any voltage above 0.6 p.u. within the time frame of 600ms, the generator may continue to operate and not disconnect from the grid while the grid voltage recovers.

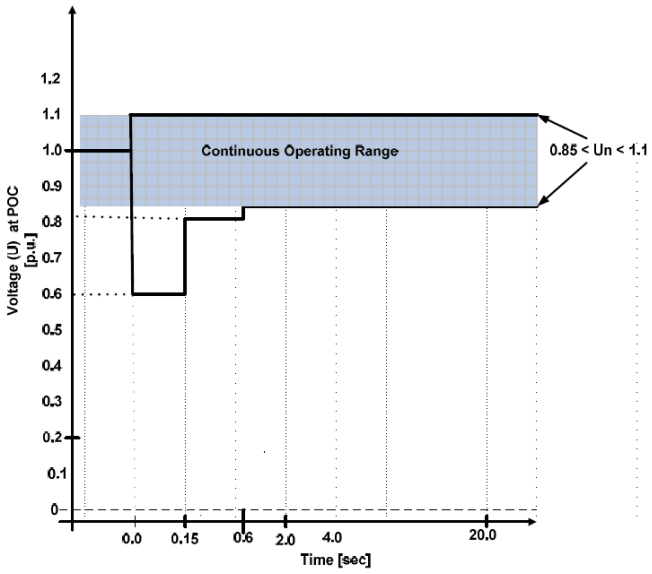

Figure 2.12: Voltage ride through capability for up to 100 kVA [37]

When the frequency of the utility grid exceeds 50.5Hz (for a 50Hz system), the plant must reduce active power as per Figure 2.13 [37].

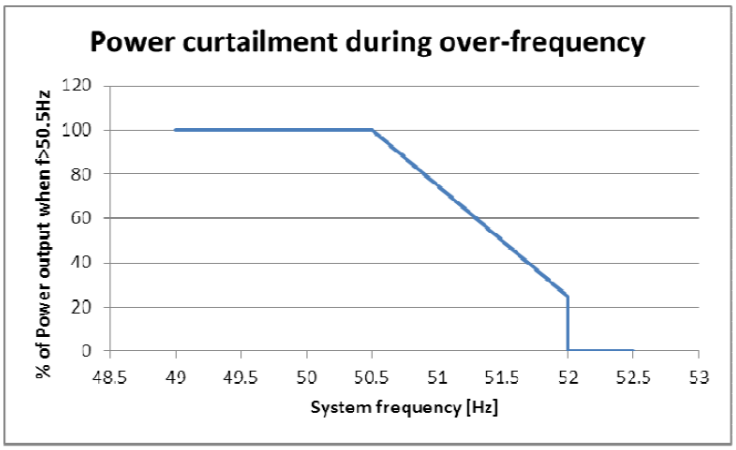

Figure 2.13: Power curtailment during over-frequency [37]

In Germany, after the “50,2Hz problem”, the grid code states that during frequency increase the generating plant has to reduce its active power by 10% of the nominal power down to 0 with 10%/min rate without the disconnection from the LV or MV network [32]. After exceeding the threshold limit the reduction of active power (P) has to be made with a gradient of 40% P/Hz.

2.4.2 Low Voltage Regulations

The NRS097 series of documents specify the minimum technical requirements for LV generators connected to the South African grid. All LV grid-connected generator

interconnection equipment must be type-test certified, as complying with the minimum technical requirements of NRS 097-2-1 [35]. Two types of generator configurations are defined as either dedicated or shared. Figure 2.14 [97] to Figure 2.17 [97] show the difference between both in a configuration that is overhead and one that is cable. A dedicated supply has a single connected customer and meter to monitor, if set, bidirectional power flows and a shared feeder has more than one connected customer taking LV supply from the same MV/LV point. Generators up to 350 kVA (PF =1) may be connected at LV with all other sizes at MV or HV. In a shared LV feeder, the maximum generation must be 25% of the supply demand up to 20 kVA [33] [35]. In a dedicated LV feeder, this is to be 75%. Dedicated single-phase supplies (e.g. 16 kVA MV/LV dedicated supplies in rural areas) shall be allowed to connect up to 13.8 kVA of generation on that single phase but within 75% of their NMD [33] [36]. The dedicated feeder cable size is limited such that the voltage rise between the point of supply and the transformer busbar is limited to 1%. The total generation (i.e. shared LV generation + dedicated LV generation) supplied by an MV/LV transformer shall be < 75% of the MV/LV transformer rating; and the total generation supplied by an MV feeder shall be < 15% of the MV feeder peak load [33] [35] [36]. All the above conditions are to be met prior to any generator connection [34].

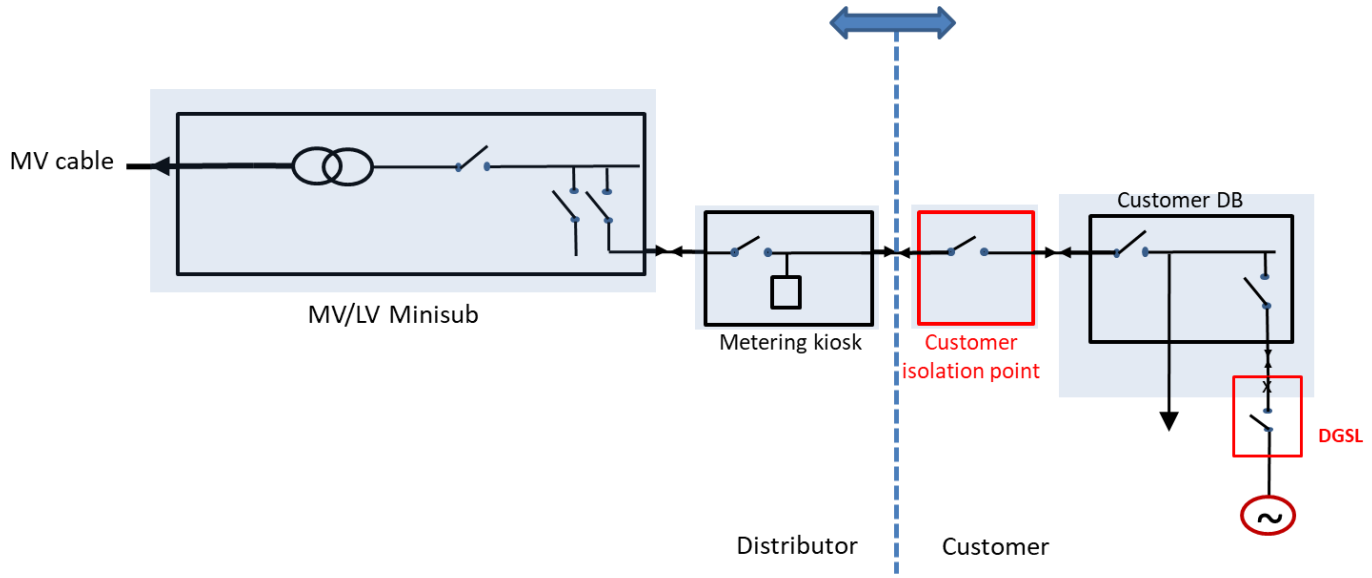

Figure 2.14: Cable - LV dedicated customer supply [97]

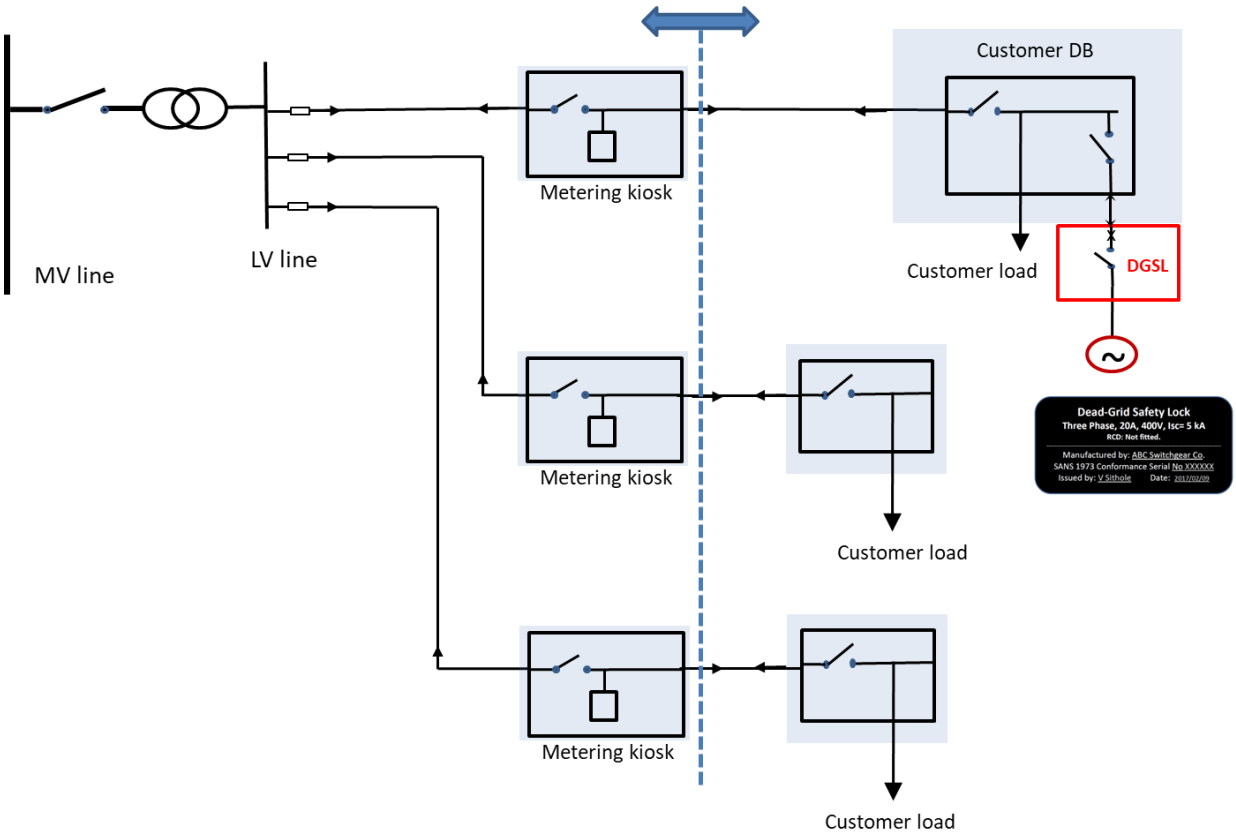

Figure 2.15: Overhead line – MV to LV shared customer supply [97]

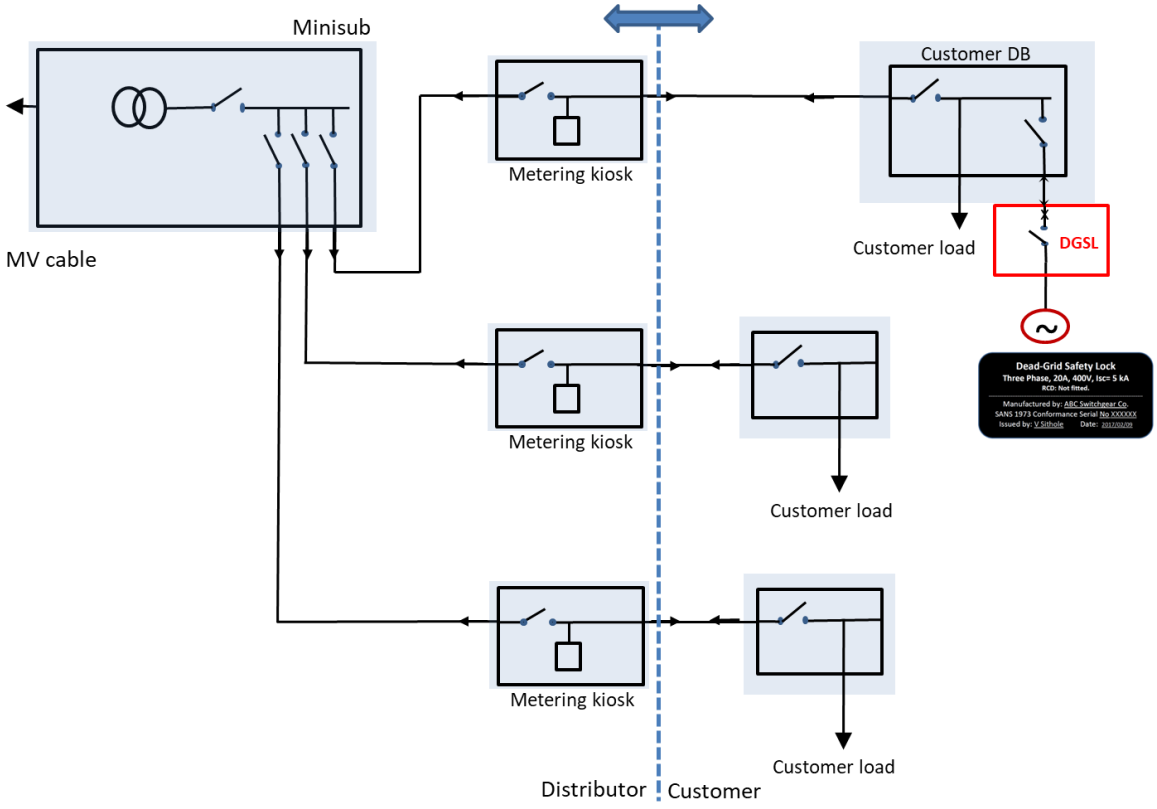

Figure 2.16: Cable – LV shared customer supply [97]

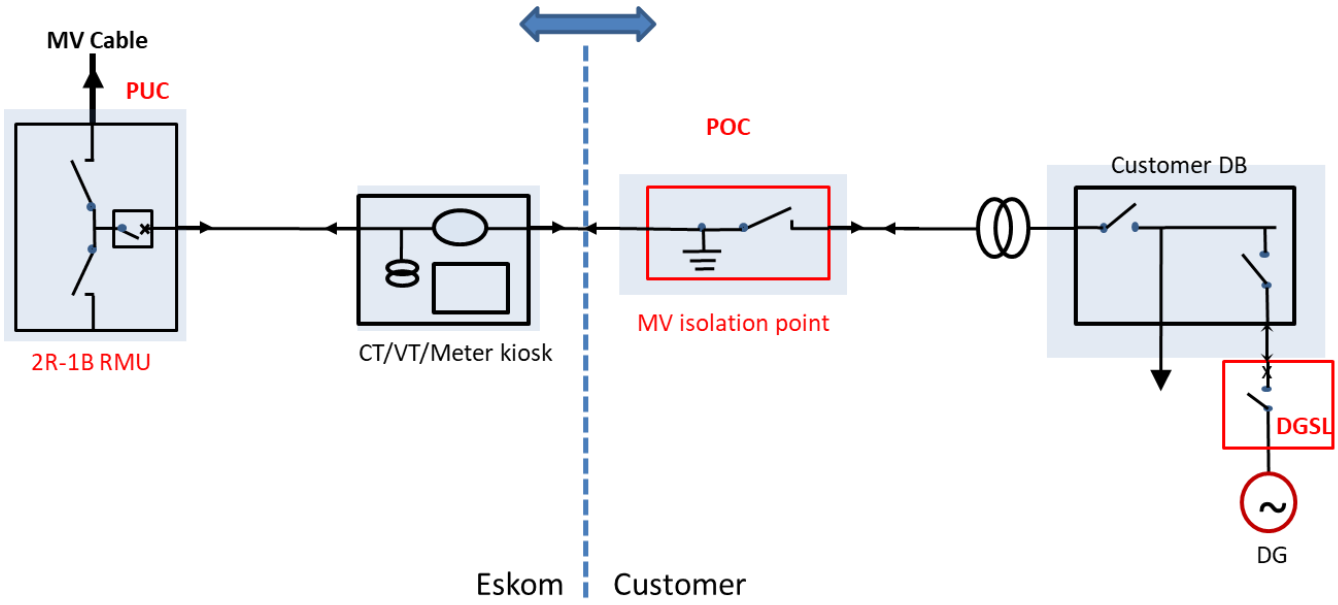

Figure 2.17: Cable – dedicated MV customer supply [97]

The summary of technical limitations that constrain LV connected generation is as follows:

- Equipment **thermal** current-carrying capacity ratings.
- Equipment short circuit current ratings**, three phase and single phase**.
- LV voltage regulation must be within the limits specified in [34] (LV voltages at the customer point of supply shall be within ±10%).
- The maximum change in LV voltage (due to voltage drop/rise in the MV/LV transformer and LV feeders) due to embedded generators is limited to 3%.
- Islanding of the utility network is *not* allowed.
- Voltage rise on LV feeders shall be limited to a maximum of 1%. This value is informed by the NRS048 voltage limits [38].
- The maximum generation connected to an MV/LV transformer is limited to 75% of the transformer rating.
- An individual limit of 25% of Notified Maximum Demand (NMD) will typically support a penetration level of 30% to 50%
- The total generation connected to an MV feeder is limited to 15% of the MV feeder maximum loading. This is used internationally where the percentage ratio is of maximum to minimum feeder loading for typical consumer load profiles. A generation limit of 15% prevents voltage rise.

2.4.3 Medium Voltage Network Classes

Medium voltage (MV) network voltages are controlled mainly by an on-load tap changer or OLTC at the distribution substation and this tap setting varies due to the voltage inputs it senses. However, LV load output voltages are fixed by manual tap setting on each individual MV/LV transformer. Due to these fixed voltages, the feeder voltage profile changes when the load changes. Each MV feeder network has been subdivided into classes. Four classes (C1-C4) exist that enable the correct tap setting to be implemented [44]. Figure 2.18 [44] shows the MV voltage profile in two scenarios, the first during peak load where the load is higher and hence the voltage drop is higher (relative to source), and the light load scenario where the voltage drop is lower (relative to source) and hence the voltage profile plot approaches the sending end voltage. Three tap zones (TZs) are also defined in Figure 2.18 [44]..

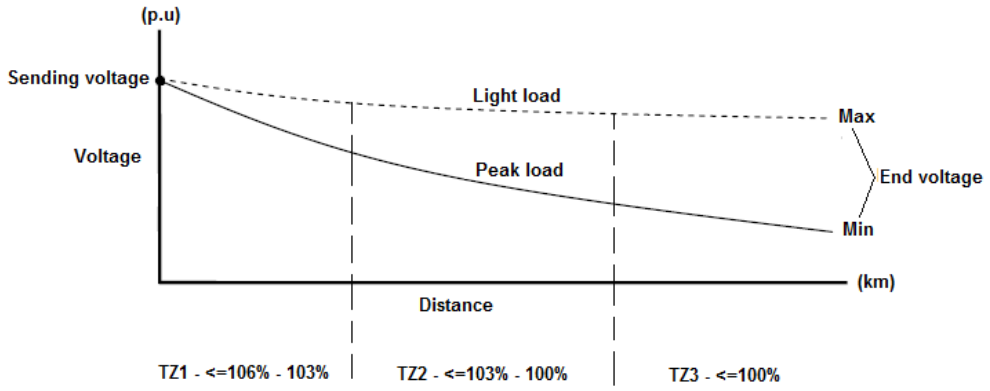

Figure 2.18: MV voltage profile definition and tap zone identification (Voltage at source is set at 103% or 1.03p.u.) [44]

By connecting more than one DG to the network, the feeder becomes unconstrained as the power drawn from the network grid is thus supplied from the DG itself. This reduces feeder stress due to loading and lengthens the operating life span of the interconnecting equipment. The voltage limits in this study case dictate the maximum DG penetration in the network. Once the network loads become dependent on DG power, the magnitude of voltage fluctuation increases as network instability events occur [51]. Un-constraining solutions such as network strengthening, i.e. decreasing impedances with larger conductor types or shunt compensation to improve downstream voltages become more complex with multiple connecting DG to the network feeder. An operating bandwidth as shown in Figure 2-19 [44] [75] [76], will enable a network feeder to function with specified limits. The optimal placement of DG determined by PSO algorithm along the feeder therefore depends on the network type, impedance ratio, installation of voltage regulating devices and MV/LV transformer tap setting. The simulation clearly illustrates that new operating bandwidths are required to maximize the amount of DG

connecting to any MV network which simultaneously results in the network capacity improvement values.

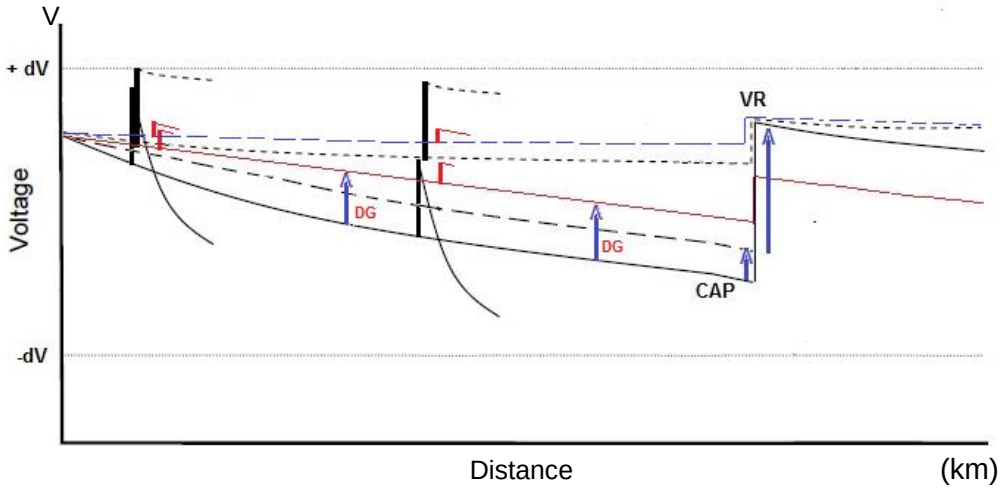

Figure 2.19: Graph showing the optimal fit of DG with voltage profile adjustment [44] [75] [76]

2.5 Increasing Network Capacity with PV and Energy Storage Technologies

The focus technology in this research is inverter-based solar PV generation and their utilization to un-constrain MV networks. Maximum power can be extracted from PV arrays using maximum power point tracking (MPPT) methods to optimize efficiencies [17]. By the end of 2010, approximately 80% of cumulative installed PV capacity, i.e. about 14 GW, was connected to the German grid via the LV distribution system [43]. Grid integration challenges for PV in Germany include the strengthening of the existing distribution networks, maintaining frequency stability and real time control of power plants less than 100 kW. In South Africa, it has been projected that the growth of the solar Energy Market share is expected to increase by 23.31TWh from 2021 to 2026, at an accelerated Compound Annual Growth Rate (CAGR) of 29.74% according to the recent market study by Technavio [74] (Figure 2.20 [74]).

Figure 2.20: High growth rate of PV with CAGR of >29% [74]

These challenges could also be mitigated by the flexible use of Energy Storage Systems (ESSs) that facilitate the management of the power system with high DG penetration [58]. Battery Energy Storage System (BESS) in particular**,** has the massive advantage of fast response, controllability, and geographical independence with technical methods to perform peak shaving, load levelling, demand response, voltage and frequency regulation and ancillary services [58]. In addition, reverse power flow and voltage rise can be managed using storage to absorb power from PV systems and should be optimally placed. Deployment of BESS in the distribution network can defer network upgrades and provide headroom for future load growth, however they do require massive charging which could cause unacceptable voltage drops [59] [60]. Storage and re-building lines with larger conductor sizes can be financially viable alternatives.

DG located near loads minimises distribution losses and can delay or possibly substitute for the establishment of new network infrastructure. Distribution grids are supplied by sources having rotating masses and these are regarded as essential for the inherent stability of the systems [28]. Solar PV facilities have inverter interfaced distributed sources that are inertia-less but can offer a more flexible operation due to grid-tied configuration which provides voltage and frequency references, or non-grid tied which uses battery storage for operation references.

2.5.1 Inverter-Based Generation with PV Installation and Power Quality

Transmission and generation facilities for PV generation often stay idle as they cannot produce electricity during night and cloudy weather. However, energy storage devices, such as batteries, can absorb fluctuation of PV generation [2] [13]. In order to drive PV installation in areas where limited or no utility supply exists, [13] proposes a DC microgrid with a redox flow (RF) battery for storage. The experimental setup demonstrated that the RF battery has great potential for balancing power supply and demand [13].

Advanced inverters that convert the DC photovoltaic output to AC have the following capabilities: A power line carrier (PLC) signal can control anti-islanding behaviour, i.e. the PLC signal received from a sub-station determines this status [14]. By controlling this signal, the utility can enable or disable PV inverters on the network feeder. This can be an important operating mechanism to allow MV network voltage control where required. Frequency droop control is stated in terms of the output angle of fast acting inverters and is able to quickly change the phase of the output voltage [15].

When DGs are connected to grid networks, they act as constant power sources which inject the demanded power into the grid. When these DG's are islanded, they are required to supply

all the power needed by the local load (accurate power sharing) and simultaneously operate within acceptable voltage and frequency ranges prescribed by the various grid codes [23]. Increasing DG penetration in a system may provide several technical problems in grid operation. A system with multiple connected DG sources that would operate in an islanded mode requires some form of storage to ensure initial energy balance [26]. At the PCC, steady state and transient stability, over or under-voltages, protection issues, fault level and power quality are the main problems that grid operators are exposed to [16]. High DG penetration levels increase network voltage to unacceptable levels when active power generation is greater than load demand [45]. PV installations on residential feeders can be considered a critical case with overvoltage where network feeder impedance plays an important role to determine the voltage rise in the feeder [46]. This is also seen in long radial distribution networks with high R/X ratios in network impedance. Optimal allocation of PV generation will support grid voltage regulation due to voltage rise and improve distribution network performance [47].

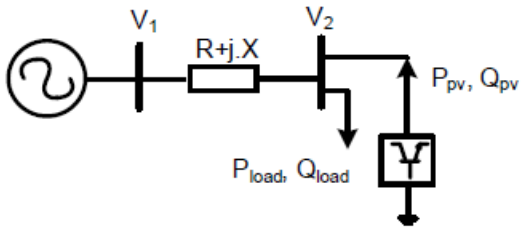

Figure 2.21: Voltage variation model with PV generation [49]

The model in Figure 2.21 [49] can be expressed as follows using equation (2.5) [49]:

$$\Delta V = V_1 - V_2 = \frac{R(Pload - Ppv) + X(Qload \pm Qpv)}{V2} \quad (2.5)\ [49]$$

Under no-load condition with $P_{load} = Q_{load} = 0$, DG can provide voltage support to raise the end voltage V_2 but with high values of R, this would result in overvoltage. This limits the DG capacity which can be installed, or, in general, the active power that can be injected at the end of the line [48] [49].

Overvoltage issues are addressed by [50] using the following approaches:

• Lowering the MV/LV transformer tap setting

• Allowing the DG's controller to absorb reactive power acting as an inductor (leading pf)

• Installing appropriately sized voltage regulators

• Reducing line impedances with larger conductors

• Employing active power curtailment strategies

2.6 PV Integration on the LV Network and its Utilization in Improving Network Capacity

In integrating solar PV DG to the MV network, which is transformed from the LV network, the response of the LV network to the addition of small-scale embedded generation (SSEGs), focuses on the following technical aspects of voltage regulation - voltage rise, voltage unbalance, cable and transformer thermal limits and network losses [30].

Control strategies of LV grid-interfaced PV inverters and relevant grid requirements differ from MV grid-interfaced inverters where grid voltage support features are included [27]. Clustered PV inverters might trigger a parallel resonance due to interaction between equivalent line inductance, capacitance of residential units, and injected harmonic currents. Resonance frequency for residential LV network might be decreased to the 5^{th} harmonic level depending on number of residential units, inverter output filter capacitance and line impedance [27].

A challenging task is to operate more than one connected DG as it is not possible to use P and Q control but necessary to regulate the voltage during islanded operation by using a voltage versus reactive power droop controller for local reliability and stability [16]. In Germany, when system frequency increases to 50.2Hz, results in [43] show that it is indeed necessary to disconnect a significant proportion of the existing PV plants when this happens. This became enforced when Germany exported to other regions. When these regions experienced sudden disturbances which led to grid failure or blackouts, the frequency increased to 50.2Hz due to an oversupply of electrical power in the Germany grid [43].

Two kinds of control strategies are used to operate an inverter, PQ inverter control and voltage source inverter (VSI) control. The PQ inverter control supplies a given active and reactive power set point whereas the VSI control has predefined values for voltage and frequency controlled through droop [16] [25]. PQ control consists of a P and Q controller. P controller adjusts the frequency-droop characteristic to produce constant value of P and Q controller adjusts the voltage-droop characteristic to produce constant reactive power output as shown in Figures 2.22 [25] and 2.23 [25]. During islanded mode local frequency control is required which uses droop control consisting of a frequency and voltage droop controller. Figures 2.24 [25] to 2.25 [25] show the droop characteristics for each controller which is typically employed by the control scheme of a flywheel often seen in a stand-alone, microgrid network. The active and reactive power output is adjusted when the frequency or voltage changes during the islanding condition.

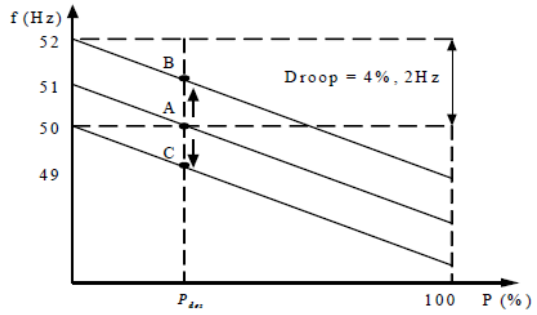

Figure 2.22: Frequency-droop characteristic [25]

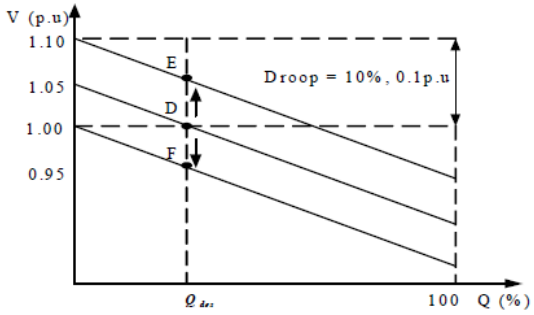

Figure 2.23: Voltage-droop characteristic [25]

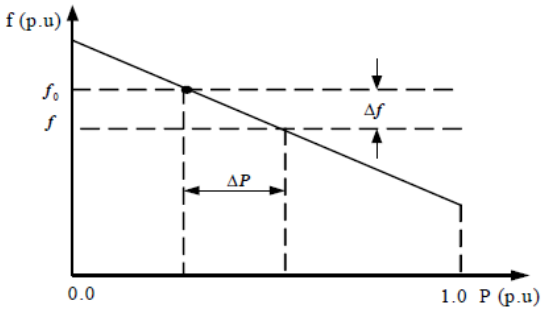

Figure 2.24: Frequency-droop characteristic for droop controller [25]

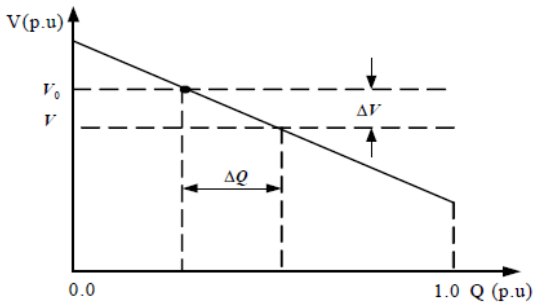

Figure 2.25: Voltage-droop characteristic for droop controller [25]

2.7 PV Integration on the MV Network and its Utilization in Improving Network Capacity

2.7.1 Steady-State Response of MV Networks

In transmission systems the X/R ratio is high. A slight change in Q can cause significantly high changes in voltages. Power factor control can result in excessive Q flow if set to account for the worst-case voltage contingency (e.g., during light load conditions), which in turn can result in increased losses [33]. Voltage control is achieved by adjusting the amount of reactive power (depending on range and connecting conductance) injected or absorbed into the network. Q control produces a constant value of reactive power, irrespective of the active power (P) output or voltage level.

Rapid Voltage Change (RVC) is a phenomenon in which there are changes in voltages noticeable by proximity customers at the Point of Connection (POC) caused by changes in generation output [33]. The phenomenon is similar to flicker that happens when large motors

are started and the network grid is relatively weaker. Checking the RVC percentage change is also known as the Voltage Variation Test (VVT).

The sudden voltage change caused by a generation connection can be estimated using equation (2.6) [33] as below:

$$\Delta U_{max}\ (\%) = \frac{\mathbf{SrE(MVA)}}{\mathbf{SkV(MVA)}} \times 100 \qquad (2.6)\ [33]$$

Where ΔU_{max} is the sudden change in voltage in percentage

$\mathbf{SrE(MVA)}$ is the rated apparent power of the generating unit

$\mathbf{SkV(MVA)}$ is the fault level of the grid at the point of connection

The short circuit contribution of an inverter-based plant is typically 1.1 - 1.2 times the plant rating [33]. RVC testing is the first step in assessing the connection of DG to the distribution grid and only then is the voltage and thermal limits checked. This is discussed in the next chapter is critical in finding the optimal location of connecting DG to MV networks.

2.7.2 Stability of MV Networks

The current practice of inverter disconnection when a voltage disturbance takes place (to avoid islanding situations) is not appropriate as it may lead to power system collapse [20]. Transitions from interconnected to islanding mode of operation are likely to cause large mismatches between generation and loads, posing a severe frequency and voltage control problem in the network [28].

Stability study of the Kythnos Island power system was investigated due to disturbances caused by weather conditions (cloudiness). Results in [20] showed that the system is generally stable for penetration lower than 50% while it becomes unstable at higher levels. It is concluded that at high levels of penetration of PV (> 60%) voltage instability occurs. In [22] simulations show that it is necessary to limit penetration levels, but a case-by-case assessment should be implemented depending on generator controller type. Results in [31] indicate that voltage stability is positively correlated with penetration of DG, but large induction type DG (e.g. Hydro power plant) may lower the voltage stability margin (VSM).

Rectifiers and voltage regulators have control loop dynamics in a similar frequency range to inverters which leads to a degradation of small-signal damping [19]. Participation analysis of the eigenvalues of the above combined system identified that the low-frequency modes are associated with the voltage controller of the active rectifier and the droop controllers of the inverters [19]. Participation Analysis allows the investigation of the sensitivity of eigenvalues

to the states of the DG integrated grid and indicates interactions between the dynamics of the inverters and the active load [19].

Droop controllers give rise to low-frequency modes. These controllers use low-pass filters to reject harmonic and negative sequence disturbances from the power measurements. As the supply demand of each inverter changes, the low-frequency modes of the power sharing dynamics drift to new locations and instability can occur. In [24], by imitating a voltage source with complex finite-output impedance, voltage droop control is achieved. Frequency droop control is further achieved from synchronizing the power source with the grid, with a phase angle difference that depends on the difference between nominal and real grid frequency. Grid interfaced inverters require output filter to attenuate low and high frequency components and coupling to the grid [27]. Inverter control is currently not operated by the Distributor but by the DG facility itself. With the integration of many inverters and the additional operation of already installed FACTs devices on MV networks, stability of the MV network becomes more of a concern when the DG facility exceeds the load demand and is suddenly disconnected from the network.

2.8 Optimization Algorithms to Determine Optimal DG Connection Points

Various publications on shunt compensation, DG and voltage regulators have been analysed on different network test cases to determine optimal location and size; by utilizing different search method techniques. Where the installation is integrated to and what the installation can deliver (control modes and ancillary services) are variables of a resultant mathematical function that can provide the most cost effective and technical feasible solution or combination thereof. In this research, network capacity needs to be maximized considering all the above variables such that all function constraints are satisfied. To optimally integrate these systems into MV networks, an optimization algorithm is required to determine the most beneficial placement and size. Once this is determined by a suitable search method for multiple PV installations, network capacity can be calculated and is proposed to be the best improvement in creating the additional capacity. Particle Swarm Optimization Algorithm (PSO) is the proposed search method for reasons further discussed.

2.8.1 Particle Swarm Optimization Algorithm (PSO)

A large number of optimization algorithms are used to solve electrical power optimization problems, for example, genetic algorithm, particle swarm optimization algorithm (PSO), seeker optimization algorithm, clustering optimization algorithm etc. Various computational algorithms exist to solve non-linear problems and the selected algorithm used in this research is the particle swarm optimization technique.

PSO does not require a good initial solution to start its iteration process and was chosen for this research as this has been used to successfully control grid reactive power and power losses reduction. PSO is considered as one of the most powerful methods' for resolving the non-smooth global optimization problems and some of the advantages are as follows [98]:

- ✓ PSO is a derivative free technique just like as other heuristic optimization techniques.
- ✓ PSO is simple in its concept and coding implementation compared to other heuristic optimization techniques.
- ✓ PSO is less sensitive to the nature of the objective function compared to the conventional mathematical approaches.
- ✓ PSO has a limited number of less sensitive parameters including only inertia weight factor and two acceleration coefficients in comparison to other techniques.
- ✓ PSO is less dependent on a set of initial points and generate high-quality solutions within shorter calculation time and stable convergence characteristics than other stochastic methods.

Particle Swarm Optimization (PSO) has many similarities with Evolutionary Computation (EC) techniques in general and Genetic Algorithms (GA) in particular as they all update the population and search. The main difference between the PSO approach compared to EC and GA is that PSO does not have genetic operators such as crossover and mutation.

In [54] a study was undertaken to assess the overall performance of various Swarm Intelligence (SI) based approaches and aimed to provide a comparison among the well-known SI-based approaches. A set of algorithm techniques including Genetic algorithm (GA), Ant Colony Optimization (ACO), Particle Swarm Optimization (PSO), Differential Evolution (DE), Artificial Bee Colony (ABC), Glowworm Swarm Optimization (GSO), and Cuckoo Search Algorithm (CSA) are considered and a selection of thirty benchmark functions that have been utilized in MATLAB to measure the performance of these approaches.

Table 2.2 [54] shows 10 out of the 30 functions used in the study for comparison. Table 2.3 [54] shows the results of the 30 functions and the number of functions each method performed at its best. DE outperformed in 24 out of the 30 functions with PSO the second-best approach. Each function has a theoretical optimal value to which each algorithm was executed to achieve.

Table 2.2: Benchmark functions selected for comparison (showing 10 out of 30) [54]

No	Function	Formula	Value	Dim	Range	Properties
1	Sumsquare	$f(x) = \sum_{i=1}^{n} i x_i^2$	0	30	[-5.12, 5.12]	Unimodal, Separable
2	Sphere	$f(x) = \sum_{i=1}^{n} x_i^2$	0	30	[−100, 100]	Unimodal, Separable
3	Beale	$f(x) = (1.5 - x_1 + x_1 x_2)^2 + (2.25 - x_1 + x_1 x_2^2)^2 + (2.625 - x_1 + x_1 x_2^3)^2$	0	2	[-4.5, 4.5]	Unimodal, Inseparable
4	Colville	$f(x) = 100(x_1^2 - x_2)^2 + (x_1 - 1)^2 + (x_3 - 1)^2 + 90(x_3^2 - x_4)^2 + 10.1((x_2 - 1)^2 + (x_4 - 1)^2) + 19.8(x_2 - 1)(x_4 - 1)$	0	4	[−10, −10]	Unimodal, Inseparable
5	Dixon-Price	$f(x) = -(x_1 - 1)^2 + \sum_{i=0}^{n} i(2x_i^2 - x_j - 1)^2$	0	24	[−5, 5]	Unimodal, Inseparable
6	Easom	$f(x) = -cos(x_1)cos(x_2) exp(-(x_1 - \pi)^2 - (x_2 - \pi)^2)$	0	30	[−30, 30]	Unimodal, Inseparable
7	Matyas	$f(x) = 0.26(x_1^2 + x_2^2) - 0.48 x_1 x_2$	0	2	[−10, 10]	Unimodal, Inseparable
8	Powell	$f(x) = \sum_{(i=1)}^{n/4} (x_{(4i-3)} + 10x_{(4i-2)})^2 + 5(x_{(4i-1)} + x_4 i)^2 + (x_{(4i-2)} + x_{(4i-1)})^4 + 10(x_{(4i-3)} + x_4 i)^4$	0	2	[−100, 100]	Unimodal, Inseparable
9	Rosenbrock	$f(x) = \sum_{i=1}^{n-1} [100(x_{i+1} - x_i^2)^2 + (x_i - 1)^2]$	-1	2	[−100, 100]	Unimodal, Inseparable
10	Schwefel	$f(x) = \sum_{i=1}^{n} -x_i \sin(\sqrt{\lvert x_i \rvert})$	0	30	[−500, 500]	Unimodal, Inseparable

Table 2.3: Best performing algorithm out of the 30 functions [54]

Category	Number of functions	GA	ACO	PSO	DE	ABC	GSO	CSA
Best performing method	30	15	13	19	24	6	0	3

Modified PSO algorithms have been discussed in [55] and show that all the PSO methods gave similar results for the optimal DG output with similar power loss values in the system. When PSO is combined with other algorithms forming a hybrid optimizer, optimal placement of feeder switches, capacitor banks and DG can be determined. In addition, the common power system applicability of the PSO or modified PSO algorithm was used to optimize reactive power flow and to minimize real system power losses. Also, the problem of optimal power flow where the goal is to find optimal settings of the control variables such that the sum of all generators cost functions is minimized, hybrid techniques improved convergence characteristics [56]. The conclusion derived from the research above indicates that adaptive/ modified PSO and basic PSO algorithm is best suited for the optimal allocation of DG on MV networks and identifying weak and strong network injection points of MV networks. Although in [57] an attempt to optimally place DG on networks using PSO was investigated, using the approach to un-constrain capacity limited MV networks is novel to the research.

PSO algorithm is based on the theory of swarm intelligence. Every candidate solution is rated as a particle with a number of candidate solutions making up a swarm. Each particle has a weight and volume, which determines its fitness with the objective function. The motion of each particle in the search space is decided by the particle velocity. Particle velocity is mainly determined by the individual optimal location and the global optimal position as in equation (2.7) [57] and (2.8) [57]. Each particle has knowledge of the location with best fitness value of the whole swarm which called the global best or (*gbest*). At each point along their path, each particle also compares the fitness value of their (*Pbest*) to that of (*gbest*). If any particle has a (*Pbest*) with better fitness value than that of current (*gbest*), then the current (*gbest*) is replaced by that particle's (*Pbest*). The movement of particles is stopped once all particles reach close to the position with best fitness value of the swarm.

The modified velocity and position of each particle can be calculated from the current velocity and the distance from particle current position to particle best position *Pbest* and to global best position *gbest* is described in the following equations (2.7) and (2.8):

$$V_i^{(t)} = w.V_i^{(t-1)} + c_1.r_1.(P_{best} - X_i^{(t-1)}) + c_2.r_2.(G_{best} - X_i^{(t-1))}) \quad (2.7)\ [57]$$

$$X_i^{(t)} = X_i^{(t-1)} + V_i^{(t)} \quad (2.8)\ [57]$$

where:

$i = 1, 2, 3\ldots..N$

$V_i(t)$ - Velocity of the particle i at iteration t (m/s)

$X_i(t)$ - The current position of particle i at iteration t

c_1 - The cognitive acceleration coefficient and it is a positive number

c_2 - Social acceleration coefficient and it is a positive number

r_1 and r_2 are random numbers obtained from function in the interval [0,1]

g_{best} - the global best position

w is the inertia weight which shows the effect of previous velocity vector on the new vector. Suitable selection of inertia weight w provides a balance between global (<w) and local exploration (>w) , thus requiring less iteration on average to find optimal solution.

2.8.2 Initialization of PSO Parameters

The control parameters of lower and upper bounds at node: voltage regulation, voltage variation (%) and fault level. Randomly generate an initial array of particles with random positions and velocities, randomly connect PV DG to multiple locations on the feeder network with small and different magnitudes of PV injections.

2.8.3 Evaluation of Fitness Function

The fitness function should be capable of reflecting the objective and directing the search towards an optimal solution. Since the PSO proceeds in the direction of evolving best-fit particles and the fitness value is the only information available to the PSO, the performance of the algorithm is highly sensitive to the fitness values. For each particle or swarm, PV generators are placed at the sensitive nodes and this updates the particles fitness function.

Information of the *best* position includes the optimal location and magnitude of generation.

2.8.4 Algorithm for Optimal Location of PV using PSO

Each test network will follow the same process. After calibration and model completion, DIgSILENT Programming Language (DPL) would be used to create the PSO algorithm presented below.

Step 1: Execute load flow and short circuit studies using system data such as generation, line, load and compensation data to obtain the MV voltages for the network feeder and record these results as the base case.

Step 2: Initialize the PSO parameters such as Number of Iterations, Number of Particles (no. of DG units), Initial value of Inertia weight (W_{max}), Final value of Inertia weight (W_{min}), Acceleration Constants (c_1 & c_2).

Step 3: Initialize the constraint parameters (voltage at MV nodes and line thermal limitations as per NRS048).

Step 4: Initialize the swarm (set of MV nodes at a particular voltage) by assigning a random position and velocity to each particle (connect PV units to random terminal nodes), where each particle is a solution of network percentage improvement calculated at the source busbar.

Step 5: Run the load flow, short circuit conditions and VVT tests and compute the fitness value of each particle using equation (the fitness value shown and elaborated further in the methodology is the difference in voltage levels after each iteration and connecting DG).

Step 6: Compare the present fitness value of i^{th} particle with its previous best fitness value. The best fitness value of the DG (P_{best}) offering the highest voltage improvement is compared in every iteration. If the present value is better than P_{best}, update the P_{best}, else retain P_{best} as same. The best voltage improvement in the entire network with all particles changing position in every iteration is defined as Global best or G_{best}.

Step 7: Find the G_{best} value from the obtained P_{best} values.

Step 8: Update the particle positions & velocity using derived equations.

Step 9: Apply boundary conditions to the particles.

Step 10: Execute steps 6-10 in a loop for maximum number of iterations.

Step 11: Stop the execution and display the G_{best} values as the set of critical nodes of best network improvement % and best generating connecting points.

Once the PSO simulation is completed, certain feeder sections will result in optimal placement of PV installations as well their magnitude. Simultaneously, network capacity is at its greatest when PV is connected at these points.

PSO as mentioned above has been chosen for this research as the algorithm does not require a good initial solution to start its iteration process and coding implementation is relatively simple when compared to other optimization techniques that was investigated as part of this review. Also, convergence is guaranteed and the solution does not depend on the initial starting positions implying that optimal positions to connect DG on MV networks can be found quickly when the executing on smaller iterations and thus is particularly suitable in its application for this research problem. The PSO equation does not have as many variables as other techniques require and so the objective function is not as sensitive to the outcome.

2.9 Integrating Microgrids to Optimal Points of Connection Determined by the PSO Strategy

Microgrids can be defined as a collection of interconnected loads & distributed energy resources (DERs) (e.g. wind turbines, PV, generators etc.) and storage devices (e.g. batteries, flywheels etc.) within clear electrical boundaries acting as a single controllable entity with respect to the utility grid [33] [78]. The grid can be operated in an islanded mode maintaining the relevant quality of supply parameters independent of any technical grid references. When well-coordinated and managed, power system efficiency can be increased by supporting large scale penetration of DG, facilitating the integration of renewable energy sources, reducing

system losses and greenhouse gas emissions; and increasing network reliability and resilience.

Microgrids are generally interconnected to the utility grid through the PCC. However, their modes of operation may be grid-connected and islanded. In grid-connected mode (default), the microgrid can import, export, or have zero power exchange with the utility grid to achieve the least-cost supply schedule. Having the capability to switch to islanded mode, isolates the microgrid from faults and/or disturbances in the utility network improving reliability; resulting in least load curtailment. To be able to successfully plan or integrate microgrids particularly to MV networks, an understanding of the current network expansion practices are required. In applying the thesis strategy to integrate microgrids as well as improving current network capacities, a further understanding of what is required to be derived from the tool is assessed in the sections that follow [94].

2.9.1 Current Network Planning Philosophy and Methodology

In planning the expansion of the network grid to accommodate new and existing load growth, a series of philosophies has to be applied to quantify what is required from a technical and financial perspective. These philosophies focus on technical criteria of voltage and regulation, fault level, load forecasting, quality of supply etc. and must adhere to categories defined under the SA Grid Code and Distribution Code [38]. The planning projects derived for grid expansion must be economically viable under the least economic cost criteria. The quality of supply criteria is stipulated in the NERSA policy [34], NRS048, and specifies compatibility levels, limits, voltage characteristics and assessment methods to the end-users point of supply. The planning methodology is sketched and depicted in Figure 2-26.

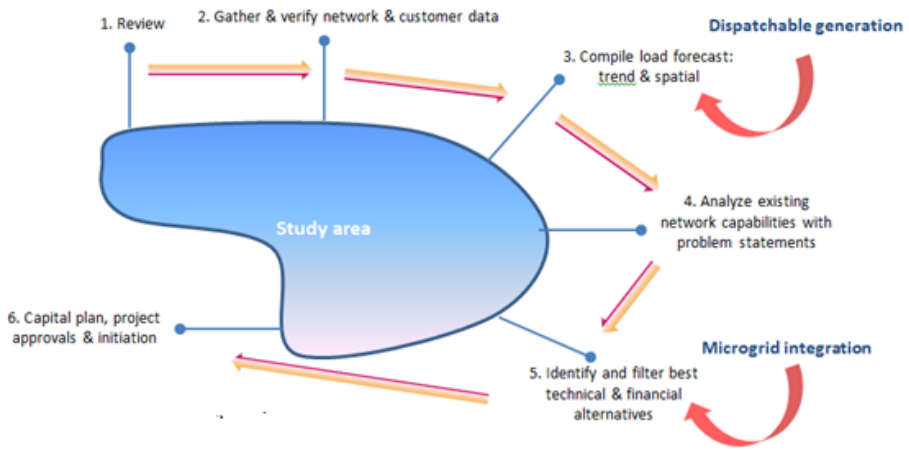

Figure 2.26: Planning methodology applied for network expansion

Application of load forecasting is an essential step in the process of infrastructure planning. Once the necessary and relevant information is quantified, the future state of networks is simulated with the new predicted loads and compared to the status quo of networks in the study area. Solutions to address the networks that contravene regulatory standards [34] are then compiled and documented in an approved Network Development Plan. In integrating microgrids in the methodology in Figure 2.26, implies a change in the approach where existing or new load is forecasted as the proposed demand is now (depending on location) dispatched from the microgrid itself. Therefore, solutions encompassing microgrids become a plausible mechanism to alleviate network constraints. A major investment in providing network capacity to a study area is typically new build of high voltage substations and its infeed line. In remote areas, this new infrastructure has several drawbacks in terms of cost, environmental impacts and time to construct and commission. This solution may not be financially viable due to losses and negative Net Present Value (NPV) generated from minimal supply demand, but is required to provide the necessary service to the study area in question. This makes the establishment and installation of microgrids an attractive alternative. Also, microgrids positively impact distribution network cost components when using optimal network planning, considering even a substantial microgrid penetration [78].

2.9.2 Microgrid Integration into MV networks

Integrated microgrid systems must satisfy all of the operational and interconnection requirements that the utility utilizes viz. all relevant Distribution Codes (Network Codes) [34], Renewable Grid Codes (Grid Connection Code for RPPs in South Africa) [37], quality of supply criteria, DG interconnection standards and all relevant guidelines and policies for infrastructure design and operation. Advanced microgrid systems will provide high-quality power to their loads with safety protection, synchronization, harmonic distortion limits, voltage limits, support for devices requiring reactive power, surge capabilities, and protection-device coordination [5]. The PCC is typically where the standards and codes by NERSA and Eskom Distribution apply.

Advanced microgrids will not exist without an energy-storage element (parameter references) and *will almost always use inverters* and controllers to interface with the EMS [79]. Whenever there is any disturbance (three phase fault being the worst scenario) in the utility grid or microgrid, the PCC is opened and the microgrid is disconnected and operates in stand-alone mode. DG should be provided at strategic points which may be load centres so that they provide voltage and capacity support, reduce line losses, and improve stability [80]. Renewable energy produced in the microgrid is classified into dispatchable (hydro, gen sets etc.) and non-dispatchable (wind and solar) production. Dispatchable production is changed upon demand and by the request of the Distribution System Operator (DSO). High penetration

of non-dispatchable DERs lead to voltage rise, voltage fluctuations, reverse power flow, changes in power factor, injection of unwanted harmonics, frequency regulation issues, fault currents, and grounding issues and unintentional islanding [81]. Also the total energy supplied to the grid from the microgrid can lead to stability issues. Voltage and frequency droop control has to be a function of the inverters to provide the relevant reactive power to the grid and operate within defined power factor range to control the grid voltage at the PCC [82] or if grid frequency exceeds the allowable limit, the inverters are required to disconnect from the grid.

Microgrids also consider the operation of electric vehicles (EVs). These, however, are represented as an additional load to the system. The aggregated effect of both DG and EV in the microgrid is positive but negative for EV charging stations alone [83].

2.10 Integrating Electric Vehicle Charging Infrastructure to Optimal Points of Connection Determined by the PSO Strategy

The electric vehicle (EV) forms an important part of the future smart grid in the control of charging or discharging power of an EV's battery for vehicle-to-grid (V2G) services. Some of the services include balancing the voltage and frequency, absorbing excessive renewable energy and supplying other ancillary services. The auto green paper released in June 2021 provides a platform advocating for a policy framework and opportunity for South Africa to facilitate and contribute to the procurement and/or production of electric vehicles and associated charging equipment [99]. What this means is that charging points are required to be integrated into MV networks that offer the same technical interface as PV systems but with the additional capability of providing power during variable times due to the additional storage. In planning for the charging infrastructure, suitable MV points are therefore required and as a result vehicle-to-grid power functionality can be utilized at the optimal positions found using the assessment tool as a result of this research. In order to accurately simulate the effects of the charger on the network, it is very important to model the behaviour of the charger.

EVs currently have not been heavily adopted in South Africa, but an increase of their usage will result in an increase in electric power demand on the electric network. Although there might be a desire to contain EV charging load to off peak hours without affecting the peak demand, the charging behaviours of different EV users has an element of randomness [84] [85].

2.10.1 Opportunities for Vehicle-to-Grid Technology (V2G)

Vehicle-to-grid (V2G) is an emerging technology which came into existence because a large number of EVs can be used as load as well as an energy storage system to support the grid. The EVs must be fully charged during off-peak time and provide power back to the grid during

peak time. The design and planning of the V2G system is implemented to solve the above-mentioned problem where EV acts as energy storage units [86]. In the residential area, the effect of EVs influences more heavily on the network, since recharging occurs mostly in the evening thus producing greater load peaks. V2G can be used to provide power supply at peak demand for an intervention time varying between four and six hours every day [85].

EV Chargers have the potential to provide reactive power for voltage support that can help solve local voltage issues in distribution networks. The charging infrastructure should have this capability. In addition, EV charger and associated infrastructure is required to align and *adhere to applicable standards for specifications and guidelines for deployment.*

2.10.2 Grid Impact and Infrastructure Placement

To mitigate negative grid impact, it is best to locate EV chargers near networks that are not constrained. Adequate grid capacity, especially for fast charging and driver demand are two key planning variables for locating EV charging infrastructure. Most EV charging in other countries typically occurs at night and during the weekends, when passenger vehicles are often not being used. However, public transport would need to charge during the day and even during peak demand periods, which could create a strain on the electricity system [2]. These aspects enable opportunity for the network assessment tool to assist in locating the EV charging infrastructure by:

a. Locating points on the network that have network capacity (22 kW AC, 50 kW DC)
b. And filtering those points that could be possible candidates for V2G opportunities

Bi-directional charging and discharging power flow can provide stability support to the power grid. In the V2G system, the main objective is to realize charging–discharging co-ordination, and maintain a charging equilibrium plan to eliminate the problems of stress on the power grid in V2G applications [87,88]. Technical planning assessment by the utility must consider and address the following:

1. Minimize active and reactive power losses
2. Minimize distance to optimal location of charger placement

Planning of EV charging infrastructure is a multi-objective and non-linear optimization problem [89]. As mentioned previously, but specifically PV technology and inverter mode of operation will enhance EV load servicing due to its ability to provide reactive power compensation. This would result in higher EV penetration with fewer grid impacts [89] [85]. The planning should in addition take into account EV forecasts, traffic flows, EV demand distribution, customer facility locations and adequate space availability [89] [85].

Bi-directional DC chargers can be used to perform voltage control on distribution grids through reactive power control in the chargers. EVs can further schedule their charging process so as to fully match renewable energy availability [90]. In [85] it concludes that the current network infrastructure has the potential to support a medium-low EV penetration (below 50%). Several organizations have sought to develop international benchmarks or quantitative guidelines for charging infrastructure as shown in Table 2.4 [91].

Table 2.4: Indicated average electric vehicle/public charge point ratios [91]

Organization	**Region**	**Electric vehicle / public charge point ratio**	**Source [91]**
European Council	European Union	10	European Parliament (2014)
NDRC	China	8 (pilot cities), 15 (other cities)	NDRC (2015)
IEA Electric Vehicle Initiative	Worldwide	8 (2015), 15 (2016)	EVI (2016,2017)
EPRI	United States	7-14	Cooper & Schefter (2017); EPRI, 2014
NREL	United States	24	Wood et al. (2017)
CEC/NREL	California	27	CEC & NREL (2017)
International Energy Agency's IEA	South Africa	7	IEA Global EV Outlook 2023 report

2.11 Conclusion

Chapter 2 concludes by highlighting possible solutions that can be applied to a network where voltage and/or thermal improvements can be made. The review discussed the implementation of DG as a voltage control device with and without shunt compensation and voltage regulation. Utilizing DG to improve network capacity was shown to be technically feasible, but multiple connecting PV systems on the same MV network has not been analysed to achieve maximum benefit both to PV output and network improvement. As a result, the conventional way of planning for forward power flow has to be changed. The next chapter of this thesis will present the methodology used to achieve the said objectives of this research. Chapter 3 on methodology will discuss the various models, load profiles, objective function and PSO algorithm used to determine the improvement in network capacity. Utilizing PSO algorithm would assist to provide optimal locations of multiple PV system integration points as well as maximize the network capacity that can be achieved with its placement. Also, two significant aspects of microgrid placement and EV charger placement can be strategized by utilizing the assessment tool.

3 Methodology

This chapter presents the methodology applied to formulate the objective function, provides details of the network models and discusses the Particle Swarm Optimization (PSO) algorithm (with its objective function and constraints) and its utilization in providing network capacity to constrained networks. Power system analysis tool, DIgSILENT Powerfactory, utilizes two scripting languages, DIgSILENT Programming Language (DPL) and Python. DPL was selected due to the researcher's knowledge of its capability in accessing network elements on a built Powerfactory model. The script was formulated incorporating load flow studies with assigned profiles to each load and PV output. This chapter starts with the definition of the objective function, the PSO optimization algorithm used and the integration of power system analysis using the algorithm.

The approach adopted is to firstly test practical electrical networks by using conventional or manual methods of connecting DG (PV) to the network model in Powerfactory. After connecting PV to different points on the network, voltage and thermal operating limits have to be checked for instance of increasing the PV size and its location on the network. Tabulated sets of results will then indicate the amount of generation and network capacity achieved by connecting PV systems to the MV network. Once this is done the DPL code is executed by using the PSO optimization technique in the code structure. The results derived from the DPL script are exported into result files which the tool interprets and displays graphically. The actual comparison between the manual method and automatic DPL method of analysis is the means to solving the research problem.

In the sections that follow, the objective function formulation is first discussed along with the constraints. The limitations to the solutions of the objective function are expressed and the direct correlation of the PSO equation parameters to the DPL scripting parameters are discussed. Flowcharts describing the general procedures and specifics are presented with a description of the two networks selected for the study, Network 1 is 11 kV and Network 2, 22 kV. Each network's loading, conductor types and attributes are also presented.

3.1 Mathematical Formulation of the Objective Function

Network capacity can be incrementally created by either increasing voltage regulation and/or increasing thermal capacity of the bottleneck lines that form the network backbone. Thus a relationship exists between either or both voltage regulation and thermal capacity and can be obtained by simulation analysis. Every network feeder as shown in Chapter 2 plots a voltage curve that radiates from the sending end voltage at the substation to the minimum voltage level at the end-of-the-line (EOL) during peak and off-peak times. With the integration of distributed generation (DG), network characteristics either improve or worsen, depending on DG magnitude and placement. Optimal placement DG is critical for deriving maximum benefit from them. One approach is to establish a relationship between what improvement in network capacity can be seen with the integration of DG installations with a focus on solar PV technology. The emphasis on this technology is due to the cost effectiveness of its supply and installation and the quantity of rapid uptake with industrial and agricultural demand not being met by conventional coal supply through the utility's generation component. This relationship is proposed as the novel contribution in this research and is defined by the objective function in equation (3.1). An additional characteristic in enhancing the novelty is that network capacity improvement is determined by utilising the optimization algorithm, PSO as discussed in Chapter 2 and below.

PSO algorithm, as introduced in Chapter 2, is a multi-agent parallel search technique which maintains a swarm of particles and each particle represents a potential solution in the swarm. To implement PSO to achieve the objectives in this research, a particle is analogous to inverter-based generation connecting at a medium voltage (MV) node in the network. Each iteration constitutes a change in the particle's position depending on its fitness value (% change p.u. value of voltage). This implies that at each iteration a connected PV is enabled at a position determined by the PSO equation. Once enabled and the simulation is complete, the relevant voltages are compared to the previous voltages (in p.u.) and the percentage improvement is the corresponding fitness value. PSO algorithm is utilized to optimize the allocation of inverter-based generation on the network and the critical component of the objective function is to maximize the improvement in network capacity and subsequently network performance.

In this optimization, the constraints are to ensure that the lower and upper bands of the voltages are within this band and as such if the upper band is breached then the magnitude of PV generation is lowered until again the calculated value is brought below the threshold. The same approach applies to thermal limitation checks and rapid voltage change percentage value checks.

The non-linear objective function per network MV terminal node is proposed as follows as per equations (3.1a) and (3.1b). Equation (3.1a) is further elaborated in the chapter. The general network capacity improvement can be defined as:

$$\boldsymbol{Nc} = \frac{\mathbf{100} * (\boldsymbol{P_{fl}} - \boldsymbol{P_{il}})}{\boldsymbol{P_{il}}} \quad \% \qquad (3.1a)$$

where, $\boldsymbol{P_{fl}}$: final loading at the source (MW),

$\boldsymbol{P_{il}}$: initial loading at the source (MW),

$$\boldsymbol{max\ f_n} = \sum_{\mathbf{1}}^{\boldsymbol{n}} (\boldsymbol{Nc_n} \ / \ \boldsymbol{P_n}) \qquad (3.1b)$$

where, n : the network node (MV terminal),

$\boldsymbol{P_n}$: DG injection at node n (kW),

$\boldsymbol{Nc_n}$: Network capacity improvement (%) at network node (or MV terminal) n,

The objective function f_n can be defined as the percentage of network capacity improvement per unit of active power injected at node *n* subject to the following constraints (unit: %/MW):

1. Voltage at each node must be within regulatory limits as defined by equations (3.2) and (3.3):

$V_{nmin} \leq V_n \leq V_{nmax}$ 0.955 p.u. <Vn,1.06 p.u. (3.2)

$$V_k = V_n + V_{sc} + V_{vr} + V_{pv} \qquad (3.3)$$

where*:*

V_k = total voltage at node n (p.u.)

V_n = voltage at node due to network (p.u.)

V_{sc} = voltage at node due to shunt cap (p.u.)

V_{vr} = voltage at node due to voltage regulator (p.u.)

V_{pv} = voltage at node due to PV inverter (p.u.)

2. Thermal limits at each node must be within regulatory limits (NERSA) as dictated by equation (3.4):

$S_n \leq S_{nmax}$ (kA) (3.4)

where S_{nmax} is the conductor rating limit measured in amperes (A).

3. Voltage variation in % at each node must be within regulatory limits as per equation (3.5):

$$RVC_n \leq 3\% \quad (3.5)$$

where RVC_n is also commonly referred to as voltage variation test (previously known as rapid voltage change or RVC) in % at node *n*.

4. Fault level at each node must remain within equipment short circuit current limitations as per equation (3.6):

$$Ikss_n \leq Ikss_{nmax} \quad (kA) \quad (3.6)$$

where $Ikss_{nmax}$ is the maximum three phase short circuit rating (A-B-C fault) of a particular equipment measured in kilo-ampere (kA).

Voltage drop on an MV feeder can be derived from the simple model shown in Figure 3.1. in this case forward power flow is shown by the arrow from voltages V_1 (sending end) to V_2 (receiving end).

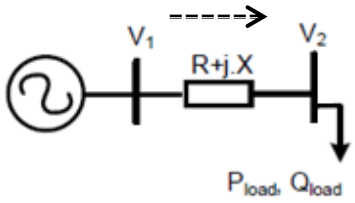

Figure 3.1: Simple source MV network with voltage drop

Power flowing through the load is defined as:

$$\boldsymbol{S_{load}} = \boldsymbol{P_l} + j\boldsymbol{Q_l} \quad (3.7)$$

$$\boldsymbol{S_{load}} = \boldsymbol{V_2}.\left(\frac{\boldsymbol{V_1}-\boldsymbol{V_2}}{\boldsymbol{R}+j\boldsymbol{X}}\right)^* \quad (3.8)$$

where*:*

V_2 = receiving end voltage at load terminals *(p.u)*

V_1 = sending end voltage at the source substation *(p.u)*

P_l = Active power of the load (same as P_{load} in Figure 3.1) *(MW)*

Q_l = *Reactive* power of the load (same as Q_{load} in Figure 3.1) (*MVAR)*

The solution to the above quadratic equation is shown in equation (3.9) [51] and is known as the exact voltage equation.

Rewriting equation (3.8) as:

$$\frac{\boldsymbol{Z.S^*}}{\mathbf{V2}} = \boldsymbol{V_1 - V_2}$$

Where $\mathbf{Z} = \boldsymbol{R + jX}$ and $\boldsymbol{S^*} = \boldsymbol{S_{load}}$ (3.8a)

Now, rearranging,

$$\boldsymbol{V_2.V_2^*} = \boldsymbol{V_1.V_2^*} + \boldsymbol{Z.S^*} \quad (3.8b)$$

With $\boldsymbol{V_2.V_2^*} = \boldsymbol{V_{2R}}^2 + \boldsymbol{V_{2I}}^2$, (3.8b) can be written as:

$$\boldsymbol{V_{2R}}^2 + \boldsymbol{V_{2I}}^2 = \boldsymbol{V_1}.(\boldsymbol{V_{2R}} - j\boldsymbol{V_{2I}}) + (\boldsymbol{R + jX}).(\boldsymbol{P_l - jQ_l}) \quad (3.8c)$$

Rearranging and isolating the imaginary part of the voltage:

$$\boldsymbol{V_{2I}} = \frac{(\boldsymbol{P_l X - jQ_l R})}{\boldsymbol{V_1}} \quad (3.8d)$$

Now inserting (3.8d) into (3.8c):

$$\boldsymbol{V_{2R}}^2 + \frac{(\boldsymbol{P_l X - jQ_l R})^2}{\boldsymbol{V_1}^2} - \boldsymbol{V_1.V_{2R}} - (\boldsymbol{RP_l + XQ_l}) = 0 \quad (3.8e)$$

Now solving using $x = \frac{-b \pm \sqrt{b^2 - 4ac}}{2a}$ and adding the imaginary part to the equation gives (3.9).

$$\boldsymbol{V_2} = \frac{1}{2}\left[\boldsymbol{V_1} \pm \sqrt{\boldsymbol{V_1}^2 - 4\left(\left(\frac{\boldsymbol{P_l X - jQ_l R}}{\boldsymbol{V_1}}\right)^2 - (\boldsymbol{P_l R + jQ_l X})\right)}\right] + \boldsymbol{j}\frac{(\boldsymbol{P_l X - jQ_l R})}{(\boldsymbol{V_1})} \quad (3.9)$$

[51]

where in addition to the defined variables above*:*

X = line reactance between voltages (ohm)

R = line resistance between voltages (ohm)

The rate of change of voltage with change in active and reactive power is found by calculating the partial derivative of equation (3.9), $\frac{\boldsymbol{\partial V_2}}{\boldsymbol{\partial P_l}}$ and $\frac{\boldsymbol{\partial V_2}}{\boldsymbol{\partial Q_l}}$. If the short circuit power at receiving end bus with voltage $\boldsymbol{V_2}$ is higher than the load power, then by calculating the first order Taylor

expansion of the derivatives with $\boldsymbol{P_l}$ and $\boldsymbol{Q_l}$ =0, the voltage drop ∆V between sending end and receiving end can be approximated by equation (3.10) [51] [52] [53].

$$\Delta \boldsymbol{V} = \boldsymbol{V_1} - \boldsymbol{V_2} \approx \frac{\boldsymbol{j(XP_l - RQ_l) + RP_l + XQ_l}}{\boldsymbol{V_2}} \quad \text{(3.10) [51]}$$

When the voltage angle ($\boldsymbol{tan^{-1}\left(\frac{XP_l - RQ_l}{RP_l + XQ_l}\right)}$) is small for small power transfer implying that term ($\boldsymbol{XP_l - RQ_l}$) is relatively small, then equation (3.10) can be approximated by equation (3.11) [57] for a change in voltage between sending end and receiving end ($\boldsymbol{V_R}$). Here V_R is the same as receiving end voltage V_2 in equation (3.10).

$$\Delta \boldsymbol{V} \approx \frac{\boldsymbol{RP_l + XQ_l}}{\boldsymbol{V_R}} \quad \text{(3.11) [57]}$$

Figure 3.2 shows multiple nodes and multiple segments on the MV feeder. Voltage drop ($\boldsymbol{\Delta V_j}$) between two nodes connected by a line segment j can be expressed with the approximation as equation (3.12). Also, in figure 3.2, V_1 is the source sending voltage.

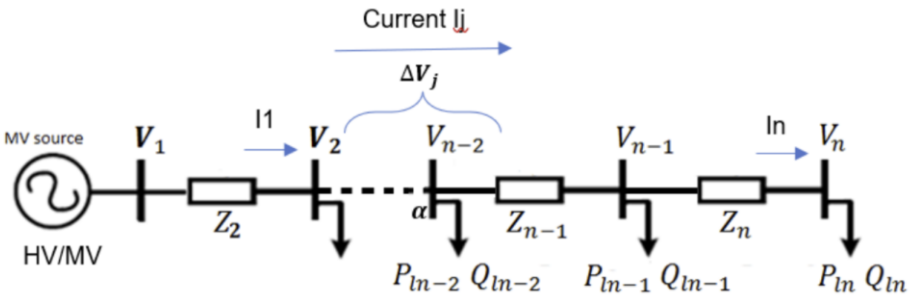

Figure 3.2: MV network with voltage drop with multiple nodes [51] [52]

$$\Delta \boldsymbol{V_j} \approx \frac{\boldsymbol{R_j P_j + X_j Q_j}}{\boldsymbol{V_j}} \quad \text{(3.12) [51]}$$

where the parameters $\boldsymbol{R_j}$ and $\boldsymbol{X_j}$ are the resistance and reactance of segment *j*, $\boldsymbol{V_j}$ is the receiving end voltage at node *j*, and $\boldsymbol{P_j}$ and $\boldsymbol{Q_j}$ are the total active power and reactive power drawn from the load at node *j* and the network; and the total current flowing through the feeder at node *i* = *j* can be calculated using equation (3.13) [51] as below:

$$\boldsymbol{I_i} = \sum_{\boldsymbol{k=i}}^{\boldsymbol{n}} \frac{\sqrt{\boldsymbol{P_k}^2 + \boldsymbol{Q_k}^2}}{\boldsymbol{V_k}} \quad \text{(3.13) [51]}$$

As the MV lines are designed using different conductors, the voltage approximation in equation (3.12) can be adjusted to accommodate the different impedances as in equation (3.14) [51] [53].

$$\Delta \boldsymbol{V} \approx \frac{\boldsymbol{R_\alpha P_l + X_\alpha Q_l}}{\boldsymbol{V_{nom}}} (\mathbf{1} - \mathbf{0.5}\boldsymbol{\alpha})$$ (3.14) [51]

where $\boldsymbol{R_\alpha}$ and $\boldsymbol{X_\alpha}$ are the summated series resistance and summated reactance of a line from the source to a point $\boldsymbol{\alpha}$ (distance in km) on the feeder network (a fraction of the total MV line length measured from the MV source substation as per Figure 3.2) and $\boldsymbol{V_{nom}}$ is the nominal per unit feeder voltage or source substation voltage.

When a voltage regulator is installed on the MV line as a combination of two or three single phase automatic voltage regulators, depending on the required configuration of open or closed delta), the secondary voltage ($\boldsymbol{V_{sec}}$) output of the regulator is calculated by equation (3.15).

$$\boldsymbol{V_{sec}} = \boldsymbol{V_{pri}} (\mathbf{1} + \boldsymbol{cVR_{tap}}) \text{ (volts)}$$ (3.15) [51]

where *c* is the per unit change in voltage per tap, $\boldsymbol{VR_{tap}}$ is the actual tap position and $\boldsymbol{V_{pri}}$ is the voltage on the primary side of the regulator in volts. If the regulator is installed beyond the point $\boldsymbol{\alpha}$ above, equation (3.14) is adjusted with the voltage regulator as in equation (3.16) [51] [52].

$$\Delta \boldsymbol{V} \approx \frac{\boldsymbol{R_\alpha P_l + X_\alpha Q_l}}{\boldsymbol{V_{nom}}} (\mathbf{1} - \mathbf{0.5}\boldsymbol{\alpha}) - \boldsymbol{cVR_{tap}}$$ (3.16) [51]

Capacitor banks improve the power factor on the feeder by supplying reactive power when needed. The approximate voltage change in the feeder by the switching of a capacitor bank at point $\boldsymbol{\alpha}$ on the network is calculated using equations (3.17) and (3.18).

$$\Delta \boldsymbol{V} \approx \frac{\boldsymbol{X_\alpha Q_{cap}}}{\boldsymbol{V_{nom}}} \qquad \boldsymbol{\alpha} \leq \boldsymbol{\alpha_{cap}}$$ (3.17) [51]

$$\Delta \boldsymbol{V} \approx \frac{\boldsymbol{X_{\alpha_{cap}} Q_{cap}}}{\boldsymbol{V_{nom}}} \qquad \boldsymbol{\alpha} > \boldsymbol{\alpha_{cap}}$$ (3.18) [51]

where $\boldsymbol{\alpha_{cap}}$ is the position of the capacitor bank relative to the position $\boldsymbol{\alpha}$ and $\boldsymbol{X_\alpha}$ and $\boldsymbol{R_\alpha}$ is the series reactance and resistance from the MV source to a point $\boldsymbol{\alpha}$ on the network. With DG now connected to the same line, its integration i.e. power injection can be defined as a negative load and the voltage drop is given by equation (3.19) [51].

$$\Delta \boldsymbol{V} \approx \frac{\boldsymbol{R(P_l - P_{DG}) + X(Q_l - [\pm Q_{DG}])}}{\boldsymbol{V_{nom}}}$$ (3.19)[51]

The connected DG increases the voltage at the integration point and influences the voltage profile along the entire feeder. DG can increase or decrease the line voltage depending on the X/R ratio of the line and the amount of reactive power it absorbs or generates. This is determined by the control mode of the DG. If the DG is set in leading power factor to act as

an inductor, then it will absorb reactive power ($+\boldsymbol{Q_{DG}}$) and if set in capacitive mode in lagging power factor the DG will generate reactive power ($-\boldsymbol{Q_{DG}}$). Similarly, as in the case of the voltage regulator and capacitor bank, the voltage drop along the feeder at a point $\boldsymbol{\alpha}$ is given by equations (3.20) and (3.21) [51].

$$\Delta \boldsymbol{V} \approx \frac{\boldsymbol{R_{\alpha}P_{DG}+X_{\alpha}Q_{DG}}}{\boldsymbol{V_{nom}}} \qquad \boldsymbol{\alpha \leq \alpha_{DG}} \qquad \text{(3.20) [51]}$$

$$\Delta \boldsymbol{V} \approx \frac{\boldsymbol{R_{\alpha_{DG}}P_{DG}+X_{\alpha_{DG}}Q_{DG}}}{\boldsymbol{V_{nom}}} \qquad \boldsymbol{\alpha > \alpha_{DG}} \qquad \text{(3.21) [51]}$$

The resultant network feeder voltage deviation from nominal with shunt compensation, voltage regulator and DG can be expressed by equations (3.22) and (3.23) [51]:

$$\Delta \boldsymbol{V} \approx \frac{\boldsymbol{R_{\alpha}P_{l}+X_{\alpha}Q_{l}}}{\boldsymbol{V_{nom}}} (\boldsymbol{1-0.5\alpha}) + \boldsymbol{cVR_{tap}} + \frac{\boldsymbol{X_{\alpha_{cap}}Q_{cap}}}{\boldsymbol{V_{nom}}} + \frac{\boldsymbol{R_{\alpha_{DG}}P_{DG}+X_{\alpha_{DG}}Q_{DG}}}{\boldsymbol{V_{nom}}} \qquad \text{(3.22)[51]}$$

$$\Delta \boldsymbol{V} \approx \frac{\boldsymbol{1}}{\boldsymbol{V_{nom}}}((\boldsymbol{R_{\alpha}P_{l}+X_{\alpha}Q_{l}})(\boldsymbol{1-0.5\alpha}) + \boldsymbol{V_{nom}.cVR_{tap}} + \boldsymbol{X_{\gamma_{cap}}Q_{cap}} + \boldsymbol{R_{\beta_{DG}}P_{DG}} + \boldsymbol{X_{\beta_{DG}}Q_{DG}}) \qquad \text{(3.23)[51]}$$

where*:*

$\mathbf{V_{nom}}$ = is the nominal or source substation voltage in p.u.

$\boldsymbol{Q_{cap}}$ = reactive power supplied from the capacitor (kVar)

$\boldsymbol{Q_{DG}}$ = reactive power supplied from the DG (kVar)

$\boldsymbol{X_{\alpha_{DG}}}$= series reactance between the DG and a point $\boldsymbol{\alpha}$ (ohms)

$\boldsymbol{R_{\alpha_{DG}}}$= series resistance between the DG and a point $\boldsymbol{\alpha}$ (ohms)

In equation (3.23) above, the resultant voltage deviations from the nominal network voltage would result in choosing the most appropriate shunt compensation and DG size to maximize the increase in feeder voltage at all load points. The parameters $\boldsymbol{\beta}$ and $\boldsymbol{\gamma}$ are the distances of the DG and capacitor bank from the source substation respectively expressed in kilometre (km) and used to show that these may be different from the $\boldsymbol{\alpha}$ parameter as these devices are referenced from the source. $\Delta \boldsymbol{V}_{\boldsymbol{max}}$ would be bound by the upper and lower limits during peak and light loads as determined by NRS048 regulations.

Percentage network capacity improvement (Nc) at each MV terminal node (as defined by equation (3.24) can be defined as increasing the voltage at that node considering proximity network devices that have an influence in the change in magnitude of the instantaneous

potential. In addition, thermal limits, voltage variation and fault levels have an influence in the search space for stability issues that may arise in the network. In this research, $\boldsymbol{Nc_n}$ is seen as a resultant percentage of the improvement in voltage and/or thermal capacity at node *n*. With the improvement in resultant voltage, the network improvement capacity for voltage regulation can be defined by equation (3.24) and a positive outcome implies a positive percentage improvement.

$$\boldsymbol{Nc_{Vn}^{k}} = \frac{\boldsymbol{100}*(\boldsymbol{V_n^{k+1}} - \boldsymbol{V_n^{k}})}{\boldsymbol{V_n^{k}}} \qquad \% \tag{3.24}$$

where k = iteration point

n = node on the MV network (medium voltage terminal)

$\boldsymbol{V_n^{k}}$ = voltage in p.u. at node n

Hence at iteration *k* which is the variable that tracks the change in position applied at node *n,* can be defined by equation (3.25) and is the percentage improvement of voltage to per kW generation (generated power $\boldsymbol{P_n^{k}}$) connecting node *n*. Using the objective function this then becomes:

$$\boldsymbol{f_{vn}^{k}} = \boldsymbol{Nc_{Vn}^{k}} \,/\, \boldsymbol{P_n^{k}} \qquad (\%/\text{MW}) \tag{3.25}$$

Applying equations (3.24) and (3.25) results in equation (3.26) where $\boldsymbol{P_{nDG}}$ (MW) is the power from the DG unit at node *n*.

$$\boldsymbol{f_{vn}} = \frac{\left(\frac{\boldsymbol{100}*\Delta \boldsymbol{V_n}}{\boldsymbol{V_n}}\right)}{\boldsymbol{P_{nDG}}} \qquad (\%/\text{MW}) \tag{3.26}$$

Similarly, for thermal limitations ($\boldsymbol{Sk}$ [%]) the network capacity improvement can be defined by equation (3.27). In this case, $\boldsymbol{Sk_{thn}^{k+1}} < \boldsymbol{Sk_{thn}^{k}}$ denotes a positive improvement in line capacity and hence in network capacity. This percentage is calculated as the difference of the conductor rated current capacity and the actual current at any particular time. However, in MV networks, voltage change to improve network capacity is far more sensitive than thermal changes and as such equation (3.26) is used further in the research work. When the magnitude of $\boldsymbol{Sk_{thn}^{k+1}}$ is lower than the previous ampere value of $\boldsymbol{Sk_{thn}^{k}}$ it implies that network capacity was created due to the conductor loading being reduced by the DG supplying more load.

$$Nc_{thn}^{k} = \frac{100 * (Sk_{thn}^{k+1} - Sk_{thn}^{k})}{Sk_{thn}^{k}} \quad (3.27)$$

Unlike in the case for positive voltage improvement, a negative percentage value here suggests that the thermal limits measured in amperes of Sk_{thn}^{k} shows that capacity was created as the new current value is lower as per the previous iteration. The order of network improvement tests would be firstly RVC, secondly voltage check, and finally thermal. P_{n}^{k} generation has to be reduced to satisfy all three criteria. For thermal limit improvement, the objective function can also be defined by equation (3.28) with same units of %/MW.

$$f_{thn}^{k} = Nc_{thn}^{k} \,/\, P_{n}^{k} \quad (3.28)$$

With these improvement factors applied to each node, two sets of solutions (A_n, B_n) for every iteration *k* in the set of all MV terminals (in the PSO execution), determine optimal points of connecting DG onto the network.

$$A_{n}^{k} = \{f_{v1}^{1}, f_{v2}^{2} \ldots\ldots f_{vn}^{k}\} \quad (3.29)$$

$$B_{n}^{k} = \{f_{th1}^{1}, f_{th2}^{2} \ldots\ldots f_{thn}^{k}\} \quad (3.30)$$

The set which defines the maximum improvement in voltage and thermal limits is given by equation (3.31) and the location common to equation sets (3.29) and (3.30), i.e. intersection of the two sets, would result in the most viable DG connecting points in the network and hence provide the best network capacity improvement per the amount of generation injected.

$$C_n = \{max\ A_n \cap max\ B_n\} \quad (3.31)$$

$$\Rightarrow \max f_n = C_n \quad (3.32)$$

In PSO all particles swarm 'fly' through a multi-dimensional search space where each particle is adjusting its position according to its own experience and that of neighbours (proximity interconnecting nodes) and its velocity decides its motion mode. In correlating this algorithm to the research objectives, each particle is represented by a PV system and the multi-dimensional space is the set of MV terminal nodes that are the building blocks of the MV network itself. Each particle has a fitness value determined by the difference between the base voltage/thermal value (however, voltage values on MV networks with respect to DG are the preferred variables for determining the fitness value as the voltage is directly affected by the system and voltage controlling devices as per equation (3.3) before and after the PV connection at that point. PSO algorithm in general is adapted as a simulation of bird flock

foraging which guides the optimization search through cooperation and competition between individuals. Velocity is mainly determined by the individual optimal location and the global optimal position and can be defined as follows:

$$\boldsymbol{V_i^{k+1}} = \boldsymbol{w}.\boldsymbol{V_i^k} + \boldsymbol{c_1 r_1}[\boldsymbol{X_{pbest}^k} - \boldsymbol{X_i^k}] + \boldsymbol{c_2 r_2}[\boldsymbol{X_{gbest}^k} - \boldsymbol{X_i^k}] \quad (3.33)$$

$$\boldsymbol{X_{gbest}^k} = \boldsymbol{X_i^k} + \boldsymbol{V_i^{k+1}} \quad (3.34)$$

where,

i = the index of the particle, referring to the *ith* PV system

$\boldsymbol{V_i^k}$, $\boldsymbol{X_i^k}$ = the velocity and position of particle i at iteration k, respectively, referring to the next connecting PV system to the MV terminal node

ω = represents inertia weight factor and is in the range [0,1],

$\boldsymbol{c_1}$ and $\boldsymbol{c_2}$ are the cognitive coefficients usually between [0,2],

$\boldsymbol{r_1}$ and $\boldsymbol{r_2}$ are random number sequences in (0, 1) which obey uniform distribution and mutual independence,

$\boldsymbol{X_{pbest}}$ represents individual optimal position (Pbest) with reference to best voltage improvement provided by an individual PV system (fitness value)

$\boldsymbol{X_{gbest}}$ represents global optimal position (Gbest) with reference to best voltage improvement provided by all PV system installations

Local optimization refers to PV generation penetration effects at network branch nodes and global penetration refers to PV generation penetration at nodes of the network to which the magnitude is at its maximum as defined in the resultant objective function in equation (3.32).

The part equation (3.33) term $\boldsymbol{c_1 r_1}[\boldsymbol{X_{pbest}^k} - \boldsymbol{X_i^k}]$ called the *cognitive component* that represents the particle's memory. The particle returns to the search space in which it has high individual fitness and the factor $\boldsymbol{c_1}$ affects the step size of the particle to move toward its local best position $\boldsymbol{X_{pbest}^k}$.

The global optimum part of the equation (3.33) term $\boldsymbol{c_2 r_2}[\boldsymbol{X_{gbest}^k} - \boldsymbol{X_i^k}]$ is called the *social component* and is responsible to move the particle toward the best region found by the swarm

so far. The social coefficient c_2 also affects the step size of the particle to find the global best position X_{gbest}, i.e. the terminal node on the network that has the best improvement in voltage, within thermal limitations and RVC percentage values.

In the equation (3.34), the particle updates itself by using the new velocity and its previous position. A new search then begins towards the global optimum solution. The algorithm searches through network nodes for solutions that satisfy the objective function of finding the maximum network capacity improvement by integrating maximum inverter-based PV DG i.e. PSO will enable the optimal placement of PV on MV feeders and as a result increase the networks' capability to supply more load (Figure 3.3 shows the geographic overview on a MV feeder and how PSO explained above is applied). The relevant generation at the POC (node in PSO calculation) would be reduced as necessary to improve the fitness values. As these are direct inputs to the equation, the next position to integrate PV would be determined as such.

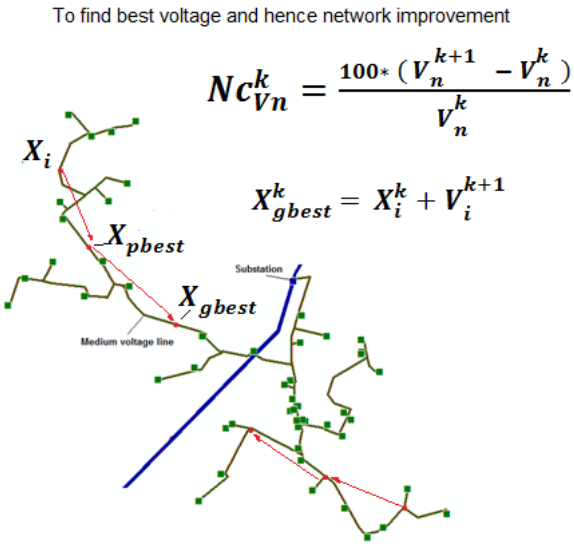

Figure 3.3: Geographic example showing how the PSO strategy is applied

PSO employed for analysis addresses the complexity of variable connecting DG points on the MV network and as such is well suited in identifying the weak and strong parts of the network. Section 3.2 that follows explains significant aspects of the methodology in the form of flowcharts.

3.2 Flowcharts in Assessing PV Integration on MV Networks for Network Capacity Improvement

3.2.1 Explanation of Flowchart 1

Flowchart 1 depicted in Figure 3.4 gives the DPL coding general procedure utilized in this research and describes the sequence of events in the code itself. It shows the initial steps taken, the integration of the PSO algorithm and the calculations that determine the end result. The main aspects are to connect PV systems according to the user's PSO inputs (no. of PV systems and iterations) and completing the necessary load flow and RVC studies. The detailed steps of the PSO methodology is presented in section 3.2.2. Matrix *bmat* contains the bus index values and base case of the MV network with no PV connected and matrix *mat* keeps track of each iteration voltage and fitness values as explained in the DPL Figure 3.28. The set *S3* stores all MV terminal nodes of the Powerfactory model and set *S9* stores the filtered out nodes of either 11 kV or 22 kV. A generic 0.5 MVA PV template is used in all calculations. In the flowchart of Figure 3.4, RVC is first calculated. The generation in the template output is adjusted to achieve the 3% limit, which is also used to satisfy the voltage and thermal criteria. The next PSO position is calculated at every iteration. Lastly, the results that provide the greatest fitness value (voltage improvement at a node) with the best network improvement is the optimal location to connect the PV system.

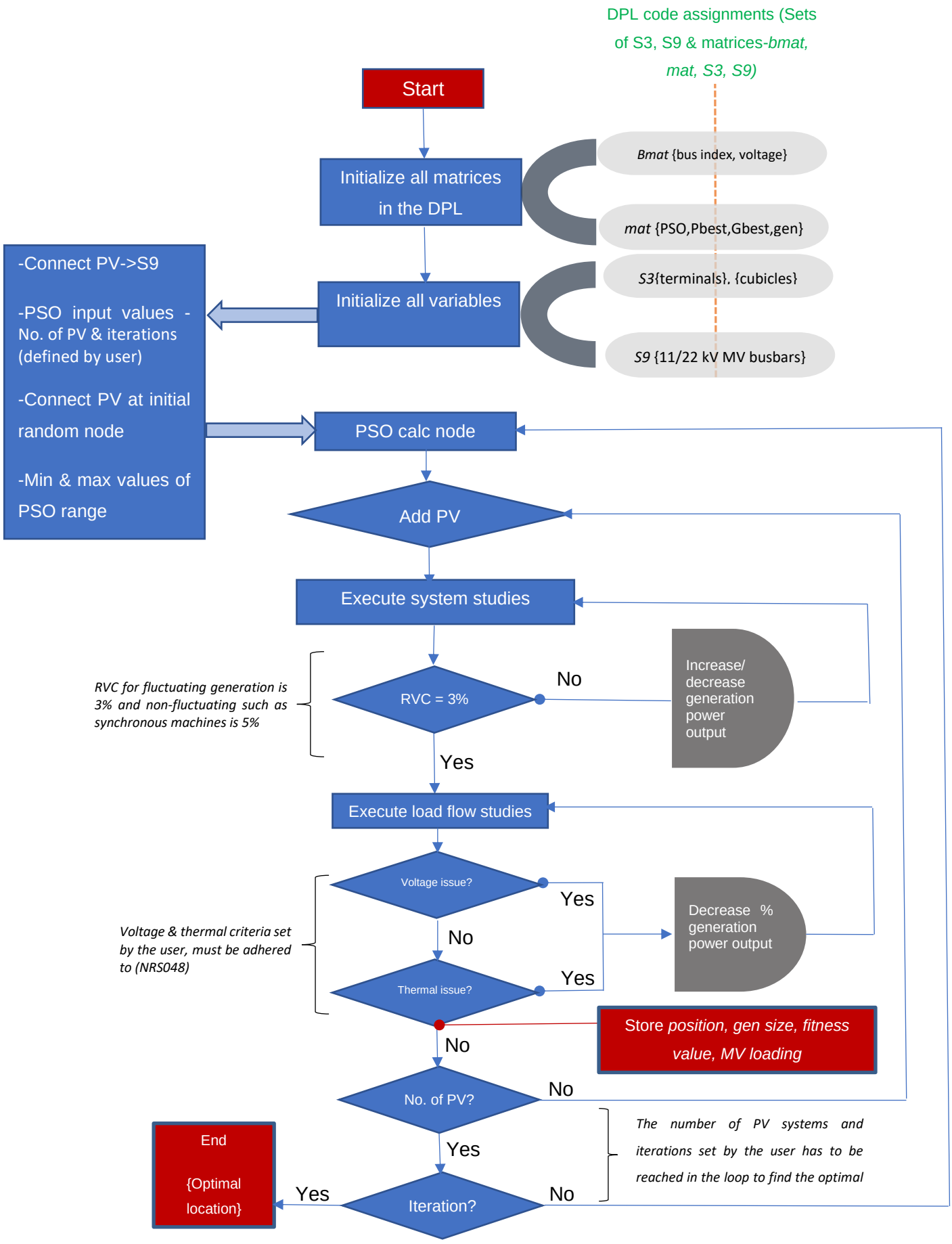

Figure 3.4: Flowchart 1: DPL coding flowchart – general procedure

3.2.2 Explanation of Flowchart 2

Flowchart 2 in Figure 3.5 shows the PSO methodology utilized and describes the sequence of events in alignment with equation (3.33) and equation (3.34). The swarm refers to the group of random PV systems. The 'velocities' in the PSO equation are determined by the fitness values of voltage improvement for a particular MV node position. Voltage improvement is therefore defined as the difference in the current and previous values of voltage at a particular node determines the fitness value bound by VTT and thermal tests. The objective function is evaluated after each system study, This general procedure is discussed in detail in Section 3.2.3 showing the electrical correlation of the PSO parameters.

Figure 3.5: Flowchart 2: PSO methodology – general procedure

3.2.3 Explanation of Flowchart 3

Flowchart 3 shown in Figure 3.6 describes the PSO methodology with MV network parameter assignment and correlation. Each circular block shows the coding interpretation of the general PSO procedure and what is in focus at that point.

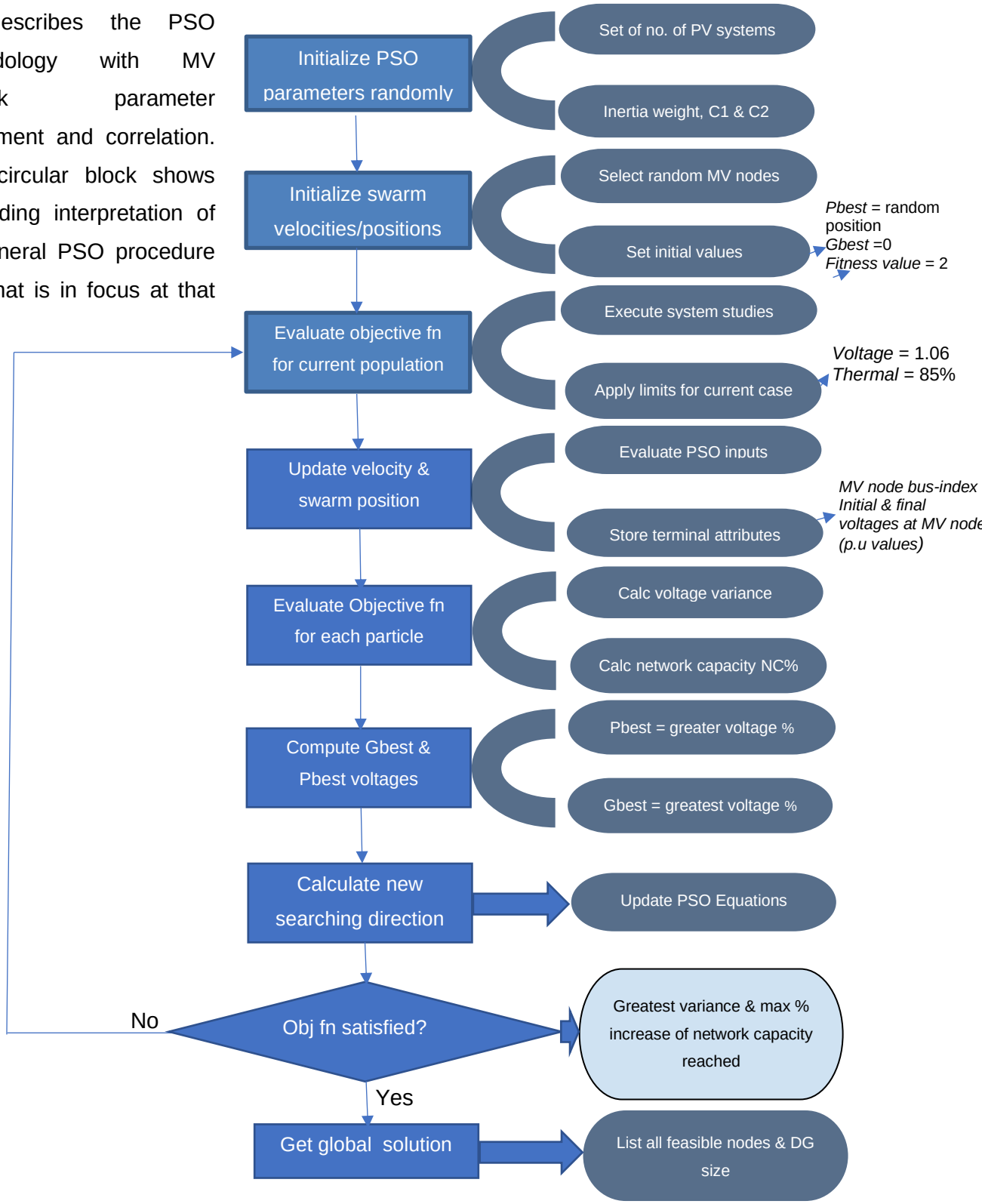

Figure 3.6: Flowchart 3: PSO methodology with medium voltage network parameter assignment and correlation

3.2.4 Explanation of Flowchart 4

.

Flowchart 4 in Figure 3.7 shows the current basic methodology for existing and *new* un-constraining network feeders and feeder assessment *(new => DG injection).* The flow of steps indicate how an MV network is assessed and the un-constraining options available to alleviate the constraint be it voltage or thermal. *DG injection* using PSO applied in the DPL script is now proposed as a new option added to the list of improving MV network capacity.

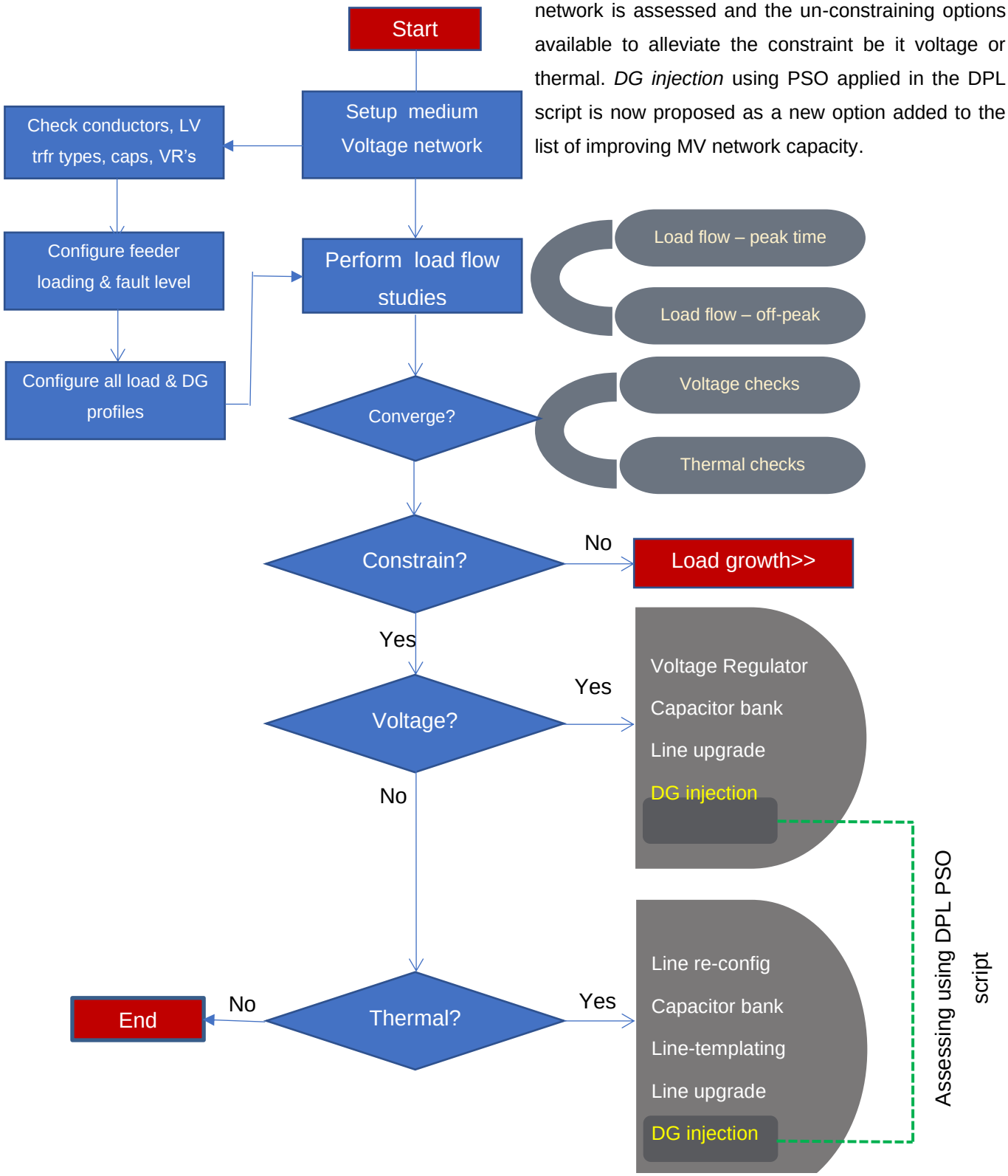

Figure 3.7: Flowchart 4: Basic methodology for un-constraining network (DG new)

3.3 Model and network data of MV feeders (11 kV and 22 kV)

3.3.1 11 kV Network 1: Geographic overview:

The geographic or geo-spatial view of 11 kV Network 1 is shown in Figure 3.8. The network has a relatively long backbone conductor with short tee-offs. Data gathered for this network is recorded every half hour and is seasonal. All load data of customer load profiles, conductor types and network type information of the Powerfactory model and geographic layout has been provided by Eskom Distribution with appropriate permissions for its usage in this study. The MV source substation has a few network feeders connected to the substation busbar and it is at this point when referred to further in this research that the feeder network is metered at.

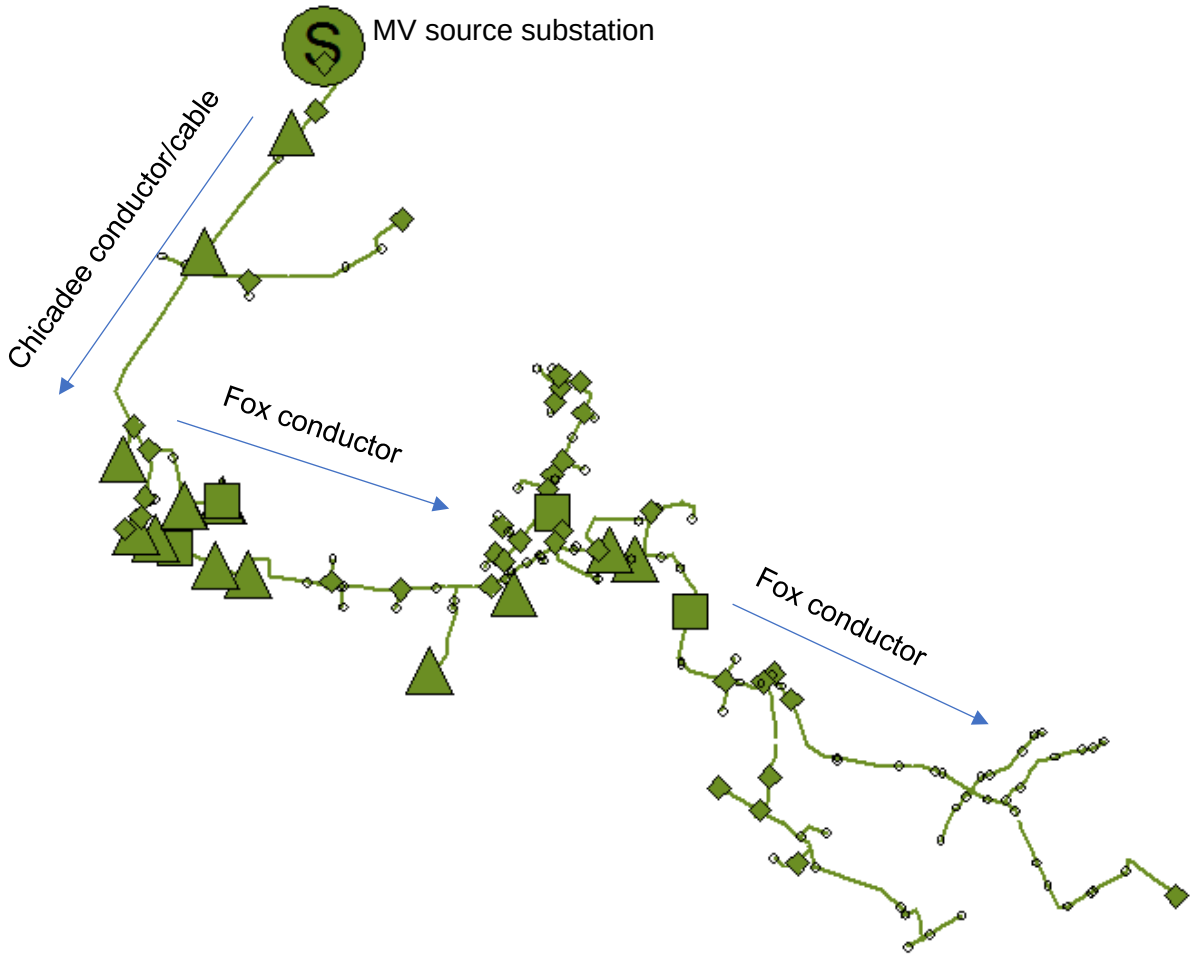

Figure 3.8: Geographic overview of 11 kV Network 1 showing main backbone conductor types

Table 3.1 shows the types of conductor current ratings that make up the network and its corresponding X/R ratios:

Table 3.1: Cables and conductors used in 11 kV Network 1

Name	Rated Current	R' (AC,20°C)	X'	L'	R0'(AC)	X0'	L0'
(XLPE/PILC – cable)	kA	Ohm/km	Ohm/km	mH/km	Ohm/km	Ohm/km	mH/km
11 kV 120mm2 Al XLPE 3Core	1	0.325	0.098	0.311944	1.102	0.143	0.455183
11 kV 120mm2 Cu PILC 3Core	1	0.153	0.251	0.798958	2.741	0.1	0.31831
11 kV 120mm2 Cu XLPE 3Core	1	0.196	0.098	0.311944	0.97	0.143	0.455183
C3/0.104 3 Delta 11.00	0.1228	1.182	0.3156	1.004586	1.328	1.649	5.24893
CHICADEE 3 Delta 11.00	0.312	0.2994	0.3156	1.004586	0.4461	1.649	5.24893
FOX 3 Delta 11.00	0.148	0.8453	0.3156	1.004586	0.992	1.649	5.24893

Figure 3.8 shows that Fox conductor makes up majority of the network with the portions of cable having the highest loading as it is used to connect the feeder to the substation 11 kV busbar. Typically, conductor or cable from the source substation or injection point must be rated at a higher fault level than conductors that radiate from this point onwards as depicted in Figure 3.9. This is due to the cumulative impedance up to the point of measurement. In Figure 3.9, the source has a strong fault level x, and due to the impedance z1-z4 between points on the line, the fault level decreases radially. The variables *a to d* in this figure are variables in the function of calculating fault level at a particular point using the cumulative impedance. For example, the fault level x-b uses sum of impedances Z1 and Z2 (Z1+Z2) and fault level value *a* to calculate the three-phase short circuit current level at that point. These levels become important to customers that require high currents for large induction and motor loads. DG technology excluding PV systems and battery technologies contribute additively to the fault current at the point of connection. PV systems and battery technologies have almost negligible fault current contribution so that network connecting points are not prone to fault levels exceeding equipment short circuit ratings.

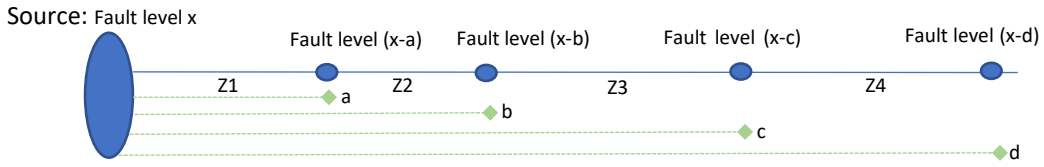

Figure 3.9: Fault level distribution along MV feeder

Also, as networks are planned for unidirectional power flow, a mixture of conductors are therefore used from a design and financial investment perspective. Figure 3.10 shows for Network 1 the proportion of conductor types used.

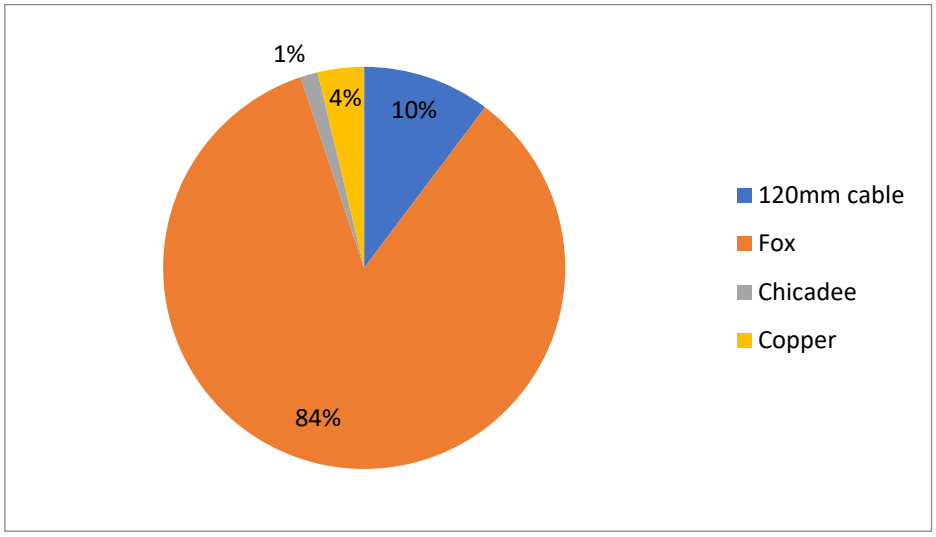

Figure 3.10: Percentage composition of network conductor

The loading of the network feeder peaks at 5.5 MVA and has a minimal load of 3 MVA (Figure 3.11). This load profile is based on annual meter readings over the four season period hence a full picture of the network load performance can be seen (Autumn-Spring-Summer-Winter-Weekday and weekend 30mins time-stamp). The network peaks indicate the times to when the network experiences maximum load and likewise for the low load periods.

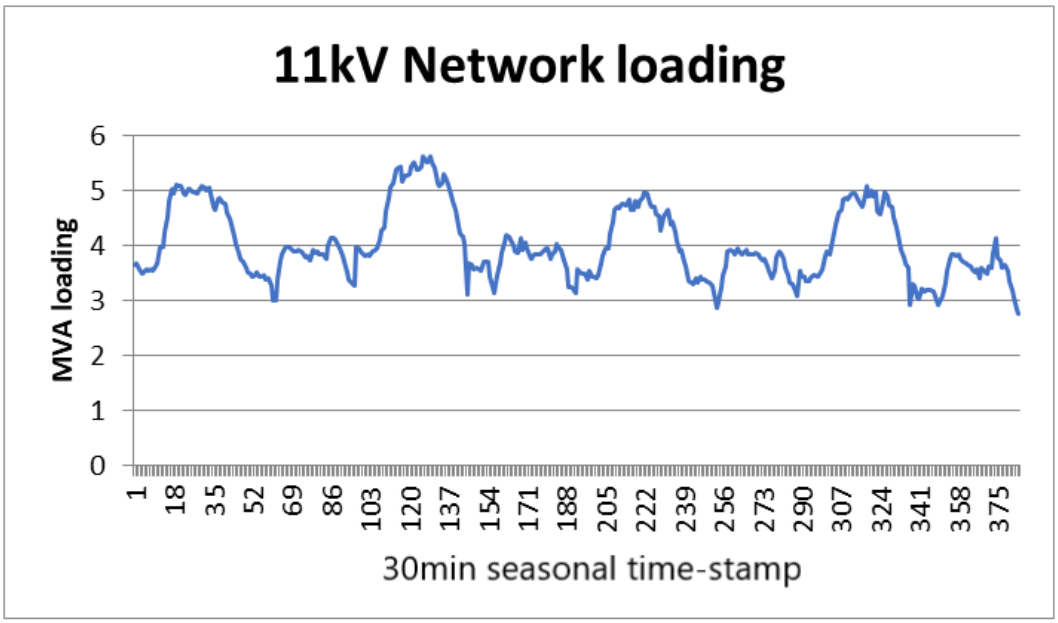

Figure 3.11: Network 1 loading (MVA)

This 11 kV Network 1 is fed from a 132 kV/11 kV substation that has two 132 kV/11 kV 40 MVA high impedance transformers coupled to the 11 kV busbar. The fault level values for this system are relatively high due to the 132 kV/11 kV substation connected to a Main Transmission Substation (MTS) at a close proximity. Any upstream upgrades of transformation size or additional transmission or distribution lines increase these short circuit levels as the upstream impedance reduces. The current fault levels are shown in Table 3.2 and the 132 kV/11 kV substation arrangement in shown in Figure 3.12.

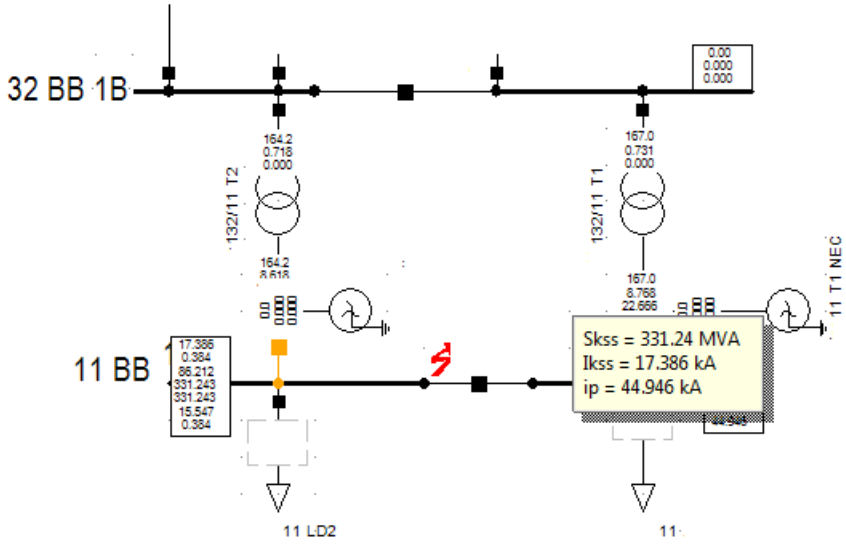

Figure 3.12: Substation 11 kV Network 1 busbar arrangement showing the transformers only

Table 3.2: Fault level values at busbars in 11 kV Network 1 substation

	3-phase	1-phase
132 kV busbar	9kA	8.8kA
11 kV busbar	18.38kA	0.667kA

The three-phase fault currents at the substation 132 kV and 11 kV busbars as per IEC60909, is 18kA and the single-phase fault current is 0.667kA. These values are entered into the external grid of the MV feeder Network 1 in the simulation model in DigSILENT Powerfactory. Figure 3.13 shows the entire single line diagram of the network feeder with Appendix A1 showing the detail mix of conductors and their respective electrical characteristics.

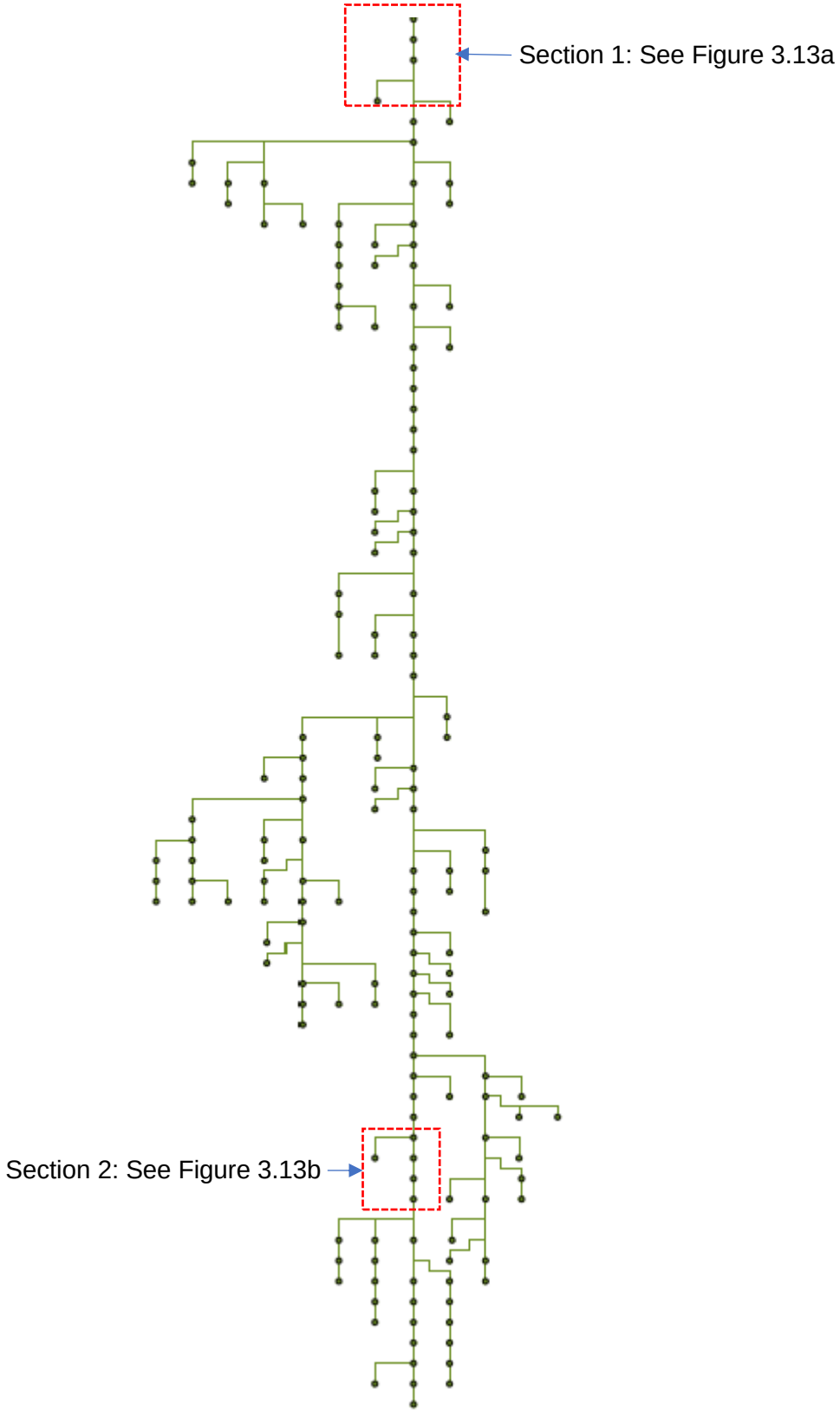

Figure 3.13:Entire single line diagram of Network 1

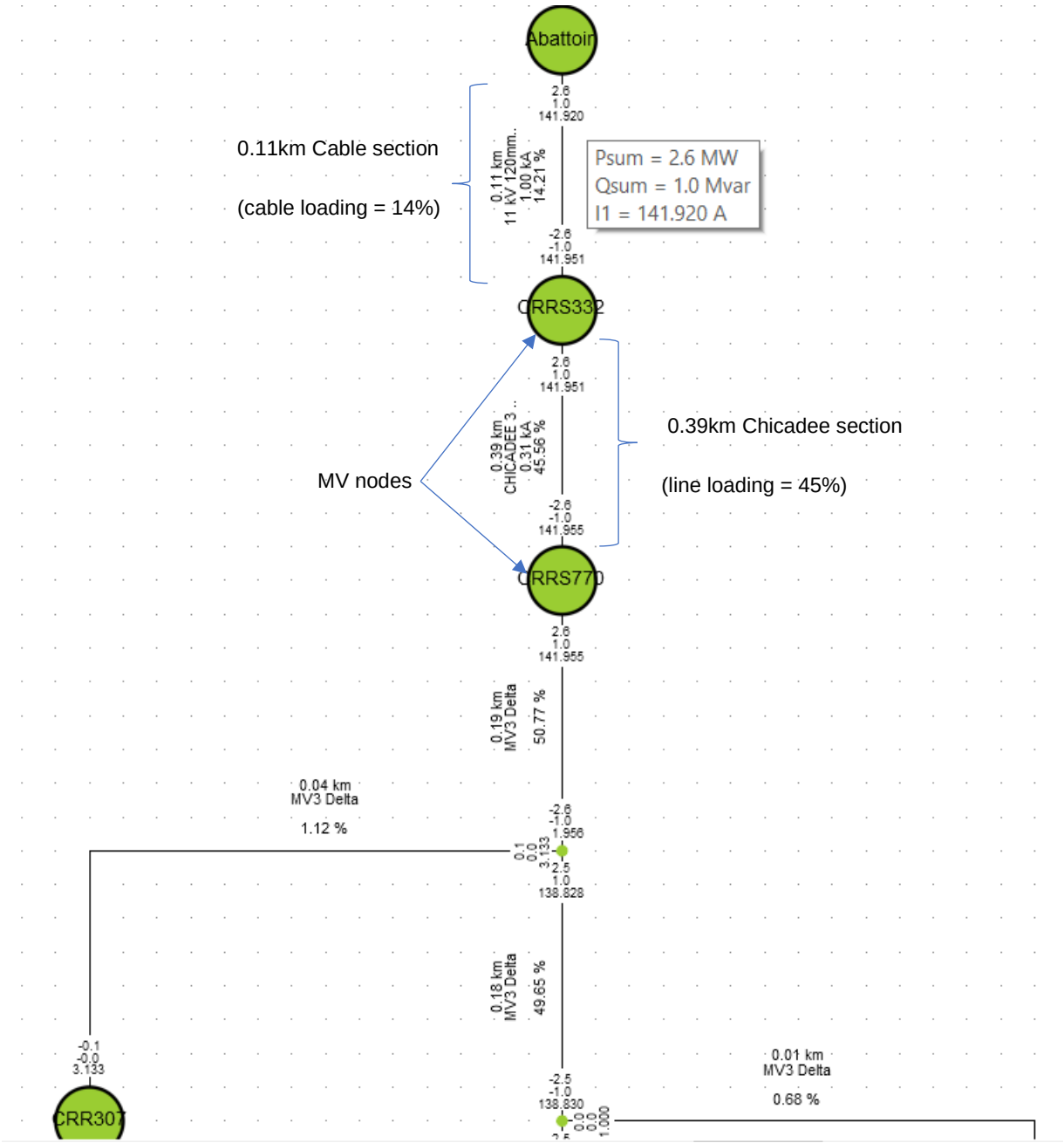

Figure 3.13(a): Section of Network 1

Figure 3.13(a), which is extracted from Figure 3.13, shows the network source and first section of the feeder. The feeder is cabled out from the substation onto the overhead line of type Chickadee which under the constrained operation scenario is loaded at 45%. Also, the feeder shows a few MV nodes which is used in the development of the DPL script. Figure 3.13 (b) shows the section of the feeder towards the end of the network. It can be seen that the line loading is around 6% with the active power 0.2 MW. Typically the fault level is at its lowest towards the end of the network.

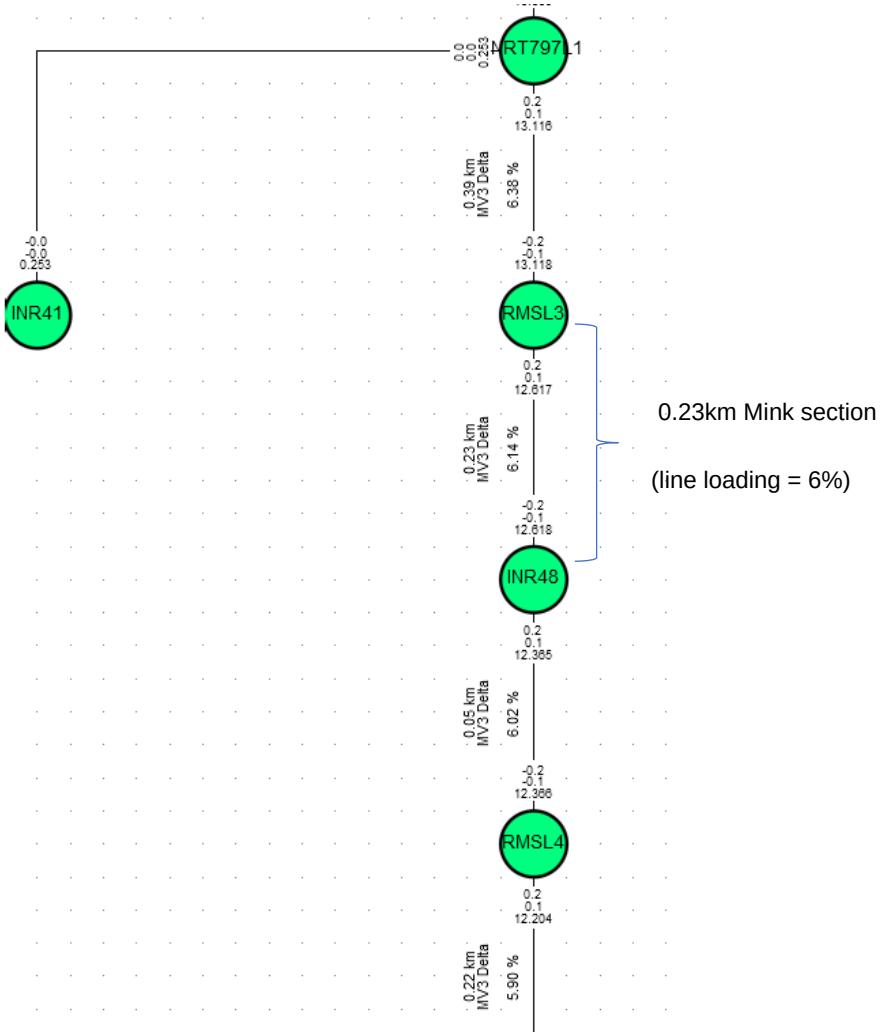

Figure 3.13(b): Section 2 of Network 1

3.3.2 Network 2 22 kV: Geographic overview:

The geographic or geospatial view of Network 2 is shown in Figure 3.14. The network has a few long tee-offs with a relatively long backbone of conductor. Data gathered for this network is recorded every half hour and is seasonal. This network is at 22 kV with all equipment and switchgear rated as such.

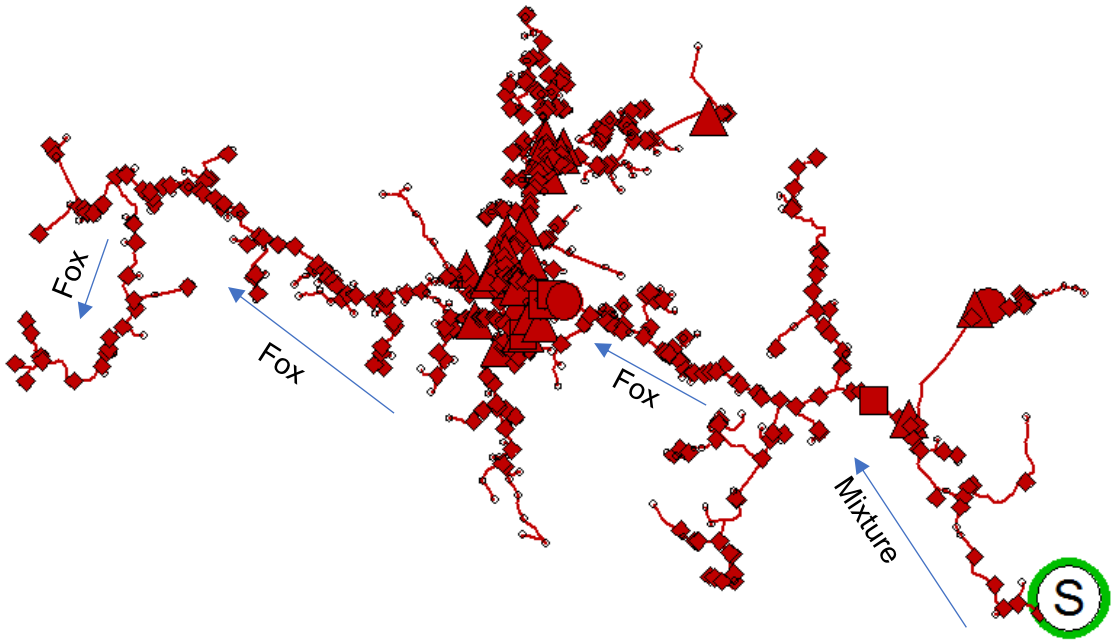

Figure 3.14: Geographic overview of Network 2

Table 3.3 shows the types of conductor current ratings that makes up the network and its corresponding X/R ratios. Appendix A2 shows the mixture of conductor data on the network.

Table 3.3: Common cables and conductor used in Network 2

Name	I rated	Z1	R 1	X1	R 0	X0
(XLPE/PILC – cable)	kA	Ohm	Ohm	Ohm	Ohm	Ohm
22 kV 120mm2 Cu XLPE	0.327	0.019865	0.017361	0.009655	0.075289	0.012932
22 kV 120mm2 Cu PILC	0.27	0.000208	0.000184	0.000096	0.001827	0.000117
FOX50	0.148	0.880281	0.785998	0.396361	0.931479	1.579407
HARE50	0.284	0.435697	0.264983	0.345856	0.403588	1.472996
MINK50	0.208	0.560184	0.431937	0.356702	0.568803	1.4697
OAK50	0.28	0.466774	0.285725	0.369106	0.431874	1.55759

Figure 3.15 shows that Fox conductor makes up majority of the network with the cable having the highest loading as it is used to connect the feeder to the substation 22 kV busbar.

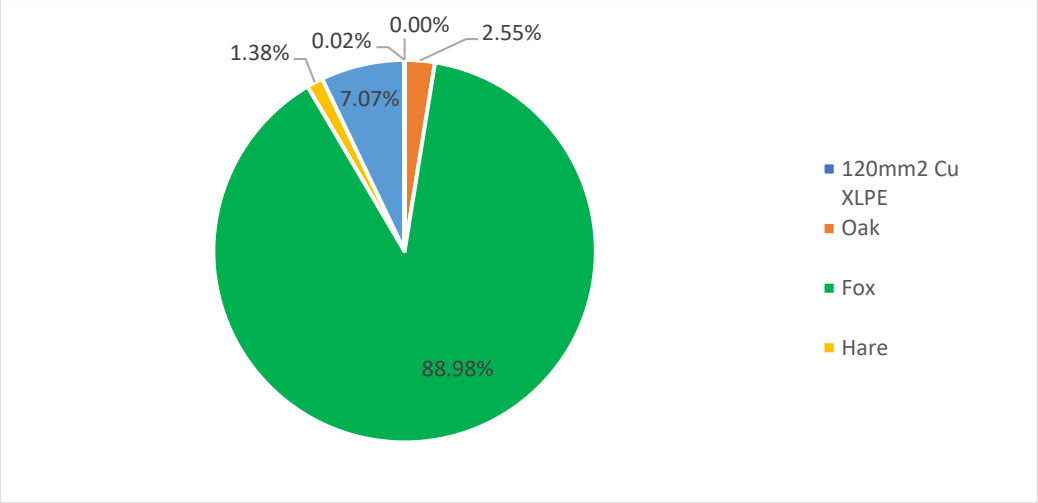

Figure 3.15: Percentage composition of network conductor

The loading of the network feeder is shown below. The network peaks at 2.4 MVA and has a minimal load of 1.1 MVA as per Figure 3.16a, with the substation busbar arrangement in Figure 3.16b showing the different voltage levels.

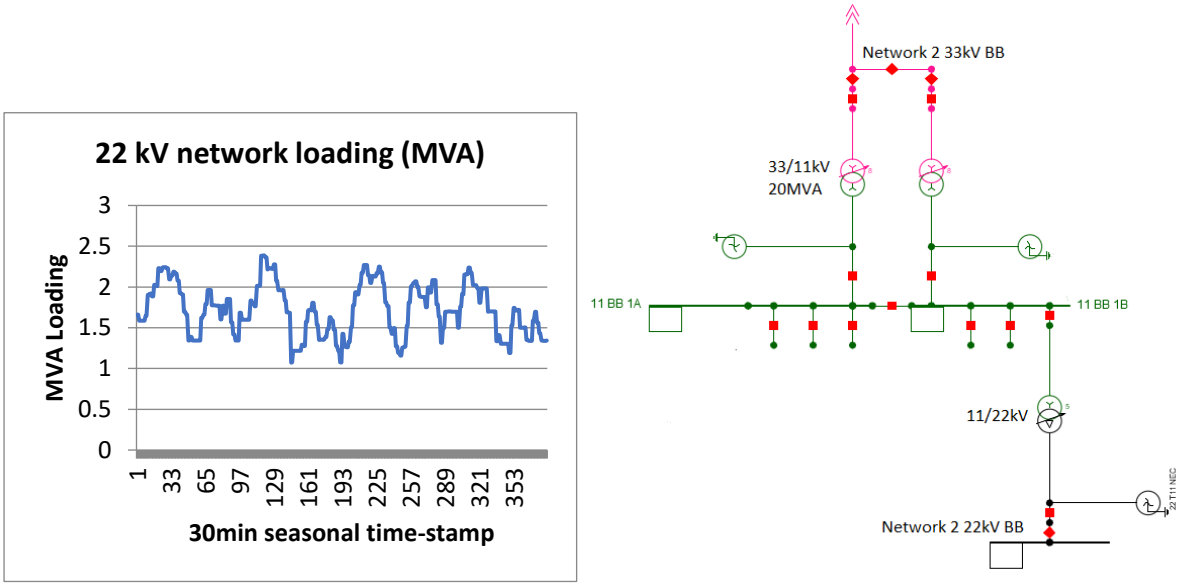

Figure 3.16: a: 22 kV Network 2 loading (MVA) b: Substation busbar arrangement

For this network to be modelled correctly all the correct data must be entered into the Powerfactory elements. Of importance is the external grid fault levels and individual loading profiles for each connected load. Network 2 substation has three voltage levels. To find the relevant busbar fault levels, three phase and single phase short circuit calculations must be completed on the 33 kV, 22 kV and 11 kV busbar of the substation as per Figure 3.16b.

Table 3.4: Fault level values for Network 2 substation 22 kV busbar

	3-phase (A-B-C)	1-phase (SLG)
33 kV busbar	2.42kA	0.54kA
11 kV busbar	7.2kA	0.6kA
22 kV busbar	1.787kA	0.3kA

Table 3.4 has three sets of fault level values. Being a Distribution substation with three transformation levels, the network was chosen to analyze the integration of PV systems using the DPL program due to this complexity. The fault levels are weak relative to Network 1 and provides a good study case to work with.

3.4 Detail explanation of DPL code and analyser interface

The DPL code is written and structured in a way that it must apply to any MV network built in DIgSILENT Powerfactory. A load flow calculation would verify that the network solution converges and that no incorrect or missing element types are connected and that the appropriate voltage levels are utilized. Different variations in Powerfactory are created to enable various conditions for modelling. Networks are typically modelled during peak and light load conditions, thus when connecting a DG to a network it is important to check both scenarios.

In order to achieve the said objective of calculating the difference and improvement in network capacity using PV integration, a method of connecting the PV system to the feeder nodes are required such that specific nodes are not individually connected and assessed. In other words, the end result should be a list of proposed integrating points of PV systems on the MV network where the optimal location is found with the maximum generation that can be connected within all regulatory conditions. The locational criteria are based on the PV system connection satisfying RVC (also referred to as voltage variation test [VVT]), voltage and thermal characteristic studies as per NRS048 and SA grid code [34]-[38]. The optimization method used and explained previously is PSO where each iteration determines the next node of PV integration and converges towards an optimal node. Figure 3.16b shows the substation layout. Network 1 is therefore connected to the 11 kV busbar of the substation arrangement. The actual transmission network is further connected upstream to the substation arrangement of Figure 3.16b and as such all fault levels are based on the actual model. The 11 kV bus also designated as source substation is marked as “11 BB” in Figure 3.16b where Network 1 is therefore metered and connected to the 11 kV bus via an 11 kV circuit breaker. The voltage plot, when running a load flow on the MV network, shows the voltage profile from the source typically set at 1.03 p.u. to the end of the network with distance on the x-axis and voltage in

per unit on the y-axis. The voltage profile also shows the tee-offs of the MV network as explained in Chapter 1. However, the data points that plot the profile are not easily obtainable and another method of extracting them was required. The significant aspect here is that each voltage point is measured and checked for compliance as discussed above. Every MV terminal, for a specific voltage of 11 kV or 22 kV, which is utilized as a busbar may have load or a PV system connected to it. It is at this terminal that integrating a PV system can be made possible. A method of referencing this busbar in Powerfactory, for ease of manipulation in the optimization equation would be to use the *bus-index* parameter. The bus-index has integer values assigned to all terminals from the source to the end of the network but due to the nature of the network the numbers are not sequential but are numbered in ascending order. This is due to tee-offs etc. that may have the same bus-index number. These values are only available once a load flow is compiled and there is convergence.

Once all terminals are identified, a new cubicle is created on each terminal (busbar) at MV voltage (11 kV or 22 kV). A copy of a 0.5 MVA PV template is created and stored as part of the DPL program, is connected to this new cubicle and placed out of service. The advantage of doing this is that the code executes faster, which when solving many iterations can take a relatively long time. By using a matrix (*bmat*), one can assign the ordered numbers to the bus-index in referencing any terminal to be used for analysis in the optimization function. Once this is done matrices are created and sized to assist in the checking and transferring of data to MS Excel. This matrix significantly also stores the base case values of the voltage (p.u) at every MV node, the corresponding node bus-index (no.) and the distance (km) of the node from the source substation. They are used to making sure that the calculations are working as they should, and to keep track of changes of values. The initial parameters of the PSO equation are stored in the matrix, *mat*, with the *Pbest* (index [no.] and fitness values [%]) and *max generation* values. The initial velocity of PSO equation (3.33) is determined as a percentage of a random number position ranging from min to max values of the bus-index. This matrix has 7 columns, the first being the current position index (having a numeric value calculated from the PSO equation), the second and third being the voltage before and after PV connection, the rest are the fitness value, *Pbest, Gbest* and generator magnitude at the *Pbest* fitness value. The next set of locations is then calculated by the PSO equation determining the new velocity and position of connecting a PV system to the MV network terminal using the current position and fitness values. The fitness values are obtained by completing the load flow studies and extracting the voltage and thermal limit values. The improvement of the voltage magnitude determines the fitness values and the highest value calculated enables saving the *Pbest* and *Gbest* values. Details of the DPL method and code structure is presented

below for a better understanding and clarity of logic. Before the script is executed, external variable values can be configured as in Figure 3.17.

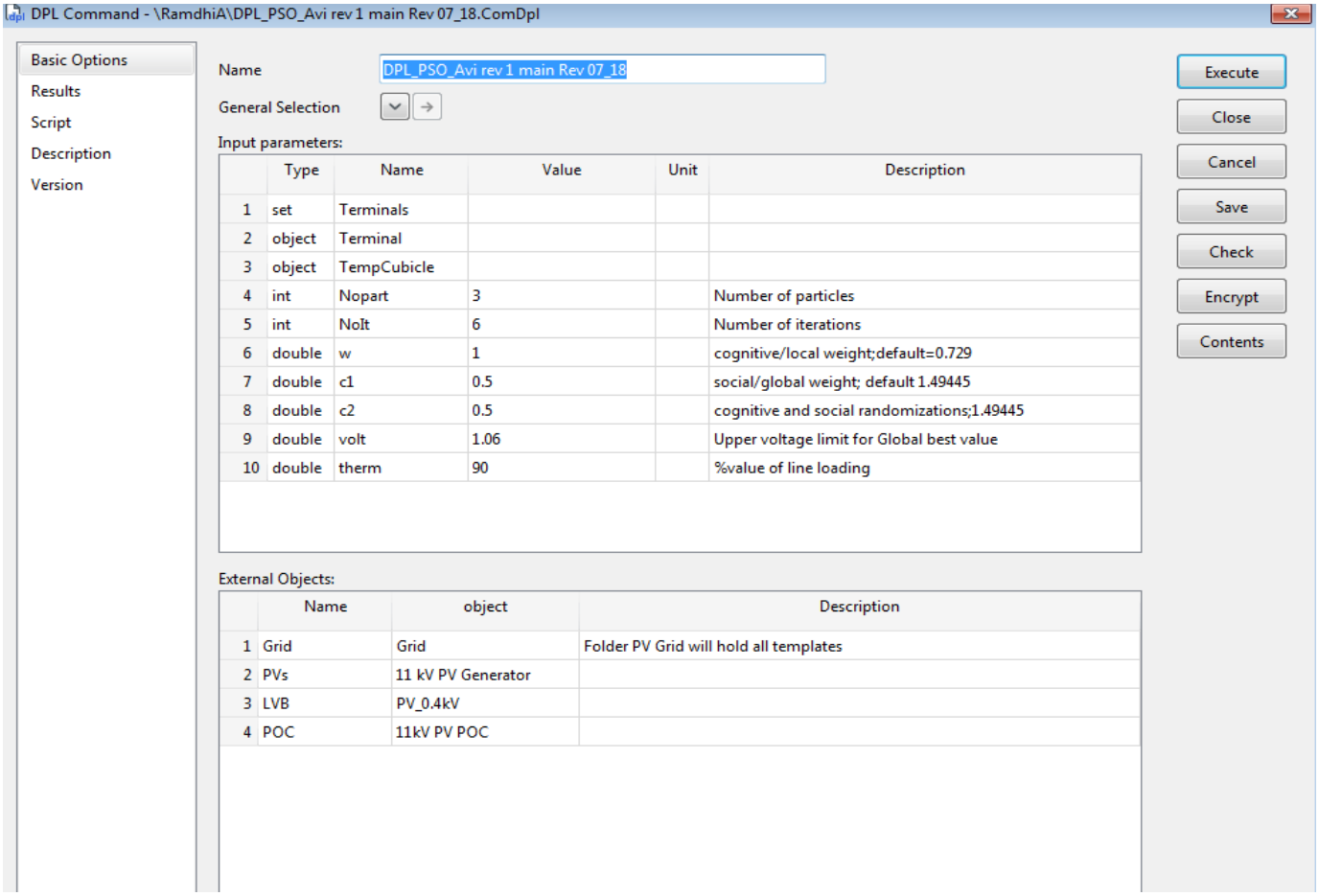

Figure 3.17: DPL input variable form

Input parameters for the PSO equation (3.33) are denoted by *w, c1, c2, Nopart* (No. of particles) and *NoIt* (No. of iterations). The MV network limits, are set by defining the voltage limit by *volt* and the thermal limits by *therm*. In addition, external objects referred to in the code have the relevant data in the *contents* part of the script, i.e. specifically referring to the type of model for the PV system. The PV system template that is been used has the following parameters as per Figure 3.18 and is discussed in section 3.4.1. The power factor at execution was set to 1.

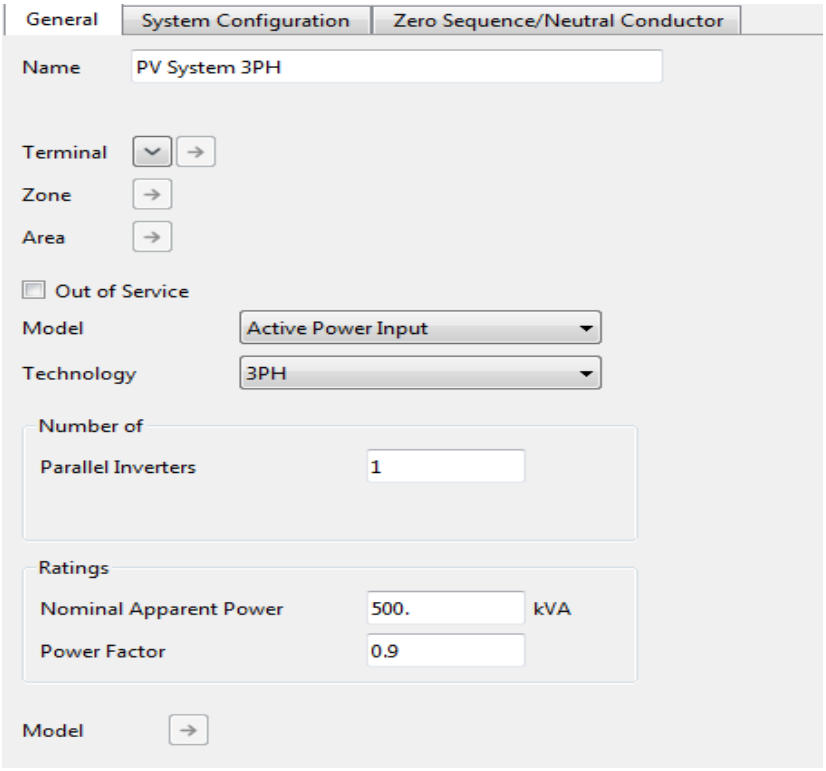

Figure 3.18: PV system template used in the code

3.4.1 PV template

The PV system in the template has a set modular rating value of 500 kVA. The amount of power dispatched can be configured as well as the number of inverters. These two values are used to calculate the optimal output to the network by increasing or decreasing their values. For the studies that follow, a 10% change was seen to be appropriate to use in the DPL script as converging to a solution was quicker, especially in the RVC calculations.

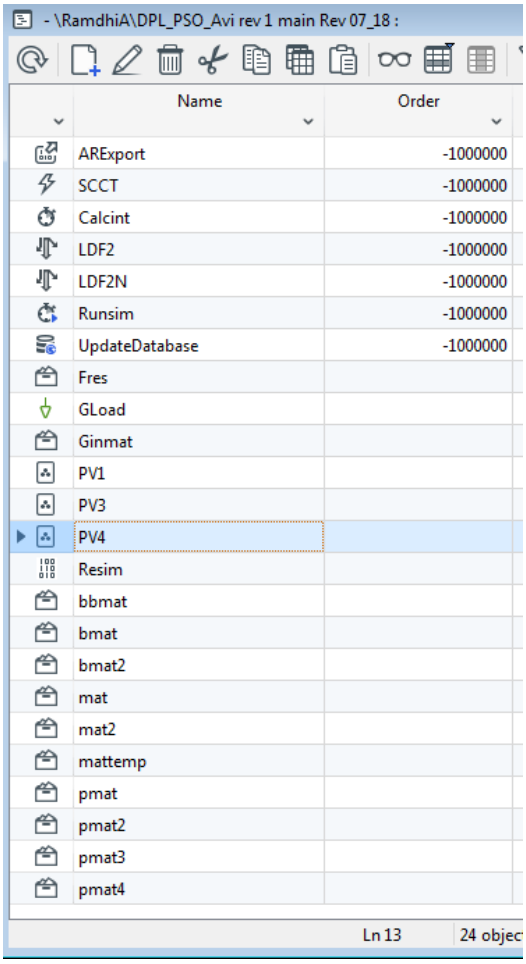

Figure 3.19: DPL code list of matrices and executable functions

3.4.2 Various matrices used

A list of matrices (as shown in Figure 3.19) is populated as the script executes. These matrices keep track of variables and enable the Excel Visual Basic interface to be more informative. Matrices are required to save the values from the *base case* load flow with no PV system connected to the network, and at each iteration, the new voltage profile and line thermal loading values are stored in *bmat* (explained above) and *bmat2* (active power [kW] and electrical losses [kW]) matrices respectively. *Fres* matrix keeps track of the PSO equation outputs of new velocities and positions (calculated using equation (3.33) and *Ginmat* (as shown in Figure 3.20) keeps track of the network initial MV feeder loading (MVA) measured at the substation 11 kV busbar and new loading after PV installation. *Gbest* values are updated and stored in this matrix as well tracking the converging of RVC values to 3% such that errors can be picked up during DPL execution run-time. *Pmat* matrix keeps track of all line loadings and electrical losses.

Ginmat		Final loading	Initial loading
Gbest	3.395373	1620.001	2.570575
Index of Gbest	65	-64.9258	0.90161

Network capacity improvement %

Figure 3.20: *Ginmat* matrix

3.4.3 Initial stages of DPL code

At the initial stage, all duplicate and old templates are deleted and a new PV template is added to the '*network data'* folder. At this stage a load flow study is then executed. All bus-indices are now available. The initial MV network loading as explained above is stored in the *Ginmat* matrix. A smaller set of terminals/busbars are filtered due to the default 11 kV MV voltage or can be changed to suit the network under assessment. This is done as other MV nodes with different voltages are also available in the set. The intention is only to model the 11 kV nodes in the model. With every iteration, data is saved in MS Excel by firstly creating a new workbook and creating a new worksheet for every iteration as determined by the PSO equation inputs. Every iteration may have many PV units selected by the user and as such the amount of data is suitably stored in the worksheet during run-time.

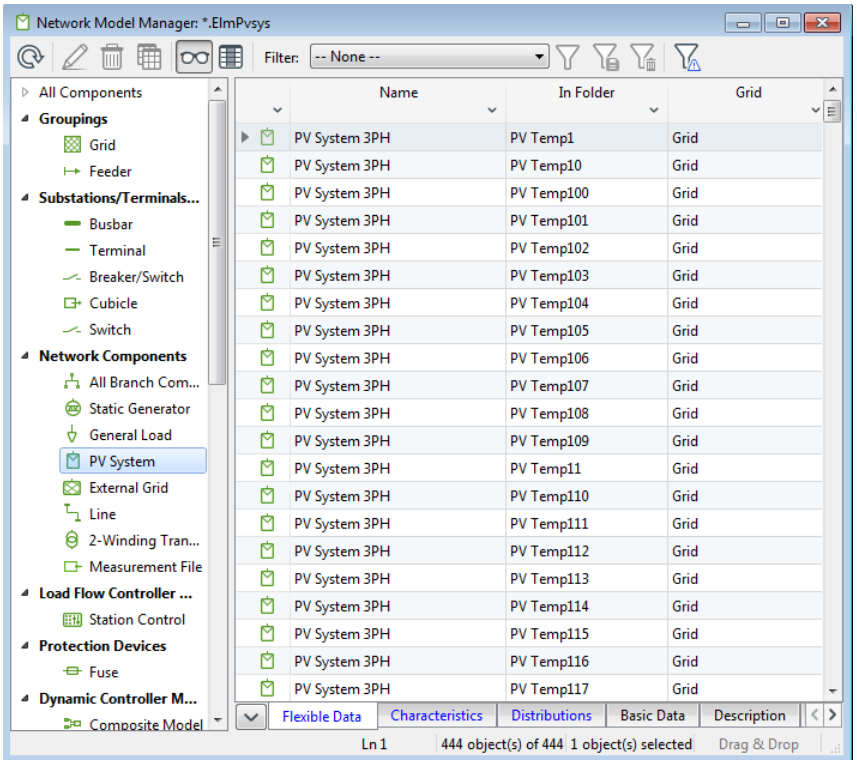

Figure 3.21: PV system templates connected to relevant MV terminals on the network

From Figure 3.21, it can be seen that the PV system template (set at 450 kW i.e. 500 kVA at 0.9 p.f. but changed to 1 at execution for testing purposes) is numbered and connected according to the *bus-index* of the network under assessment and is kept out of service. The *bmat* matrix shows the initial base case load flow (before entering the PSO calculations in the DPL code) and three columns of data that is generated for each iteration in the same matrix; the bus-index, bus voltage in per unit and distance in km from the 11 kV source substation as marked in Figure 3.12. The leftmost column shaded is the matrix row number and is applicable to all matrices used in DPL.

The PSO equation (3.33) references the row values *(bus-position)* of the bus-index rather than the index value itself as this varies per network. This means that if the position of the 'particle' determined in the PSO equation is 5, then the bus-index value is 14 as per Figure 3.23 showing the *bmat* matrix values. This implies that this assignment is done every time the particle position is under scrutiny. Also, the distance in kilometre (km) from the MV source node starting at the 11 kV source substation point, is also saved noting that the more than one bus-index can be in close proximity to each other. Figure 3.22 shows the DPL extract and the use of the "AddCopy" function to create PV templates in folder "PV Temp".

```
!Add PV generator to every MV terminal
count2 = 1;
p = S9.First();
while (p)                    {                          !Create a temporary cubicle on the terminal
        TempCubicle=p.CreateObject('StaCubic','TempCubicle ', count2);
        p = S9.Next();
        count2 = count2 +1;
                              };
sob = AllRelevant('Temp*.StaCubic');
count8 =1;
pg = sob.First();
while (pg)                   {
        op1 = ppp.AddCopy(PV4,'PV Temp',count8);
        sob2 = op1.GetContents('*.ElmPvsys');
        p2 = sob2.First();
        p2:bus1 = pg;
        p2:outserv = 1;                          !connect all gens but take them out of service
        count8=count8+1;
        pg = sob.Next();  };
```

Figure 3.22: PV system connecting to created cubicle on all relevant terminals

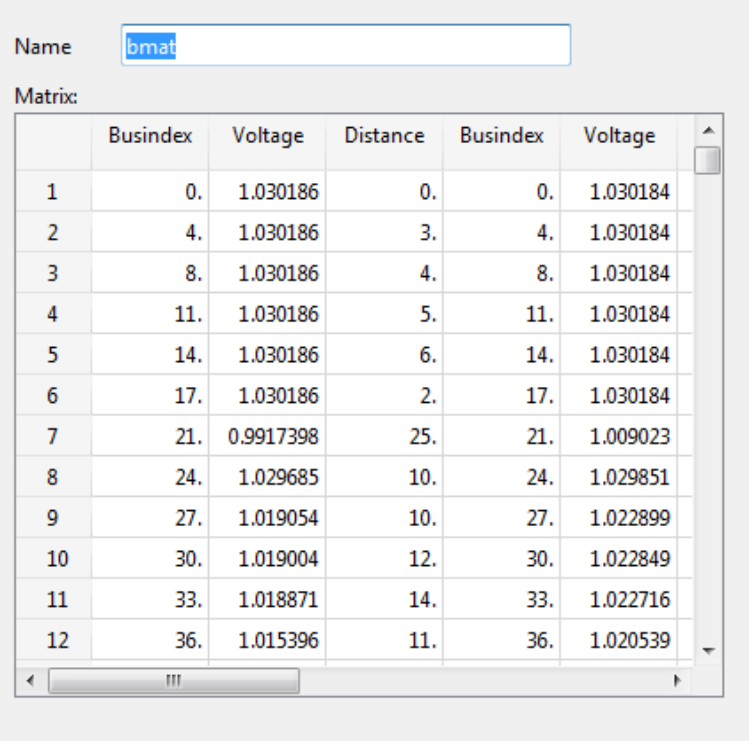

	Busindex	Voltage	Distance	Busindex	Voltage
1	0.	1.030186	0.	0.	1.030184
2	4.	1.030186	3.	4.	1.030184
3	8.	1.030186	4.	8.	1.030184
4	11.	1.030186	5.	11.	1.030184
5	14.	1.030186	6.	14.	1.030184
6	17.	1.030186	2.	17.	1.030184
7	21.	0.9917398	25.	21.	1.009023
8	24.	1.029685	10.	24.	1.029851
9	27.	1.019054	10.	27.	1.022899
10	30.	1.019004	12.	30.	1.022849
11	33.	1.018871	14.	33.	1.022716
12	36.	1.015396	11.	36.	1.020539

Figure 3.23: *bmat* matrix showing assignment to column 1 bus-index

The *bmat* matrix in Figure 3.23 shows the voltage at each bus or terminal in column 2 with the distance in km from the MV source substation in column 3. The most significant aspect of this matrix is that each row number (bus-position) has a bus-index value attached to it. The DPL code hence uses the row number in the PSO equation thus preventing errors due to duplicate bus-index numbers corresponding to the same MV node. Code extract in Figure 3.24 filters out all 11 kV terminals /nodes and populates *bmat* matrix as shown above. Initial MV feeder loading (MVA) measured at the 11 kV source substation loading is also saved.

```
!Base case results first, initial conditions

S9.Clear();
S10.Clear();
count2=1;
LDF2.Execute();
p = S3.First();                          !all relevant terminals
while (p)                                {
!filter for all 11 kV terminals and save base value for load value
if (p:uknom = 11)                        {
            bmat.Set(count2,1,p:b:index);    !busindex
            bmat.Set(count2,2,p:m:u);        !voltage p.u
            bmat.Set(count2,3,p:b:dist1);    !distance from source in km
```

```
            !save initial loadings in kW
           if (p:b:index = 0)  {
                 g10 = p:m:Pflow;
                 Ginmat.Set(1,3,g10);
                                 };
            count2 = count2 +1;
            S9.Add(p);                          !Filtered sets of values
           S10.Add(p);
                                                 };
p = S3.Next();                                  };
```

Figure 3.24: DPL code extract for generating reduced set of MV terminals and initial loading set in *Ginmat* matrix

The MV loading measured at the 11 kV busbar at the substation is achieved by measuring the power flow at bus index 0 allocated by Powerfactory. Typically, the *bmat2* matrix (as shown in Figure 3.25) stores the relevant and associated thermal line loading (%), active power at each bus (MW) and the electrical losses (kW) for every interconnecting MV line at each iteration. Therefore, when iteration 1 is complete, the next three columns of data for the *bmat2* matrix is populated, i.e., the dimension of the matrices are determined by 3 x the number of selected iterations. Once this is completed for the PV system connection, as per the flowchart in Figure 3.4, and if more PV systems are to be connected with user requirements, the matrix values, except the first three base case data columns, are transferred into Microsoft excel in the result file.

Name bmat2

Matrix:

	1	2	3
1	48.98215	935.7521	0.00079866
2	93.26549	893.328	0.07682323
3	2.305144	21.53247	0.1196909
4	92.70523	884.7745	0.05416085
5	70.89449	672.8154	0.1800607
6	18.77418	172.5884	0.1365935
7	3.917763	37.0572	0.00419331
8	0.3582126	3.316101	0.07734071
9	4.08193	36.91971	0.00235737

Figure 3.25: *bmat2* matrix storing active power and electrical losses

```
!store base case lines
count2=1;
p = S5.First();
while (p)           {
!filter for all 11 kV terminals and save base vales for load value
                        bmat2.Set(count2,1,p:c:loading); !line loading
                        bmat2.Set(count2,2,p:m:P:bus1); !active power
                        bmat2.Set(count2,3,p:c:Cload); !electrical losses
                        count2 = count2 +1;
                        p = S5.Next();
};
```

Figure 3.26: DPL code for generating *bmat2*

The *bmat2* matrix generated by the code shown in Figure 3.26 stores the line loadings (%), active power (kW) and electrical losses (kW) of the network. The first three column sets of data in the *bmat* and *bmat2* matrices store the base case values, i.e., with no PV connected. This is used to visually see the difference in the PV tool analyzer in the improvement at each iteration when a PV system is connected. If for example, in an iteration where three columns of data in a particular iteration is plotted against the first three columns of data in the base case, it is possible depending on the proximity of load from the PV system on the network, that the interconnecting MV lines may see a reduction in power drawn from the MV source at the substation and as a result, the network capacity will increase. This would be clearly seen in the simulations that follow. It is also possible that when the load is less than the amount of generation on the network the electrical losses may increase too. This is due to the nature of the network and its design build. The philosophy is that the network conductor is under-sized as power flows to the end of the network and as a result the impedance from the source is higher as explained in Figure 3.9. When a new source of active power connects to this part of the network, the resultant electrical losses may increase and this may further be exacerbated by non-technical losses such as theft and meter tampering. This is also an important aspect to consider when determining the optimal location of the PV connection. Now that *bmat* and *bmat2* store the base values (bus voltage and line loading values before PV integration) for comparison, the appropriate technical limitations can be applied at each further iteration. These limitations are documented in chapter 2 and are either the NRS048 or NRS097.

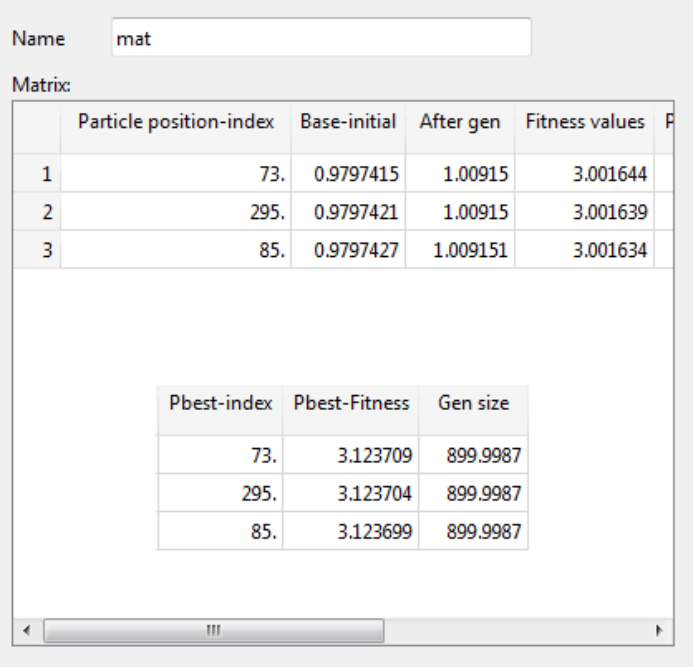

Figure 3.27: The main *mat* matrix which stores the before and after PV integration values

The matrix *mat* as shown in Figure 3.27 is the main matrix to which the PSO equation outputs are stored. As mentioned in the summary earlier in this section, *mat* matrix has 7 columns, the first being the current position index (extracted from *Fres* matrix that keeps track of all calculated PSO positions and explained further in this section), the second (extracted from the *bmat* matrix) and third being the voltage before and after PV connection, the rest are the fitness value, *Pbest, Gbest* and generator magnitude at the *Pbest* fitness value. The first column replaces the previous value with the new row position found by applying the relevant inputs into the PSO equation (3.33).

There are practical instances where the need arises to model and assess the integration of more than one PV system on the MV feeder simultaneously. A selection of how many units can be monitored is optional. In the simulations that follow to show the applicability, a number of DG's set at 5 triggers the multiple DG function. This simultaneously connects all DG units in the set and calculates the relevant voltage, thermal and RVC (or RVC) values. The most appropriate generation value applied to all PSO generated connection points gives different combination of locations on the MV network to which PV systems can connect without any technical issues and whose values are stored in matrix *mat2* (Figure 3.28).

Name mat2

Matrix:

	1	2	3	4
1	71.	0.9846924	1.016374	3.217442
2	332.	1.007478	1.022632	1.504115
3	85.	0.9969432	1.014849	1.796089
4	67.	0.987872	1.020469	3.299686
5	314.	0.9853941	1.031653	4.694453
6	80.	1.001695	1.018479	1.675593
7	70.	0.9867586	1.013361	2.69594
8	304.	1.014139	1.022489	0.8233012
9	83.	0.995236	1.011525	1.636738
10	73.	0.9836817	1.025026	4.203024
11	295.	0.9915277	1.025244	3.400488
12	85.	1.00665	1.025163	1.839057

Figure 3.28: *mat2* matrix which stores all connecting PV systems simultaneously

The PSO algorithm requires a set of initial conditions and random positions for the selected number of particles (Figure 3.29). The random number is selected based on the total bus-indices and using the matrix row linked to the index. In Figure 3.30, the Fres matrix stores all PSO positions.

```
! initialize all particles with fitness value 1, and assign random positions
tempm.Clear();
for (count4=1; count4<=Nopart; count4=count4+1)                    {
        ran = GetRandomNumber(1,max2);
        Info('Random index row no: %d',ran);
        countB = bmat.Get(ran,1);    !bmat matrix has bas values
        Info('Matrix index value %d',countB);
        mat.Set(count4,1,ran);        !associated busindex
        Fres.Set(count4,1,ran);
        mattemp.Set(count4,1,ran);  !duplicate first col-tracking only
        count6 = mat.Get(count4,1); !Base index is PBest initially
        mat.Set(count4,5,count6);     !Stores Pbest_index values
        mat.Set(count4,6,2);          !initial fitness value/voltage imp
        mat.Set(count4,7,450);        !initial gen size
                                                                   };
```

Figure 3.29: DPL code for initial PSO setup

So for example, with *three* iterations and *three* PV systems the *Fres* matrix shown below keeps track of the next position as input to the PSO equation (3.33). *Pbest* initial value would be the current position of the PV system i.e., the first random MV terminal found for PV connection and *Gbest* is set to 0. The initial fitness value is then set to 0. In Figure 3.30, the PSO equation would calculate positions in each column i.e every column except column 1, is populated at each iteration; and every row shows the trajectory of a single PV system. For example, a PV system randomly positioned at MV node 332 (row no. of bus-index), would then move to position 314 and eventually to position 295 depending on the PSO equation (3.33) inputs and outputs.

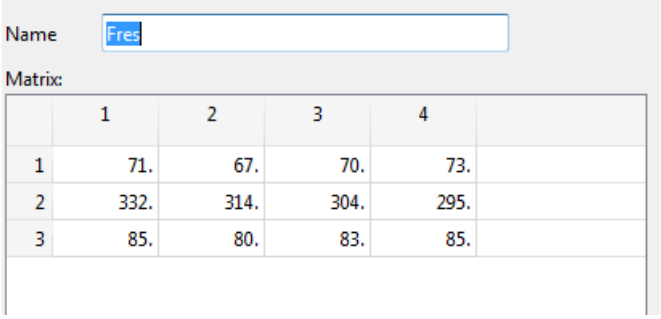
Name Fres

Matrix:

	1	2	3	4
1	71.	67.	70.	73.
2	332.	314.	304.	295.
3	85.	80.	83.	85.

Figure 3.30: *Fres* matrix to keep track of all positions calculated using the DPL code

Figure 3.31 shows the PSO equation and initial parameters set in the code as well as the actual equation calculation *(h4).* Once each node position for PV placement is calculated using *h4*, the bus index value is found and the 500 kW PV system that is connected to the new cubicle is placed in service. This means that PV connected here is now ready to be studied in the system studies that follow. The cubicle here refers to the node created with code shown in Figure 3.22 which adds a PV template copy for each MV node *(sob).*

```
!for each iteration produce new positions for each particle
for (o=1; o<=Nopart; o=o+1) {     !Nopart is the number of particles
temp2 = mat.Get(o,1);             !current position of matrix mat
temp1 = mat.Get(o,5);             !Pbest – initial value
temp = Ginmat.Get(2,1);           !Gbest value stored in matrix Ginmat
!New velocity is determined by next equation h4 as the velocity of the particle
h4 = round((0.05*temp2) + r1*c1*(temp1 – temp2) + r2*c2*(temp – temp2));
!h4 the new velocity + current position is the next position for calculating
!if the new position is out of bound then the value is the max value
if (h4+temp2 > max2)  {
    mat.Set(o,1,max2);
    Fres.Set(o,iter+1,max2);
```

```
                    };
if (h4+temp2 < max2) {
mat.Set(o,1,h4+temp2);
!track each new set per iteration
Fres.Set(o,iter+1,h4+temp2);
                    };
                        };
```

Figure 3.31: DPL code for PSO equation

Once the initial values and positions are determined and stored in the *Fres* and *mat* matrix, the base case values stored in the *bmat* and *bmat2* matrix, system studies can commence. The RVC calculation code is first executed. It is the first requirement to be adhered to before voltage and thermal values are checked. The code in Figure 3.32 increases the PV size (*p6:ngnum)* by first increasing the number of PV systems and then if need be, decrease the PV system output value (kW) *(p6:pgini)* until the RVC criteria for fluctuating generation (PV) of 3% is met (*2.8 < rvc < 3.3*) thereafter the other two checks above are completed (see flowchart in Figure 3.4).

```
rvc = 0;
grow = 1;
while (rvc <> 3) {                          !3% for PV
      p6:outserv = 0;                       !PV in service
      LDF2.Execute();                       !All consideration ticked
      rvc1 = p5:m:u1pc;
      Ginmat.Set(count4,8,rvc1);            !Save first value
      UpdateDatabase.Execute();             !update database
      p6:outserv = 1;                       !PV out service
      LDF2N.Execute();                      !All consideration unticked
      rvc2 = p5:m:u1pc;                     !Save second value
      Ginmat.Set(count4,9,rvc2);
      rvc = abs(100*(rvc2-rvc1)/rvc1);      !Calculate diff wrt 1st
      Ginmat.Set(count4*2+8,grow,rvc);      !Store RVC & gen size
      Ginmat.Set(count4*2+9,grow,p6:ngnum*p6:pgini);
      grow = grow +1;
if (rvc <= 2.8) {
p6:ngnum = p6:ngnum + 1;
};
if (rvc > 3.3) {
```

```
p6:pgini = p6:pgini – 0.1 * p6:pgini;
};
if (rvc < 3.3) {
if (rvc > 2.8) {
   genvari = rvc;
   rvc = 3;
                    };
                   };
};
p6:outserv = 0;
LDF2.Execute();
```

Figure 3.32: DPL code for RVC checks

The PV system at the node is placed in and out of service and the database updated when doing a comparison of voltage values at the point of connection as mentioned earlier. At runtime, the code executes much faster by having the physical connection of the PV system connected to the node already in place hence using the out of service part on the template. In the PV template, the parameters are either increased or decreased by changing the number of machines and /or the magnitude of PV output to satisfy the RVC conditions as explained above.

As the code executes, *Ginmat* matrix used also as a storage array uses the relative generator magnitude with RVC calculation to keep track of the convergence to a value most suited to proceed further. As can be seen in Table 3.5, the RVC value for 3 PV systems increases as the PV generator output increases. This is done for each PV system. For example, for 3 PV systems, in table 3.5 RVC of 3% is achieved after the relevant and corresponding adjustment of the PV output.

The network is then checked for voltage and thermal issue contraventions, against the limits set in the NRS048 standard; that may arise from the excessive generation or increased losses as a result of the connection (Figure 3.32).

Table 3.5: RVC (%) values vs PV generator output (kW)

RVC values stored in matrix *Ginmat*						
Iteration		**1**	**2**	**3**	**4**	**5**
PV1	RVC%	1.349453	2.626477	3.837971	3.481027	3.155075
	PV size(kW)	449.9996	899.9989	1349.998	1214.997	1093.497
PV2	RVC%	1.349448	2.626468	3.837958	3.481015	3.155064
	PV size(kW)	449.9996	899.9989	1349.998	1214.997	1093.497
PV3	RVC%	1.349443	2.626459	3.837945	3.481003	3.155053
	PV size (kW)	449.9996	899.9989	1349.998	1214.997	1093.497

All the terminal voltages are checked and if the user set parameter (*volt – 1.06p.u*) is exceeded the PV size is further reduced by 10% and rechecked until this condition is met. Similarly, thermal conditions against user set parameters (therm – 90%) are validated and the same reduction applies. This is highlighted in the code in red below as shown in Figure 3.33 with the voltage and thermal checks (*volt and therm*). Only the parameter *p6:pgini* is adjusted here as these checks are a finer adjustment to the already calculated RVC percentage. Matrices *pmat* and *pmat2* are created to keep track of the thermal line loading (%) for all calculations. In *pmat* the machine size in every 2nd column from a set of 3 columns keep track of the machine size (kW) decreasing in value if the value is too big when doing voltage check. Similarly, the voltage (p.u) is tracked in every 3rd column from a set of 3. In matrix *pmat2*, for thermal checks, from a set of 3 columns, the line thermal loading (%) and the corresponding machine size (kW) are tracked in columns 2 and 3. Matrices *pmat* and *pmat2* are only used to keep track of the changes that happen in the adjustment of the voltage and thermal values after the RVC is completed and is not transferred to the tool analyzer.

```
Stat3 = 1;
stat5 = 0;
while (stat3 < 10) {
stat1 = 0;
stat2 = 0;
!voltage check constraint
count12 = 1;
p8 = S10.First();
while (p8) {
        count14=count14+1;
```

```
        pmat.Set(count12,iter*3-2,count14);
        pmat.Set(count12,iter*3-1,p6:pgini*p6:ngnum);
        pmat.Set(count12,iter*3,p8:m:u);
if (p8:m:u > volt) {
stat1 = 1;
};
count12=count12+1;
p8 = S10.Next();
};
!thermal check constraint
count12 = 1;
p9 = S5.First();
while (p9) {
            pmat2.Set(count12,iter*3,p9:c:loading);
            pmat2.Set(count12,iter*3-2,p9:ciDistAll);
            pmat2.Set(count12,iter*3-1,p6:pgini*p6:ngnum);
if (p9:c:loading > therm) {                    !after gen con, thermal high
stat2 = 1;
};
count12=count12+1;
p9 = S5.Next();
};
!if both stats are 0, implies gen size is adequate at this node
if (stat1 = stat2 = 0) {
if (stat5 = 1) {
      stat3 = 9;
      Ginmat.Set(count4,4,p6:pgini);
      Ginmat.Set(count4,5,p6:ngnum);
      Ginmat.Set(count4,6,p5:b:index);
      Ginmat.Set(count4,7,p5:m:u);
};
if (stat5 = 0) {
stat3 = 9;
      Ginmat.Set(count4,4,p6:pgini);
      Ginmat.Set(count4,5,p6:ngnum);
      Ginmat.Set(count4,6,p5:b:index);
Ginmat.Set(count4,7,p5:m:u);
};
};
!if either stat is 1, implies gen value size has to be reduced
```

```
if (stat1 + stat2 >= 1) {

if (stat1 = 1) {
p6:pgini = p6:pgini – 0.1 * p6:pgini;
stat5 = 1;
};

if (stat2 = 1) {
p6:pgini = p6:pgini – 0.1 * p6:pgini;
stat5 = 1;
};
};
stat3 = stat3 + 1;
LDF2.Execute();
};
```

Figure 3.33: DPL code for voltage and thermal checks

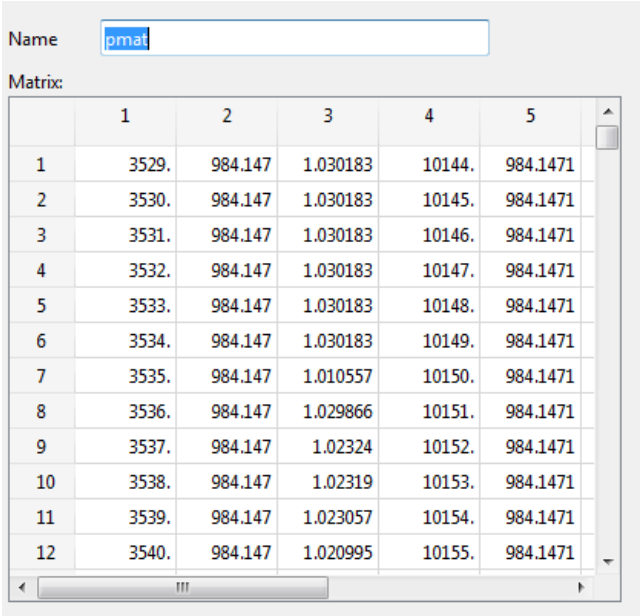

	1	2	3	4	5
1	3529.	984.147	1.030183	10144.	984.1471
2	3530.	984.147	1.030183	10145.	984.1471
3	3531.	984.147	1.030183	10146.	984.1471
4	3532.	984.147	1.030183	10147.	984.1471
5	3533.	984.147	1.030183	10148.	984.1471
6	3534.	984.147	1.030183	10149.	984.1471
7	3535.	984.147	1.010557	10150.	984.1471
8	3536.	984.147	1.029866	10151.	984.1471
9	3537.	984.147	1.02324	10152.	984.1471
10	3538.	984.147	1.02319	10153.	984.1471
11	3539.	984.147	1.023057	10154.	984.1471
12	3540.	984.147	1.020995	10155.	984.1471

Figure 3.34: *pmat* matrix

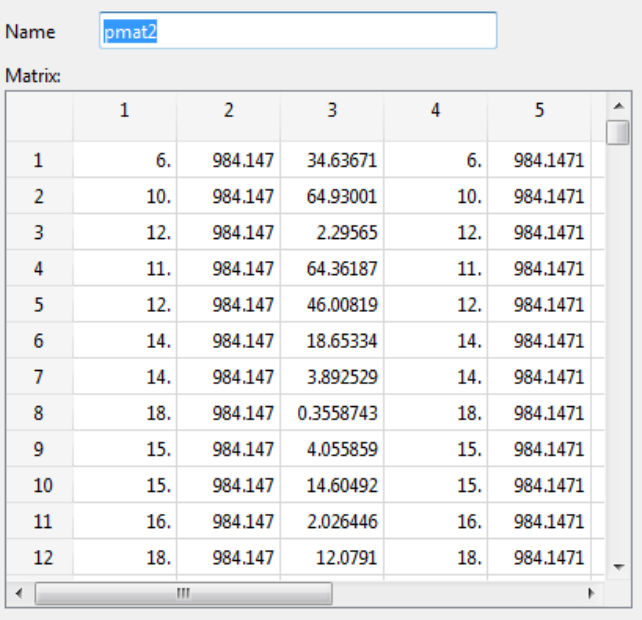

	1	2	3	4	5
1	6.	984.147	34.63671	6.	984.1471
2	10.	984.147	64.93001	10.	984.1471
3	12.	984.147	2.29565	12.	984.1471
4	11.	984.147	64.36187	11.	984.1471
5	12.	984.147	46.00819	12.	984.1471
6	14.	984.147	18.65334	14.	984.1471
7	14.	984.147	3.892529	14.	984.1471
8	18.	984.147	0.3558743	18.	984.1471
9	15.	984.147	4.055859	15.	984.1471
10	15.	984.147	14.60492	15.	984.1471
11	16.	984.147	2.026446	16.	984.1471
12	18.	984.147	12.0791	18.	984.1471

Figure 3.35: p*mat2* matrix which stores very iteration for thermal checks

Once the maximum PV size is reached, the same process is repeated for each new position identified in the matrix *Fres*. In Figure 3.33, this adjustment is highlighted in red where *pgini* is reduced for PV output in the actual PV system. With reference to Figure 3.36, at the current location, the fitness value is calculated and compared to the previous value as well as the global best (*Gbest*) value. If at this position the improvement in voltage is higher than the existing *Pbest* position fitness value (*h3>h1*), this position becomes the new best particle position and similarly checked with the global best value as well *(h3>h6).* The new network capacity improvement is calculated by the difference before the PV is applied and after the PV is applied at this position (*g7*).

```
P6:pgini = Ginmat.Get(count4,4);
p6:ngnum = Ginmat.Get(count4,5);
LDF2.Execute();
        mat.Set(count4,n+2,p5:m:u);          !voltage p.u after gen
        x1 = mat.Get(count4,n+1);
        x2 = mat.Get(count4,n+2);
        h3 = 100*(x2-x1)/x1;
        mat.Set(count4, n+3, h3);            !fitness value
        h1 = mat.Get(count4,6);              !Pbest fitness value
        h2 = mat.Get(count4,1);
        h6 = Ginmat.Get(1,1);                !global best position
if (h3 > h1) {
        mat.Set(count4,6,h3);                !Fitness value at Pbest
```

```
        mat.Set(count4,5,h2);                    !Pbest position
        mat.Set(count4,7,p6:pgini*p6:ngnum);     !gen size
};
if (h3 > h6) {
   Ginmat.Set(1,1,h3);                           !Fitness value at Gbest position
   Ginmat.Set(2,1,h2);                           !Global best gets current index
   Ginmat.Set(1,2,p6:pgini*p6:ngnum);            !Fitness value at Gbest position
   count12 = 1;
   p8 = S10.First();
  while (p8) {
     if (p8:b:index = 0) {
   g6 = p8:m:Pflow;
                              };
  count12=count12+1;
  p8 = S10.Next();
                               };
  Ginmat.Set(2+iter,2,g6);
  g8 = Ginmat.Get(1,3);                         !initial loading
  g7 = 100*(g6-g8)/g8;
  Ginmat.Set(2+iter,3,g7);
                              };
count12 = 1;
p8 = S9.First();
while (p8) {
bmat.Set(count12,count4*3+1,p8:b:index);
bmat.Set(count12,count4*3+2,p8:m:u);
bmat.Set(count12,count4*3+3,p6:pgini*p6:ngnum);
```

Figure 3.36: DPL code setting the *Pbest* and *Gbest* values

This process is repeated with many user defined iterations as possible noting the network capacity with the application of each selected PV system particle connecting to the MV network. A resultant load flow in comparison to the initial load flow graph is saved in the matrix *bmat* and the data is transferred to MS Excel for analysis. The Excel file is saved as *Results_PSO* and once the simulation completes, the data is manipulated (arranged in specific order) and analysed by an MS Excel built interface using Visual Basic. All the required data from the relevant matrices in Powerfactory are transferred during runtime (using *xlSetValue*) as per Figure 3.37. Every iteration is stored as a new sheet storing the *bmat* and *pmat* matrix values. Once the tool is started, and PSO is selected, the result file is opened and the data in

each sheet is sorted and plotted in the tool when requested with the final results of the *Ginmat* matrix (*g1,g2,g11*) displayed on the interface.

```
xlSetWorksheetName(iter, 'Iteration start');
kk2 = mat.Get(count4,1);
g1 = Ginmat.Get(count4,4);
g2 = Ginmat.Get(count4,5);
g11 = Ginmat.Get(2,3);
    xlSetValue((count4-1)*3+1, 1,kk2);
    xlSetValue((count4-1)*3+1, 2,g1*g2 );
    xlSetValue((count4-1)*3+2, 1,g11 );
    xlSetValue((count4-1)*3+1, count12+2, p8:b:index);
    xlSetValue((count4-1)*3+2, count12+2, p8:m:u);
    xlSetValue((count4-1)*3+3, count12+2, p8:b:dist1);
    bmat.ColLbl('Busindex',count4*3+1);
    bmat.ColLbl('Voltage',count4*3+2);
    bmat.ColLbl('Distance',count4*3+3);
count12=count12+1;
p8 = S9.Next();
};
count12 = 1;
p9 = S5.First();

while (p9) {
xlSetValue((count4-1)*3+2+Nopart*3, 1,kk2 );
xlSetValue((count4-1)*3+2+Nopart*3, 2,g1*g2 );
xlSetValue((count4-1)*3+2+Nopart*3, count12+2, p9:m:P:bus1);
xlSetValue((count4-1)*3+3+Nopart*3,count12+2, p9:c:loading);
xlSetValue((count4-1)*3+4+Nopart*3,count12+2, p9:c:Cload);
count12=count12+1;
p9 = S5.Next();
};
p6:outserv = 1;
p6:ngnum = 1; !1 machine
p6:pgini = 450;
p5 = sterm1.Next();
};                                                    !end while loop
```

Figure 3.37: DPL code for data transfer to excel

The interface provides a simplistic but significant insight into the manner in which PV systems are integrated into MV networks and its ability to provide additional capacity to networks that are particularly constrained. Using Visual Basic in Excel, a *frame* is created with a *multipage tab menu*, which are suitable functions for the interface. The interface is shown in Figure 3.38. The user should be able to open a result file from any directory and have the tool populate all *picture, combo* and *text boxes* with the appropriate data from the result file. In the multipage function part of the interface, all graphics are displayed here using the *chart.SeriesCollection* and *Shapes.Addchart(type)* functions in basic with the *chart.SetSourceData* pointing to the appropriate rows and columns in the result file.

Figure 3.38: Interface in Microsoft excel designed and used to analyse results from the DPL script

The result file has to be first opened so that the interface can sort and order the data to be plotted as shown in Figure 3.39.

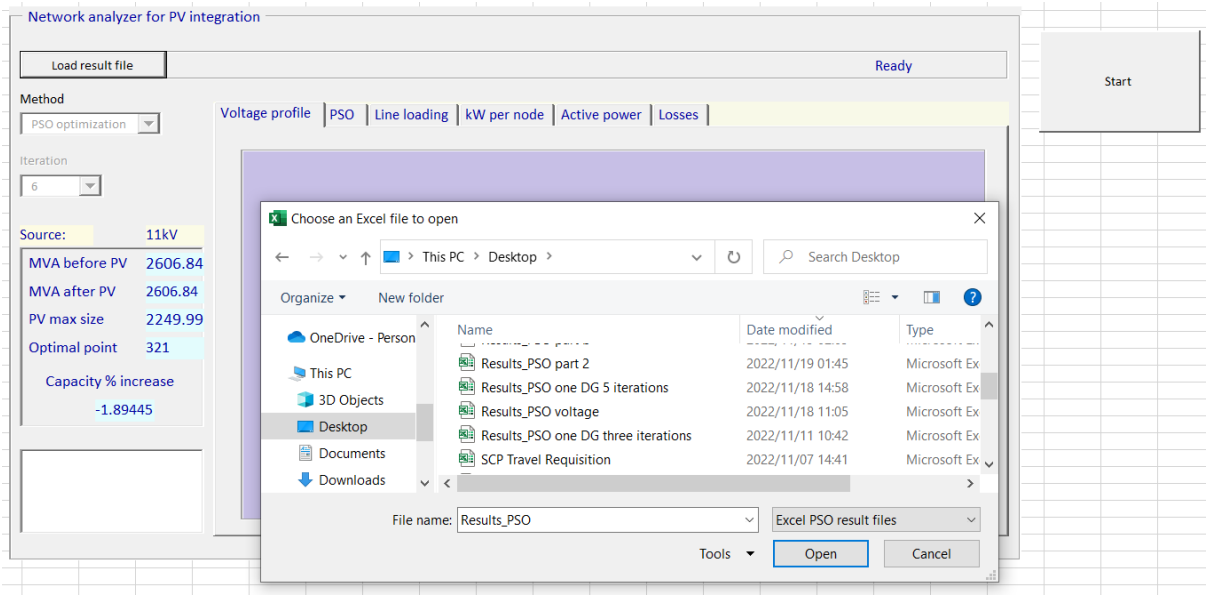

Figure 3.39: Interface with file open dialog box locating a results file

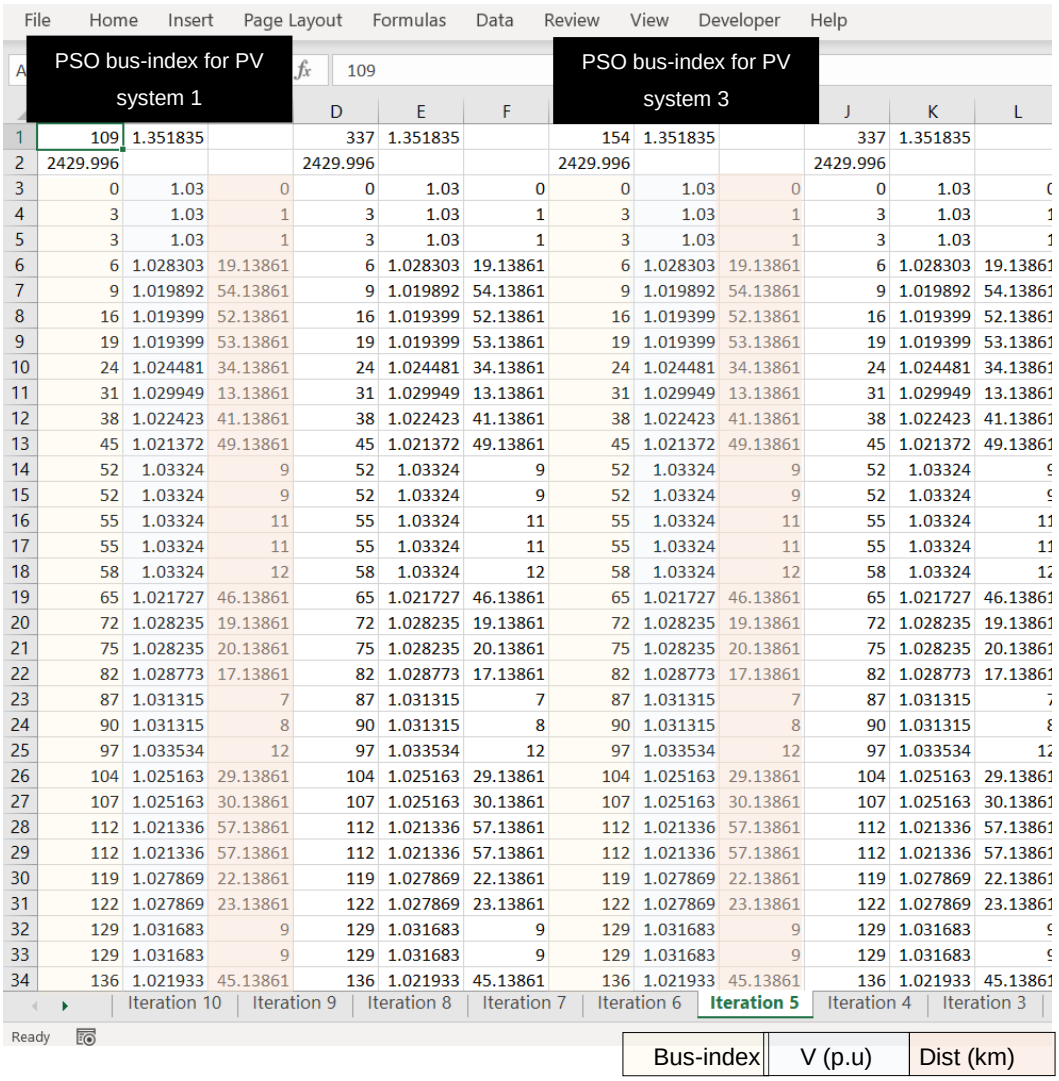

Figure 3.40: Example of a result file with unsorted data

In Figure 3.40 it can be seen that every tab is an iteration with several user defined particles for every three columns. For example, the current tab selected is Iteration 5. Every 3 sets of columns are the data from the *bmat* matrix where the figure in column A, row 1 is the PSO position from the Fres matrix for PV system 1 i.e., bus-index 109 (corresponding to a MV bus node) and for PV system 2, is bus-index position 337 and so forth. Coulmn 2 is the voltage (p.u) after the PV connects at that bus-index and column three is the distance from the source (km) as per the legend below Figure 3.40. When the result file is opened, PSO can be selected as the optimization algorithm and a particular iteration number can be chosen. With each iteration changing position, all the relevant voltage plots can be graphically shown at once. The tabs, voltage profile, line loadings, active power and technical losses show the technical data extracted from Powerfactory matrices. The PSO plot shows how each particle converges with each iteration to an optimal position. Figure 3.41 shows an example of selecting PSO and 5^{th} iteration (base case and 5^{th} iteration profile marked in Figure 3.41) and Figure 3.42 shows an example of the convergence of PSO particles in the search space converging to a solution. In Figure 3.41, the bus-position is marked on the x-axis and the voltage (p.u) marked on the y-axis. The different colour graphs shows the voltage profile for that iteration at the bus-position labelled per graph. In Figure 3.41, the base case is typically the plot that sits the lowest compared to the other profiles. When a particular iteration is selected, the relevant plot and base case is plotted for the voltage profile and line loading. The voltage profile here shows the iteration with the base case value, i.e. with no PV connected. The info frame on the interface shows the loading (MVA) before and after with the max PV that can be connected, the optimal point on the network to achieve this and the network capacity increase due to this integration.

Simultaneously, results shown on the left of the interface shows the capacity improvement made. Figure 3.42 plot is the data from the *Fres* matrix which is the calculated positions of the PV system to the MV network in each iteration. In the results, the graph will show how the convergence to a particular node is found through the calculation of the optimal fitness values.

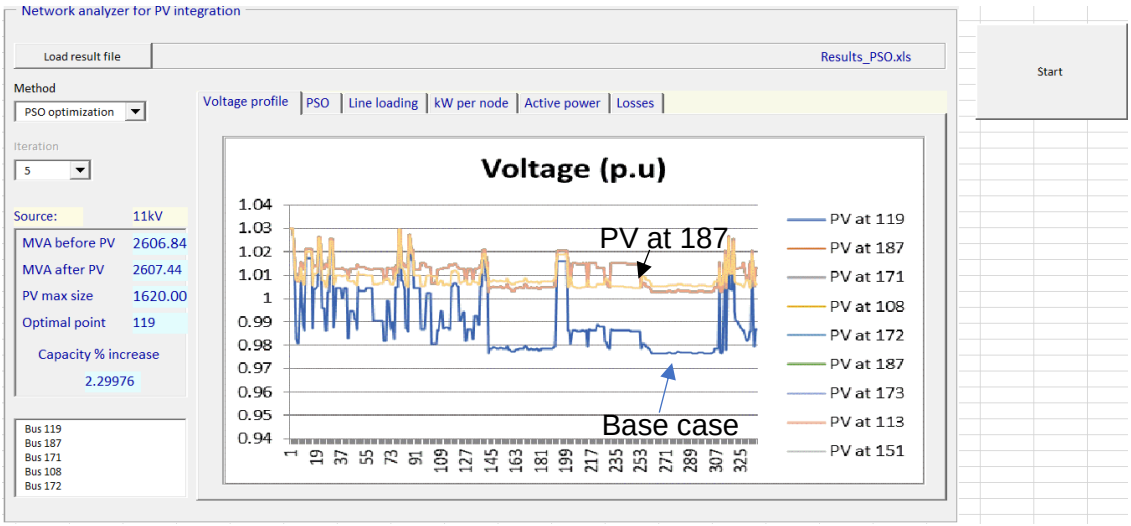

Figure 3.41: Example of selecting PSO and 5th iteration

Practically, rural networks that have high non-technical loss rates have a low probability of applying this approach due to the nature of unplanned load growth. This is elaborated more in the discussion chapter of this research. In Figure 3.41, the number of iterations is shown on the x-axis and the y-axis is the bus-position. As the next position is calculated for every iteration, the results converge to a particular MV node that would have the greatest fitness value (voltage improvement) and hence network capacity improvement. In this case for 10 iterations and 5 PV systems, starting at different MV bus positions (bus-indices are assigned through a look-up table in Appendix B onwards), the graphs converge to optimal position between 180 and 200 and which corresponds to approximately 50% of the feeder length from the MV source node. In the next chapter, the simulations plot the Fres matrix values and show the convergence of the PV systems to a particular node (MV position). However, it must be noted that the node is an approximate position to which the PV system should connect to.

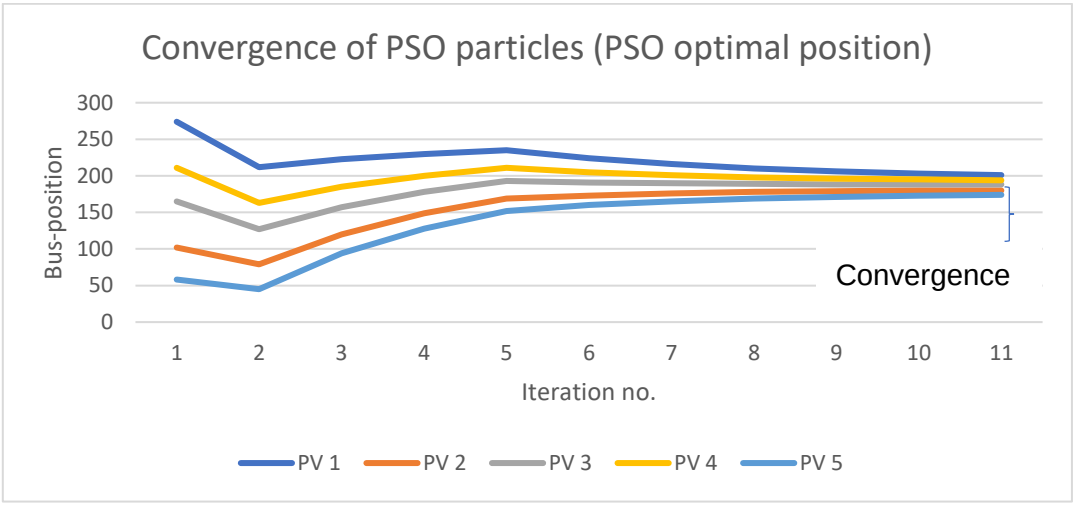

Figure 3.42: Example of PSO particle convergence (extraction from PSO *Fres* matrix)

3.5 Conclusions

Chapter 3 has presented the methodology used in this thesis to meet the objectives discussed in Chapter 1. The derivation and limitations of the equations for the objective function to establish the network capacity have been documented. The corresponding flowcharts were also presented to describe the process used in the DPL code and the assessment of un-constraining MV networks. Also, the correlation between the selected optimization algorithm of Particle Swarm Optimization (PSO) parameters and DPL code were presented diagrammatically. Although limitations of low convergence rate and local optimum for the PSO technique are well-documented, however, two ways of over-coming this was addressed in the proposed method. The MV feeder had inconsistent and duplicate bus-indices which would throw the results far off from convergence; However, this issue was addressed by re-assigning these indices in a numeric sequence. Also, *max* and *min* parameters were defined allowing the search space to remain within a fixed range of MV terminals and initial random positions to be selected appropriately. A detail analysis of the DPL code covering the significant variables, matrices and procedures used were presented and discussed with appropriate examples. Also, chapter three has in detail discussed the nature and characteristics of the two test networks that are used in Chapter 4 of the simulations. Network 1 is 11 kV and Network 2 is 22 kV. All relevant technical data has been documented and discussed for clarity to the inputs of the simulations covered in Chapter 4.

The next chapter documents the simulations and results of two test networks, 11 kV and 22 kV. The number of particles (PV systems} and iterations are changed. Also, connecting PV systems to the network without the DPL program is also done to compare to results by using PSO thereafter. Chapter 4 presents the results by manually connecting PV systems to the MV network in three positions. Middle, end-of-line (EOL) and both. This is done during peak and off-peak operating times of the network. The next part of the results present the analyser tool results using the PSO technique in Powerfactory as explained and documented in chapter 3. These results are an indication as to how the script and tool can be used to analyse PV integrated networks but not explicitly formulating rules to MV networks.

4 Network Simulations and Analysis of Results

4.1 Conventional modelling and results for Network 1

The modelling and simulations presented in this chapter for test Network 1 and test Network 2 are performed in DIgSILENT Powerfactory power system simulator. Network 1 MV voltage is at 11 kV and represents majority of feeder networks utilized in Eskom Distribution including municipalities. The nature of the network in terms of its length, electrical characteristics (conductor impedances and fault levels) and types of load represents an urban and industrial type zone and is quite apt as a test network. Also, the same network when scaled up to achieve a constrained network state represents network feeders that cannot enable load growth and implementing short term solutions as explained previously may not be cost effective and network operational improvement is limited by existing voltage control devices. It is due to these reasons that this section models the normal type and constrained type network. The approach as discussed in the methodology Chapter 3 is to model the network by firstly the conventional or manual method (without using any DPL script) and secondly by executing the DPL script with different input values for the PSO equation part of the code. The input values here would be 11 kV voltage level for Network 1 as well as the number of PV systems and iterations. The conventional method is executed in DIgSILENT Powerfactory by physically connecting a PV system (as the DG) by estimating the location down the feeder and linking the PV system to that node. The 11 kV Network 1 was setup as explained in Chapter 3 and load flow studies were conducted using the Newton-Raphson method to get the current peak apparent (MVA), active (MW), reactive (MVAR) power of the 11 kV network as shown in Figure 4.1. The electrical losses of the same network are shown in Figure 4.2. These plots consider seasonal data and hence show peak and off-peak curves on a 30min seasonal time-stamp i.e., day and night per season per every 30min period. The network data with respect to the conductor type, geographic layout and seasonal load is documented in the methodology section of Chapter 3.

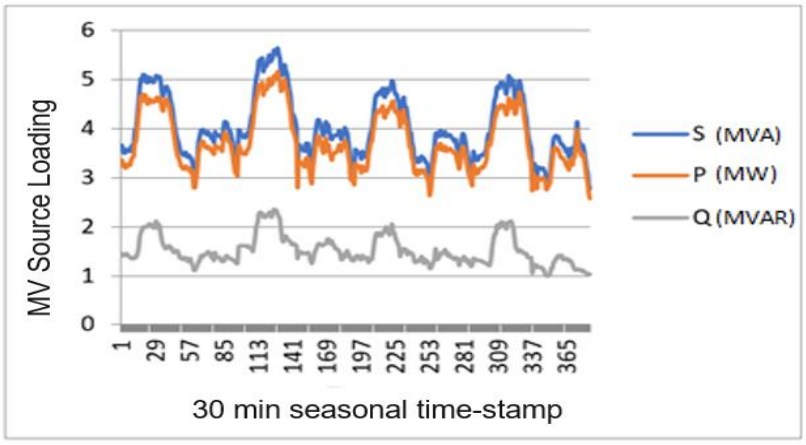

Figure 4.1: Apparent, active and reactive power values for Network 1

Figure 4.1 depicts that the active power peaks at 5 MW while the reactive power peaks at 2.4 MVAR. At low load, the active power is just below 3 MW and reactive power above 1 MVAR. These figures give an indication how much PV generation could be added to this feeder to supply loads at times when the PV output power is available and loads need not be fed directly from the MV feeder source. This however will depend on the PV location. For example, 3 MW of generation could be added as either lumped at a point or as distributed such that existing load can be supplied while additional capacity becomes available. Also, the reactive power can be supplied from capacitor banks to increase network capacity and hence to allow more inductive load to be connected. In Figure 4.2, the electrical losses are shown, but another significant factor that negatively contribute to problematic network capacity issues are *non-technical* losses due to theft or meter tampering. In some cases, the feeder trips on overload and unbalance where non-technical losses play a major role [33] [51]. The graph in Figure 4.2 has the same time-stamp on the x-axis as in Figure 4.1. The total grid electrical losses (entire network feeder including all interconnecting lines) is plotted on the y-axis corresponding to the time stamp on the x-axis.

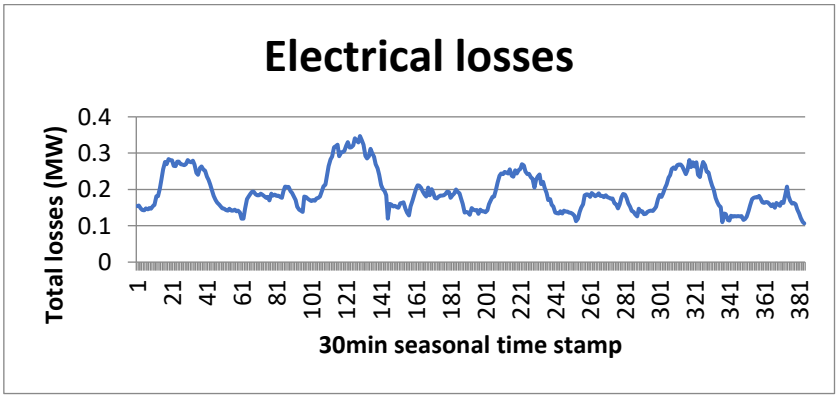

Figure 4.2: Electrical losses of Network 1

Figure 4.3 shows the voltage variation over the same period of time. During peak loads, it can be seen that the voltage drops below 0.92 p.u. which contravenes the legal limit of 0.95 p.u. (NRS048). All the voltage points in Figure 4.3 are the minimum voltage point in each load flow corresponding to a particular time-stamp.

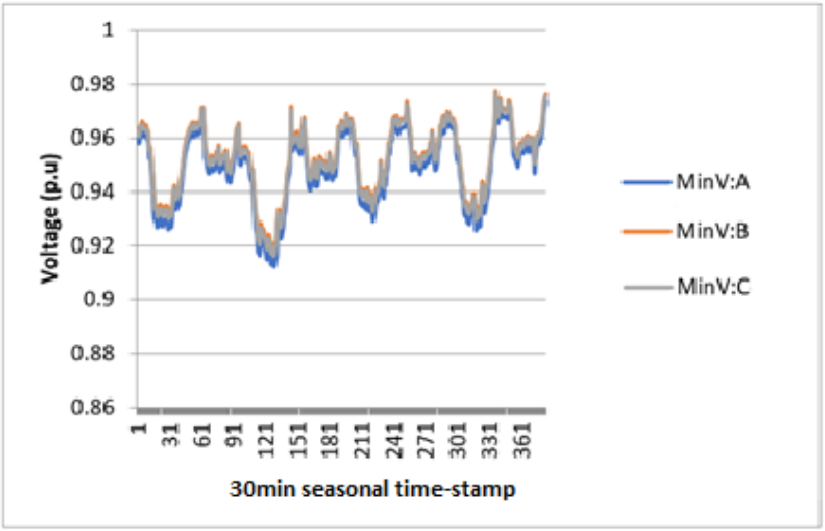

Figure 4.3: Voltage variation in Network 1

4.1.1 Connecting PV at 50% of the MV feeder:

In connecting solar PV DG to this network, the PV system is integrated at approximately 50% of the network backbone (~ 13 km in total length) from the 11 kV source substation estimated from the geographic layout of the network (please see Chapter 3, Figure 3.8 and approximately 7 km from the MV source substation). Different scenarios of normal and constrained network operation with peak and off-peak load variations are modelled and simulated. Normal networks here refer to those that operate with *no voltage or thermal limit issues* during peak or off-peak times and constrained networks either have voltages under normal limits (<95% as defined by NRS0480) or have conductors with thermal issues. When more load is added to a constrained network, the network will either trip due to over-current or conductors will sag more, or customers will experience flickering or low voltage in their supply. Therefore, as that these two scenarios represent many other practical MV networks in the utility, they are modelled accordingly thus covering a wide range of practical Distribution networks. In this research, the normal network under steady state conditions has been modelled to have an end-of-line (EOL) voltage greater than 0.95 p.u which is operated and classified by definition as un-constrained. This network's loads were then scaled to a scaling factor of 142% to mimic a constrained peak load network such that the EOL voltage becomes

lower than the 0.95 p.u mark and scaled to 40% to mimic a light loaded network for both normal and constrained scenarios.

4.1.1.1 Normal feeder peak load

At 50% of the MV network feeder 1 (please see Figure 3.8 in Chapter 3 for geographic overview of feeder 1), the MV terminal is the bus-index 536 in the simulated model built in Powerfactory. Scaling factor 1 implies that each load in the normal network scenario is multiplied by a factor of 1. The network as per Figure 3.8 was built using Powerfactory elements with relevant loads, conductor types and dimensions. Table 4.1 shows the load flow study results for different sizes of PV systems connected at this point (bus-index 536) with the corresponding voltages before and after at this MV node as well. There were no backbone feeder thermal issues in all the PV capacity variations. Once the Rapid Voltage Change (RVC) reaches 3% the final capacity improvement would therefore be determined as this is the limit for varying the PV generation (NRS097). For this study for normal network loading with peak load, it is found that 1.4 MW of PV generation can be connected at bus-index 536 maximizing network capacity limited by RVC values. By running a load flow study without any PV (base case), the 11 kV source substation source loading was found to be 2.6 MVA. With reference to Figure 4.1, the peak load is at 5 MW. The voltage per phase shown in Figure 4.3 is not balanced and exceeds the voltage limits set for this network. In other words, the network is constrained due to the EOL voltage profile being below 0.95 p.u (NRS048). To generalise, to an extent, the MV networks that are operating throughout the utility, the MV source loading at the substation is required to be scaled down to mimic an un-constrained network. A scaling factor derived from Figure 4.1 is 0.5 and results in 2.6 MW at peak load. Similarly, for light loads, a scaling factor of 0.4 was further used (industrial type scaling factor) to achieve 1.1 MW. While using the PV template with rated power of 500 kVA, the number of PV units were increased by adjusting the number of PV installations (multiples of 500 kVA installations as user-defined inputs). Following this, the magnitude of the PV system output (was adjusted on the PV template) to reach a RVC of 3% while the bus voltages and line thermal limits were checked in addition. If the source substation loading decreases, it means that more capacity can be connected, as part of the load will then be supplied from the connected PV source. From equation (3.24) in chapter 3, the capacity improvement in column 6 of Table 4.1, can be calculated as:

$$\boldsymbol{Network\ capacity\ improvement} = \frac{\mathbf{100} * (\ \mathbf{Final\ source\ loading} - \boldsymbol{Initial\ source\ loading}\ )}{\boldsymbol{Initial\ source\ loading}}\ \% \qquad (4.1)$$

Equation (4.1) is used in each study case for calculating network capacity improvement. The PV magnitude here is defined as the PV power injected at bus-index 536. But due to transformer electrical losses, the 450 kW output is slightly reduced to 448 kW. To site an example, a PV size of 1.344 MW has 3 installations, each of 448 kW PV plant, and this results in an increase in voltage of 1.01 p.u at bus-index 536 with a 53% network capacity improvement. The RVC% in this case is still within the 3% range indicating an acceptable configuration.

Table 4.1: Normal feeder peak load results with different PV sizes connected at bus-index 536 (at 50% of feeder length)

PV size At 50% of feeder	Voltage before (p.u)	Voltage after (p.u)	Initial Loading at source substation	Final Loading at source substation	Capacity Improvement (as per equation 4.1)	Rapid Voltage Change%
0.448 MW	0.985	0.99	2.6 MW, 1 MVAR	2.1 MW, 1 MVAR	19%	1%
1.344 MW	0.985	1.01	2.6 MW, 1 MVAR	1.2 MW, 1 MVAR	53%	2.72%
1.4 MW	0.985	1.01	2.6 MW, 1 MVAR	1.2 MW, 1 MVAR	54%	3%

Figure 4.4 shows the corresponding voltage profile (plotted in p.u on the y-axis) from the base case (no PV) to the 1.4 MW increase in PV generation. The voltage graphs are plotted from the MV source substation (distance in km on the x-axis) to the end-of-line (EOL). This in practical terms can allow up to >1000 households to be connected or alternately provide power to several electric vehicle charging points.

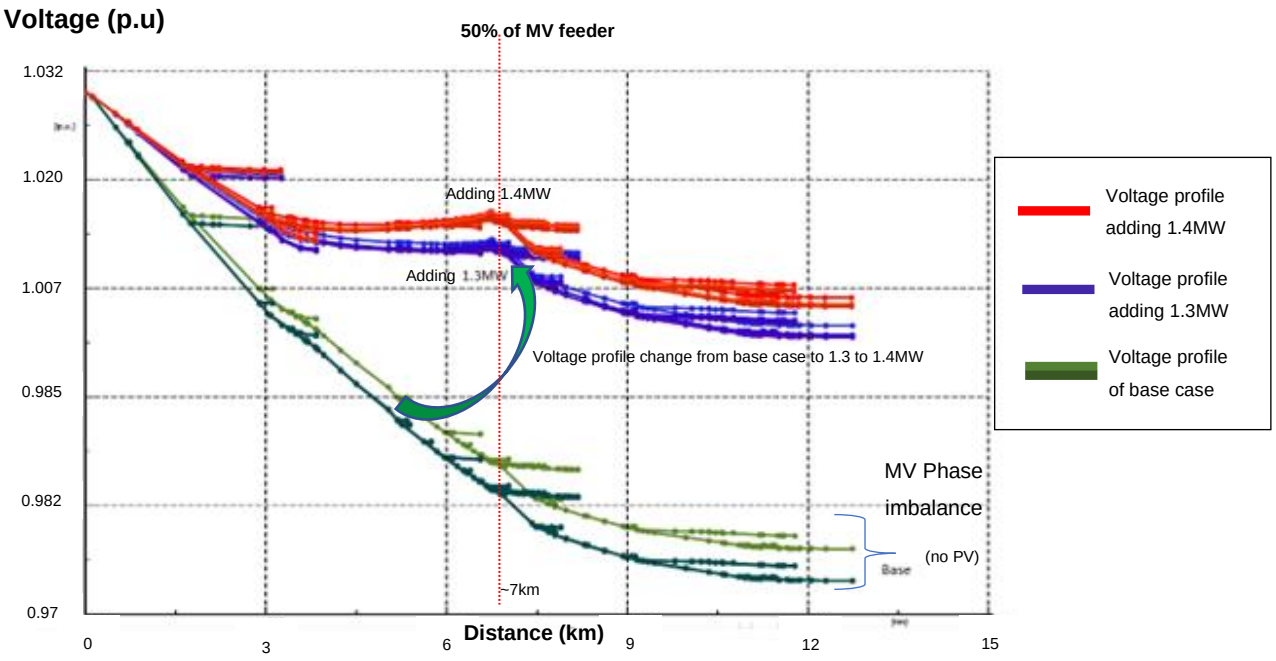

Figure 4.4: Normal feeder peak load: Voltage profile for Network 1 for base case and integration of different PV sizes at 50% feeder location

Figure 4.4 shows that the voltage profile has improved from the base case to when the PV systems were connected at half-way down the feeder. The base case is represented in this figure by two green curves each representing a single and two (2) phases of the network. In Network 1, two phases are almost balanced but as seen in Figure 4.4, the light green phase is rather unbalanced, i.e., more load is connected to this phase. This could be due to incomplete phase balancing projects or non-technical losses loading this phase. Each voltage per unit value has shown improvement at each point on the network (the graph colours differentiate the base case from the PV-connected cases). Connection of 1.344 MW (blue graph) and 1.4 MW (red graph) PV connections do lead to appreciable voltage improvement along the feeder even though the feeder in the base case is not completely balanced phase-wise. As the RVC approximated 3% the entire improvement in the voltage profile is still within the technical limitations for up to 1.4 MW PV connection.

On Network 1, the MV backbone compared to other rural loaded networks is relatively strong, i.e., the conductors used have low impedances and as such only voltage limits are the constraint here. The substation loading also referred to as the maximum demand when divided by the sum of each individual customer maximum demand presents the *factor of coincidence*. During light loaded conditions a typical coincidence factor of 0.2-0.4 is used to approximate the overall feeder loading and as that this feeder has a good portion of industrial load connected, 0.4 coincidence factor is acceptable to be used.

4.1.1.2 Normal feeder light load

As in the previous scenario, PV with different sizes are connected at 50% of the MV feeder at bus-index 536. A scaling factor of 0.4 is used to multiply normal feeder loading to simulate a light load condition while the study is executed. As previously indicated, once the relevant RVC% value of 3% is reached, results presented in Table 4.2 show that 1.6 MW capacity of PV generation can be connected at lightly loaded conditions with no power quality issues. Equation 4.1 is used to calculate the network capacity improvement at each different PV size in Table 4.2. To site an example, a PV size of 0.9 MW has 2 installations (each of 448 kW) and results in an increase in voltage to 1.03 p.u at bus-index 536 with an 81% network capacity improvement. The RVC% remains within the 3% range to be an acceptable configuration.

Figure 4.5 shows the relative voltage profiles and voltage improvement for the base case and with different PV capacities connected at half-way down the feeder. This figure indicates that the profile has improved from the base case (no PV) to cases where the PV was connected at 50% of the network. However, at light load, all voltage values (in p.u) are increased so the voltage rise seen by the PV installation then becomes critical on its position and magnitude. It was found that the there was a relatively larger voltage rise (voltage in p.u on the y-axis) due to the amount of load been much less than in peak load conditions. The voltage profile is plotted from the MV source substation to the EOL.

The base case is represented by two colours as explained in the previous section. Connecting 1.3 MW of PV generation, the voltage profile is represented by the blue curve in Figure 4.5. In Figure 4.6, however, the voltage profile curve for 1.6 MW PV connection in the feeder is seen to be quite sensitive due to the drastic voltage rise seen during light loading condition, when PV generation is connected at 50% of the the feeder length. Due to different y-axis scales, the comparison is shown on two different graphs.

Also, in Table 4.2, the source loading is negative (-) implying that power is been exported upstream into the MV source substation. In this case, several factors have to be considered, such as, are the MV/LV transformers capable of allowing the export generation as most are configured to be protected to trip on reverse power? And does the export magnitude of generation increase upstream system losses? The former can be managed and some work may be needed in this case to re-configure or bypass the reverse power protection. The latter factor is dependent of the strength of the distribtuion system and has to be assesed on a case by case study. It is to be noted here that all PV installations must conform to the specifications set out in NRS097 documents for embedded generation specifically PV.

All installations that have no back-up battery storage require the electrical grid to operate and synchronize and as such, require a connection agreement with the utility. The installation then becomes un-authorized if non-compliance is observed and the system needs to be disconnected off the network. Concurrently, a technical study by the utility has to be completed to address the export power and quantify the scope of work and cost required to allow the export of the excess generation. However, there are many cases where this is problematic in that not all installations are declared to be functional and ways to resolve this significant safety issue is still being addressed [35] [36].

This study in this section, has the advantage to provide network capacity during the times when PV is at its strongest as typical peak load on most feeders occur during the early mornings and late evenings where PV is at its weakest. A typical application of this has been discussed in Chapter 2 where electric vehicle charging infrastructure can charge vehicles during those times allowing the utilization of relevant cost-reflective tariffs for the customer or charging hub owner. In this particular feeder of Network 1, majority of load is classified industrial, meaning that the times of operation provide a peak load different from that of rural feeders.

As mentioned in the literature review, rural feeders have a typical coincidence factor of 0.2-0.3 of the feeder installed capacity and have peak loads similar to residential behavioural load patterns. Hence, *PV to industrial customers can be of great benefit during light and normal load conditions*. Also, a supplement to the existing conventional supply is also of great benefit where loadshedding can assist customers that rely on power for their daily operations, a scenario that would always persist in the current depleting coal-fired power generation.

Table 4.2: Normal feeder light load results with PV connected at bus-index 536 (50%)

PV size at 50% of feeder	Voltage before (p.u)	Voltage after (p.u)	Initial Loading at source substation	Final Loading at source substation	Capacity Improvement (as per equation 4.1)	Rapid Voltage Change%
0.448 MW	1.01	1.02	1.1 MW, 0.4 MVAR	0.6 MW, 0.4 MVAR	45%	0.9%
0.9 MW	1.01	1.03	1.1 MW, 0.4 MVAR	0.2 MW, 0.4 MVAR	81%	1.75%
1.3 MW	1.01	1.04	1.1 MW, 0.4 MVAR	-0.3 MW, 0.4 MVAR	127%	2.56%
1.6 MW	1.01	1.04	1.1 MW, 0.4 MVAR	-0.5 MW, 0.4 MVAR	145%	3%

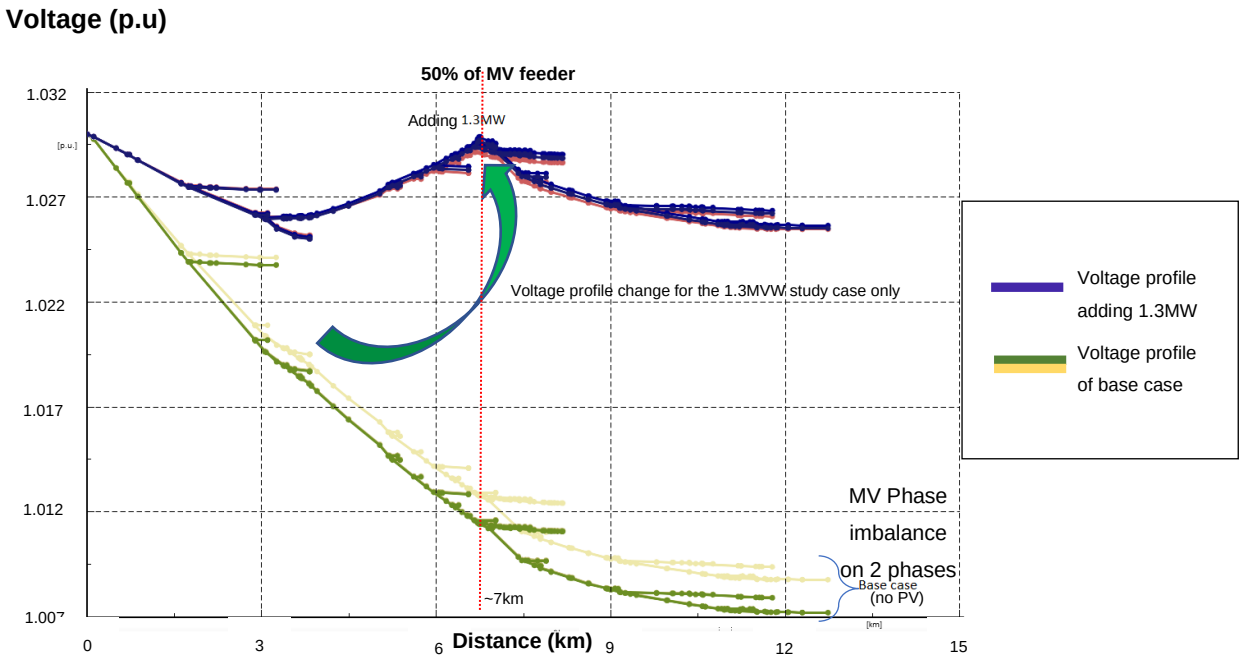

Figure 4.5: Normal feeder light load: Voltage profile of base case and 1.3 MW PV integration at 50% feeder location

The studies covered in sections 4.1.1.1 to 4.1.1.2 have focused on a typical conventional 11 kV network. There are many capacity constrained networks for various reasons explained in Chapter 2.

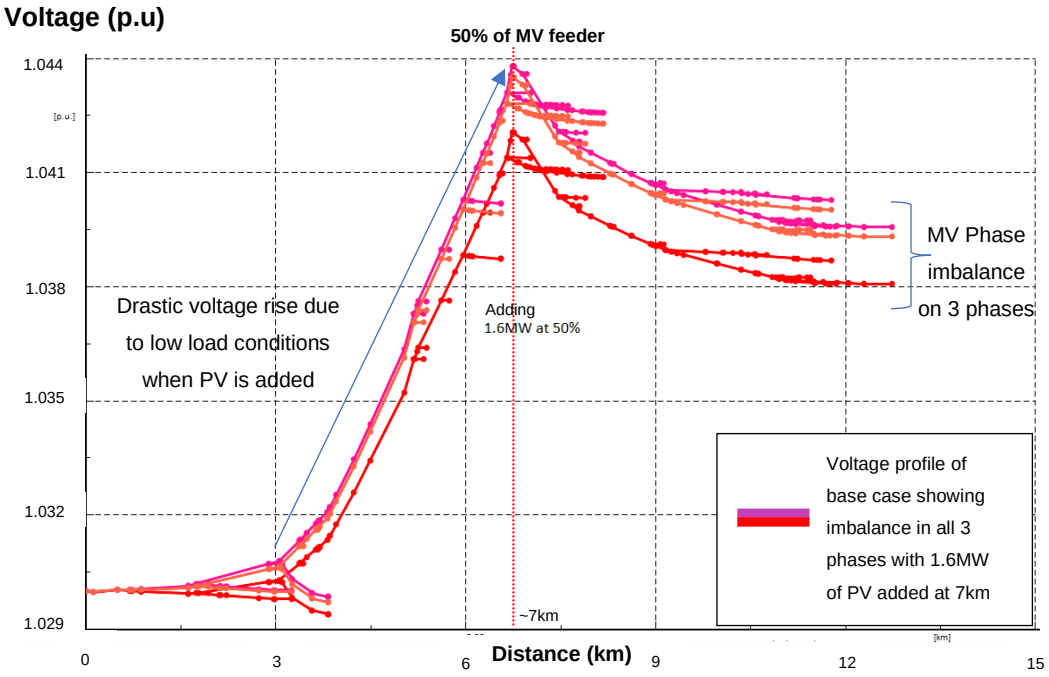

Figure 4.6: Normal feeder light load: Voltage profile of 1.6 MW PV integration at 50% feeder location

The next set of studies are also modelled during peak and off-peak conditions and at 50% down the feeder backbone from the MV source substation (~7 km). The only change in the MV feeder model is that each load has been scaled up such that the network voltage profile during peak load conditions is below the 0.95 p.u value.

4.1.1.3 Constrained feeder peak load

Table 4.3 of results shows that connecting 1.44 MW of PV improves the network capacity by 38% and voltage to 1.0 p.u while RVC remains at an acceptable value of 3%. For lower PV capacities integrated, network capacity improvement of 13% and RVC of 1% is achieved for 0.448 MW PV integration while an improvement of RVC close to 3% is seen when three times the amount of PV is added. On this constrained network, the initial source loading is 3.7 MW scaled up from 2.6 MW to achieve an EOL voltage of just below 0.95 p.u as per constrained feeder definition [33] [51] and as explained in the previous sections.

Table 4.3: Constrained feeder peak load

PV size at 50% of feeder	Voltage before (p.u)	Voltage after (p.u)	Initial Loading at source substation	Final Loading at source substation	Capacity Improvement (as per equation 4.1)	Rapid Voltage Change%
0.448 MW	0.97	0.97	3.7 MW, 1.5 MVAR	3.2 MW, 1.5 MVAR	13.5%	1%
1.3 MW	0.97	0.99	3.7 MW, 1.5 MVAR	2.4 MW, 1.5 MVAR	35%	2.77%
1.44 MW	0.97	1.0	3.7 MW, 1.5 MVAR	2.3 MW, 1.5 MVAR	38%	3%

Figure 4.7 shows the corresponding relevant voltage profile of Network 1 with 1.44 MW of PV generation connected at approximately 7 km down the feeder. It should be noted here that for both loading conditions (*normal peak and constrained peak),* the PV input result is the approximately same but the network capacity is different and *lower* in the constrained network. The shape of the curve is therefore exactly the same due to the linear scaling of the current loads. It is apparent that for any particular network type, the RVC% calculation is first significant in determining the maximum amount of PV that can be connected to an MV network and should therefore be checked first prior to checking voltage and/or thermal issues. The next section models Network 1 with scaled up loads to reach just below 0.95p.u EOL voltage and is then checked during light loaded conditions.

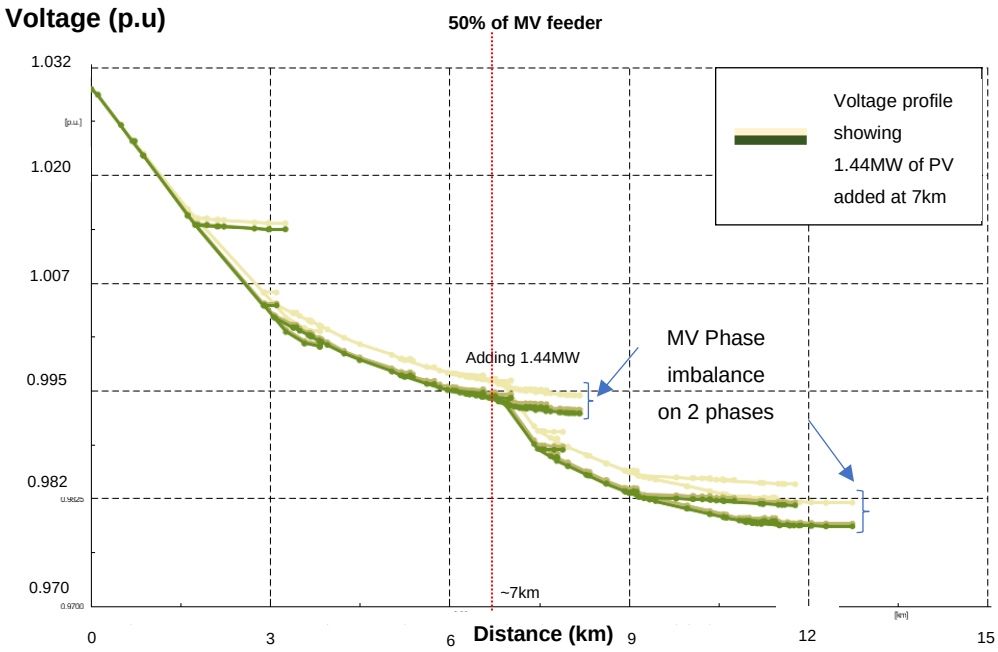

Figure 4.7:Constrained feeder peak load: Voltage profile of 1.44 MW PV integration at 50% feeder location

4.1.1.4 Constrained feeder light load

On this constrained network, the initial source loading as explained in section 4.1.1.1 is 1.5 MW scaled down by a factor of 0.4 from 3.7 MW, to achieve an EOL voltage just below 0.95 p.u as per constrained feeder definition [33] [51]. The EOL of 0.95 p.u is the normal voltage limit set by the NRS048 regulator standard.

Results in Table 4.4 show that when integrating PV at 50% down the feeder, 1.3 MW of PV generation improves the network capacity by 87% while the RVC value of 2.5% remains within limits. Adding another PV installation and reducing the generation output to achieve 1.56 MW, connected to bus-index 536, resulted in 106% network capacity improvement while 60 kVA of power is exported upstream into the MV source. The capacity improvement is lower than the previous study of section 4.1.1.2 of 145% in Table 4.2. Figure 4.8 shows the resulting voltage profile improvement of integrating 1.56 MW of PV generation and is seen to be within set legal limits (< 1.06 p.u). The resultant voltage profile (green colour graph) follows a similar shape in the normal light load scenario (Figure 4.6) as the loads are scaled linearly. Under this scenario, as explained in the previous sections, reverse power into the upstream network has to be technically accounted for in terms of enabling or disabling the flow of excess PV generation.

Table 4.4: Constrained feeder light load

PV size at 50% of feeder	Voltage before (p.u)	Voltage after (p.u)	Initial Loading at source substation	Final Loading at source substation	Capacity Improvement (as per equation 4.1)	Rapid Voltage Change%
1.3 MW	1.0	1.03	1.5 MW, 0.6 MVAR	0.2 MW, 0.6 MVAR	87%	2.52%
1.56 MW	1.0	1.04	1.5 MW, 0.6 MVAR	-0.06 MW, 0.6 MVAR	106%	3%

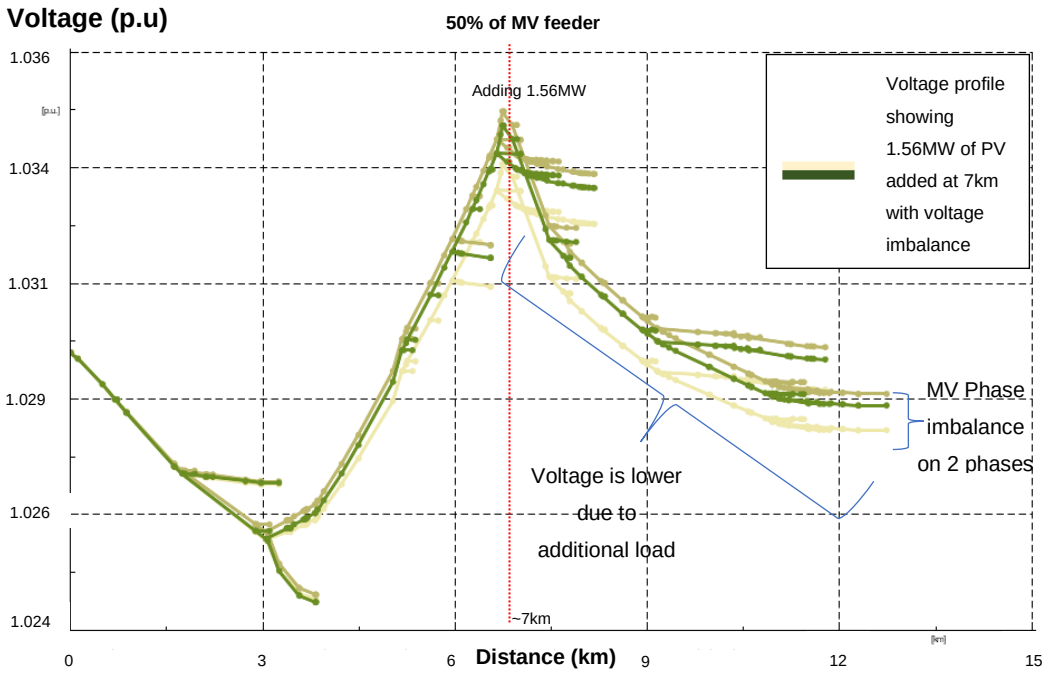

Figure 4.8: Constrained feeder light load: Voltage profile of 1.56 MW PV integration at 50% feeder location

4.1.2 Connecting PV at the End-of-line (EOL) of the MV feeder

All the simulations done so far have considered the middle part of the network for connecting the PV systems and modelled Network 1 with different sizes of PV plant integration at 50% feeder location. The next set of simulations looks at connecting PV to the end of Network 1, i.e., at the End-of-Line (EOL) which means at 100% of the MV feeder length (~13 km backbone, as per geographic in chapter 3, Figure 3.8). In this case, EOL is simulated as the bus-index RMSL14 in the 11 kV network with a scaling factor of 1.0 for peak load and 0.4 for light load. Similar to section 4.1.1, different scenarios of normal and constrained network operation with peak and off-peak or light load variations are modelled and simulated in this study case. As in the previous section, normal network refers to those that operate with no

voltage or thermal limit issues during peak and off-peak times and constrained networks either have voltages under normal limits (<95% as defined by NRS048) or have conductors with thermal issues due to load growth or non-technical energy losses due to theft and meter tampering.

4.1.2.1 Normal feeder peak load

Network 1 is now modelled as per section 4.1.1.1 with the same scaling factors but with the exception that PV systems are connected at the EOL instead of 50% feeder location. Table 4.5 shows the results at peak load with different capacity PV systems connected at the EOL.

In this study, connecting 0.448 MW of PV generation resulted in 19% network capacity improvement while the RVC value remains at an acceptable low of 2%. Adding another PV installation by increasing the number of units of the PV template, and lowering the generation output by 10%-20%, it is found that only 0.65 MW of PV generation can be connected to the network EOL before RVC of 3% is exceeded.

Figure 4.9 shows only the corresponding voltage profile when 0.65 MW of PV generation is added at EOL. The resultant curve becomes more parabolic as the amount of generation increases and the curve eventually reaches the 1.06 p.u mark. The network capacity in this case is relatively lower than any other scenario previously modelled (almost half compared to when PV systems were connected halfway down the feeder) due to high RVC values. This gives a clear indication of the MV network strength at the EOL. This implies that the impedance is relatively high at this part of the MV backbone (13 km down Network 1) than upstream conductor sizes due to older radial network designs and as a result the fault level is relatively lower. If the backbone conductor was consistently the same throughout the feeder, more network capacity could be achieved. However, it must be mentioned here that if the potential of a renewable project such as a PV plant requires to be connected within this lower part of the network, mitigation plans to technically accommodate the set size of the PV plant must be put in place and designed suitably to accommodate this project. Once such solution would be to decrease the impedance by upgrading the weak part of the existing MV backbone. In some cases this would mean a new build or re-build of the existing line and would therefore have a cost implication to the project.

Table 4.5: Normal feeder peak load

PV size at EOL	Voltage before (p.u)	Voltage after (p.u)	Initial Loading at source substation	Final Loading at source substation	Capacity Improvement (as per equation 4.1)	Rapid Voltage Change%
0.448 MW	0.98	1.0	2.6 MW, 1 MVAR	2.1 MW, 1 MVAR	19%	2%
0.650 MW	0.98	1.0	2.6 MW, 1 MVAR	1.9 MW, 1 MVAR	27%	3%

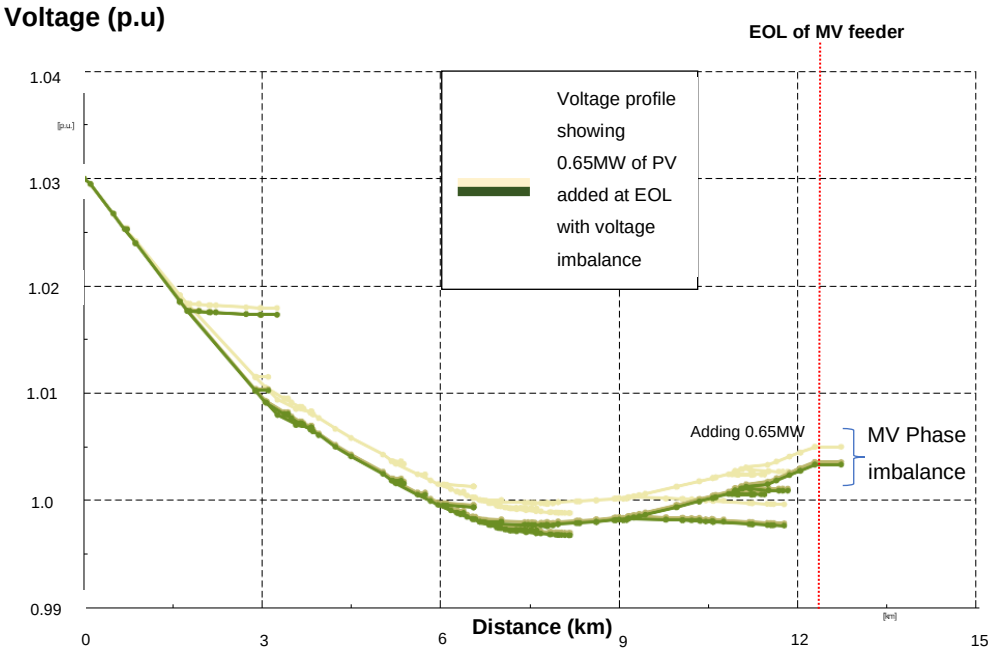

Figure 4.9: Normal feeder peak load: Voltage profile of base case and 0.65 MW PV integration at feeder EOL

4.1.2.2 Normal feeder light load

As in the previous sections, a scaling factor of 0.4 is used to multiply normal feeder loading to simulate a light load condition while this study is executed. As indicated earlier, once the relevant RVC% value of 3% is reached, results presented in Table 4.6 show for EOL bus-index RMSL14, only 0.7 MW capacity of PV generation can be integrated at this point with no power quality issues. Utilizing equation 4.1, network capacity improvement is found to be 63% but with no more generation as compared to peak load conditions. The relevant voltage profile for the EOL connection is shown in Figure 4.10. With 0.7 MW connected to the EOL, the profile is parabolic compared to the base case and it can be seen that even if RVC% was not an issue, the voltage limit of 1.06p.u would be quickly reached for the voltage rise due to this

weak part of the network. Due to the RVC% calculation approximating around 3%, no export of power is seen as in the previous case of connecting PV at 50% during light load conditions. This is due to the location of the PV not connected close enough to the MV source substation and as such due to the length of the MV backbone, connected load would sink whatever PV is connected at the EOL resulting in a cap of the magnitude of PV size due to high RVC values. In the development of the DPL code, this once again highlights the sequence of studies that first determines the limits of calculating PV integration to an MV network, i.e., RVC is checked first, then voltage and lastly thermal tests.

Table 4.6: Normal feeder light load

PV size at EOL	Voltage before (p.u)	Voltage after (p.u)	Initial Loading at source substation	Final Loading at source substation	Capacity Improvement (as per equation 4.1)	Rapid Voltage Change%
0.3 MW	1.01	1.02	1.1 MW, 0.4 MVAR	0.8 MW, 0.4 MVAR	27%	1.3%
0.7 MW	1.01	1.04	1.1 MW, 0.4 MVAR	0.4 MW, 0.4 MVAR	63%	2.97%

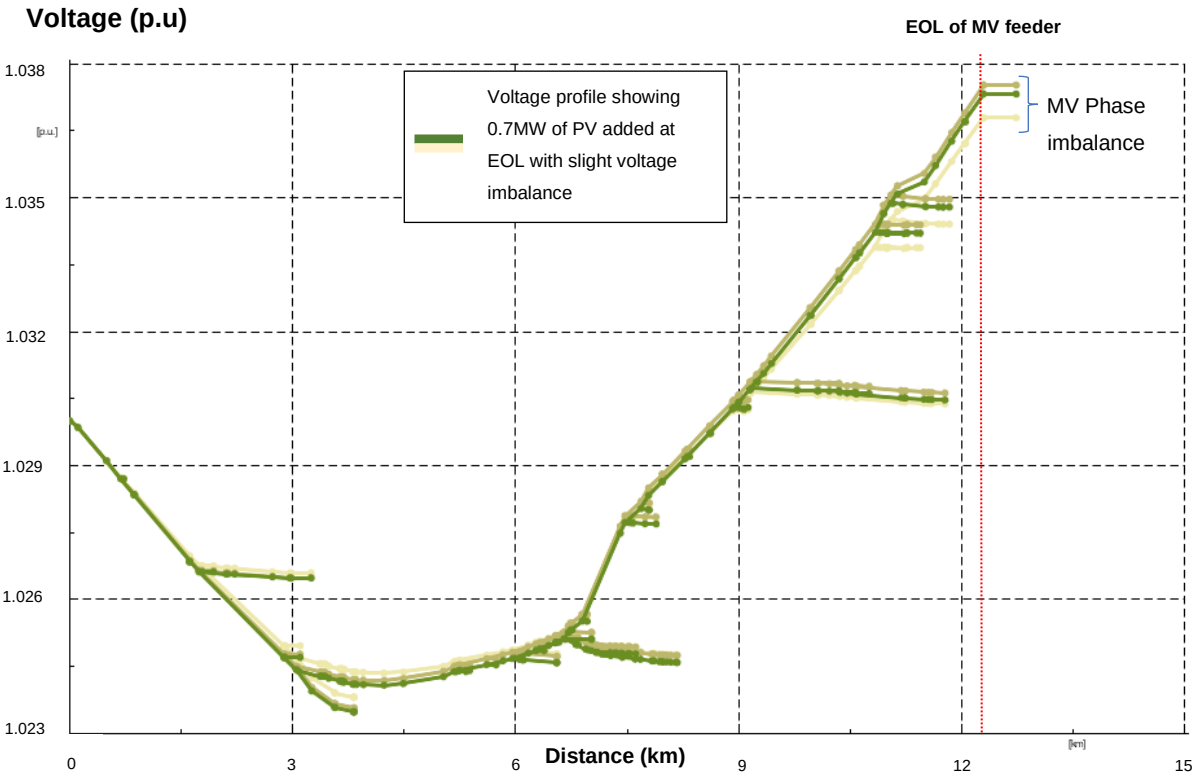

Figure 4.10: Normal feeder light load: Voltage profile of 0.7 MW PV integration to feeder EOL

As per previous studies, the next sets of results have been applied to a constrained network. The resultant voltage profiles are very similar to Figures 4.9 and 4.10 and are therefore omitted

as that the loads are scaled linearly. Only the capacity improvement changes due to connecting PV generation to the feeder are documented in Tables 4.7 and 4.8. Sections 4.1.2.3 to section 4.1.2.4 are modelled and documented for completeness to the study.

4.1.2.3 Constrained feeder peak load

Table 4.7 indicates that 0.64 MW PV generation added to the EOL of network feeder 1 resulted in a slight network capacity improvement of 16.2% as the RVC value of 3% was quickly reached.

Table 4.7: Constrained feeder peak load

PV size at EOL	Voltage before (p.u)	Voltage after (p.u)	Initial Loading at source substation	Final Loading at source substation	Capacity Improvement (as per equation 4.1)	Rapid Voltage Change%
0.448 MW	0.95	0.97	3.7 MW, 1.5 MVAR	3.2 MW, 1.5 MVAR	13.5%	2.15%
0.64 MW	0.97	0.98	3.7 MW, 1.5 MVAR	3.1 MW, 1.5 MVAR	16.2%	3%

4.1.2.4 Constrained feeder light load

Table 4.8 indicates that 0.7 MW PV generation added to the EOL in the network feeder 1 resulted in a better network capacity improvement of 47% as the RVC value of 3% was also quickly reached.

Table 4.8: Constrained feeder light load

PV size at EOL	Voltage before (p.u)	Voltage after (p.u)	Initial Loading at source substation	Final Loading at source substation	Capacity Improvement (as per equation 4.1)	Rapid Voltage Change%
0.7 MW	1.0	1.03	1.5 MW, 0.6 MVAR	0.8 MW, 0.6 MVAR	47%	2.94%

Both network capacity improvements in Table 4.7 and Table 4.8 are relatively lower than in the normal network models due to the linear scaling of all loads, but what is of significance is, the approximate amount of PV generation that can be integrated at the EOL is approximately *constant*. This implies that the impedance of the MV line, especially throughout the MV backbone, is critical in determining the amount of voltage rise when a considerable amount of

PV generation is added and shown in the literature review of chapter 2. As that upgrading long lengths of MV conductor to lower impedance conductors, is not cost effective, other mitigation solutions such as new MV injections from proximity networks would assist. The next section therefore investigates adding PV to 50% down the MV feeder and the EOL and then to calculate the network capacity from the results obtained.

4.1.3 Connecting PV at 50% of the MV feeder and at End-of-Line of the MV feeder

Sub-sections 4.1.1 and 4.1.2 tested Network 1 with PV connected at 50% of the MV network down the feeder backbone (~7 km) and at the EOL (~13 km) respectively. The next set of simulations involves connecting PV systems both at 50% *and* at EOL of the MV feeder. The same study cases as per the previous sections apply.

4.1.3.1 Normal feeder peak load

At 50% of the MV network feeder 1 (please see Figure 3.8 in Chapter 3 for geographic overview of feeder 1), the MV terminal is again the bus-index 536 and at the End-of-Line (EOL) i.e. 100% of the MV feeder length (~13 km backbone) is bus-index RMSL14 in the 11 kV network with a scaling factor of 1.0 for peak load and scaling factor of 0.4 for light load.

In the simulations that follow, there were no backbone feeder thermal issues in all the PV capacity variations. Once the RVC reaches 3% the final capacity improvement would therefore be determined as this is the limit for varying the PV generation (NRS097) as applied to all previous simulations as well.

Table 4.9 shows the results of both injections and Figure 4.11 shows the relevant voltage profile. In Table 4.9, results indicate the total installed PV generation to Network 1 without any RVC issues would be 1.34 MW with a network capacity of 54%. When comparing this result to the installation of PV at 50% and EOL of the feeder under the normal network peak load, it is seen that the RVC value of 3% is reached quicker as the amount of PV generation at the EOL is limited at 0.14 MW.

Table 4.9: Normal feeder peak load – 50% feeder location and EOL

PV size located at	Voltage before (p.u)	Voltage after (p.u)	Initial Loading at source substation	Final Loading at source substation	Capacity Improvement (as per equation 4.1)	Rapid Voltage Change%
1.2 MW at 50% and 0.14 MW at EOL	0.99	1.00	2.6 MW, 1 MVAR	1.2 MW, 1 MVAR	54%	3%

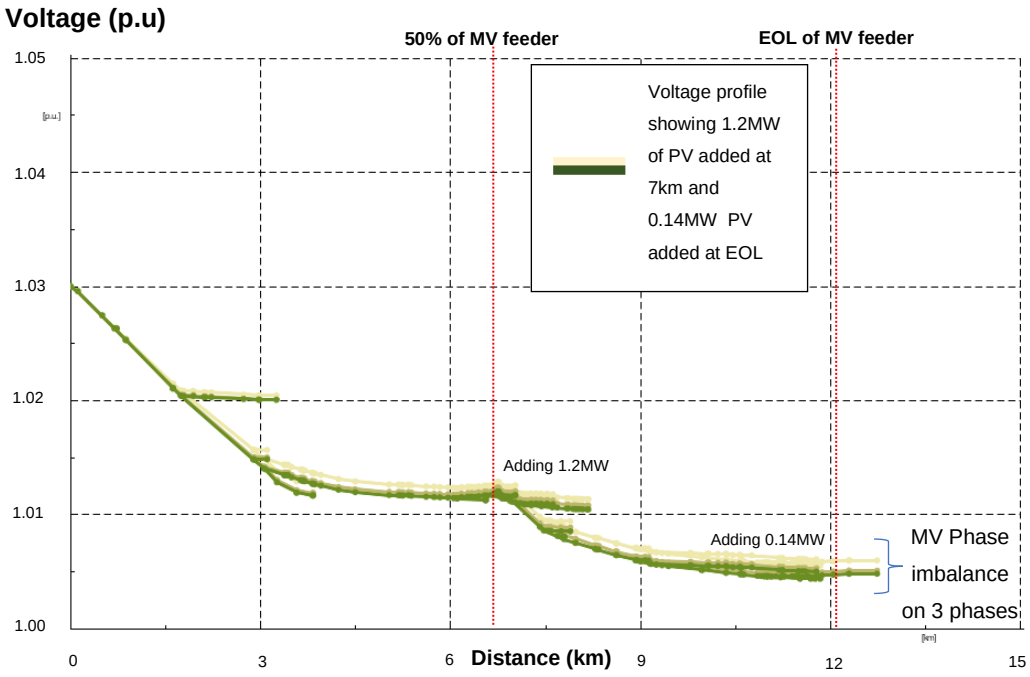

Figure 4.11: Normal feeder peak load: Resultant voltage profile of 1.2 MW PV connected at 50% feeder location and 0.14 MW PV connected at EOL

In Figure 4.11, both injections are shown with RVC the determining factor on the penetration levels of PV on MV networks. Sections 4.1.3.2 to 4.1.3.4 show the results for the remaining three scenarios.

4.1.3.2 Normal feeder light load

A scaling factor of 0.4 is used to multiply normal feeder loading to simulate a light load condition while the study is executed. As previously indicated, once the relevant RVC% value of 3% is reached, results are presented in Table 4.10.

Table 4.10: Normal feeder light load – 50% feeder location and EOL

PV size	Voltage before (p.u)	Voltage after (p.u)	Initial Loading at source substation	Final Loading at source substation	Capacity Improvement (as per equation 4.1)	Rapid Voltage Change%
1.2 MW at 50% And 0.2 MW at EOL	1.01	1.04	1.1 MW, 0.4 MVAR	-0.3 MW, 0.4 MVAR	127%	3%

Table 4.10 shows the results of both injections and Figure 4.12 shows the resultant voltage profile. In Table 4.10, results indicate that by installing PV at both parts of the network, the network capacity is increased, however, PV connected to half-way down the feeder was a major factor in this increase. As per previous results in Table 4.9, the amount of PV connected at the EOL is not as significant in this location where other PV installations are connected closer to the load demand. In Figure 4.12, the resultant voltage profile is very similar to the graph in Figure 4.6 while the connected PV at 50% is slightly lower. The total PV connected is 1.4 MW in this scenario.

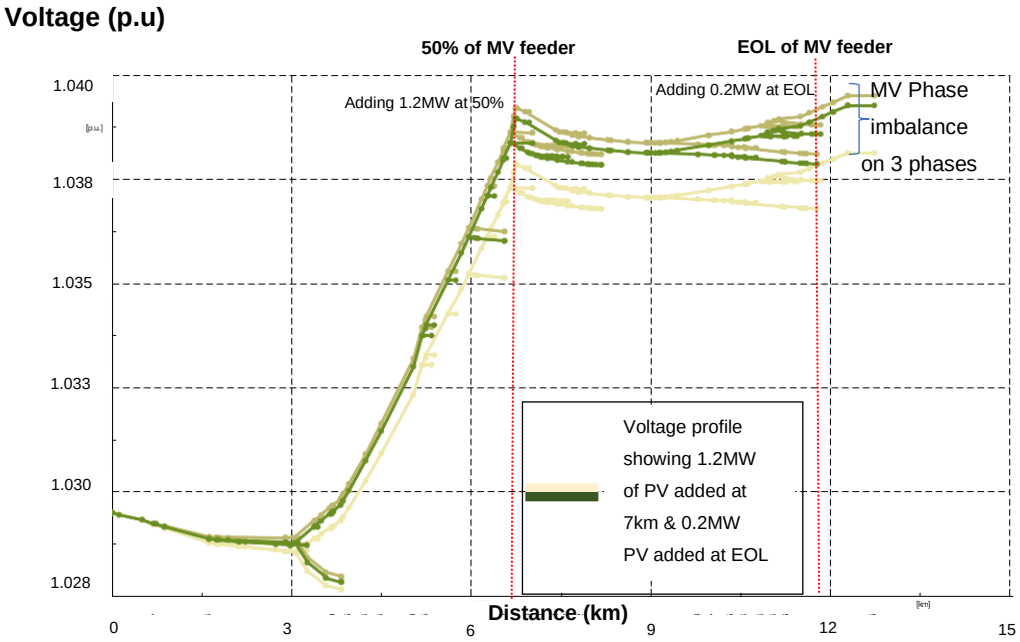

Figure 4.12: Normal feeder light load: Resultant voltage profile of 1.2 MW PV connected at 50% feeder location and 0.2 MW PV connected at EOL

As per previous studies, the next sets of results have been applied to a constrained network. The constrained feeder loads are scaled up as explained in section 4.1.1. PV generation is again connected at 50% down the feeder network and at the EOL.

4.1.3.3 Constrained feeder peak load

Table 4.11 shows the results of both injections and Figure 4.13 shows the corresponding resultant voltage profile. In Table 4.11 results indicate the total installed PV generation to Network 1 with RVC values of 2.96% and 3% would be 1.4 MW with a network capacity improvement of 35%. *It must be noted that in this study case the voltage p.u value and RVC % value are different in each location (2.96% for 1.2 MW PV at 50% and 3% for 0.2 MW PV at EOL) and as such are shown in different rows in Table 4.11 albeit PV is connected at both locations.* In Figure 4.13, the resultant voltage profile improves all voltages throughout the network and exhibits similar behaviour in the nature of the curve as in the normal load scenario.

Table 4.11: Constrained feeder peak load – 50% and EOL

PV size *1.2 MW at 50% and 0.2 MW at EOL*	Voltage before (p.u)	Voltage after (p.u)	Initial Loading at source substation	Final Loading at source substation	Capacity Improvement (as per equation 4.1)	Rapid Voltage Change%
At 50%	0.97	0.99	3.7 MW, 1.5 MVAR	2.4 MW, 1.5 MVAR	35%	2.8%
At EOL	0.95	0.98	3.7 MW, 1.5 MVAR	2.4 MW, 1.5 MVAR	35%	3%

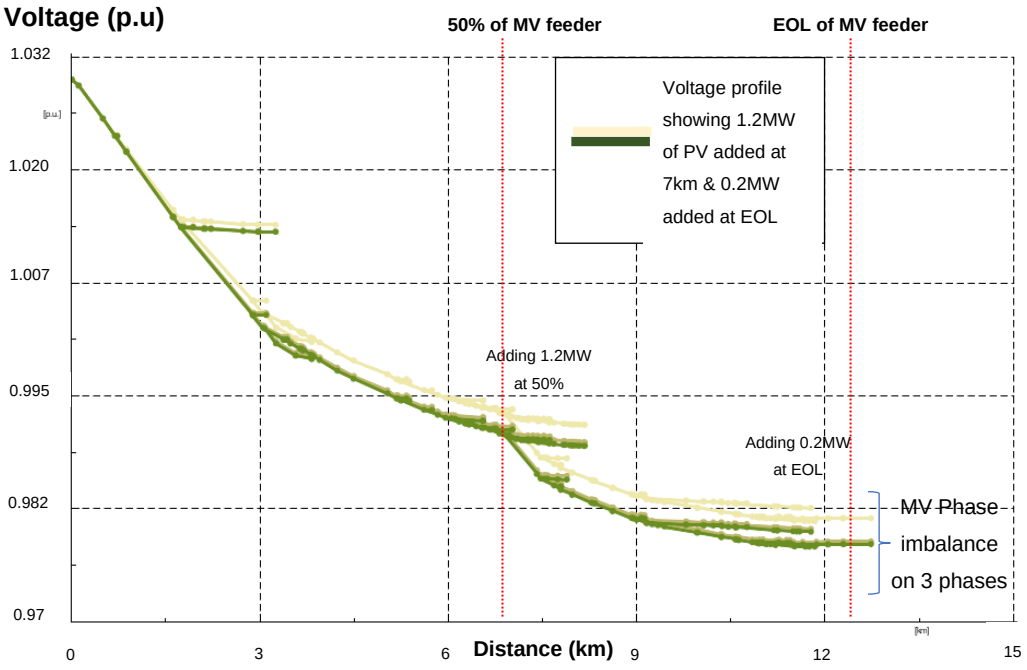

Figure 4.13: Constrained feeder peak load: Resultant voltage profile of PV connected to 50% and EOL during peak conditions

4.1.3.4 Constrained feeder light load

Table 4.12 shows the results of both integrating points and Figure 4.14 shows the resultant voltage profile. In Table 4.12 results indicate the total network capacity improvement is 93% when 1.4 MW of PV is connected to the network. *Only the RVC % value is different at each location with both PV systems connected simultaneously and as such are shown in different rows in Table 4.12 to show this difference.* In Figure 4.14, the resultant voltage profile improves all voltages but reaches the 1.06 p.u limit very quickly as per the light loaded scenario behaviour identified in the previous simulations. This implies that voltage fluctuation is far more sensitive when it comes to PV integration at the EOL as shown in Figure 4.6 as well.

Table 4.12: Constrained feeder light load – 50% and EOL

PV size *1.2 MW at 50% and 0.2 MW at EOL*	Voltage before (p.u)	Voltage after (p.u)	Initial Loading at source substation	Final Loading at source substation	Capacity Improvement (as per equation 4.1)	Rapid Voltage Change%
At 50%	1.0	1.03	1.5 MW, 0.6 MVAR	0.1 MW, 0.6 MVAR	93%	2.71%
At EOL	1.0	1.03	1.5 MW, 0.6 MVAR	0.1 MW, 0.6 MVAR	93%	2.95%

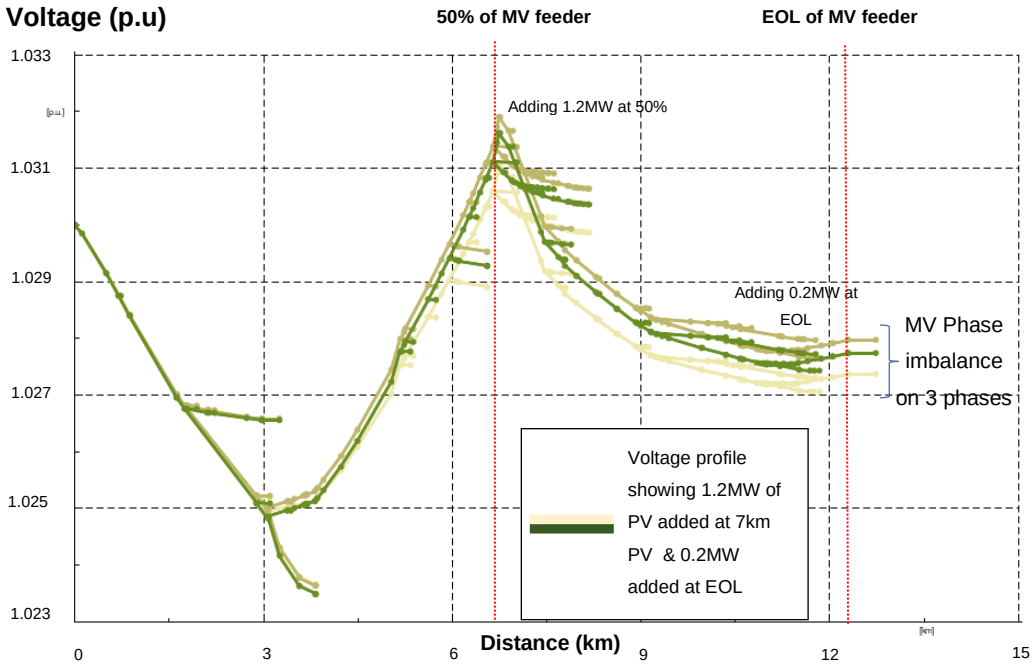

Figure 4.14: Constrained feeder light load: Resultant voltage profile for the constrained feeder in light load conditions – 50% and EOL

In the next section of 4.2, the tool is applied to the feeder network and the expected result is that the scenarios above feature in the results obtained when running the DPL script. A summary of all simulations and results are presented towards the end of this chapter.

4.2 PV placement using the PSO tool applied to Network 1

The PV placement scenarios simulated in DIgSILENT Powerfactory in the conventional manner as presented in section 4.1 to assess the network improvement, were also used to compare the effectiveness of the DPL-based PSO tool with respect to the manual method (as a reference base case). For the PSO tool, the values for the number of iterations and number of PV systems can be selected by the user in the input page of the DPL script for analysis.

In section 4.1, three PV placement configurations were considered, namely, PV systems connected halfway (50%) down the feeder, PV systems connected at the EOL and PV systems connected at 50% feeder and EOL simultaneously. In each of these configurations, the four scenarios of normal and constrained feeders with peak and off-peak (light) loadings were studied in the simulations. These same scenarios are again applied while utilizing the proposed tool to assess the network improvement with the developed DPL script.

In each scenario, the Fres matrix values are presented graphically showing the progression of the PV connection as determined by the PSO tool in the MV network. The Fres matrix has been explained in Chapter 3, Figure 3.28 where every row represents a PV system and every column for that row represents the new MV bus placement position (connection point) calculated by PSO equation (3.33). As mentioned in Chapter 3 when explaining the Fres matrix, all MV bus positions displayed graphically from the matrix is assigned a bus-index value to which the look-up table is provided in Appendix B for Network 1 and Appendix C for Network 2. The voltage profile of the feeder for the optimal PV connection point determined is displayed through an extract from the tool, and a summary of results showing values of the Ginmat matrix (please see Chapter 3, Figure 3.20), i.e. optimal connection point found, maximum PV size at that point and the source loading before and after the connection of the PV system. Lastly, the tool extract also displays the network capacity improvement in percentage calculated by the tool.

4.2.1 Normal feeder peak load scenario

For this scenario all of the feeder load is scaled as per section 4.1 with a scaling factor 1 to represent peak loading. The selected input on the DPL input page was number of PV system=1 and number of iterations=5. The *Fres* matrix values were calculated for every

iteration as per the PSO equation (3.33) in the code where each new MV bus position (i.e., PV connection point) is determined by the calculated fitness values (change in voltage [p.u]) before and after the PV connection. Figure 4.15 represents the *Fres* matrix graphically starting at iteration 1 at an initial random position of *256* (bus-index 812) and progressing through to position *268* (bus-index 853) as the code is executed from iteration 1 to iteration 6. Appendix B shows the lookup table of positions with their corresponding feeder bus-index values with the highest 1096 and is used to determine the MV percentage position along the feeder. It is to be noted that initial iteration is 1 and then 5 more iterations are executed up to iteration 6. The x-axis of Figure 4.15 gives the iteration number and the y-axis gives the MV bus-positions as calculated by the PSO equation (3.33).

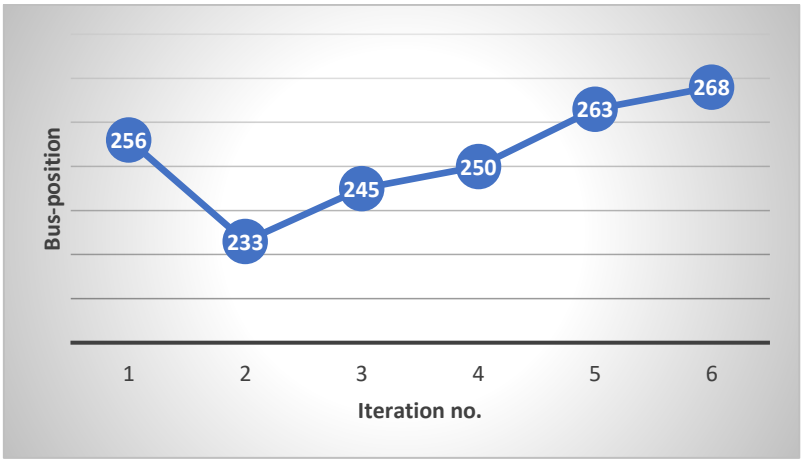

Figure 4.15: Normal feeder peak load*:* *Fres* matrix values for PV connection positions calculated from the PSO equation (PV system=1, iterations=5)

Figure 4.16 shows the tool display extract where the optimal PV connection point found for 5 iterations (2 to 6) was position 250 corresponding to a bus-index of 803. In the tool interface, as discussed in Chapter 3, the block with information highlighted in red in Figure 4.16, shows the source voltage (in this case 11 kV) and loading (2.57 MVA). As per the display, the optimal point of 250 found, to which the PV of 1 MW is connected, results in a loading of 1.44 MVA at that connection point (power factor =1). Each coloured voltage profile shown in Figure 4.16 represents the voltage profile at every new position calculated (for each column value in the *Fres* matrix) , i.e., at every iteration for the connected PV system as well as the base case. This for clarity, is extracted from the tool and is shown in Figure 4.17 where the voltage profile for the optimal point is found.

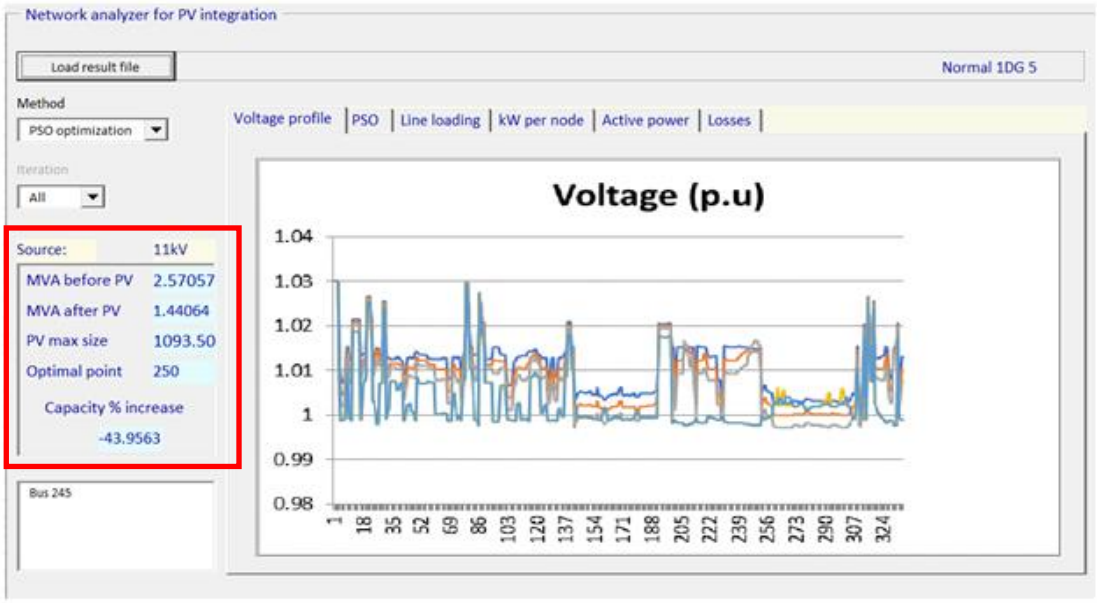

Figure 4.16: Normal feeder peak load: Extract from PSO tool (PV system=1, iterations=5)

As shown in Figure 4.17, every position as displayed in Figure 4.15 has an optimised voltage profile. The profile highlighted in red is the optimised voltage profile found for the optimal position, 250, which had the greatest change in voltage before and after the connection of the PV system (that is the greatest fitness value). Similarly, this approach has been applied to all voltage profile extracts further documented in this section. It must be noted here that the optimal point is found, only once the PV generation connected at the position in Figure 4.15, satisfies firstly the RVC requirements. The network capacity is only determined once this is completed using equation (4.1).

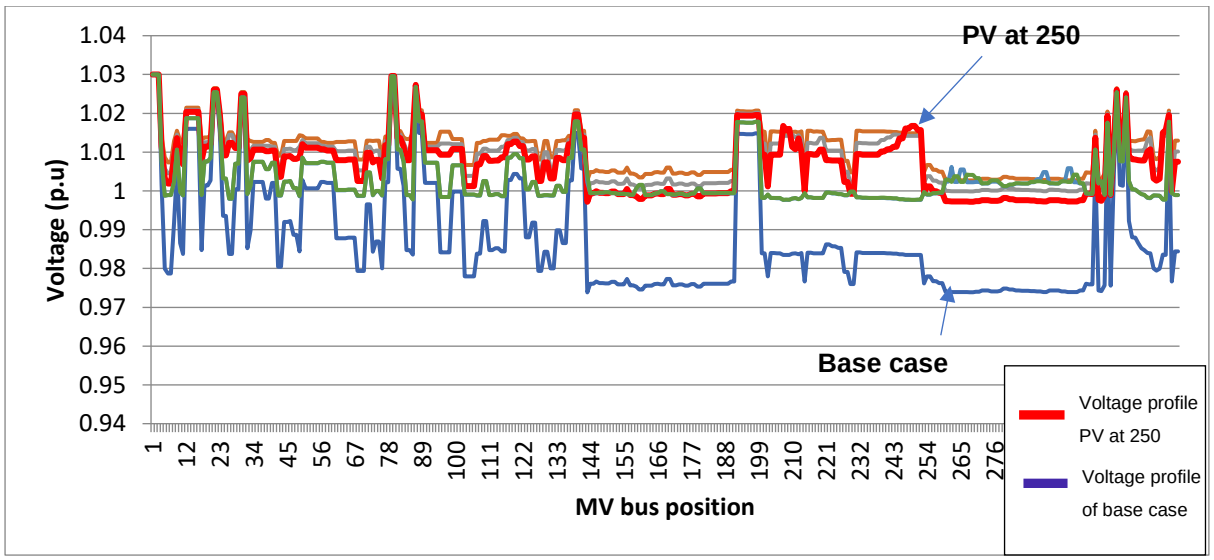

Figure 4.17: Normal feeder peak load: Feeder voltage profile with optimal PV connection point 250 (PV system=1, iterations=5)

In Figure 4.17, the plot labelled “PV at 250” shows the optimal connection position found after 5 iterations relative to the base case (before the PV connection) for Network 1. It can be seen that all the voltage profiles at MV positions (plotted along x-axis) are improved by installing PV of 1 MW. The extract of the tool results are shown in Figure 4.19. With final results of the *Ginmat* matrix, Figure 4.19 shows the before and after source loading of the connection of the PV system, maximum PV size and network capacity found. Figure 4.18 shows that all thermal line loadings are within the threshold of 85% which is set by the user [33] [34]. As mentioned previously, feeder line loadings for Network 1 are not as significant when compared to networks that have high impedance conductors. Hence Figure 4.18 shows that thermal line loadings do not exceed 40% for every new position of Figure 4.15 of the *Fres* matrix.

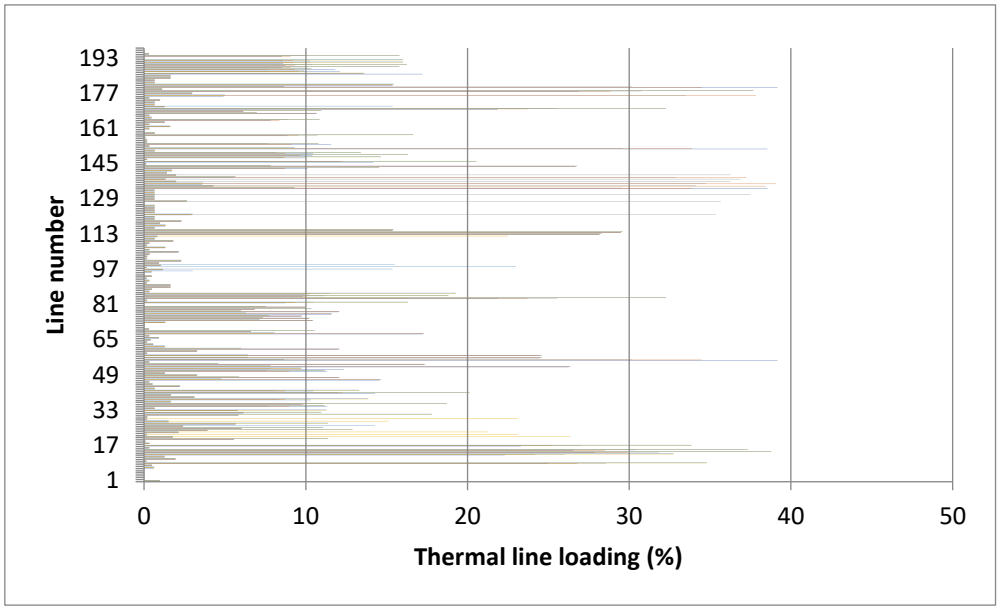

Figure 4.18: Normal feeder peak load: Thermal line loadings (PV systems=1, iterations=5)

MVA before PV	2.57057
MVA after PV	1.44064
PV max size	1093.50
Optimal point	250
Capacity % increase	-43.9563

Figure 4.19: Normal feeder peak load: PSO tool screenshot indicating the network capacity improvement of 43% (PV system=1, iterations=5)

In comparison to the conventional modelling, this scenario indicates a position 73% down the MV feeder from the MV source substation and as a result only 43% of network improvement is achieved compared to the 57% improvement achieved with conventional modelling as listed in Table 4.1 where the PV was installed at 50% i.e. halfway down the feeder in Network 1. As

mentioned above, position 250 corresponds to a bus index of 803. Hence the 73% value is calculated as 803/1096x100% which is equal to optimal point divided by the highest bus-index and computed for all scenarios and calculations and multiplied by 100.

To further test this network, the next selected input was modelled to have PV system=5 and number of iterations=10. The *Fres* matrix values were calculated for every iteration. It can be seen in Figure 4.20 that the displayed values converge to a particular MV connection position when more than 1 PV system is added, and the PV system in this figure *only* is plotted on the x-axis to display this convergence with each colour representing a different iteration. For example, in Figure 4.20, the graph labelled 'A' represents iteration 1. PV system 1 is connected at random position 66, PV system 2 is connected at random position 181, PV system 5 at random position 213 and so forth. At each of these random positions, the next position is calculated using equation (3.33) of Chapter 3 to populate the *Fres* matrix, so PV system 5 at position 213 moves to 164, then 145 and so forth for each PV system. Each transition to a new position for each PV system starts converging to position 65.

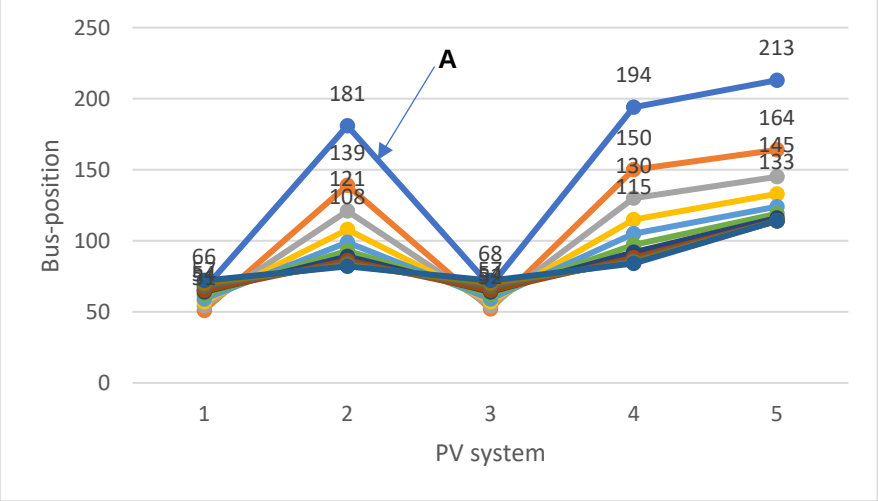

Figure 4.20: Normal feeder peak load*: Fres* matrix values for PV connection positions calculated from the PSO equation (PV system=5, iterations=10)

The voltage (p.u) profiles of the feeder network and the improvement at the iteration with the optimal connecting position found, is shown in Figure 4.21. The plot labelled "PV at 65" shows the optimised voltage profile (out of 5) for the iteration that determined the optimal location for installing PV to be position 65. It can be seen that the voltage profiles at all MV positions or connection points are improved by installing PV of 1.620 MW. The tool results show a 64% network capacity improvement with PV to be installed about 22% (position 65, bus-index 245

[Appendix B] down the network from the MV source. Figure 4.22 is a check to ensure line loadings are still within technical limits and are under 70% for this study.

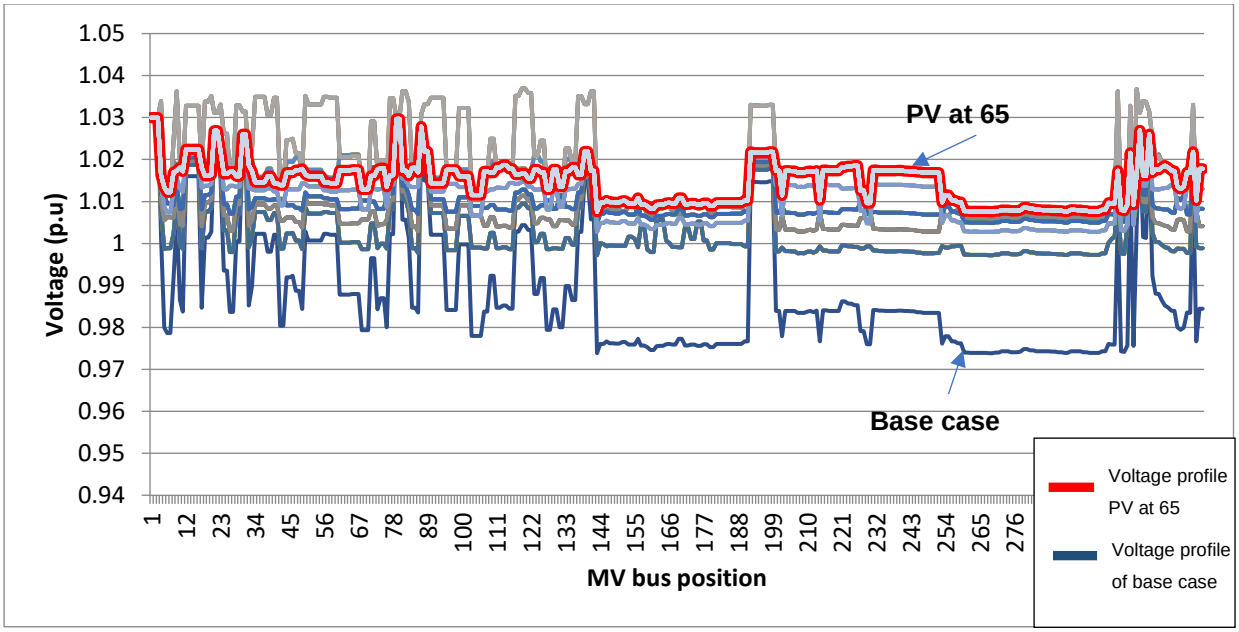

Figure 4.21: Normal feeder peak load: Feeder voltage profile with optimal PV connection point 65 (PV system=5, iterations=10)

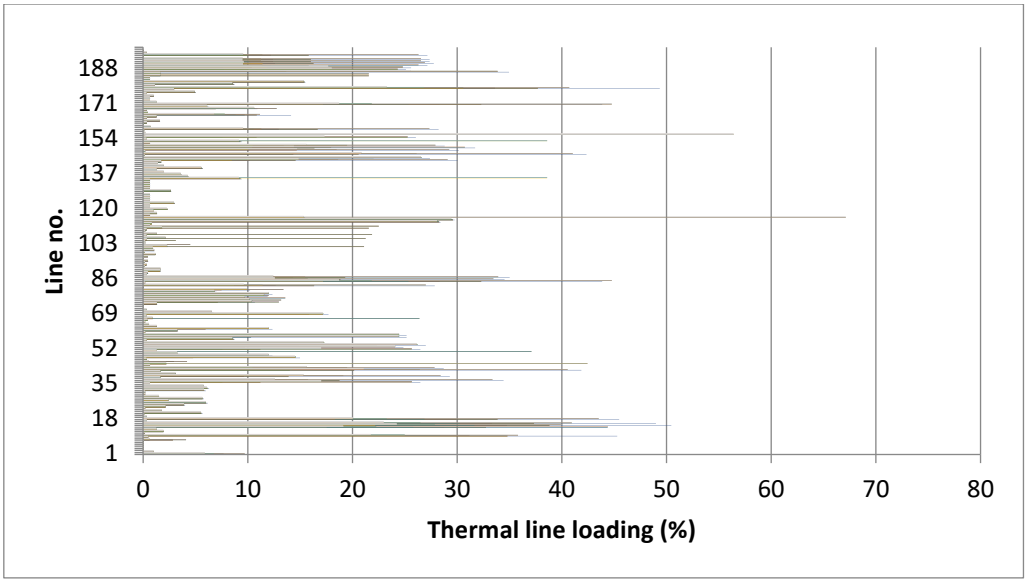

Figure 4.22: Normal feeder peak load: Thermal line loadings (PV system=5, iterations=10)

The third selected input to test Network 1 was PV system=10 and number of iterations=15. The *Fres* matrix values were again calculated in every iteration in the DPL script. Figure 4.23 shows this matrix on the assessment tool itself and with the *'PSO'* tab selected, shows particle convergence (PV connection point) to position 18 (bus-index 72). This plot will always have the iteration numbers on the x-axis with the MV positions on the y-axis. Results show that the more PV systems are to be connected, the optimal MV positions or collection of points shift

towards the MV source itself and this results also proves to be an accuracy check on the tool itself. The legend in Figure 4.23 shows the starting random PV connection points of the study before progression to convergence.

.

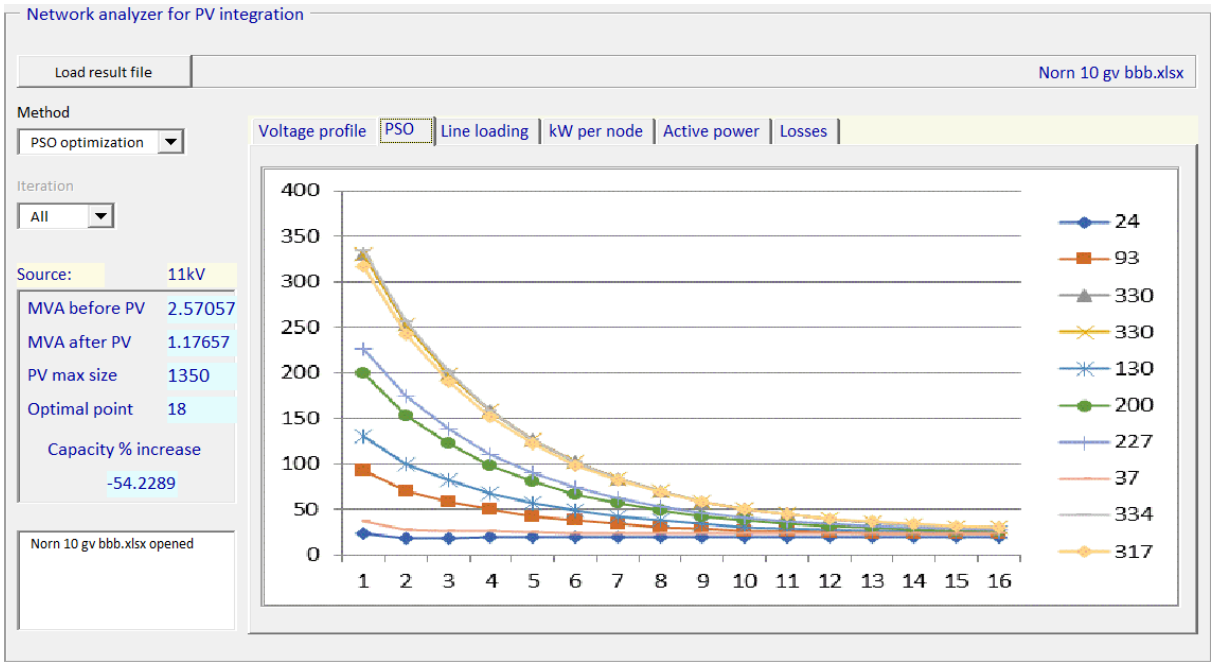

Figure 4.23: Normal feeder peak load: *Fres* matrix values calculated from the PSO equation (PV systems=10, iterations=15)

Figure 4.24 shows the amount of generation to MV position values for the entire feeder based on having all the PV connection points with generators per *Fres* matrix column in service. In other words, all the PV systems were modelled simultaneously. As presented in Figure 4.24, MV positions 1-11 can connect just over 1 MW of PV generation, while positions 61-71 can connect just over 300 kW of generation and so forth. This function of the tool is significant to understand how much of PV generation this feeder can host and how this hosting capacity reduces as the position or connection point moves away from the MV source. The optimised voltage profile (10 PV systems per iteration) is shown in Figure 4.25 (in red) corresponding to optimal connection point 18 with a maximum PV size of 1350 kW and 54% network capacity increase.

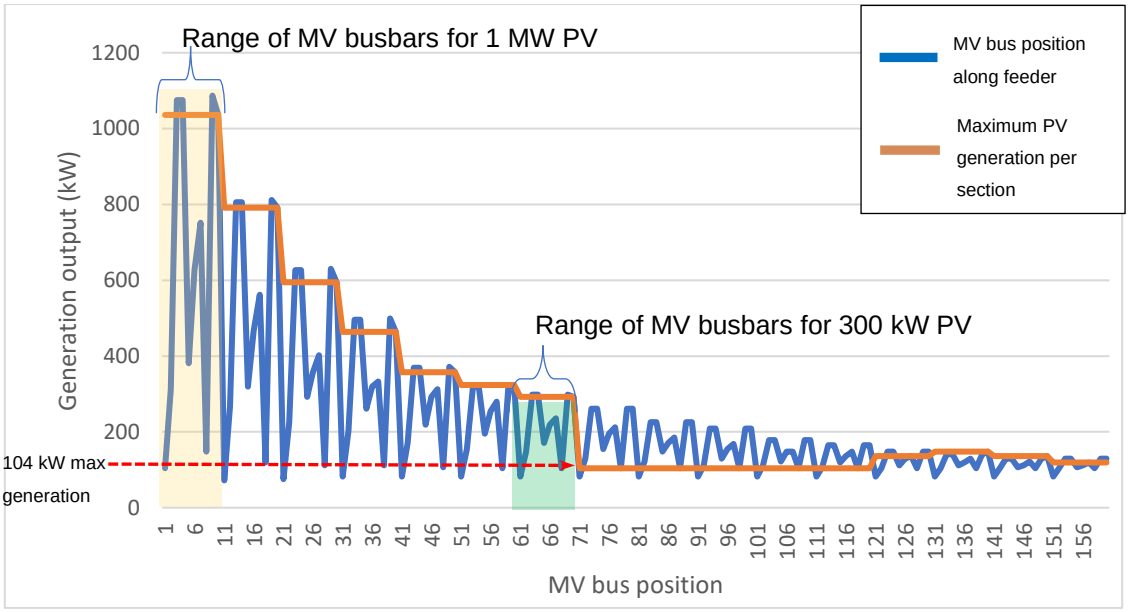

Figure 4.24: Normal feeder peak load: PV Generation with multiple PVs vs MV positions (PV systems=10, iterations=15)

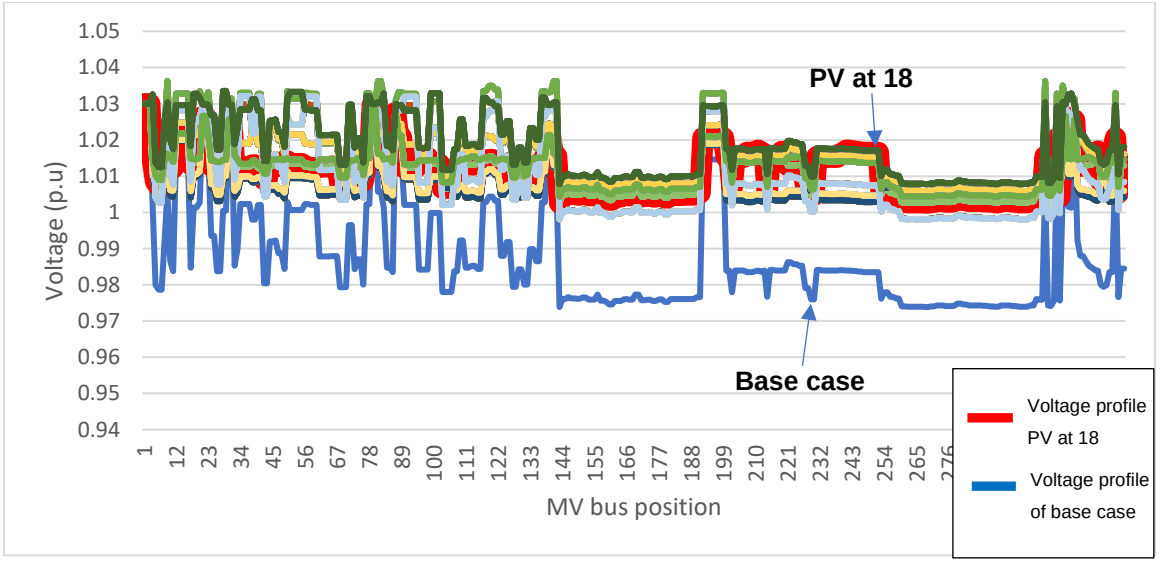

Figure 4.25: Normal feeder peak load: Feeder voltage profile with optimal PV connection position 18 (PV system=10, iterations=15)

4.2.2 Normal feeder light load scenario

In this scenario the DPL script is applied to Network 1 where the study case represents the off-peak or light load scenario with all feeder loads scaled with a scaling factor of 0.4. The selected input in the DPL input page was PV system=1 and number of iterations=5. The *Fres* matrix values were calculated in every iteration in the code where each new position (i.e., PV connection point) is determined by the calculated fitness (change in voltage [p.u]) values before and after the PV connection and is shown in Figure 4.26. The starting bus position was randomly selected at *139* (bus-index 405, Appendix B) with each new position calculated using

equation (3.33) of Chapter 3. The x-axis of Figure 4.15 gives the iteration number, and the y-axis gives the MV bus-positions as calculated by the PSO equation (3.33) in the DPL script.

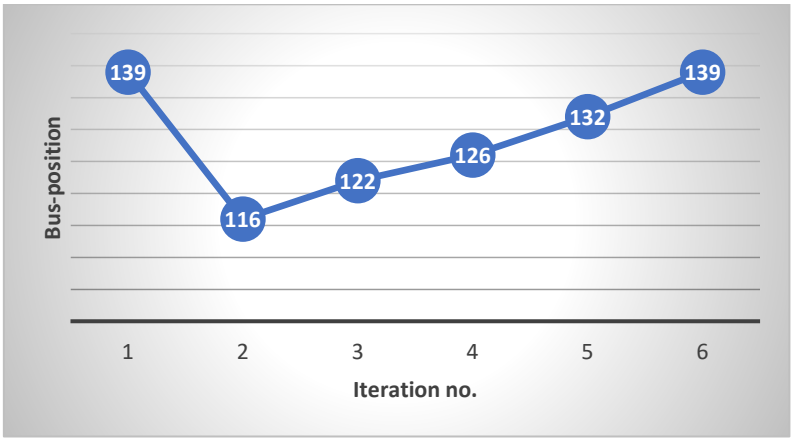

Figure 4.26: Normal feeder light load: *Fres* matrix values for PV connection positions calculated from the PSO equation (PV system=1, iterations=5)

The voltage profile in Figure 4.27, is extracted from the tool and each colour represents the voltage profile for every PSO location calculated in the *Fres* matrix and graphically shown in Figure 4.26. The plot labelled “PV at 132” corresponding to a bus-index of 390 (36% down the feeder network, calculated as 360/1096x100% as explained in section 4.2.1), shows the optimal location determined in iteration 4 (as compared to the base case before PV connection). It can be seen that the voltage profile where PV is connected at position 132 is optimised and Figure 4.28 shows that all thermal line loadings are within the threshold of 85% which is set by the user [33][34].

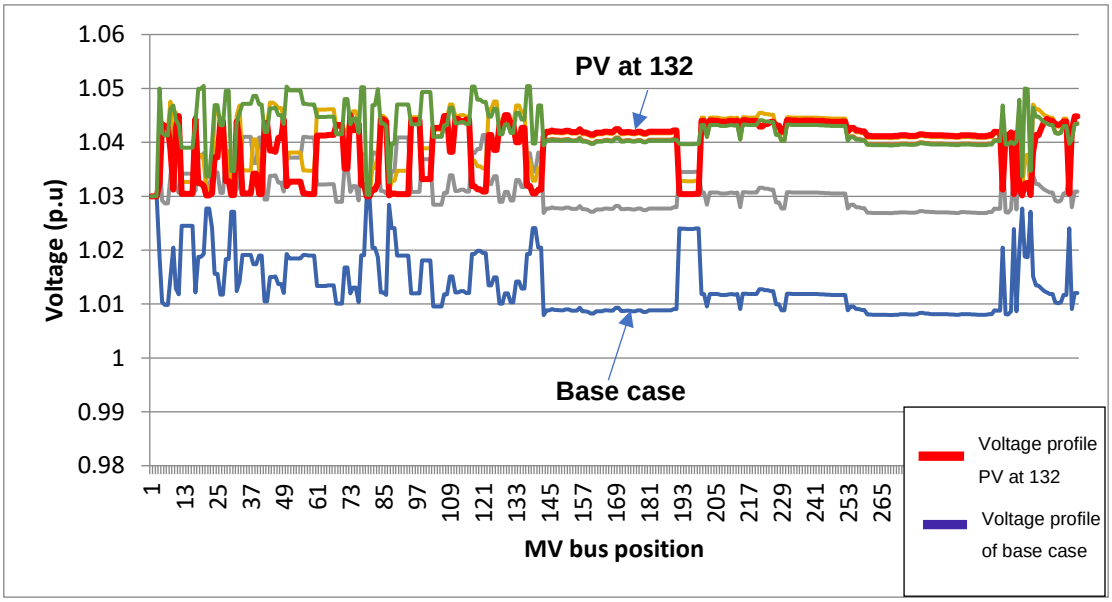

Figure 4.27: Normal feeder light load: Feeder voltage profile with optimal PV connection point 132 (PV system=1, iterations=5)

These thermal loading values are not as significant when compared to networks that have high impedance conductors and the results will always be below the upper limit of 85%.

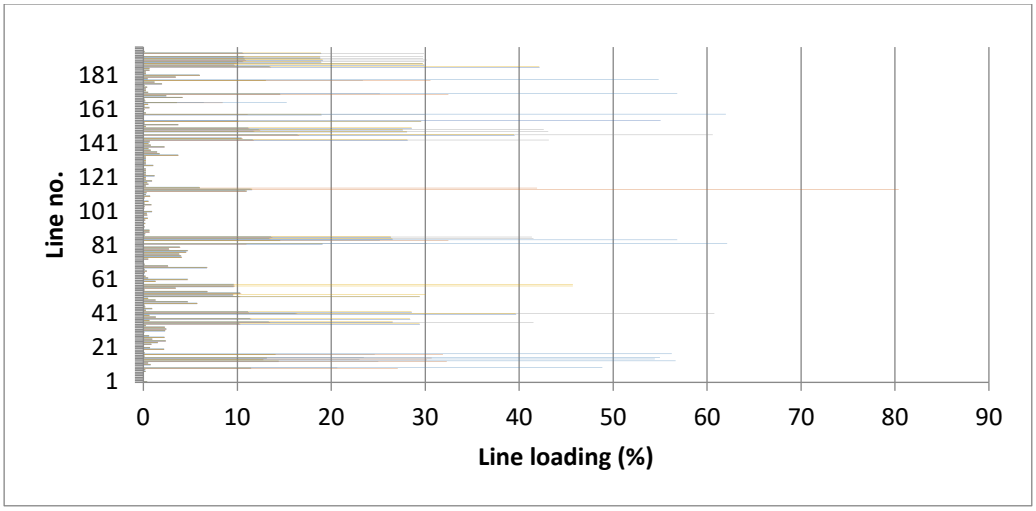

Figure 4.28: Normal feeder light load: Thermal line loadings (PV system=1, iterations=5)

Figure 4.29 shows the summary of the DPL results extracted from the tool. The largest magnitude of PV that can be connected at position 132 is found to be 1.6 MW.

MVA before PV	1.03191
MVA after PV	0.57607
PV max size	1619.99
Optimal point	132
Capacity % increase	
155%	

Figure 4.29: Normal feeder light load: PSO tool screenshot indicating the network capacity improvement of 155% at optimal point 132 (PV system=1, iterations=5)

In comparison to the conventional modelling of section 4.1, this scenario achieved a network capacity improvement of 155% as compared to the 145% in Figure 4.5 (manual method) where the PV was installed at mid-way (50%) of Network 1.

To further test this network, the next selected input was PV system=5 and number of iterations=10 for the next sets of simulations. The *Fres* matrix values were again calculated in every iteration and shown in Figure 4.30. The tool extract in Figure 4.31 shows that the optimal position or connection point found is 143 (corresponding bus-index 417, Appendix B) which is 39% down the feeder network and may connect up to 1.2 MW of PV and results in an 117% network capacity improvement. Figures 4.32 and 4.33 show the corresponding optimised voltage profiles with the MV positions on the x-axis and voltage (p.u) on the y-axis. It can be seen that the voltage profile when connecting the PV at position 143 has slightly higher MV

voltages along the network feeder when compared to all the displayed graphs in Figure 4.33 but optimised to be below the 1.06 p.u mark. Also, 176 kW of power is exported upstream and has to be technically managed. A convenient function of the tool, is that for a particular position, demonstrated in Figure 4.32, the profile for a particular iteration can be selected and shown only, i.e. iteration 2 was selected in the drop-down menu and the corresponding voltage profile to the base case was displayed. All thermal line loadings were checked to be within limits.

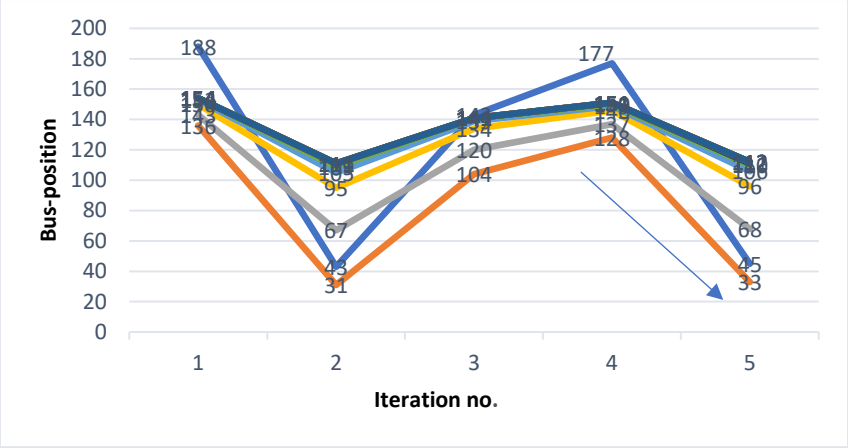

Figure 4.30: Normal feeder light load*: Fres* matrix values for PV connection positions calculated from the PSO equation (PV system=5, iterations=10)

Figure 4.31: Normal feeder light load: Extract from PSO tool (PV system=5, iterations=10)

From the previous simulation using 1 PV system and executing 5 iterations, a 6% difference of location is seen when testing with more PV systems during the light load scenario where

voltages are higher than in the peak load scenario. For this length of network and point of connection, this difference is not as significant. It is as also seen that in the peak load condition, the more PV that was tested the more the location moved towards the MV source but in the light load scenario the locational points found remained to be within the first half of the network but with limited amount of PV generation added.

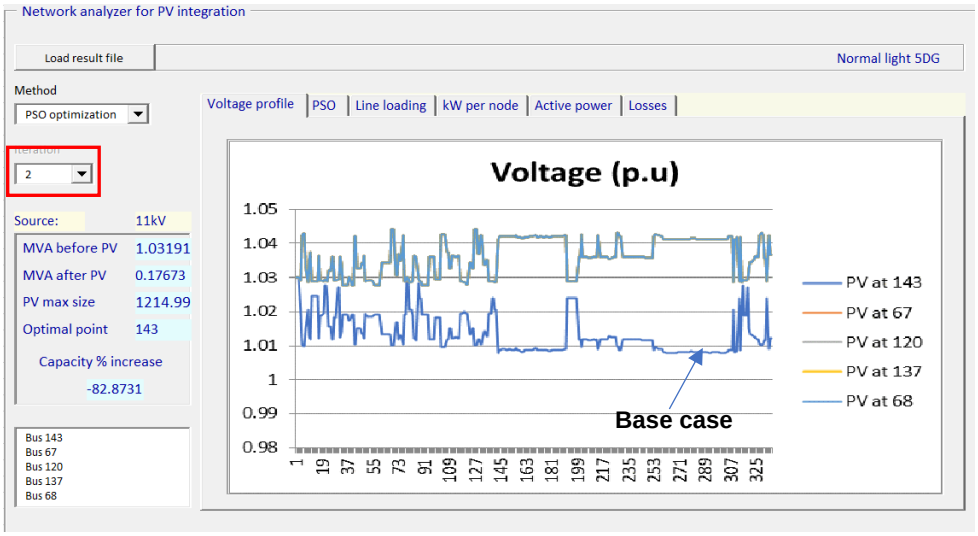

Figure 4.32: Normal feeder light load: Extract from PSO tool (PV system=5, iterations=10) - position 143 voltage profile for iteration 2 selected

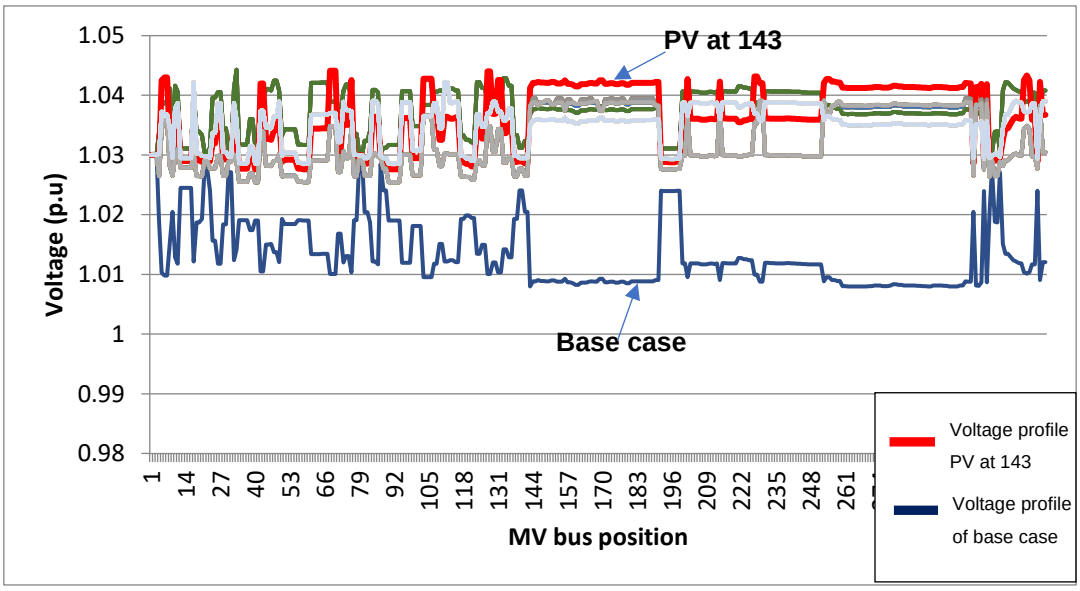

Figure 4.33: Normal feeder light load: Feeder voltage profile with optimal PV connection point 143 (PV system=5, iterations=10)

The next test applied to Network 1 was to select input of PV system=10 and number of iterations=15 on the DPL input page. All the feeder loads are kept scaled at 0.4 and checked before each time the DPL script executes. The *Fres* matrix values are shown graphically in Figure 4.34 and were again calculated in every iteration using PSO equation (3.33). The

positions calculated with PSO can be seen to converge just before position 200 as shown in Figure 4.34. It is also noted that results deviate when too many iterations are selected as shown in Figure 4.34, but the tool filters out the significant results that is needed when completing the analysis of calculating network capacity improvement using PV integration. Figure 4.35 shows the optimised voltage profile extracted from the tool and result summary from the *Ginmat* matrix shows that the optimal position is 198 (bus-index 624) which is located 57% down the network feeder. A network capacity improvement of 78% is seen with 809 kW of generation added at this point (198). Figure 4.35 also indicates that the optimised voltage profile corresponding to the optimal position found does not necessarily have all its voltages higher than other voltage profiles when PV is integrated at different PSO locations. This is due to the DPL code filtering the greatest voltage change but with the maximum RVC % change possible within limits.

Also, from the two sets of iterations (10 and 15), all further PSO calculated points start to move towards the MV source as shown in Figures 4.30 and 4.34. The optimal point found in this case is also network dependent in terms of the position and magnitude of load to where the PV connects. A minimal voltage increase can be seen where more PV is added due to the load sinking the generated power. It is this very reason that many scenarios are completed to gain a better understanding of the network itself to PV integration.

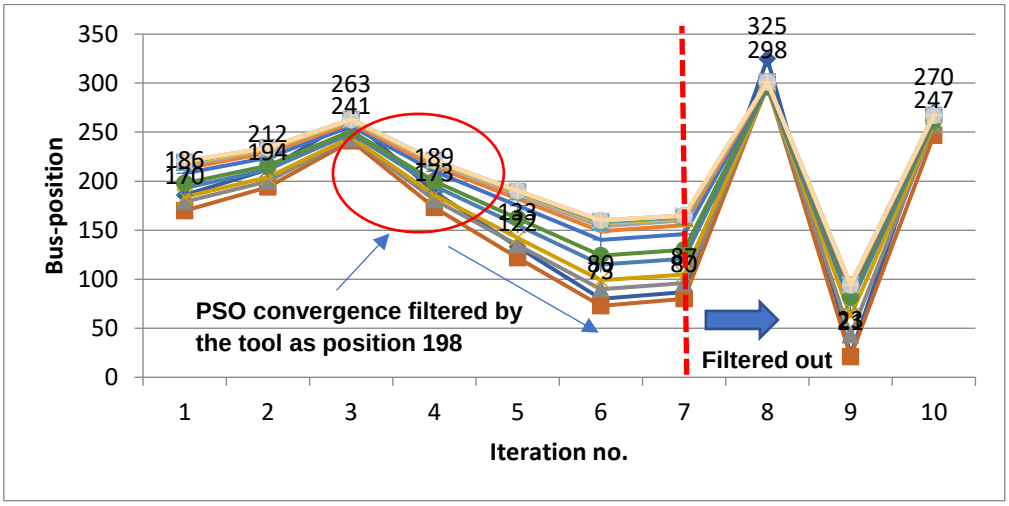

Figure 4.34: Normal feeder light load: *Fres* matrix values for PV connection positions calculated from the PSO equation (PV system=10, iterations=15)

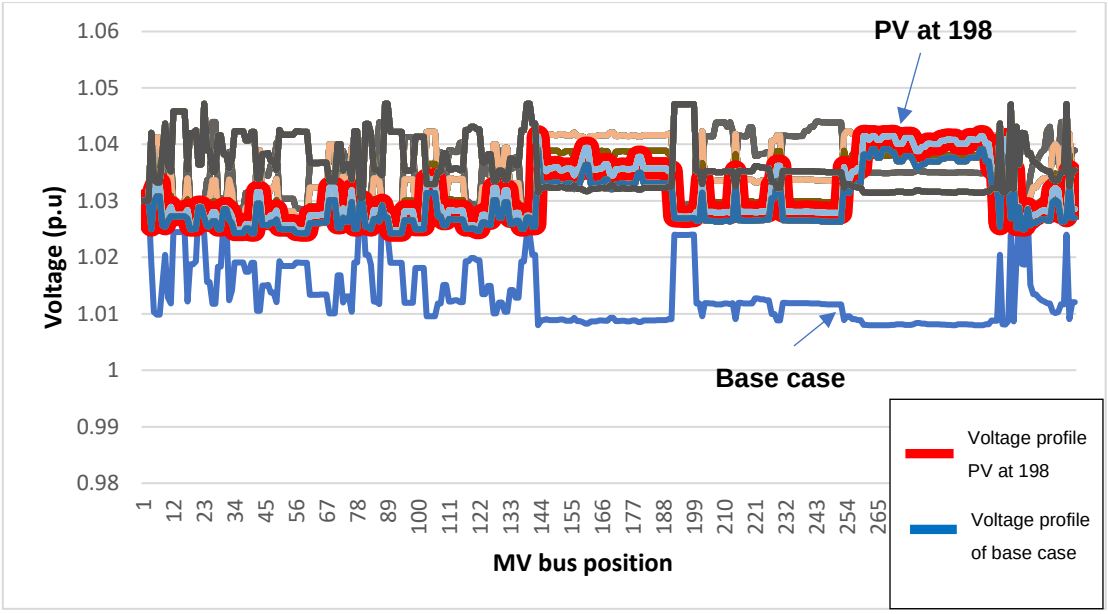

Figure 4.35: Normal feeder light load: Feeder voltage profile with optimal PV connection point 198 (PV system=5, iterations=10)

4.2.3 Constrained peak load scenario

The third scenario modelled on the DPL script for Network 1 tests the constrained network where all the loads are scaled up, i.e., a factor (142%) higher than their normal individual demand as explained in section 4.1. The selected input in the DPL script, was PV system=1 and number of iterations=5. The *Fres* matrix values were again calculated in every iteration and is shown in Figure 4.36 with the iteration on the x-axis and the MV position or PV connection point on the y-axis. The initial random position selected by the DPL script was 298 while the last position calculated by PSO in iteration 5 was bus position 191. Figure 4.37 shows the optimised voltage profile of the network feeder (green colour) for iteration 3 which determines the optimal PV position to be 178 (corresponding bus-index 571, Appendix B). All voltages are seen to be improved with PV connected at this position relative to the base case but also within the upper limit of 1.06 p.u. From previous results, the expected PV generation should not be more than 1 MW. The result summary transferred from the DPL matrix *Ginmat* to the tool analyser, shows that the optimal bus position is located 52% (calculated as 571/1096x100% as explained in section 4.2.1) down the network feeder. A network capacity improvement of 23% is seen with 809 kW of generation added at this position of 178. Figure 4.38 shows the tool functionality displaying the line thermal loadings which are under 60% for this study. The x-axis is the percentage thermal rating of the conductor and the y-axis is the line number on the feeder network.

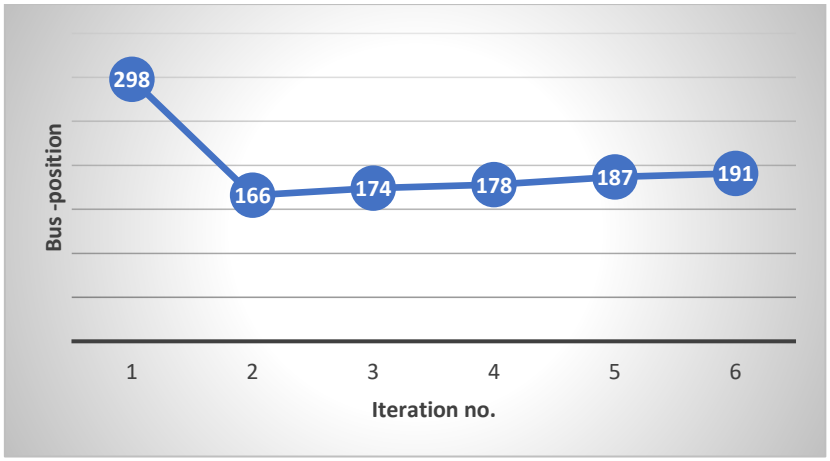

Figure 4.36: Constrained feeder peak load: *Fres* matrix values for PV connection positions calculated from the PSO equation (PV system=1, iterations=5)

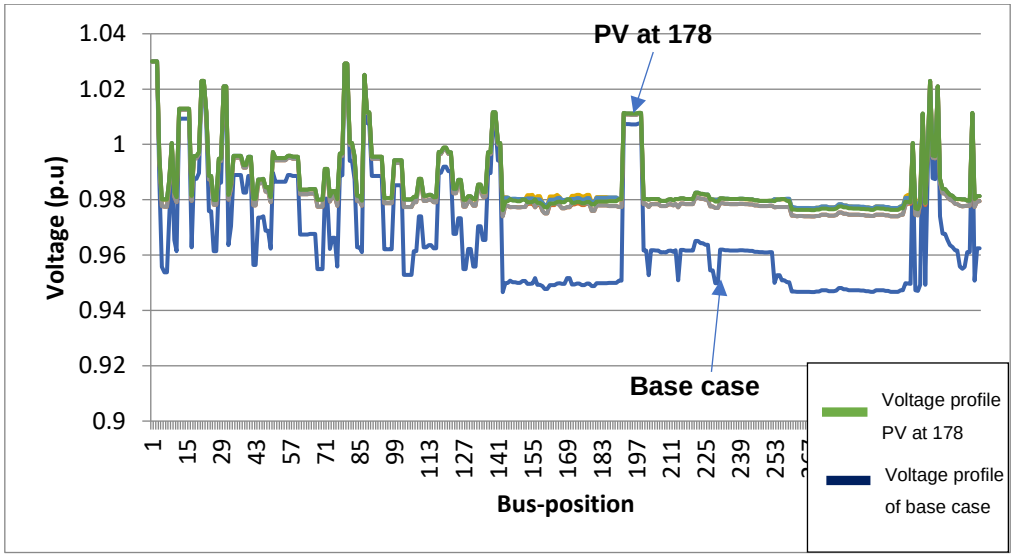

Figure 4.37: Constrained feeder peak load: Voltage profile of the MV feeder with optimal PV connected at position 178 (PV system=1, iterations=5)

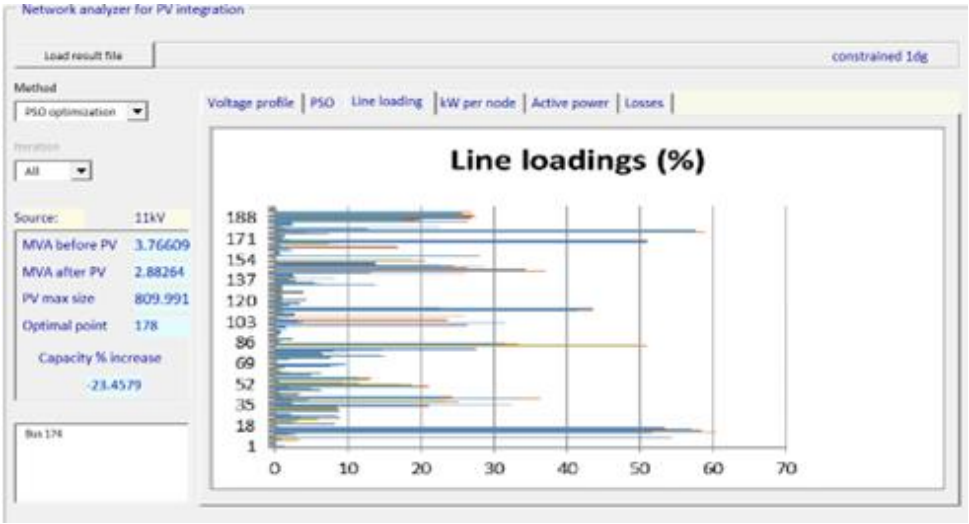

Figure 4.38: Constrained feeder peak load: Line loadings extract from the tool

The next selected input to test the network with the tool was to use PV system=5 and number of iterations=10 on the DPL input page. The *Fres* matrix values of the PSO positions were calculated in every iteration and is shown graphically in Figure 4.39. It can be seen that on connecting 5 PV systems, the convergence moves to a location closer to the MV source substation. The optimised voltage profile (green colour) is shown in Figure 4.40 and is extracted from the tool. All MV voltages are well above the base values and the result summary from the *Ginmat* matrix shows that the optimal PV connection position is found to be 26, located 10% down the network feeder. A resultant network capacity improvement of 62% is seen with 2249 kW of generation added at this position 26. As mentioned in previous sections, that higher penetration of PV becomes greater as the integration point moves closer to the MV source due to the backbone conductor having lower impedances and higher fault levels thus minimising stability issues.

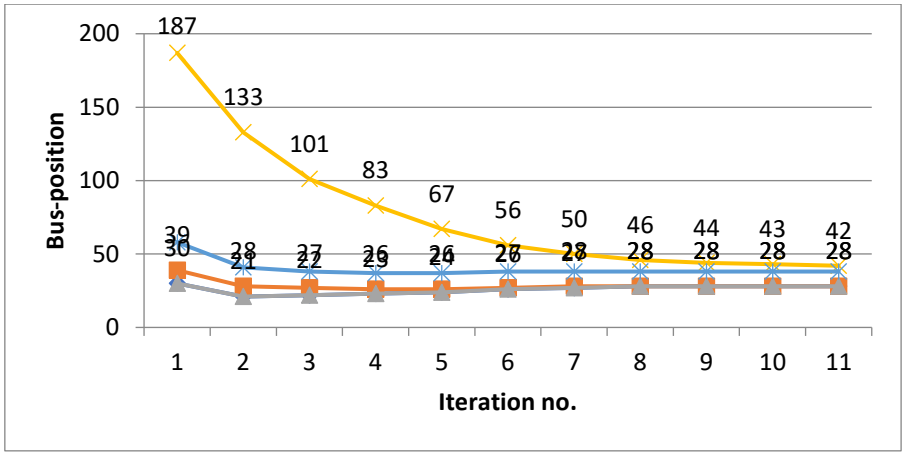

Figure 4.39: Constrained feeder peak load: *Fres* matrix values for PV connection positions calculated from the PSO equation (PV system=5, iterations=10) ‘

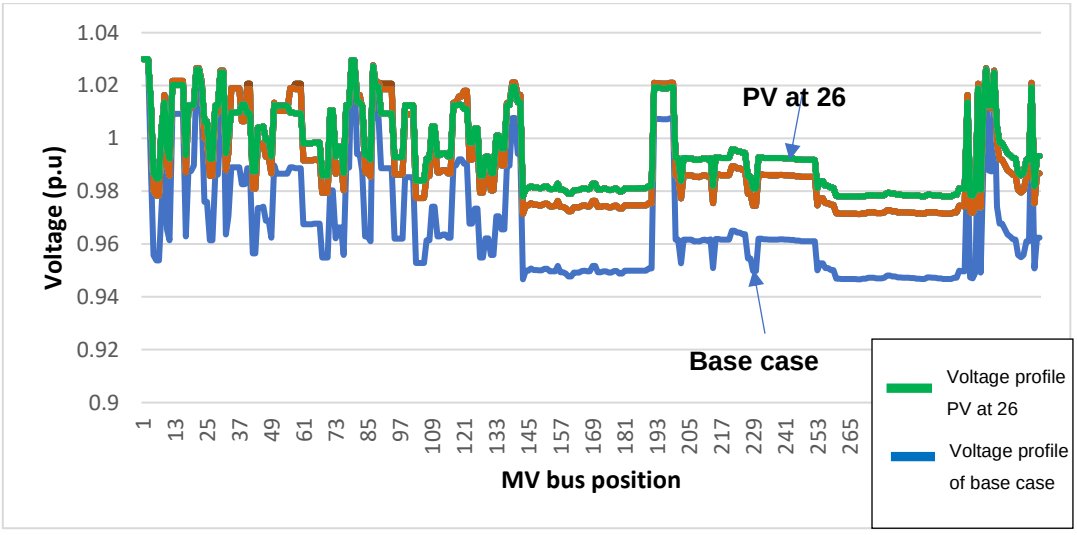

Figure 4.40: Constrained feeder peak load: Voltage profile (green colour) of the MV feeder with optimal PV connected at position 26 (PV system=5, iterations=10)

Also, for constrained feeder, the amount of PV generation is higher than in the *normal feeder peak scenario* due to the additional load of 1 MW sinking the PV generation when PV is added to this part of the network.

The next selected study case using Network 1 had the following input of PV system=10 and number of iterations=10 for the next set of simulations. All loads were again checked that they were scaled accordingly prior to the DPL code execution. The *Fres* matrix values converged to a particular MV bus-position as presented is Figure 4.41. The starting positions of the PSO positions were quite spread although randomly selected. The optimised voltage profile (red colour) is shown in Figure 4.42 and is also extracted from the tool. Voltages are above the base case but lower than in the other iterations of different PSO locations due to the upper voltage limits applied in the DPL script and the RVC results. The result summary is extracted from the *Ginmat* matrix and shows that the optimal position 263 (corresponding bus-index 831, Appendix B) is located 75% (=831/1096x100% as per section 4.2.1) down the network feeder. A resultant network capacity improvement of 94% is seen with 2900 kW of generation added at this position 263.

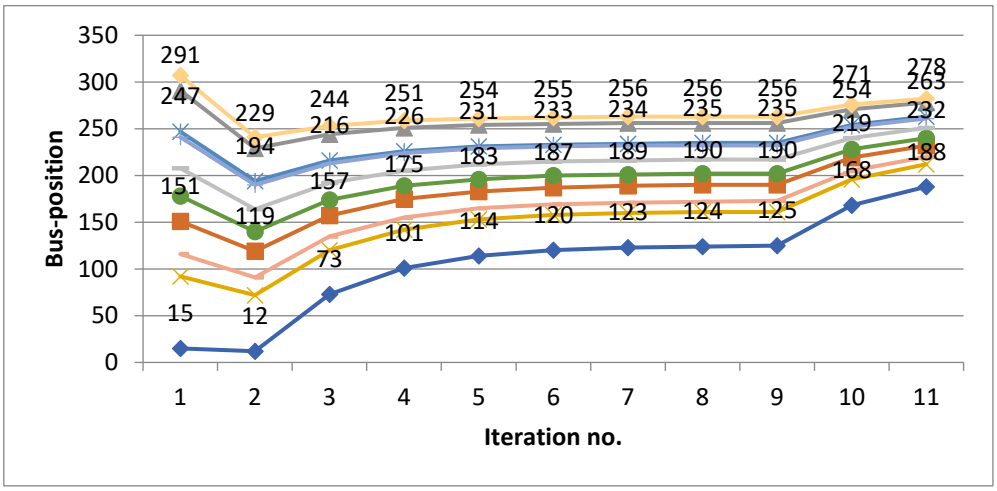

Figure 4.41: Constrained feeder peak load: *Fres* matrix values for PV connection positions calculated from the PSO equation (PV system=10, iterations=10) ‘

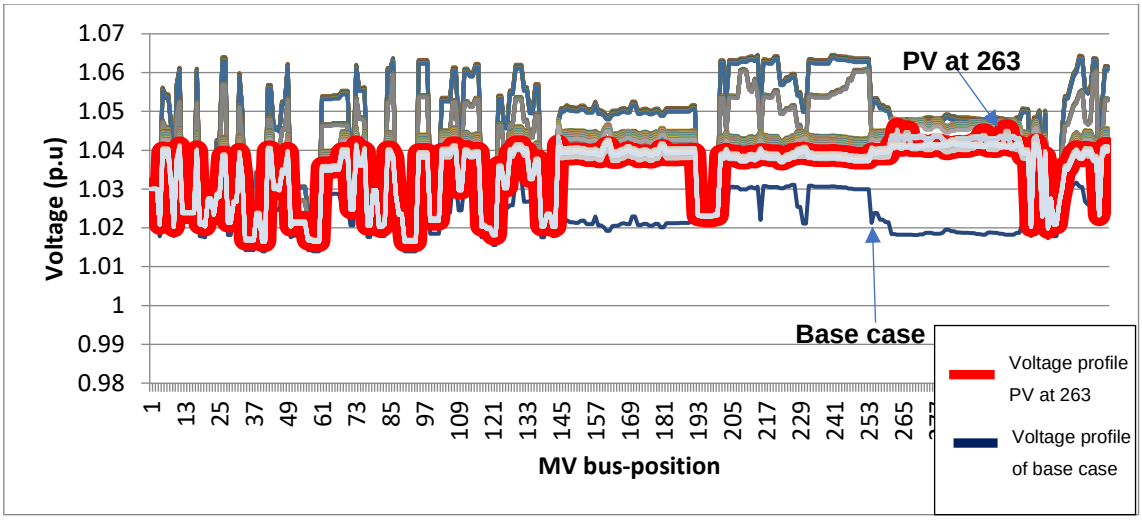

Figure 4.42: Constrained feeder peak load: Voltage profile of the MV feeder with optimal PV connected at position 263 (PV system=10, iterations=10)

Figure 4.43 shows a significant function of the tool that can be extracted. The graph shows each of 10 PV systems connected at a bus position determined from the PSO equation with the relevant fitness values for one of 10 iterations. All the PV systems connected at bus position in Figure 4.43 shows the corresponding fitness values or in this case, voltage improvement when PV is connected. This study is also significant when planning PV integration projects. For example, in Figure 4.43, the PV system number 3 connected at bus position 225 would have a voltage improvement value of 2.2%. Similarly, for each PV system the same approach is used to determine the corresponding fitness value.

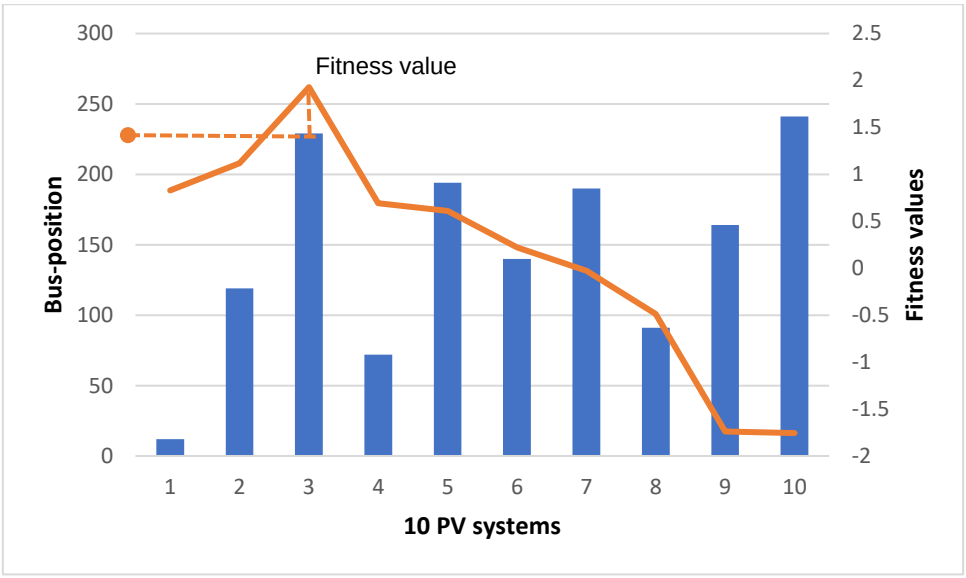

Figure 4.43: Constrained feeder peak load: Bus-position vs Fitness % value for iteration with the greatest fitness values

4.2.4 Constrained feeder light load scenario

The fourth scenario modelled on the DPL script for Network 1 tests the constrained network where all the loads are scaled down (0.57 scaling factor applied), i.e., a factor much lower than the individual demand to mimic the light load times as explained in section 4.1. The selected input to the DPL input page was PV system=1 and number of iterations=5. The *Fres* matrix values were shown in previous simulations but are not displayed in this section as that the results converged and what is of significance is the network capacity value and feeder location. Figure 4.44 results show the tool extract of the optimised voltage profile for the feeder corresponding to optimal position 313 (bus-index 1024) and is located 94% down the network feeder. The voltage (p.u) is shown on the y-axis and the MV bus-position is shown on the x-axis. A network capacity improvement of 55% is seen with 810 kW of generation added at this connection point (=1024/1096x100%)

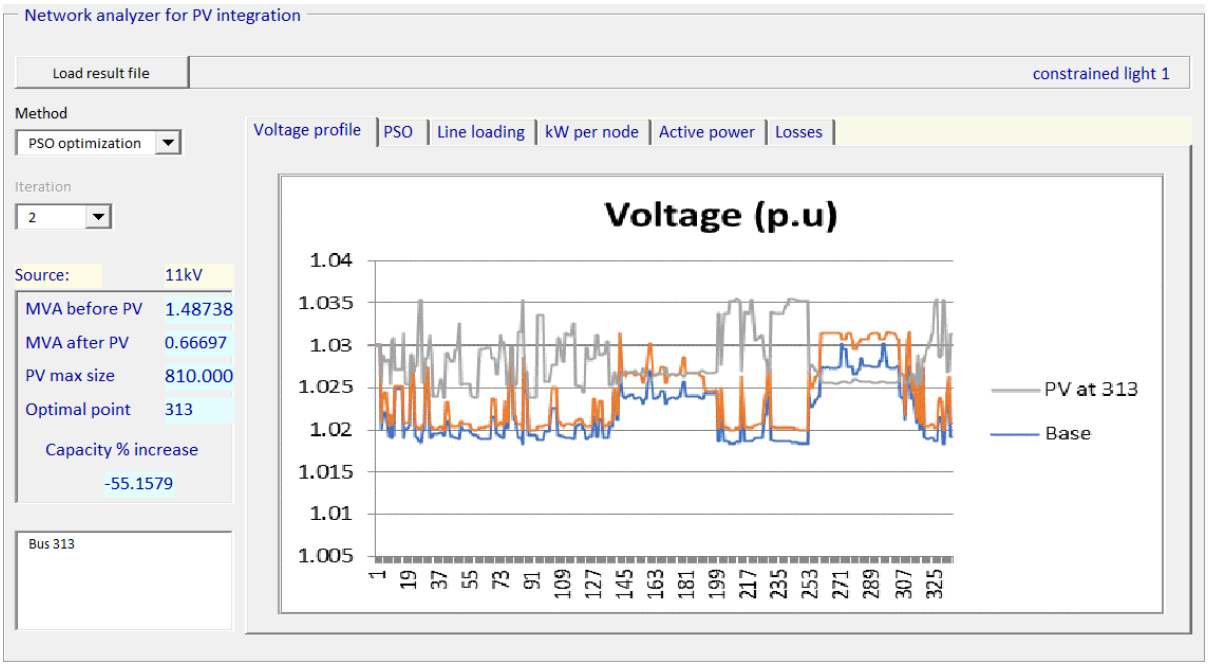

Figure 4.44: Constrained feeder light load: Voltage profile of the MV feeder with optimal PV connected at position 313 (PV system=1, iterations=5)

The next selected input was PV system=5 and number of iterations=10 for the constrained light load scenario. Result summary from the *Ginmat* matrix shows that the optimal bus position is found to be 144 (bus-index 420) which is located 38% down the network feeder. A network capacity improvement of 55% is seen, also with 810 kW of generation added at this point (144). The optimised voltage profile (red colour) is shown in Figure 4.45 and is extracted from the tool.

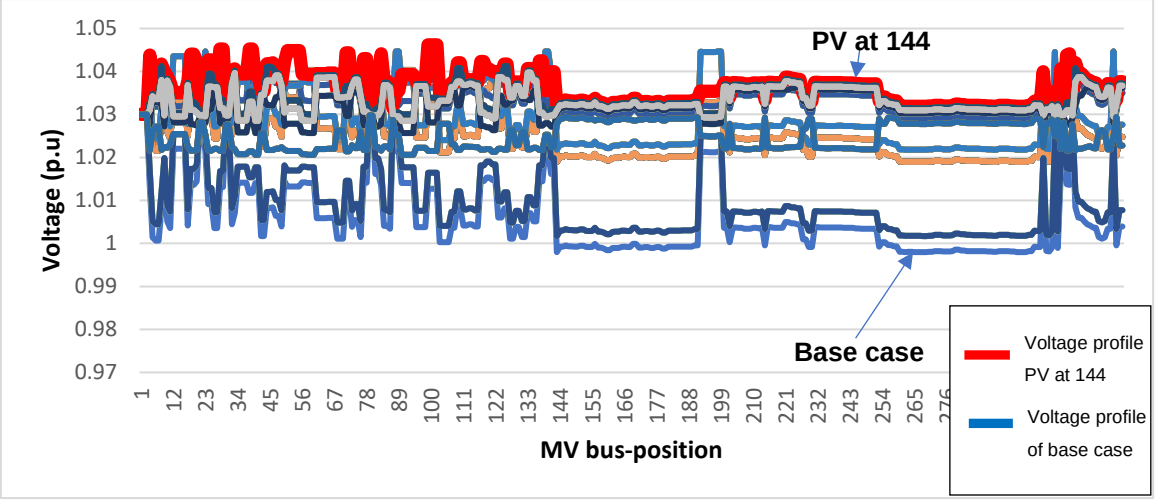

Figure 4.45: Constrained feeder peak load: Voltage profile of the MV feeder with optimal PV connected at position 144 (PV system=5, iterations=10)

In sections 4.1 and 4.2, the manual method of connecting PV and the method using the DPL script and tool analyser were presented. Each case result is extracted and summarised in section 4.5. In the next section of 4.3, the exact methodology of assessment is executed on Network 2.

4.3 Conventional modelling and results of Network 2

In this section, Network 2 has an MV voltage of 22 kV and represents a rural type of network where the MV backbone is quite longer with much higher bus-indices. This type of network of 22 kV is used when load is far from the source and in most cases 3 or 4 times that of an 11 kV network in backbone length. To deliver the same amount of power to a load, the higher voltage of 22 kV results in lower currents compared to the 11 kV system and as such conductor thermal limits are typically not a constraint. Network 2 has in addition a voltage control device of an open-delta configured regulator and makes this network a suitable test network to apply the developed DPL script and tool. The approach as discussed in the methodology of Chapter 3 and section 4.1 is to model Network 2 by first using the manual method (without using any DPL script) and secondly by executing the DPL script with different input values for the PSO equation part of the code. The input values here would be 22 kV voltage level for Network 2 as well as the number of PV systems and iterations. The 22 kV Network 2 was setup as explained in Chapter 3 and load flow studies were conducted using the Newton-Raphson method to get the current peak apparent (MVA), active (MW), reactive (MVAR) power of the 22 kV network as shown in Figure 4.46. The total electrical loss of the same network is shown in Figure 4.47. These plots also consider seasonal data and hence show peak and off-peak curves on a 30min seasonal time-stamp i.e., day and night per season per every 30min period similarly to the graphs of Network 1. Figure 4.46 depicts that the active power peaks at 2.3

MW while the reactive power peaks at 0.75 MVAR. At low load, the active power is 1 MW and reactive power of 0.4 MVAR. In Figure 4.47, the electrical losses are shown and can also be exacerbated by *non-technical* losses due to theft or meter tampering. The total grid electrical losses (entire network feeder including all interconnecting lines) is plotted on the y-axis corresponding to the time stamp on the x-axis. Network 2 has a voltage regulator which assists the feeder with respect to voltage regulation during peak load times.

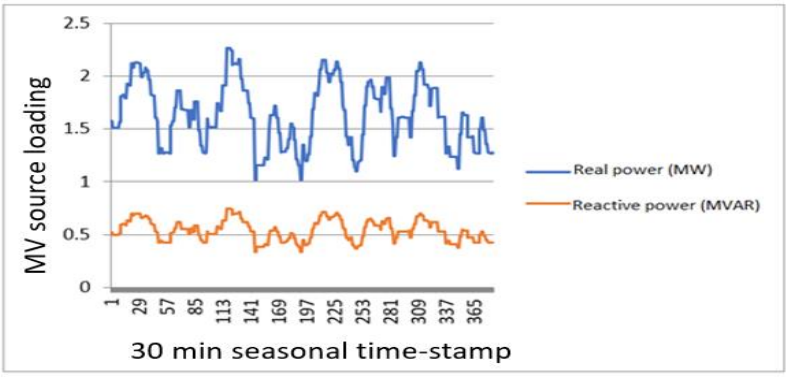

Figure 4.46: Active (MW) and reactive power (MVAR) values of Network 2

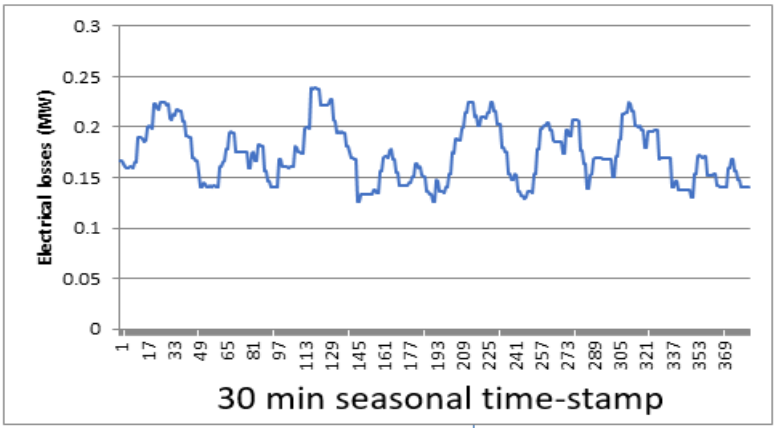

Figure 4.47: Total electrical losses (MW) of Network 2

Figure 4.48 shows the voltage profile of Network 2 during light load conditions (scaling factor 0.4) with and without the voltage regulator and as such, PV systems in the simulations that follow, are connected during the different scenarios with this variation of voltage control. Figure 4.49 shows the voltage profile of Network 2 during peak load conditions (scaling factor 1) with and without the voltage regulator. Figure 4.50 shows the geographic layout of the 22 kV network and the positions referred to in the different simulated scenarios. Also, the position of the VR is indicated by a solid grey circle.

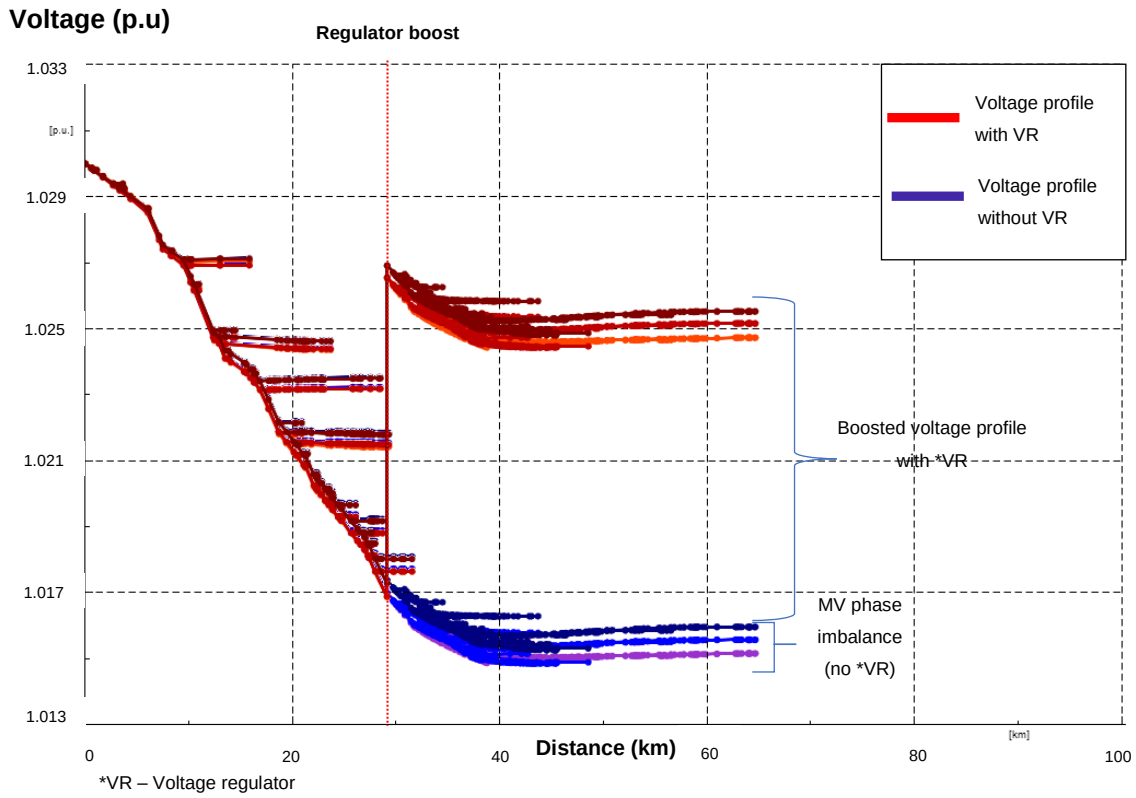

Figure 4.48: Voltage profile of Network 2 with and without the voltage regulator for light load condition

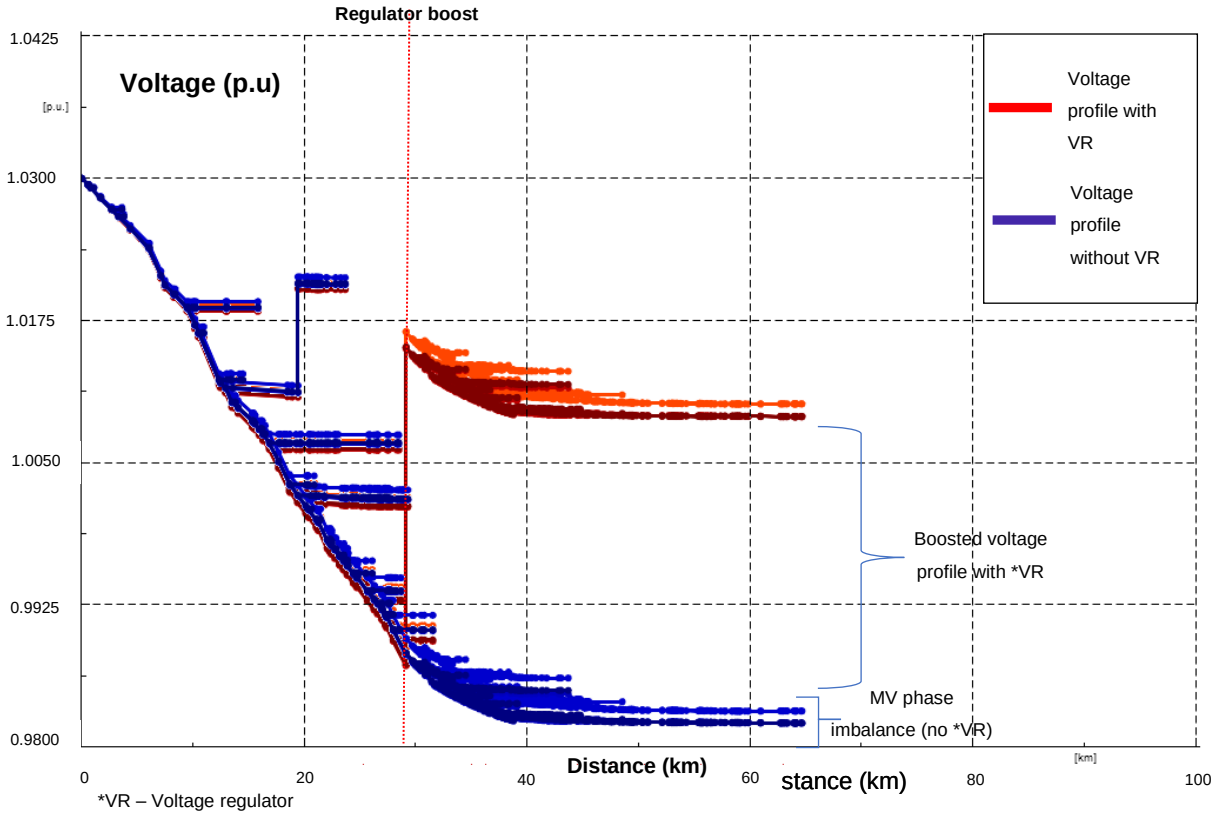

Figure 4.49: Voltage profile of Network 2 with and without the voltage regulator for peak load condition

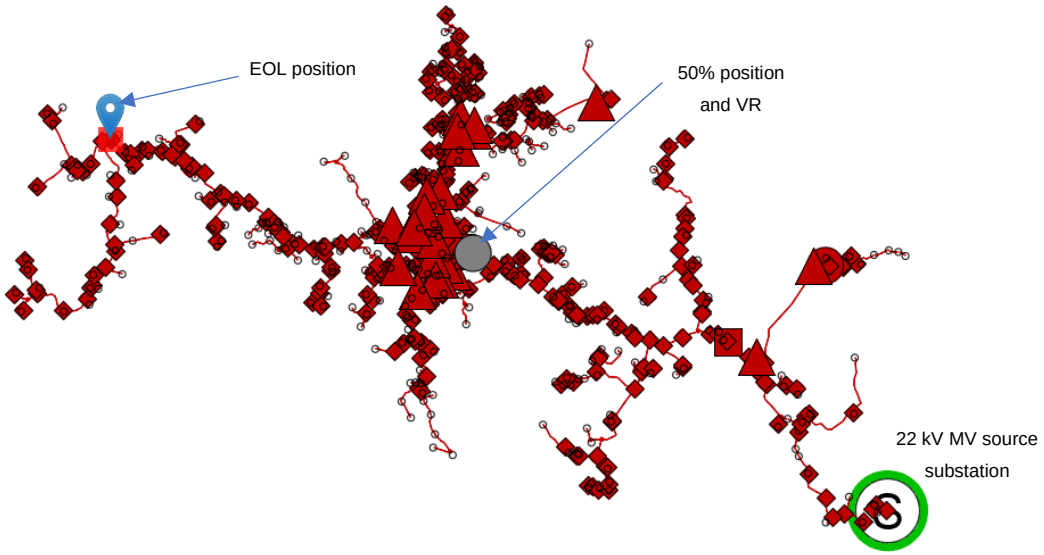

Figure 4.50: Geographic overview of 50% position, Voltage regulator and EOL position referred to in the simulations that follow

4.3.1 Connecting PV at 50% of the MV feeder

In connecting solar PV DG to this network, the PV system is integrated at approximately 50% (30 km) of the network backbone (~ 65 km in total length) from the 22 kV MV source substation estimated from the geographic layout of the network (Figure 4.50). Different scenarios of network operation with peak and off-peak (light) load variations are modelled and simulated with and without the voltage regulator in service.

4.3.1.1 Peak load without regulator and with PV installed

In this scenario, all loads have a scaling factor of 1 in Network 2 for peak load simulation. The network model was modelled using DIgSILENT Powerfactory. Table 4.13 shows the load flow study results for the PV system connected at MV bus-index 1864 with the corresponding voltages before and after at this position as well. No backbone feeder thermal issues were found in the simulations that follow. Once the Rapid Voltage Change (RVC) test reached 3% the final capacity improvement would therefore be determined by equation 4.1.

Results presented in Table 4.13 shows that 0.99 MW of PV generation can be connected at peak load conditions without the regulator in service. The PV size of 0.99 MW has 3 installations (each of 330 kW) and results in an increase in voltage to 1.02 p.u with a 75% network capacity improvement. The RVC% remains within an acceptable configuration. Figure 4.51 shows the corresponding voltage profile (voltage plotted in p.u on the y-axis). All voltage

graphs are plotted from the 22 kV MV source substation (distance in km on the x-axis) to the end-of-line (EOL). An appreciable voltage improvement is seen throughout the network.

Table 4.13: Peak load without regulator – PV at 50% feeder location

PV size	Voltage before (p.u)	Voltage after (p.u)	Initial Loading at source substation	Final Loading at source substation	Capacity Improvement (as per equation 4.1)	Rapid Voltage Change%
0.99 MW	0.99	1.02	1.2 MW, 0.4 MVAR	0.3 MW, 0.4 MVAR	75%	3%

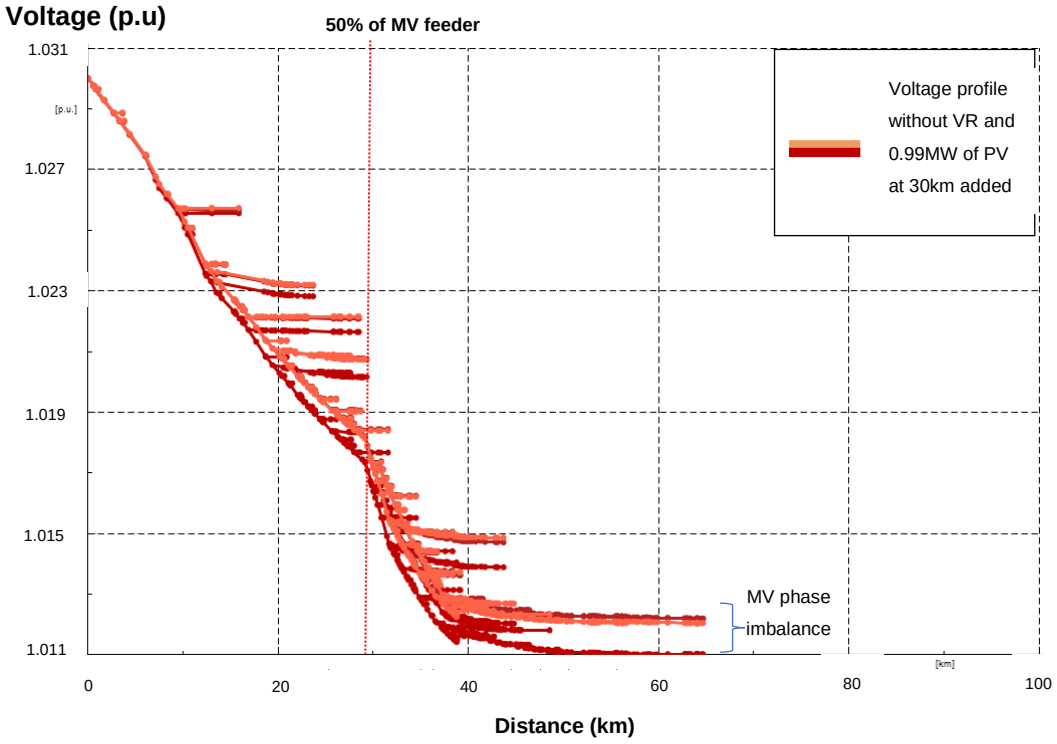

Figure 4.51: Peak load without regulator: Voltage profile of Network 2 with PV at 50% feeder location

4.3.1.2 Peak load with regulator and with PV installed

In the next scenario, the open-delta regulator (two cans) is placed into service. This implies that two phases will be boosted accordingly. In Table 4.14, results show that there is no change to the results obtained in Table 4.13. The reason is that the regulator settings and its position determine the operation in which the regulator will either boost or buck the input voltage. In this case, the controller tap settings are shown in Figure 4.52 and were set for Network 2 by the utility to have a lower bound of 1.015. Hence, the voltage profile would be more or less the same as in the previous simulation and is shown in Figure 4.53 for completeness.

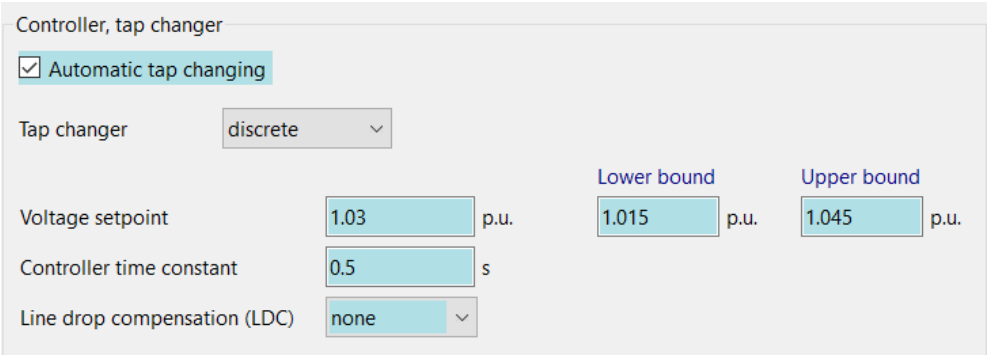

Figure 4.52: Voltage regulator (VR) controller settings

Table 4.14: Peak load with regulator - PV at 50% feeder location

PV size	Voltage before (p.u)	Voltage after (p.u)	Initial Loading at source substation	Final Loading at source substation	Capacity Improvement (as per equation 4.1)	Rapid Voltage Change%
0.99 MW	0.99	1.02	1.2 MW, 0.4 MVAR	0.3 MW, 1 MVAR	75%	3%

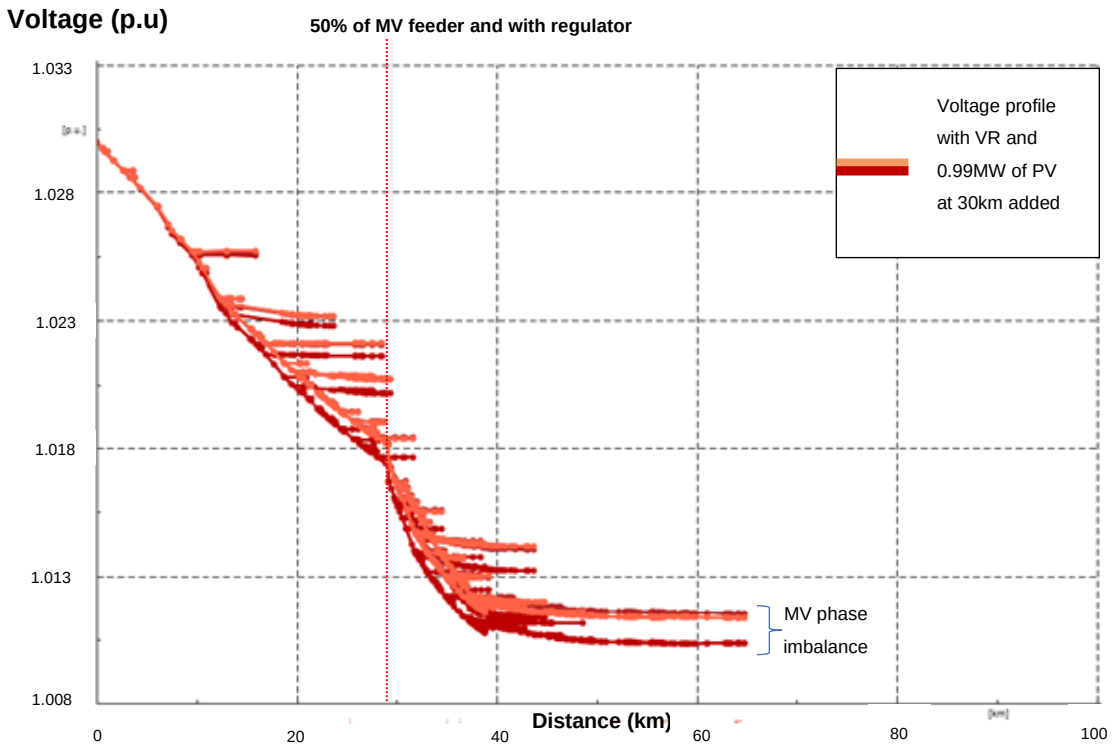

Figure 4.53: Peak load with regulator: Voltage profile of Network 2 with PV at 50% feeder location

4.3.1.3 Light load with regulator and with PV installed

In this study, all loads are scaled to 0.4 for simulating light load conditions. The MV source substation loading is adjusted to 0.5 MW. A PV size of 0.99 MW was connected to bus-position

1864 and the results are shown in Table 4.15. The new MV source loading shows that 400 kW of power is exported upstream into the network grid due to the connected PV generation exceeding the connected load during off-peak times. *Also, the final loading has a negative VAR flow due to cables and line capacitance on this network.* The voltage at bus-index 1864 is raised to 1.05 p.u with an acceptable RVC value of 3% and calculated network capacity of 180%. As mentioned in section 4.1.1.2, several factors have to be considered for the exported power, such that the MV/LV transformer has to be configured to allow reverse power by disabling any switching relays that prevent this, provided this has been deemed technically and financlially acceptable. It is noted here as well, that all PV installations must conform to the specifications set out in NRS097 documents for embedded generation. Figure 4.54 shows the voltage profile tapped down due to the controller settings and that only two phases are well balanced.

Table 4.15: Light load with regulator – PV at 50% feeder location

PV size	Voltage before (p.u)	Voltage after (p.u)	Initial Loading at source substation	Final Loading at source substation	Capacity Improvement (as per equation 4.1)	Rapid Voltage Change%
0.99 MW	1.02	1.05	0.5 MW, -0.1 MVAR	-0.4 MW, -0.1 MVAR	180%	2.9%

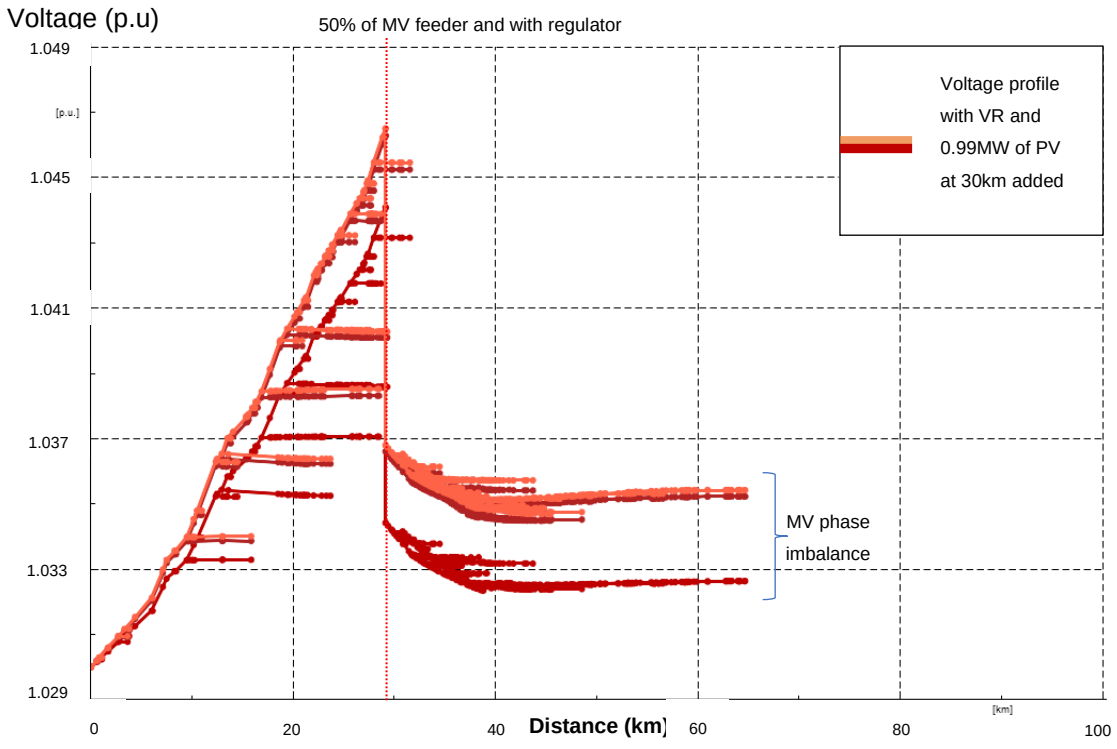

Figure 4.54: Light load with regulator: Voltage profile of Network 2 with PV at 50% feeder location

4.3.1.4 Light load without regulator and with PV installed

In this study, the regulator is taken out of service. The results in Table 4.16 are exactly the same as in Table 4.15. However, the voltage profile in Figure 4.55 shows that the voltage rise seen at the EOL is much greater than the previous study with the voltage regulator in service. This again, is due to the upper bound set on the controller of the voltage regulator. As in section 4.3.1.3 the export power of 400 kW (shown as negative loading of -0.4 MW) in Table 4.16 also must be technically managed.

Table 4.16: Light load without regulator – PV at 50% feeder location

Max PV size	Voltage before (p.u)	Voltage after (p.u)	Power initial at source	Power final at source	Capacity improvement	RVC%
0.99 MW	1.02	1.05	0.5 MW, -0.1 MVAR	-0.4 MW, -0.1 MVAR	180%	2.9%

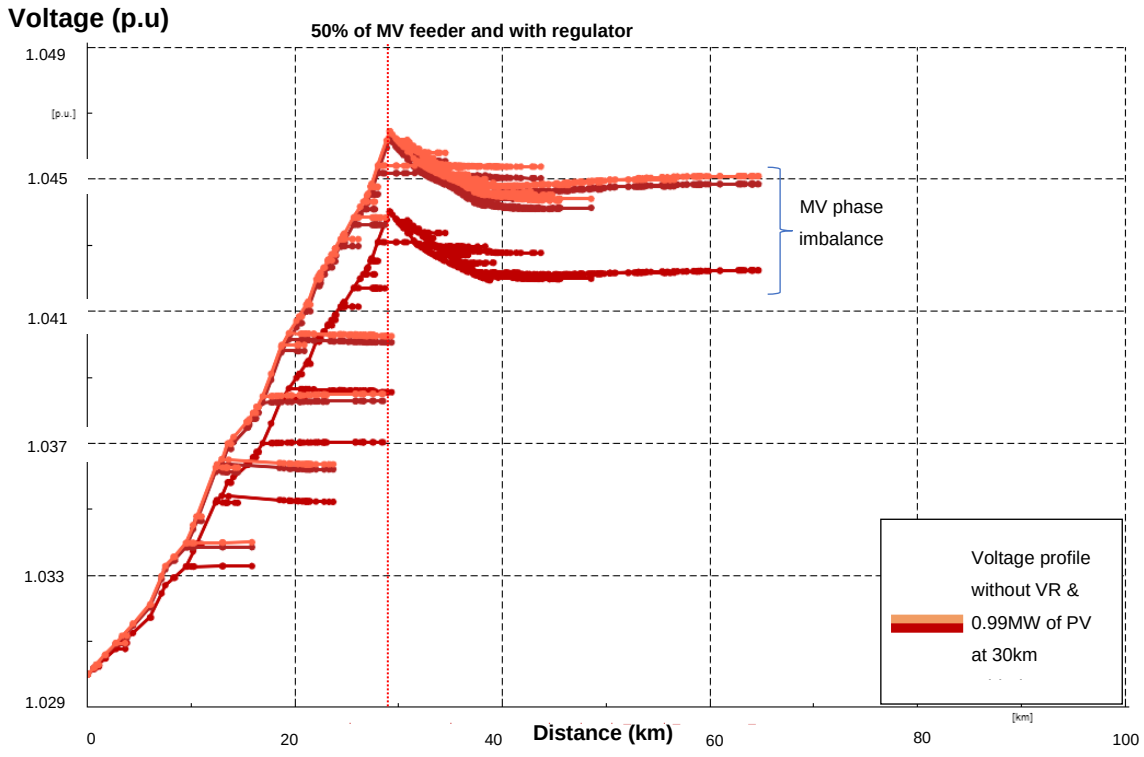

Figure 4.55: Light load without regulator**:** Voltage profile of Network 2 with PV at 50% feeder location

4.3.2 Connecting PV at the End-of-line (EOL) of the MV feeder

The simulations in section 4.3.1 have considered the middle part of the network for connecting the PV system and modelled Network 2 with the feeder voltage regulator at 50% feeder location. The next set of simulations looks at connecting PV to the end of Network 1, i.e., at the End-of-Line (EOL) at bus-index 6269 as indicated in Figure 4.60. Similar to section 4.3.1, different scenarios with and without the voltage regulator during peak and light load variations are modelled and simulated in this study case. Two sets of results for peak and light load are presented in sub-section 4.3.2.1 and 4.3.2.2 with and without the voltage regulator. From the previous analysis, the voltage regulator does not change the network capacity improvement or RVC % value and for this network does not play a major role in determining these results. With the voltage regulator controller settings fixed for this network, graphs for the voltage profile presented in Figures 4.54 and 4.55 would have similar results in sections 4.3.2.1 and 4.3.2.2 and are therefore not presented here.

4.3.2.1 Peak load with and without regulator and with PV installed

All loads here are scaled back to 1 here, to simulate peak load. The maximum PV size connected to bus-index 6289 was found to be 0.48 MW with or without the regulator in service and the maximum improvement in network capacity capped by the RVC % value was 38%. Figure 4.17 tabulates these results and shows, as previously indicated that the network capacity improvement and RVC % value have no effect with the location of the voltage regulator on Network 2. The regulator keeps the output voltage within the set bounds in the controller settings and would therefore boost accordingly.

Table 4.17: Peak load – PV at EOL

Regulator	Max PV size	Voltage before (p.u)	Voltage after (p.u)	Power initial at source	Power final at source	Capacity improvement	RVC%
With VR	0.48 MW	1.01	1.03	1.3 MW, 0.4 MVAR	0.8 MW, 0.4 MVAR	38%	3%
Without VR	0.48 MW	0.98	1.01	1.3 MW, -0.4 MVAR	0.8 MW, -0.4 MVAR	38%	3%

4.3.2.2 Light load with and without regulator and with PV installed

All loads in this study case are scaled back to 0.4 to simulate light or off-peak feeder loading. The maximum PV size connected to bus-index 6289 at the EOL, was found to be 0.5 MW with or without the regulator in service and the maximum improvement in network capacity capped

by the RVC % value was 80%. Figure 4.18 tabulates these results. With the voltage regulator in service, the voltage is controlled not to exceed the upper bound and as such with the PV installed, the voltage upper limit is reduced from 1.05p.u to 1.04 p.u. The regulator keeps the output voltage within the set bounds in the controller settings and would therefore in this study buck accordingly. Also, the final loading has no export of real power but a negative VAR flow due to cables and line capacitance on this network.

Table 4.18: Light load – PV at EOL

Regulator	Max PV size	Voltage before (p.u)	Voltage after (p.u)	Power initial at source	Power final at source	Capacity improvement	RVC%
With VR	0.5 MW	1.02	1.04	0.5 MW, -0.1 MVAR	0.1 MW, -0.1 MVAR	80%	3%
Without VR	0.5 MW	1.02	1.05	0.5 MW, -0.1 MVAR	0.1 MW, -0.1 MVAR	80%	3%

4.3.3 Connecting PV at 50% of the MV feeder and at End-of-Line (EOL) of the MV feeder

Sub-sections 4.3.1 and 4.3.2 tested Network 2 with PV connected at 50% of the MV network down the feeder backbone (~30 km) and at the EOL (~65 km) respectively. The next set of simulations involves connecting PV systems both at 50% *and* at EOL of the MV feeder. The same study cases as per the previous sections of 4.3.1 and 4.3.2 apply in this case.

4.3.3.1 Peak load with regulator and with PV installed

In this study, 0.56 MW of PV was installed at 50% down the feeder and 0.22 MW of PV was installed at the EOL. Results in Table 4.19 show that a 62% improvement in network capacity was seen with the RVC at the EOL reaching an acceptable value of 3%. Figure 4.56 shows the corresponding voltage profile with the voltage regulator boosting the voltage at the EOL as the connected point of the regulator falls below the lower limit in the controller setting.

It must be noted that in the study cases that follow, the voltage p.u value and RVC % value are different in each location and as such are shown in different rows in Tables 4.19 - 4.22 albeit PV is connected at both locations.

Table 4.19: Peak load with regulator – PV at 50% and EOL

PV size located at	Voltage before (p.u)	Voltage after (p.u)	Power initial at source	Power final at source	Capacity improvement	RVC%
0.56 MW at 50% and 0.22 MW at	0.99	1.01	1.3 MW, 0.4 MVAR	0.5 MW, 0.4 MVAR	62%	2.3%
	1.01	1.03	1.3 MW, 0.4 MVAR	0.5 MW, 0.4 MVAR	62%	3%

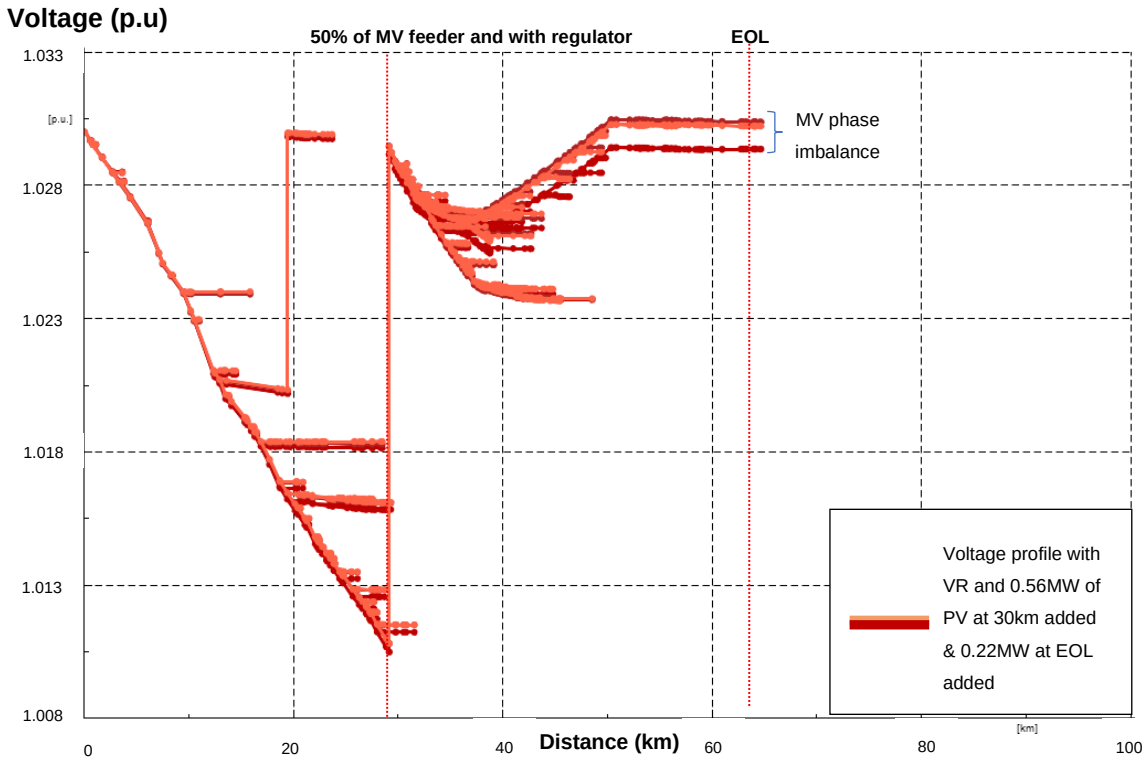

Figure 4.56: Peak load with regulator: Voltage profile of Network 2 with PV at 50% and EOL

4.3.3.2 Peak load without regulator and with PV installed

In this study, 0.56 MW of PV was installed at 50% down the feeder and 0.2 MW of PV was installed at the EOL. Results in Table 4.20 show that a 62% improvement in network capacity was also seen with the RVC at the EOL reaching an acceptable value of 2.9%. Figure 4.57 shows the corresponding voltage profile without the voltage regulator. No changes are seen from Table 4.19 except the voltage at the connecting point of the PV system. Voltage regulation is better with the regulator installed.

Table 4.20: Peak load without regulator – PV at 50% and EOL

PV size located at	Voltage before (p.u)	Voltage after (p.u)	Power initial at source	Power final at source	Capacity improvement	RVC%
0.56 MW at 50% and 0.2 MW at EOL	0.99	1.01	1.3 MW, 0.4 MVAR	0.5 MW, 0.4 MVAR	62%	2.3%
	0.98	1.01	1.3 MW, 0.4 MVAR	0.5 MW, 0.4 MVAR	62%	2.9%

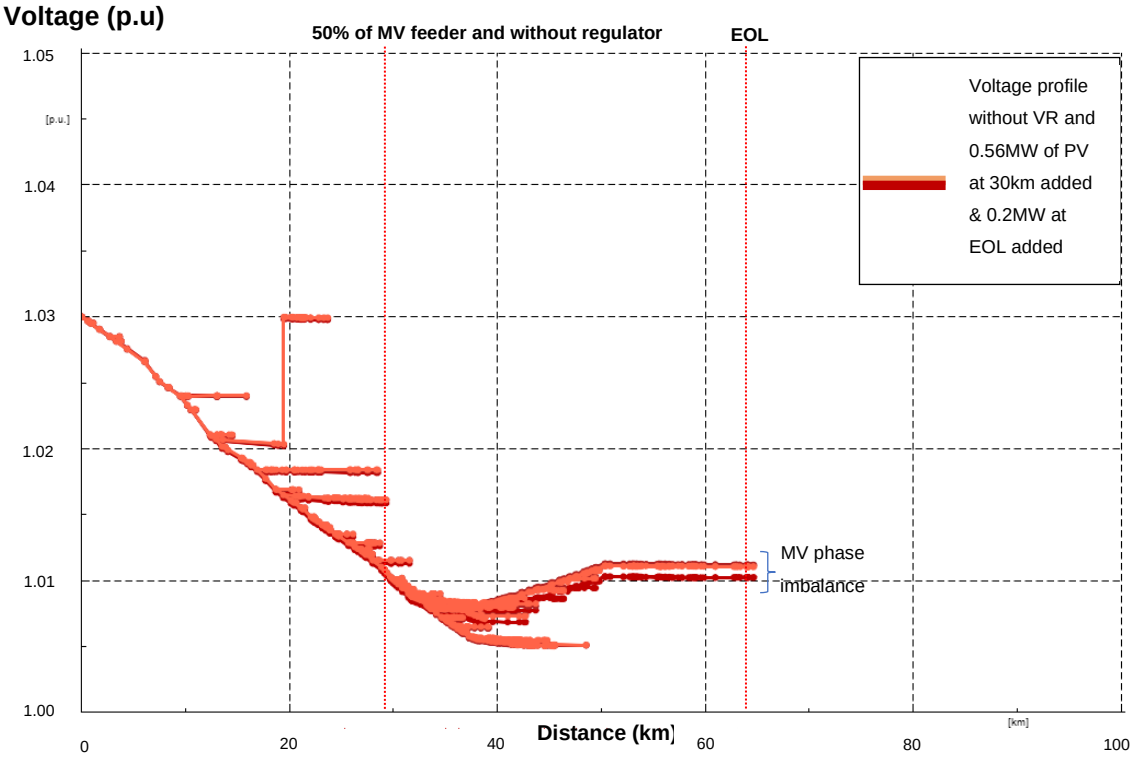

Figure 4.57: Peak load without regulator: Voltage profile of Network 2 with PV at 50% and EOL

4.3.3.3 Light load with regulator and with PV installed

In this study, 0.56 MW of PV was installed at 50% down the feeder and 0.22 MW of PV was installed at the EOL. Results in Table 4.21 show that a 133% improvement in network capacity was also seen with the RVC at the EOL reaching an acceptable value of 2.9%. As in the sections with light loading, the final loading has a negative VAR flow due to cables and line capacitance on this network**.** Figure 4.58 shows the corresponding voltage profile with the voltage regulator.

Table 4.21: Light load with regulator – PV at 50% and EOL

PV size located at	Voltage before (p.u)	Voltage after (p.u)	Power initial at source	Power final at source	Capacity improvement	RVC%
0.56 MW at 50% and 0.22 MW at	1.02	1.04	0.6 MW, -0.1 MVAR	-0.2 MW, -0.1 MVAR	133%	2.3%
	1.02	1.04	0.6 MW, -0.1 MVAR	-0.2 MW, 0.1 MVAR	133%	2.9%

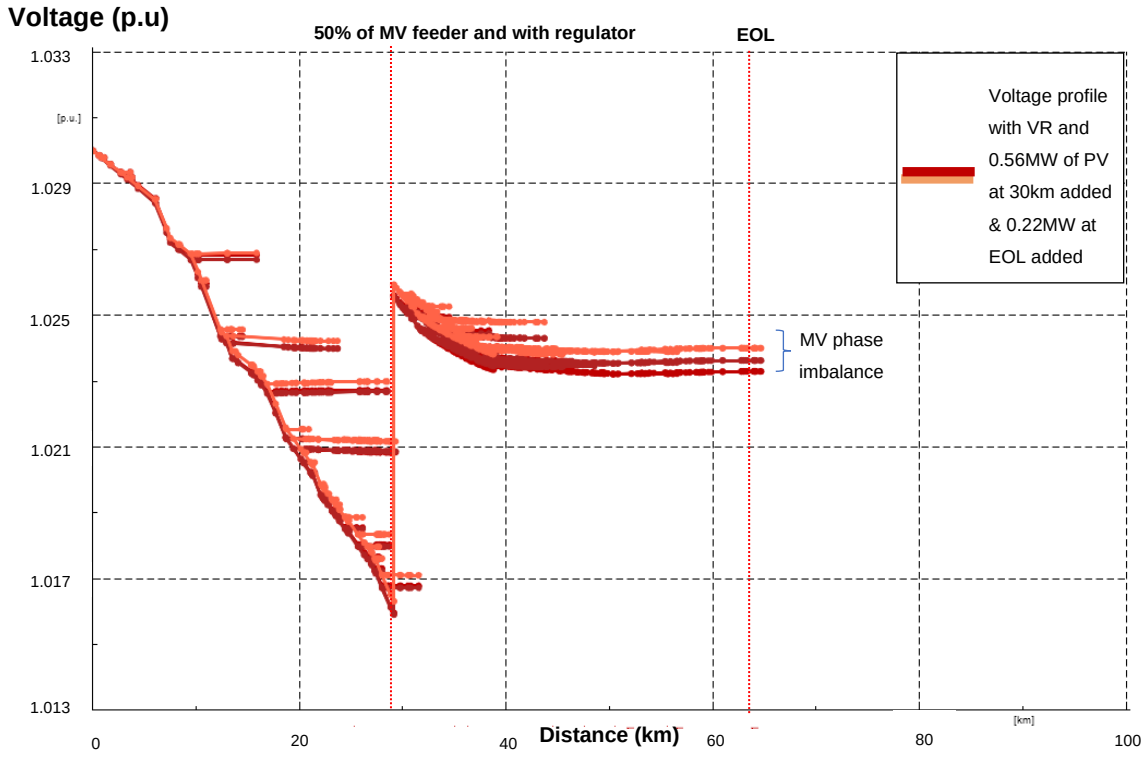

Figure 4.58: Light load with regulator: Voltage profile of Network 2 with PV at 50% and EOL

4.3.3.4 Light load without regulator and with PV installed

In this study, 0.56 MW of PV was installed at 50% down the feeder and 0.22 MW of PV was installed at the EOL. Results in Table 4.22 show that a 133% improvement in network capacity was also seen with the RVC at the EOL reaching an acceptable value of 2.9%. Figure 4.59 shows the corresponding voltage profile without the voltage regulator. No changes are seen from Table 4.21 except that once again, the voltage at the connecting point of the PV system has improved voltage regulation with the regulator installed.

Table 4.22: Light load without regulator – PV at 50% and EOL

PV size located at	Voltage before (p.u)	Voltage after (p.u)	Power initial at source	Power final at source	Capacity improvement	RVC%
0.56 MW at 50% and 0.22 MW at	1.02	1.04	0.6 MW, -0.1 MVAR	-0.2 MW, -0.1 MVAR	133%	2.3%
	1.01	1.04	0.6 MW, -0.1 MVAR	-0.2 MW, -0.1 MVAR	133%	2.9%

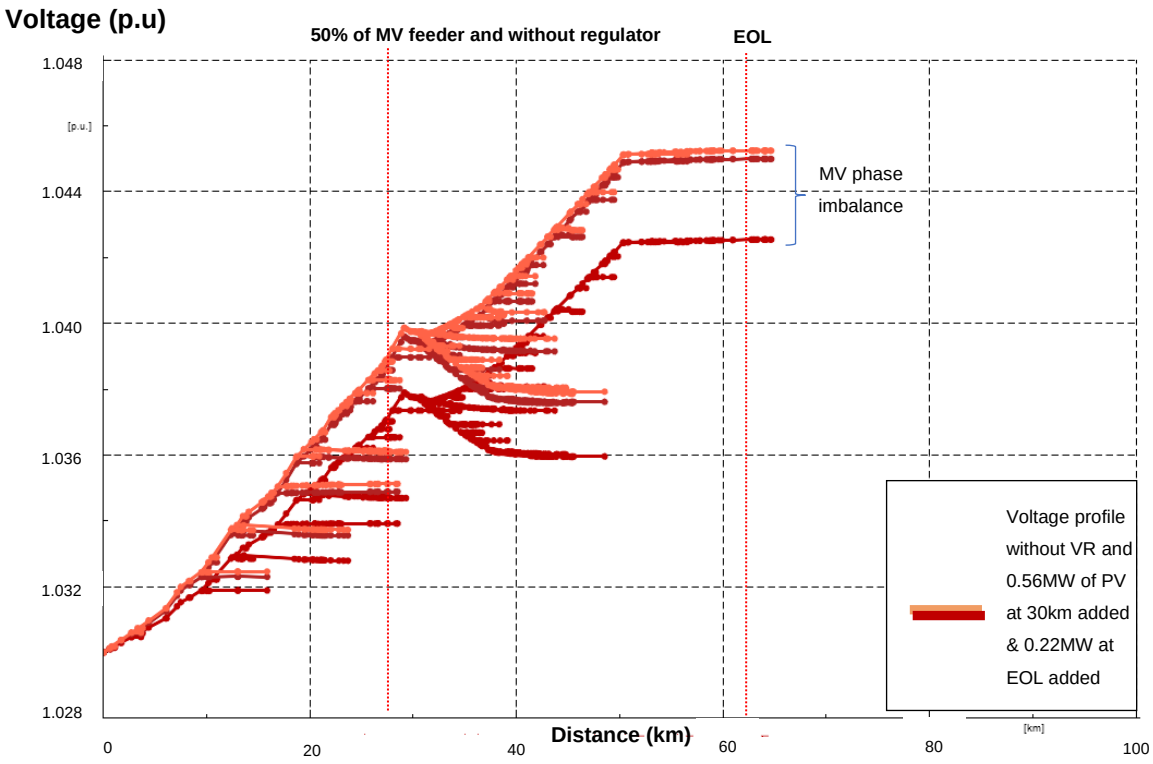

Figure 4.59: Light load without regulator: Voltage profile of Network 2 with PV at 50% and EOL

4.4 PV placement using the PSO tool applied to Network 2:

The scenarios simulated in the conventional manner in section 4.3 with Network 2, assessed the network capacity improvement by connecting PV to strategic MV positions as in section 4.1 Section 4.4 applies the PSO DPL script and assessment tool analyser to Network 2 and the results obtained is used to compare the effectiveness of the tool to the manual method as a reference base case in section 4.3. For the PSO tool, the values for the number of iterations

number of PV systems and network voltage (here 22 kV for Network 2) can be selected by the user in the input page of the DPL script for analysis.

In section 4.3, the network improvement using the manual method of connecting PV systems halfway (50%) down Network 2 feeder, at the EOL and at both positions simultaneously (Figure 4.50 shows these positions), were conducted and discussed. In each of the three PV connection configurations, the four scenarios of having the regulator in and out of service operating during peak and off-peak (light load) times were applied in the simulations. These scenarios are again applied while utilizing the proposed tool to assess the network improvement with the developed DPL script.

In each scenario as previously discussed, the *Fres* matrix values are presented graphically (matrix explained in Chapter 3, Figure 3.28 where every row is a PV system and every column for that row is the new MV position calculated by equation (3.33)), showing the progression of the PV connection as determined by the PSO calculations in the MV network. The voltage profile for Network 2 for the optimal PV connection point obtained, is displayed through an extract from the tool and a summary of results showing values of the *Ginmat* matrix (Chapter 3, Figure 3.20), is presented including the network capacity found.

4.4.1 Light load with regulator and with PV system installed

In this scenario all loads are scaled to 0.4 to obtain a voltage profile during off-peak load times. The DPL script is applied to Network 2 where the selected input in the DPL input page was PV system=1 and number of iterations=5. The *Fres* matrix values were calculated in every iteration as per the PSO equation in the DPL code where each new position is determined by the calculated fitness (voltage) values and is shown in Figure 4.60. The starting position was randomly selected at 1171 with each new position calculated using equation (3.33) of Chapter 3. The x-axis scale is the iteration number and the y-axis is the MV bus-position.

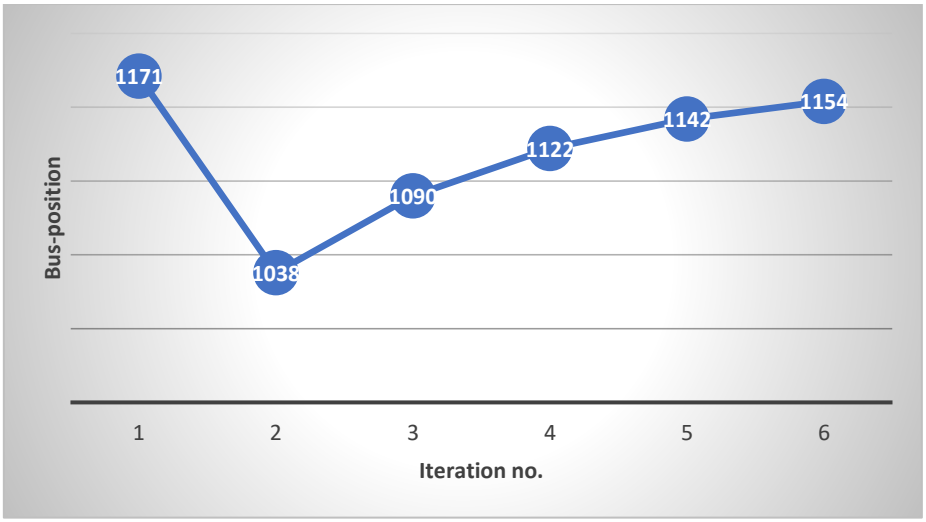

Figure 4.60: Light load with regulator: *Fres* matrix values for PV connection positions calculated from the PSO equation (PV system=1, iterations=5)

The voltage profile in Figure 4.61 is extracted from the tool and each colour represents the voltage profile for every PSO location calculated in the *Fres* matrix which is shown graphically in Figure 4.60. The plot labelled PV at position 1038 corresponding to a bus-index of 2869 (64% down the feeder network, please refer to Appendix C, look-up table for MV position to bus-index), shows the optimal location found to the base case (before the connected PV). An improved voltage profile is seen (green colour) with respect to the base case (blue colour) but optimised by the set upper limit in the DPL script.

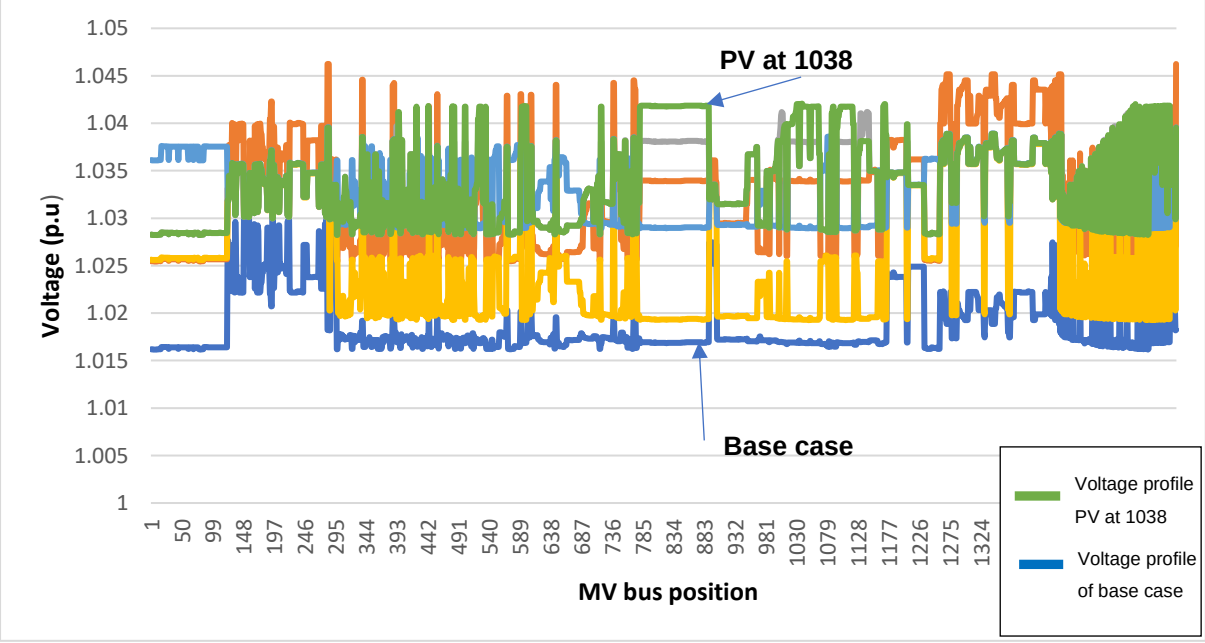

Figure 4.61: Light load with regulator: Voltage profile of the MV feeder with optimal PV connected at position 1038 (PV system=1, iterations=5)

The *Ginmat* matrix results shows a 143% network capacity improvement with PV to be installed 64% down the network from the MV source with an initial loading of 0.489 MW to a final loading of -0.21 MW export and maximum PV size of 706 kW. As mentioned previously, the 210 kW exported power has to be technically managed. All line loadings were checked to be within set limits.

To further test this network, the next selected input was PV systems=3 and number of iterations=6 for the light load scenario with the regulator in service and PV installed. Figure 4.62 shows the progression of the PSO location for each connected PV and each iteration of the 3 PV systems from random starting positions 1250, 395 and 70. The displayed values converge to a particular MV bus-position. The *Ginmat* matrix results show a 242% network capacity improvement with PV to be installed at optimal position 725 (bus-index 2009) which is 45% down the network from the 22 kV MV source with an initial loading of 0.489 MW to a final loading of -0.707 MW export and maximum PV size of 1220 kW.

The tool extract of the optimised voltage profile for the feeder corresponding to the iteration where the optimal position 725 was found is shown in Figure 4.63. The voltage is just below the 1.06 p.u.

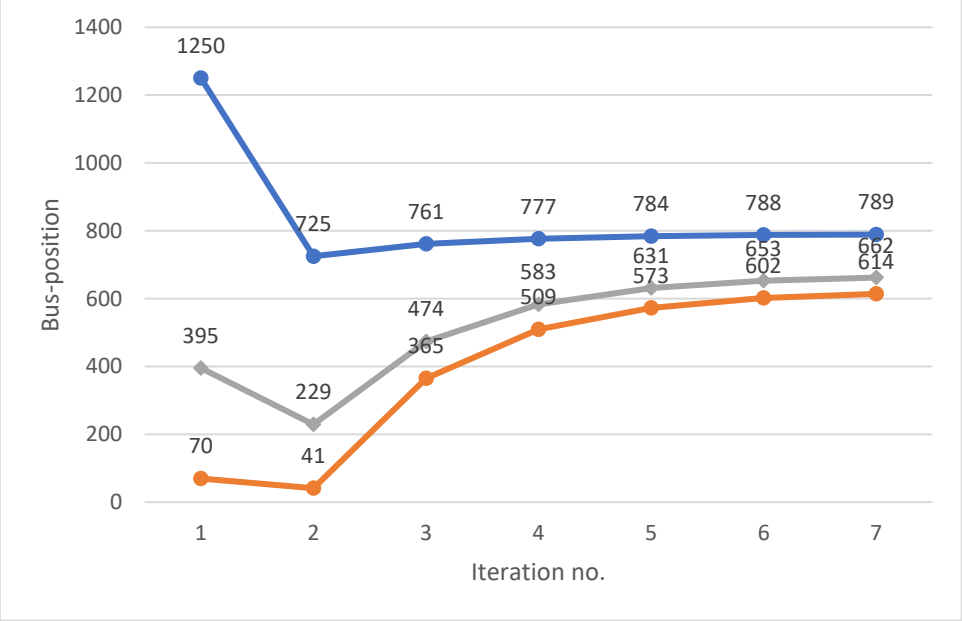

Figure 4.62: Light load with regulator: *Fres* matrix values for PV connection positions calculated from the PSO equation (PV system=3, iterations=6)

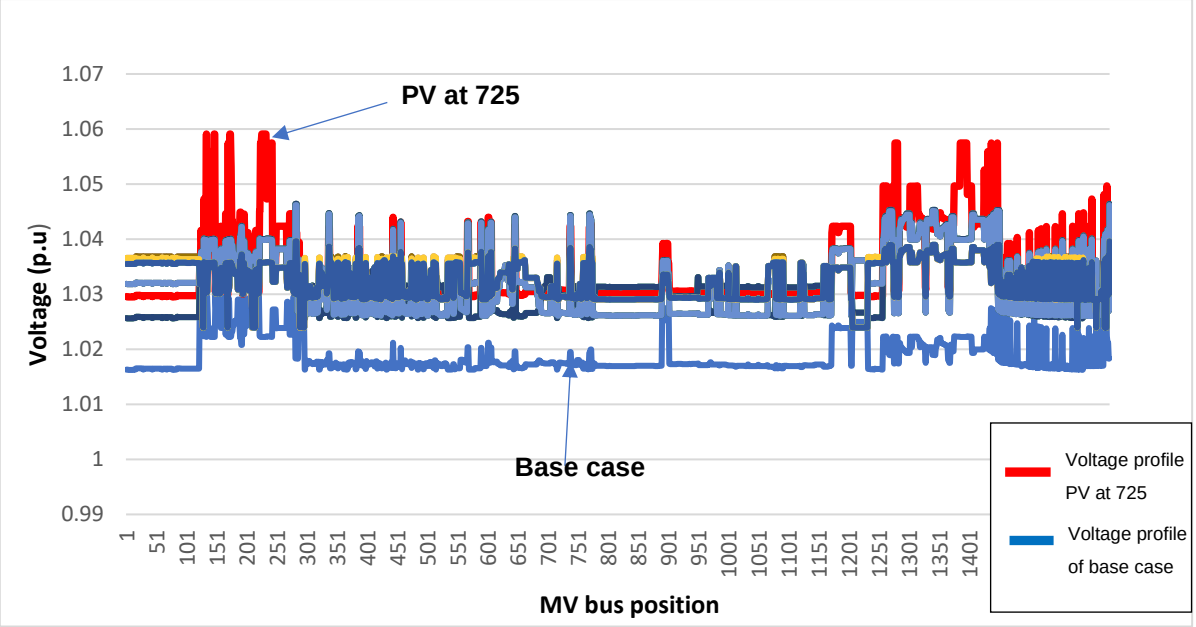

Figure 4.63**:** Light load with regulator: Voltage profile of the MV feeder with optimal PV connected at position 725 (PV system=3, iterations=6)

4.4.2 Light load without regulator and with PV system installed

The second scenario using the DPL script for Network 2 utilizes the same parameters for light load, no. of PV systems=1 and iterations=5 but without the regulator in service. Figure 4.64 shows the progression of the PSO location for connected PV and each iteration, from position 1107 to 1306 calculated using equation (3.33) in Chapter 3. The tool extract of the optimised voltage profile for the feeder corresponding to optimal position 1244 (bus-index 3363) is shown to be located 74% down the network feeder as presented in Figure 4.65. A network capacity improvement of 143% is seen with 706 kW of generation added at this point (1244). All voltages along the MV feeder are kept within the upper bound of 1.06 p.u and provides voltage regulation much higher than the base case profile.

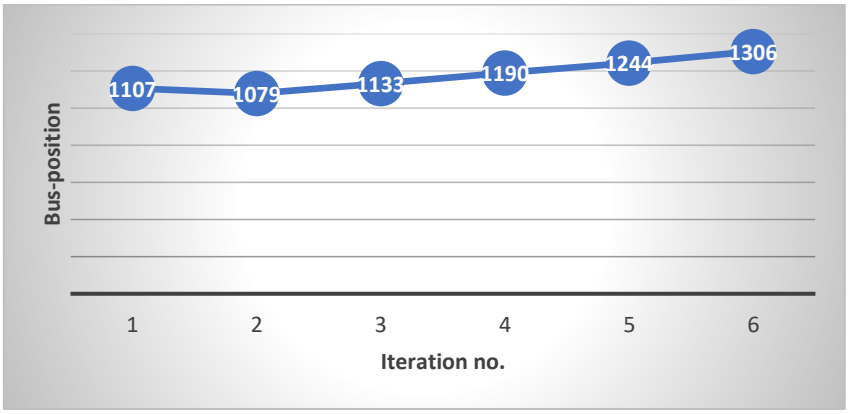

Figure 4.64: Light load without regulator: *Fres* matrix values for PV connection positions calculated from the PSO equation (PV system=1, iterations=5)

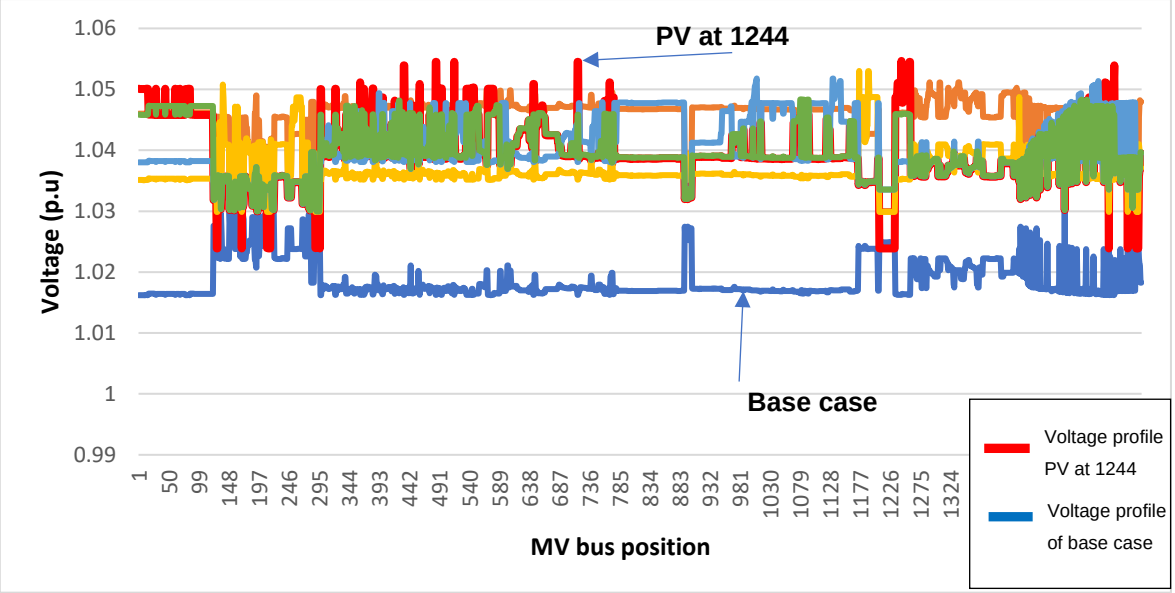

Figure 4.65: Light load without regulator: Voltage profile of the MV feeder with optimal PV connected at position 1244 (PV system=1, iterations=5)

The next selected input was PV system=3 and number of iterations=6 for the light load scenario and the regulator out of service. Figure 4.66 displays the calculated PSO points of the *Fres* matrix and is shown graphically. All 3 PV systems is seen to converge as more iterations are executed. Result summary from the *Ginmat* matrix shows that the optimal position is found to be 1523 (bus-index 4155) located 93% down the network feeder. A network capacity improvement of 142% is seen, also with 706 kW of generation added at this point (1523). The optimised voltage profile is shown in Figure 4.67 and is extracted from the tool. The 22 kV MV source has an initial loading of 0.489 MW and with the PV installed has a final loading of -0.208 MW, where 208 kW of power is exported into the upstream network.

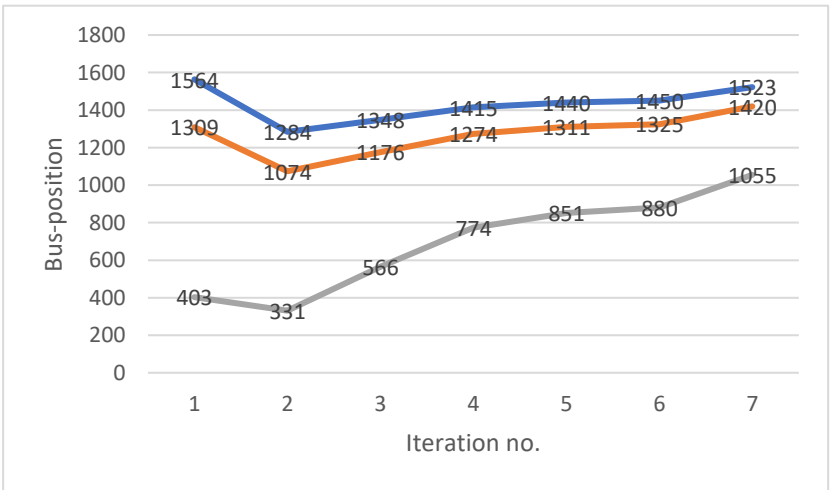

Figure 4.66**:** Light load without regulator: *Fres* matrix values for PV connection positions calculated from the PSO equation (PV system=3, iterations=6)

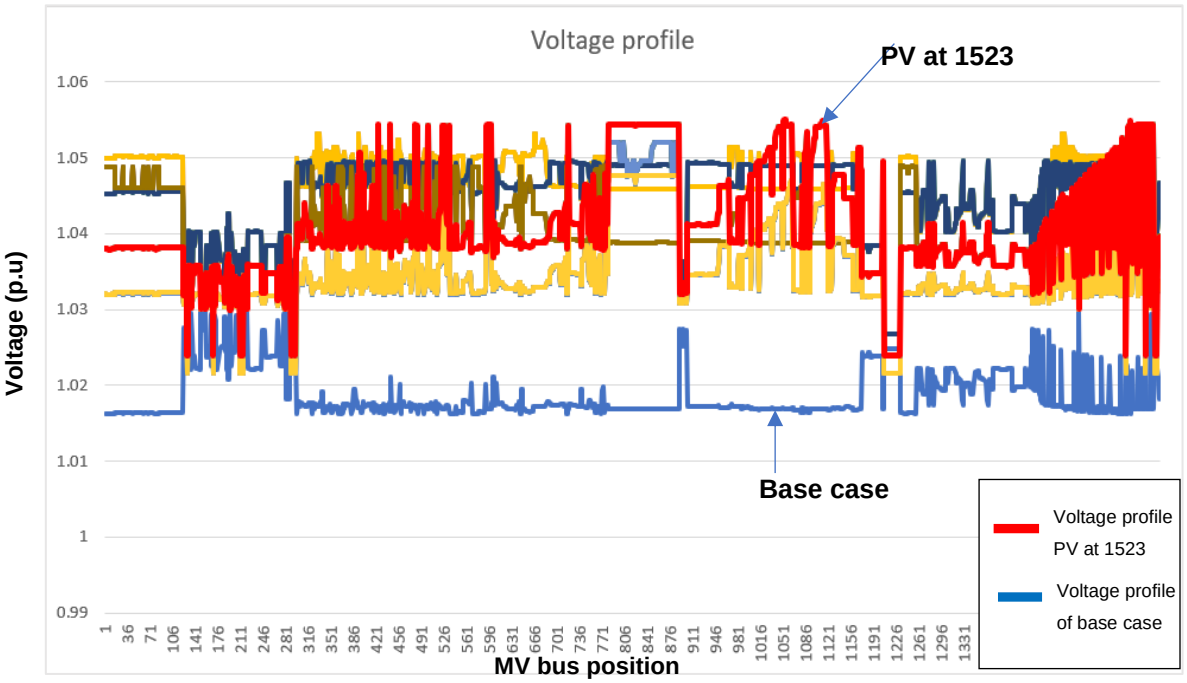

Figure 4.67: Light load without regulator: Voltage profile of the MV feeder with optimal PV connected at position 1523 (PV system=3, iterations=6)

4.4.3 Peak load with regulator and with PV system installed

For this scenario all scaling for the feeder load is applied as per section 4.1 (scaling factor 1). The selected input on the DPL input page was number of PV system=1 and number of iterations=5. The *Fres* matrix values were calculated for every iteration as per the PSO equation (Chapter 3, equation (3.33)) in the code where each new position (i.e., PV connection point) is determined by the calculated fitness values (change in voltage [p.u]) before and after the PV connection. Figure 4.68 represents the *Fres* matrix graphically starting at iteration 1 at an initial random position of *1353* (bus-index 3756) and progressing through to position *1297* (bus-index 3560) as the code is executed from iteration 1 to iteration 6. Appendix C shows the lookup table of MV positions to feeder bus-index values. It is to be noted that initial iteration is 1 and then 5 more iterations are executed up to iteration 6. The x-axis of Figure 4.68 gives the iteration number and the y-axis gives the calculated positions.

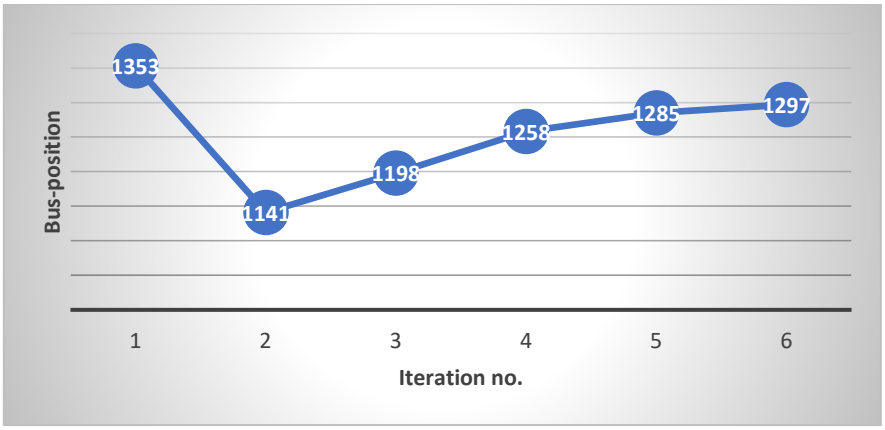

Figure 4.68: Peak load with regulator: *Fres* matrix values for PV connection positions calculated from the PSO equation (PV system=1, iterations=5)

Figure 4.69 shows the tool extract where the optimal PV connection point found for 5 iterations (2 to 6) was 1297 corresponding to a bus-index of 3560. The profile highlighted in red is the optimised voltage profile found for the optimal position that had the greatest change in voltage before and after the connection of the PV system (greatest fitness value). It must be noted here also that the optimal position is found, only once the PV generation connection satisfies the RVC requirements. The network capacity is only determined once this completed by equation 4.1. It can be seen that all MV terminal points are improved relative to the base case (labelled 'base case', blue colour graph) by installing PV of 1.22 MW. A network capacity improvement of 104% is seen, also with 1.22W of generation added at this point (1297). The 22 kV MV source has an initial loading of 1.195 MW and with the PV installed has a final loading of -0.05 MW, where 50 kW of power is exported into the upstream network.

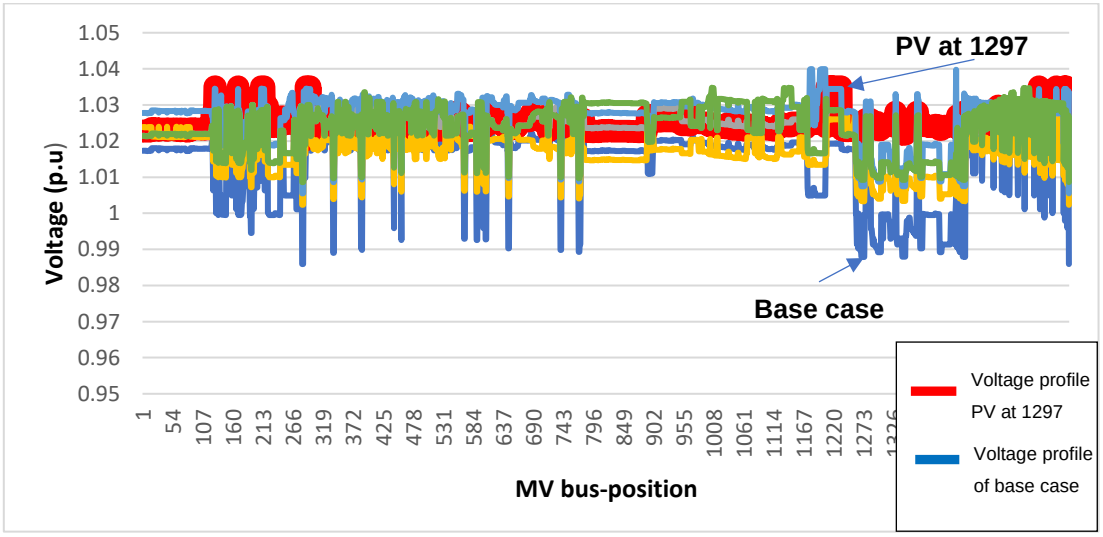

Figure 4.69**:** Peak load with regulator: Voltage profile of the MV feeder with optimal PV connected at position 1297 (PV system=1, iterations=5)

To further test this network, the next selected input was PV system=3 and number of iterations=6 for the peak load scenario with the regulator in service and PV installed. Figure 4.70 shows the progression of the PSO location for each connected PV and each iteration of the 3 PV systems from random starting positions 1029, 285 and 115. The displayed values converge to a particular MV bus-position. The *Ginmat* matrix results show a 103% network capacity improvement with PV to be installed at optimal position 71 (bus-index 285) which is 6% down the network from the 22 kV MV source with an initial loading of 1.195 MW to a final loading of -0.0387 MW export and maximum PV size of 1220 kW. The tool extract of the optimised voltage profile for the feeder corresponding to the iteration where the optimal position 71 was found is shown in Figure 4.71. The voltage throughout the network is kept within regulation limits.

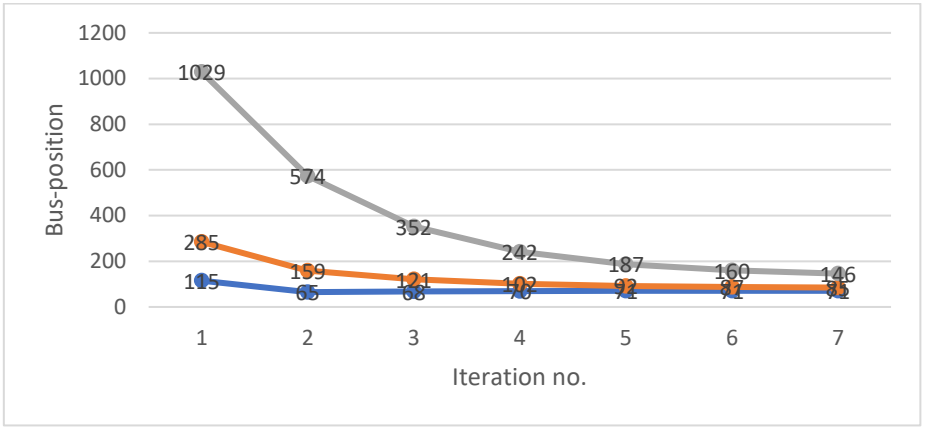

Figure 4.70: Peak load with regulator: *Fres* matrix values for PV connection positions calculated from the PSO equation (PV system=3, iterations=6)

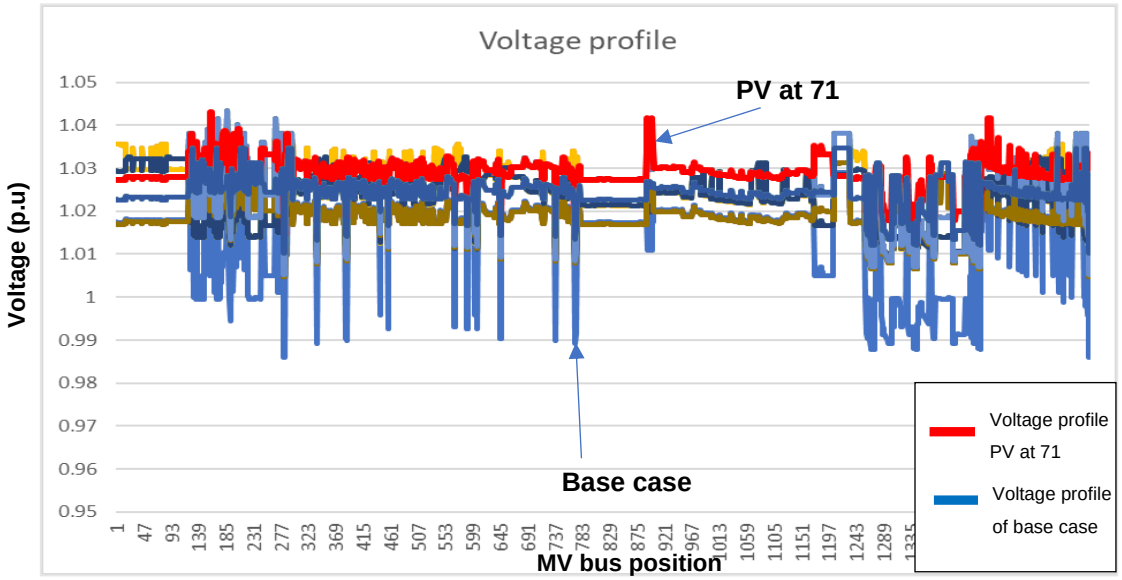

Figure 4.71**:** Peak load with regulator: Voltage profile of the MV feeder with optimal PV connected at position 71 (PV system=3, iterations=6)

4.4.4 Peak load without regulator and with PV system installed

The selected input in the DPL script for this scenario, was PV system=1 and number of iterations=5. The regulator here is out of service and all loads remain to be scaled by a factor of 1 representing a peak load profile. The *Fres* matrix values were again calculated in every iteration and is shown in Figure 4.72. Figure 4.73 shows the optimised voltage profile of the network feeder for the iteration where the optimal position 697 (bus-index 1967) is found. Result summary from the *Ginmat* matrix shows that the optimal bus position is located 44% down the network feeder. A network capacity improvement of 81% is seen with 941 kW of generation added at this connection point (697). A final loading of 0.222 MW is noted.

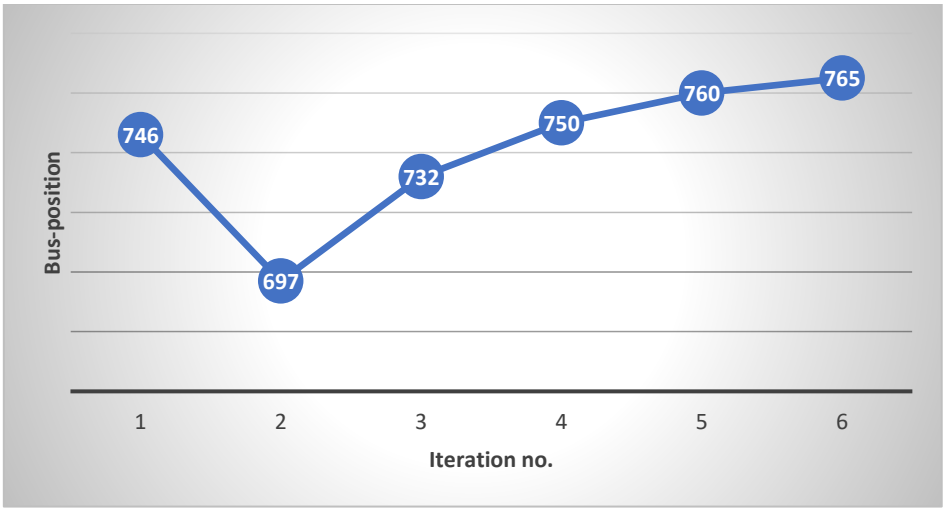

Figure 4.72: Peak load without regulator: *Fres* matrix values for PV connection positions calculated from the PSO equation (PV system=1, iterations=5)

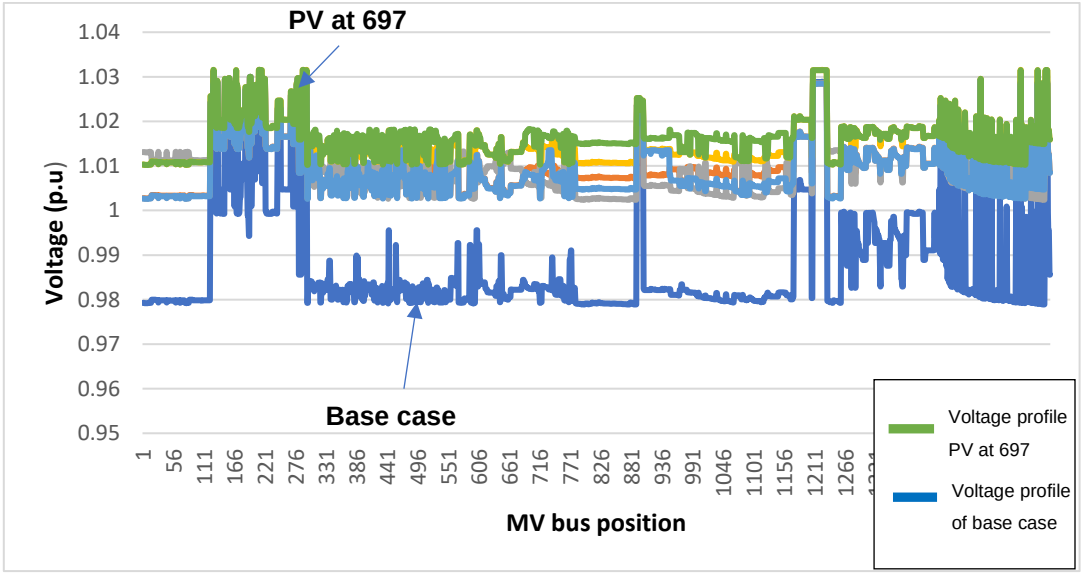

Figure 4.73**:** Peak load without regulator: Voltage profile of the MV feeder with optimal PV connected at position 697 (PV system=1, iterations=5)

To further test this network, the next selected input was PV system=3 and number of iterations=6 for the peak load scenario with the regulator is placed out of service. Figure 4.74 shows the progression of the PSO location for each connected PV and each iteration of the 3 PV systems from random starting positions 1562, 740 and 172. The displayed values do not converge with 6 iterations but if more iterations were executed convergence is possible. The *Ginmat* matrix results show a 44% network capacity improvement with PV to be installed at optimal position 858 (bus-index 2326) which is 52% down the network. A final loading of 0.67 MW and maximum PV size of 508 kW is seen. The tool extract of the optimised voltage profile is shown in Figure 4.75. The voltage throughout the network is kept within regulation limits.

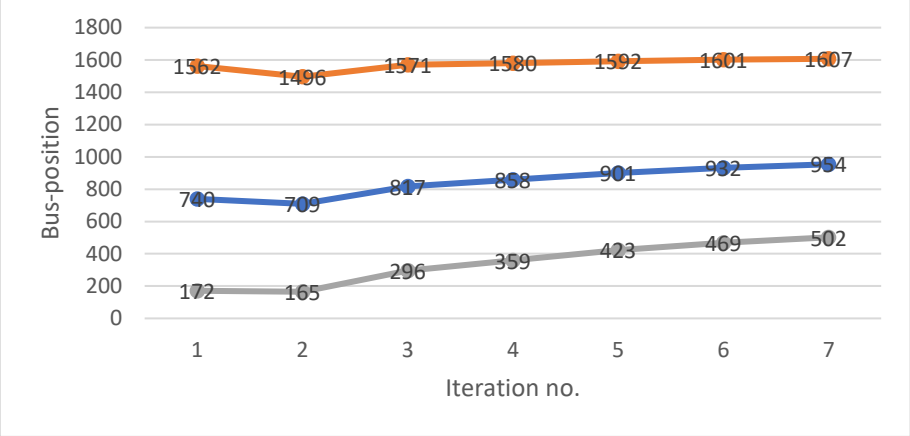

Figure 4.74: Peak load without regulator: *Fres* matrix values for PV connection positions calculated from the PSO equation (PV system=3, iterations=6)

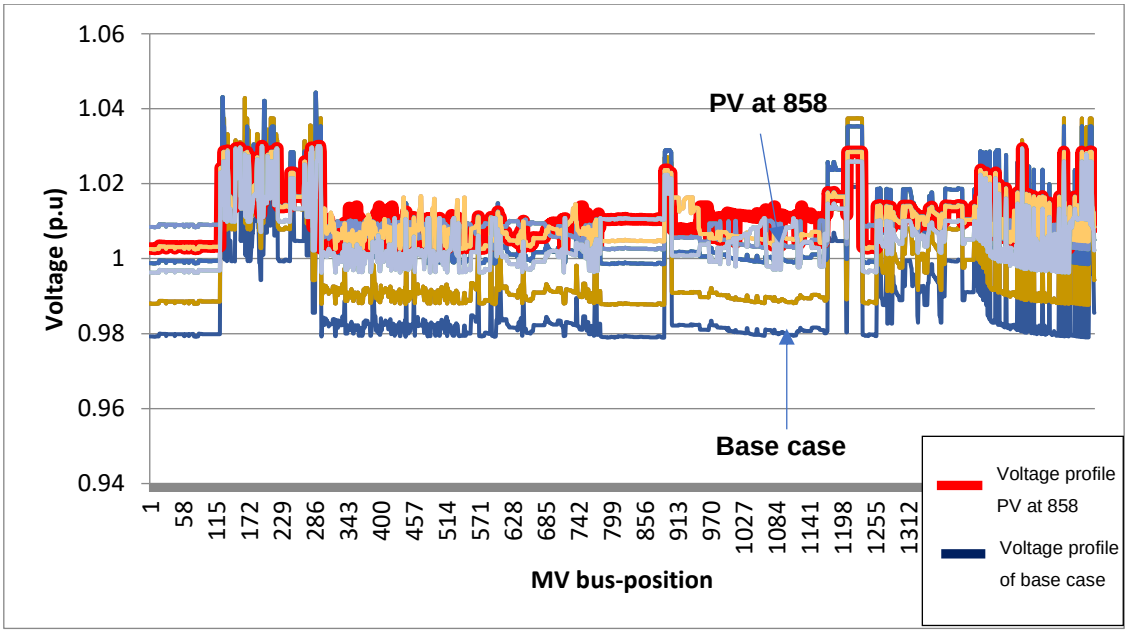

Figure 4.75: Peak load without regulator: Voltage profile of the MV feeder with optimal PV connected at position 858 (PV system=3, iterations=6)

The next section of 4.5 summarizes all results for both networks and is tabulated accordingly. The summary of results are extracted from sections 4.1 – 4.4 and are collated and presented in this section. The method or scenario, the position on the feeder, the network capacity created and total amount of generation are the columns for the relevant tables that follow.

4.5 Summary of results and objective function values

4.5.1 Network 1 results summary

Table 4.23 presents the summary for Network 1, comparing the conventional method of modelling and the results from applying the tool to that network. The scenario, the placement of the PV system on the feeder (MV bus-position) and the amount of generation maximized to achieve the network capacity is summarized. Table 4.24 presents the calculation of the objective function for Network 1.

Table 4.23: Summary of all results for Network 1

Method Utilized and PV placement point on the feeder	% down the feeder	Bus-index	% Network capacity improvement	Total PV generation(kW)
Scenario: Normal Feeder Peak Load				
Conventional 50%	50%	550	54%	1400 kW
Conventional EOL	100%	1090	27%	650 kW
Conventional 50% & EOL	50% + EOL	550+1090	54%	1340 kW
1 PV & 5 Iterations	73%	803	43%	1093 kW
5 PV & 10 Iterations	22%	245	64%	1620 kW
10 PV & 15 Iterations	7%	72	54%	1350 kW
Scenario: Normal Feeder Light Load				
Conventional 50%	50%	550	145%	1600 kW
Conventional EOL	100%	1090	63%	700 kW
Conventional 50% & EOL	50% + EOL	550+1090	127%	1400 kW
1 PV & 5 Iterations	36%	390	155%	1619 kW
5 PV & 10 Iterations	39%	417	83%	1214 kW
10 PV & 15 Iterations	57%	624	78%	809 kW
Scenario: Constrained Feeder Peak Load				
Conventional 50%	50%	550	38%	1440 kW
Conventional EOL	100%	1090	16%	640 kW
Conventional 50% & EOL	50% + EOL	550+1090	35%	1400 kW
1 PV & 5 Iterations	52%	571	23%	809 kW
5 PV & 10 Iterations	10%	112	62%	2249 kW
10 PV & 10 Iterations	75%	831	94%	2900 kW
Scenario: Constrained Feeder Light Load				
Conventional 50%	50%	550	106%	1560 kW
Conventional EOL	100%	1090	47%	700 kW
Conventional 50% & EOL	50% + EOL	550+1090	93%	1400 kW
1 PV & 5 Iterations	94%	1024	55%	810 kW
5 PV & 10 Iterations	38%	420	55%	810 kW

Table 4.24: Summary of all results for Network 1: Objective function calculation

Method Utilized	% down the feeder	% Network capacity improvement	Total PV generation (kW)	Objective fn [%/MW]
Scenario: Normal Feeder Peak Load				
Conventional 50%	50%	54%	1400 kW	39
Conventional EOL	100%	27%	650 kW	39
Conventional 50% & EOL	50% + EOL	54%	1340 kW	40
1 PV & 5 Iterations	73%	43%	1093 kW	39
5 PV & 10 Iterations	22%	64%	1620 kW	40
10 PV & 15 Iterations	7%	54%	1350 kW	40
Scenario: Normal Feeder Light Load				
Conventional 50%	50%	145%	1600 kW	90
Conventional EOL	100%	63%	700 kW	90
Conventional 50% & EOL	50% + EOL	127%	1400 kW	91
1 PV & 5 Iterations	36%	155%	1619 kW	96
5 PV & 10 Iterations	39%	117%	1214 kW	96
10 PV & 15 Iterations	57%	78%	809 kW	96
Scenario: Constrained Feeder Peak Load				
Conventional 50%	50%	38%	1440 kW	26
Conventional EOL	100%	16%	640 kW	25
Conventional 50% & EOL	50% + EOL	35%	1400 kW	25
1 PV & 5 Iterations	52%	23%	809 kW	28
5 PV & 10 Iterations	10%	62%	2249 kW	28
10 PV & 10 Iterations	75%	94%	2900 kW	32
Scenario: Constrained Feeder Light Load				
Conventional 50%	50%	106%	1560 kW	68
Conventional EOL	100%	47%	700 kW	67
Conventional 50% & EOL	50% + EOL	93%	1400 kW	67
1 PV & 5 Iterations	94%	55%	810 kW	68
5 PV & 10 Iterations	38%	55%	810 kW	68

A very interesting relationship is seen when calculating the objective function to achieve the percentage improvement per of generation added to the network. For example, with the constrained feeder light load scenario above, the *network capacity to PV generation ratio* (objective function) indicates that the network capacity improvement is 67% per MW of generation added. Similarly, for the *normal feeder peak* load scenario, the objective function (%/MW) is approximated around 40%/MW. In the multiple DG scenario various optimal points are found from the tool in which different integrating points can be used for PV systems. This is filtered out by not having any of the set of DG units exceeding the 3% RVC limits. The developed tool results, therefore, correlates closely with the results from the manual/conventional studies executed in Section 4.1 and 4.3 but provides an extensive range of analysis capabilities as presented in Section 4.2, 4.4 and 4.5. Figure 4.76 shows the

average network capacity improvement (%) to the network scenarios identified. For example, if one is to install 400 kW of PV on the network, the objective function for the peak times is 39%/MW so for 0.4 MW, the network capacity improvement is calculated by 39% x 0.4 = 15.6%.

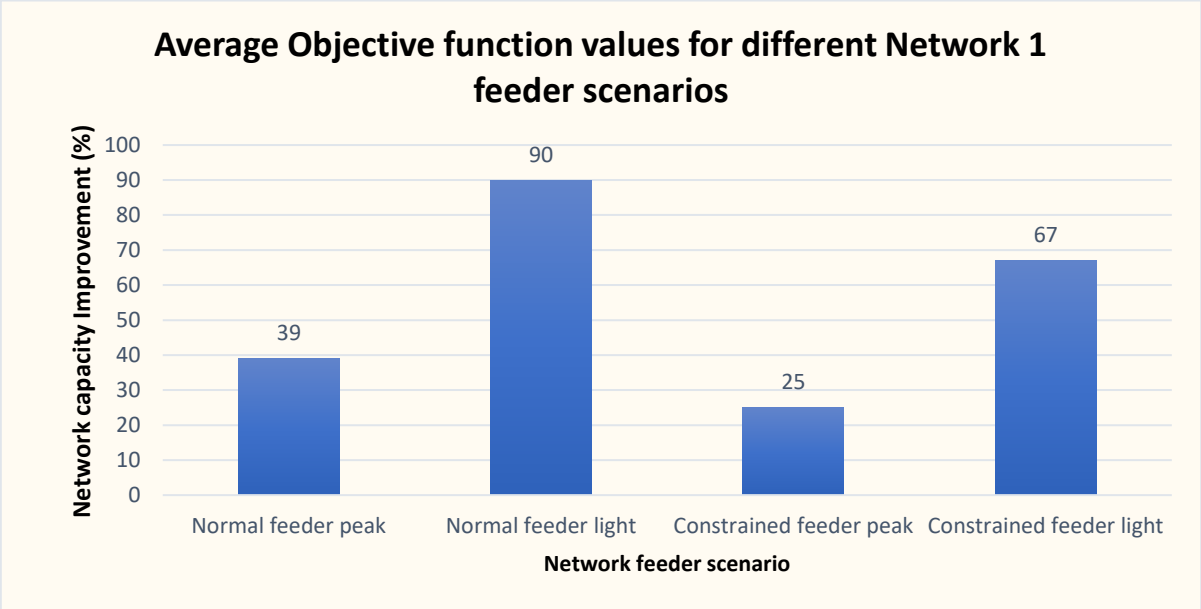

Figure 4.76: Graphical representation of average percentage of network capacity improvement per MW added to Network 1

4.5.2 Network 2 results summary

The summary of Network 2 results are presented in this section. Table 4.25 compares the conventional method of modelling and the results from applying the tool to that network. The scenario, the placement of the PV system on the feeder (bus-index) and the amount of generation maximized to achieve the network capacity is also summarized. Table 4.26 presents the calculation of the objective function for Network 2.

Table 4.25: Summary of all results for Network 2

Method Utilized	% down the feeder	Bus-index	% Network capacity improvement	Total PV generation (kW)
Scenario: Peak load without regulator				
Conventional 50%	50%	1864	75%	999 kW
Conventional EOL	100%	4491	38%	480 kW
Conventional 50% & EOL	50% + EOL	1864+4491	62%	760 kW
1 PV & 5 Iterations	44%	1967	81%	941 kW
3 PV & 6 Iterations	52%	2326	44%	508 kW
Scenario: Peak load with regulator				
Conventional 50%	50%	1864	75%	999 kW
Conventional EOL	100%	4491	38%	480 kW
Conventional 50% & EOL	50% + EOL	1864+4491	62%	780 kW
1 PV & 5 Iterations	80%	3560	104%	1220 kW
3 PV & 6 Iterations	6%	285	103%	1220 kW
Scenario: Light load with regulator				
Conventional 50%	50%	1864	180%	999 kW
Conventional EOL	100%	4491	80%	500 kW
Conventional 50% & EOL	50% + EOL	1864+4491	133%	780 kW
1 PV & 5 Iterations	64%	2869	143%	706 kW
3 PV & 6 Iterations	45%	2009	242%	1220 kW
Scenario: Light load without regulator				
Conventional 50%	50%	1864	180%	999 kW
Conventional EOL	100%	4491	80%	500 kW
Conventional 50% & EOL	50% + EOL	1864+4491	133%	780 kW
1 PV & 5 Iterations	74%	3363	143%	706 kW
3 PV & 6 Iterations	93%	4155	142%	706 kW

Table 4.26: Summary of all results for Network 2: Objective function calculation

Method Utilized	% down the feeder	% Network capacity improvement	Total PV generation (kW)	Objective fn [%/MW]
Scenario: Peak load without regulator				
Conventional 50%	50%	75%	999 kW	75
Conventional EOL	100%	38%	480 kW	76
Conventional 50% &	50% + EOL	62%	760 kW	81
1 PV & 5 Iterations	44%	81%	941 kW	86
3 PV & 6 Iterations	52%	44%	508 kW	86
Scenario: Peak load with regulator				
Conventional 50%	50%	75%	999 kW	75
Conventional EOL	100%	38%	480 kW	76
Conventional 50% &	50% + EOL	62%	780 kW	79
1 PV & 5 Iterations	80%	104%	1220 kW	85
3 PV & 6 Iterations	6%	103%	1220 kW	84
Scenario: Light load with regulator				
Conventional 50%	50%	180%	999 kW	182
Conventional EOL	100%	80%	500 kW	160
Conventional 50% &	50% + EOL	133%	780 kW	170
1 PV & 5 Iterations	64%	143%	706 kW	202
3 PV & 6 Iterations	45%	242%	1220 kW	198
Scenario: Light load without regulator				
Conventional 50%	50%	180%	999 kW	182
Conventional EOL	100%	80%	500 kW	160
Conventional 50% &	50% + EOL	133%	780 kW	170
1 PV & 5 Iterations	74%	143%	706 kW	202
3 PV & 6 Iterations	93%	142%	706 kW	201

Similarly, a very interesting relationship is also seen when calculating the objective function to achieve the percentage improvement per MW of generation added to Network 2. Figure 4.77 summarises this relationship. For each scenario, a minimum and maximum range is derived but with a minimal change in ratio between them.

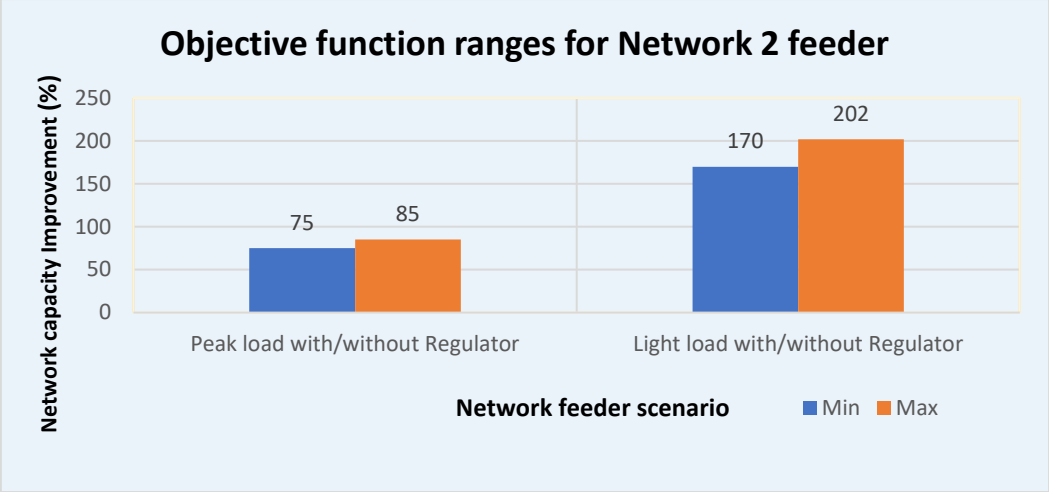

Figure 4.77: Graphical representation of average range percentage (min & max) of network capacity improvement per MW added to Network 2

The above analysis shows that there is no direct link or linear relationship on the amount of generation and position to which it may be installed. As that there are many tee-off points on the backbone and the variation of load with respect to its location, it can be concluded that every network is unique and a general rule to apply in integrating PV cannot be made, however, the ratio of the network capacity increase to the amount of generation is more or less consistent for every scenario. In Figure 4.78 below, a graphical illustration showing the feeder and positions with the manual method and DPL PSO script applied, supports the above observations.

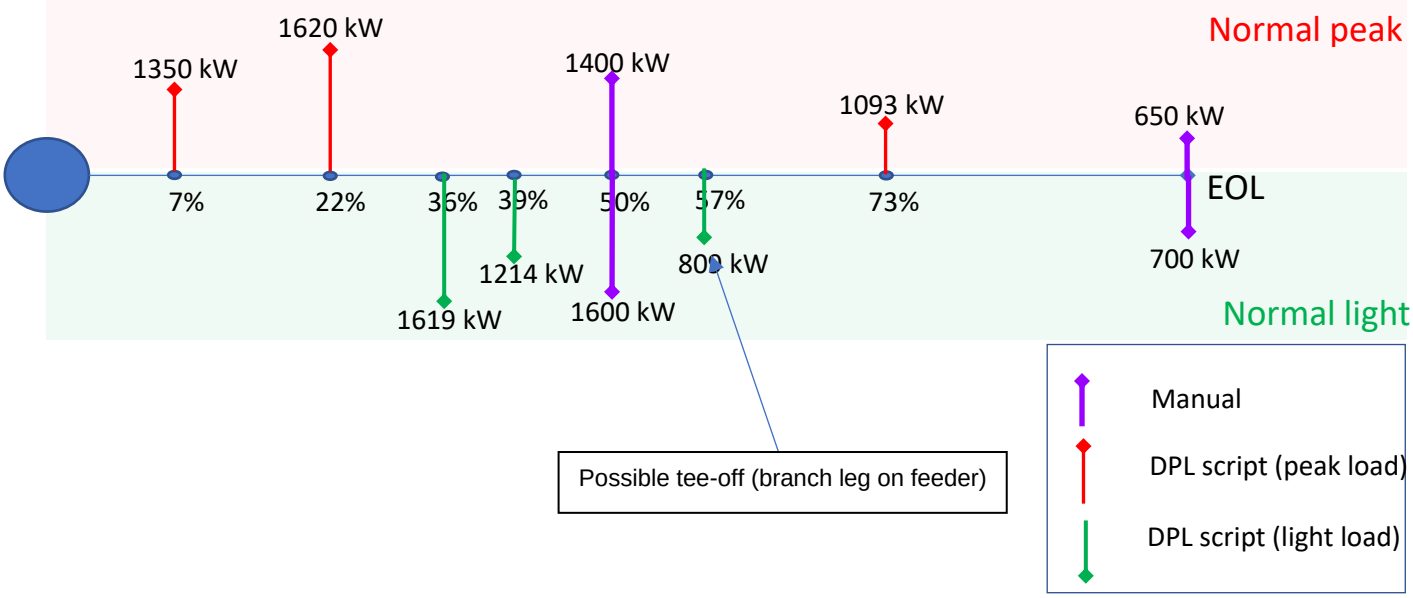

Figure 4.78: PV generation distribution along Network 1 feeder

4.6 Conclusions

Chapter 4 presented all the relevant simulations on two test networks 1 and 2 of 11 kV and 22 kV ratings. Firstly, the conventional method proposed in Section 4.1, was to manually connect a PV system to the Network 1 feeder and the results were obtained when integrated at three different positions, viz, at 50%, at the End-of-line and at both locations simultaneously. The voltage profile was presented for each location and at peak and off-peak loading scenarios. In section 4.2, the PSO tool with DPL script was applied to the same Network 1 feeder with different PV systems and iterations to the DPL input page. The results derived from the PSO tool, i.e. the optimal connecting position (bus-index) value, the optimal voltage profile, thermal limits check and the PSO position for each PV system were presented with all relevant results summarised in Section 4.5. Section 4.3 modelled Network 2 in the same manner as above and Section 4.4 documented the results achieved when the DPL script was applied to Network 2. Again with the relevant results summarized in Section 4.5.

The results derived in Section 4.5 has shown that the Objective function is consistent for each scenario and can be used as a method of approximating the amount of network capacity that can be created when a certain amount of generation that can be added to that network.

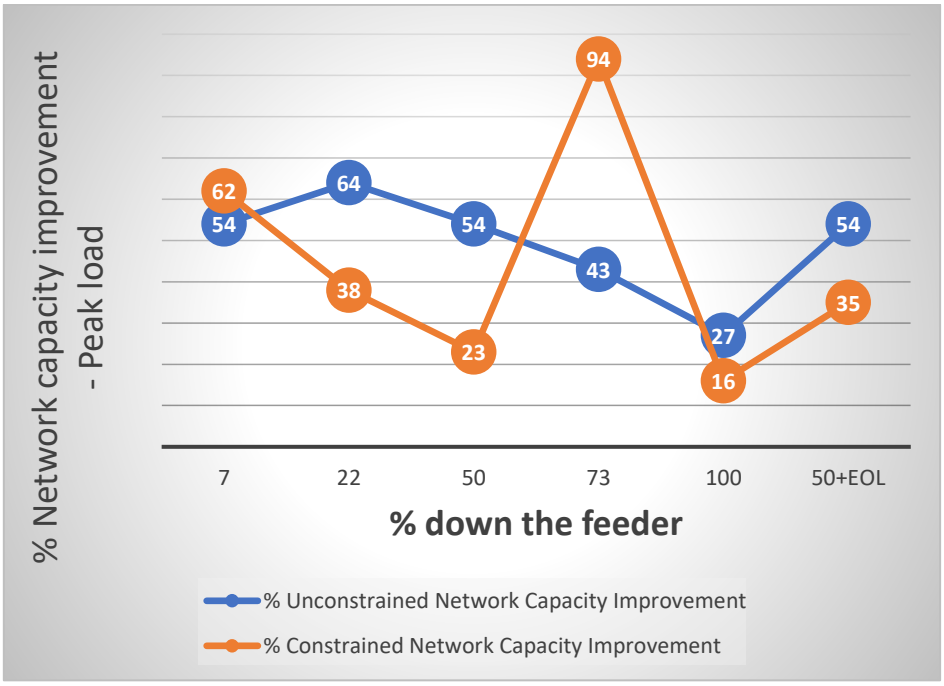

Figure 4.79: Network capacity improvement of Network 1 when the network is constrained and unconstrained and when PV is optimally allocated

Figure 4.79 graphically summarizes the peak load scenario results of Network 1, showing that, the unconstrained network can yield the greatest improvement in network capacity when PV is optimally added to the network.

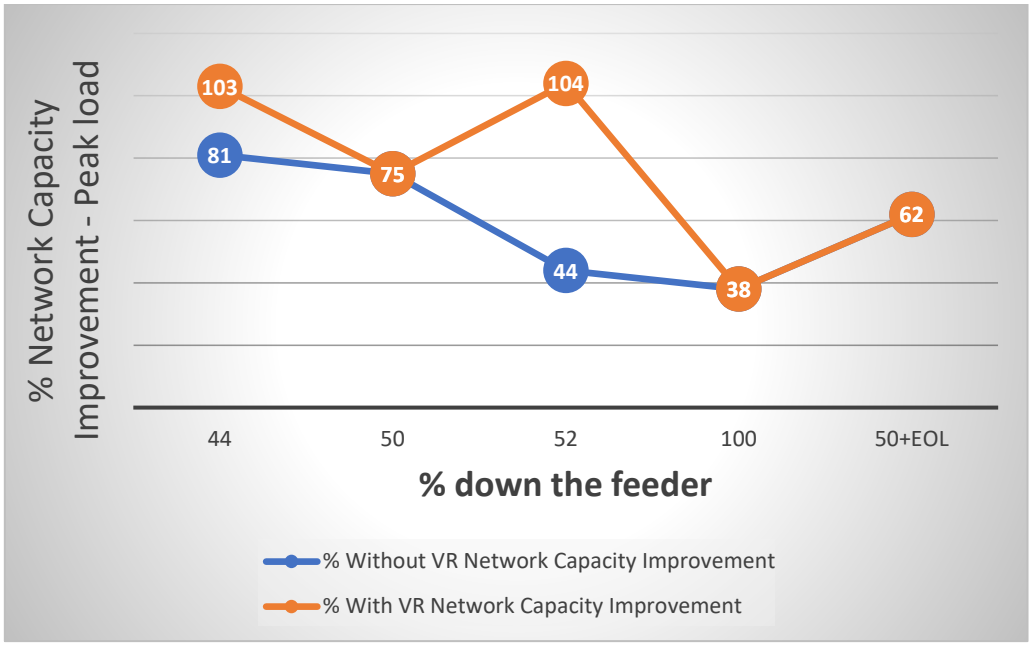

Figure 4.80: Network capacity improvement of Network 2 with and without the Voltage Regulator when PV is optimally allocated

Figure 4.80 graphically summarizes the peak load scenario results of Network 2, showing that, the network can further benefit with the inclusion of a voltage regulator and yield the greatest improvement in network capacity when PV is optimally added to the network.

5 Conclusions

5.1 Summary of Research

MV networks are becoming capacity-constrained resulting in the exceedance of line conductor and equipment thermal and network end of line voltage operating limits. As a result, no new load or increase in existing load can be accommodated and the network is now defined as a constrained MV network. A network is termed un-constrained when additional load can be connected to the network and the operating limits of thermal and voltage are not contravened for that particular network class. For example, if the new load increases the thermal capacity from 65% to 75% the network remains unconstrained provided the end-of-line voltage remains above 0.95 p.u. Significantly, MV networks have seen a huge influx of PV inverter-based systems predominantly due to loadshedding and the increasing prices of the electricity tariff. PV has certainly become cost-effective. Growing industrial type loads are serviced by strong and large roof structures and PV installation is becoming a much needed part of the business. The DPL script-based PSO tool derived from this thesis can certainly reduce the amount of time to assess DG integration (PV and/or electric vehicle charging infrastructure) as well provide a profound insight on the nature of the network when assessing optimal location and maximum network capacity benefit.

Voltage devices for shunt compensation and voltage regulators are employed as short-term solutions to partially mitigate the constraints on MV networks. In addition, shifting load to adjacent networks having the same operating voltage and phase configuration and line re-templating are also feasible and cost-effective solutions. Long term solutions as discussed in Chapter 2, are to upgrade the existing network by replacing high impedance conductors with low impedance conductors, splitting the feeder by moving a portion of load onto a new feeder source at the same substation (if practically possible) or with the establishment of a new substation. These solutions require substantial CAPEX and have extremely long lead times of implementation.

However, this thesis has shown through simulations, that inverter-based generation of solar PV connecting into these MV networks may alleviate these constraints if located appropriately and results in an improvement in network capacity. Utilizing DG as a mechanism to un-constrain MV networks through their optimal allocation using Particle Swarm Optimization

(PSO) algorithm has been addressed through the development of a DPL script to assist in this analysis and an excel based tool to interface to the corresponding result files. Due to the existing nature of the MV feeder where the fault level is higher at the source and the network impedance is lower at the source, the ideal location integrating the maximum amount of PV generation should be at the beginning of the source (initial section of the feeder), however, simulations have shown that this location is also dependent on the load at that point.

This PhD thesis has addressed the research question of integrating inverter-based generation of solar PV systems using PSO optimization technique to improve MV network feeder capacity. This thesis firstly provided an introduction to the short-term and long-term solutions applied to limited capacity MV networks and documented the design criteria that exists for the current MV networks. A comprehensive literature review was completed on the nature of MV networks and technical solutions with standards, guidelines and specifications that are applied to these networks. The review includes DG in the mix of solutions and motivates the need for the optimization algorithm selected for the study. A simple change in operating mode of the inverter unit to voltage control in the DG system would be able to assist to un-constrain the MV network at that point by adjusting the amount of reactive power that can be supplied by the inverter to the network thus increasing the voltage at the point of connection. However, this operation is not implemented with ease as regulation and policy prevents the DG system to control the utility operating voltage of the network as the quality of supply of the Distribution network is the responsibility of the licenced Distributor unless an appropriate operational agreement is in place.

An objective function was derived that best describes the relationship between network capacity and DG integration and how can this be applied to many connecting DG based systems integrating into the same MV network using the %/MW method. The focus technology and capability of PV as mentioned in Chapter 2 (literature review) is due to the influx of PV applications and proposed integration to the utilities medium voltage networks and the augmentation of PV installations due to the commercial availability and progressive reduction of material costs.

Two common utility grid networks (with their different components and load characteristics) were modelled during steady state conditions with study cases that represent all load conditions, peak and off-peak. The approach to model the two networks was firstly, the conventional modelling of connecting PV systems to the network, i.e. manually connecting PV to different parts of the network and documenting results and secondly executing the developed DPL script to solve the same objective. The comparison between the manual method and DPL method indicates the accuracy of the script function considering all input and

output variables of the algorithm. The proposed optimization algorithm selected was Particle Swarm Optimization (PSO). The discussion on the different optimization algorithms was covered in Chapter 2, Section 2.8., however a summary tabulating the different methods in optimally allocating DG to the Distribution network is provided in Table 5.1.

Table 5.1: Optimization methods in comparison to PSO

Optimization Algorithm	Merits and Demerits			Utilization
	Optimal location	Optimal size	Analysis	
Genetic algorithm (GA)	Y	Y	Faster, easier and gives more accurate solutions	Power losses reduction and voltage profile improvement
Algorithm with elitism strategy (EGA)	Y	Y	Outperformed the original GA and a bit better than PSO	Solve the size and location of multi DG
Particle swarm optimization (PSO)	Y	Y (for 2 & 3 only)	1. Easy to implement 2. Fast and accurate in determining the sizes and location 3. Effectiveness to search optimum point and the size of DGs	1. Placement of Solar PV with minimum active power losses 2. Minimizing the total real power loss 3. Minimize the total cost of the system
Non-dominated Sorting Genetic Algorithm II (NSGAII)	Y	Y	Improvement of steady state system performance	Determine the optimal locations and sizes of DG
Artificial Bee Colony algorithm (ABC)	Y	N	Close agreement with grid search method	Minimize total system real power loss
Simulated annealing (SA)	Y	N	The proper selection of parameters could assure global optimum	Optimal location and sizes of DG units in a microgrid
Improved Bat Algorithm (IBA)	Y	N	Significant reduction in power losses and an increase in the minimal node voltage	Minimize energy losses and to improve voltage profile
Analytical Method AM +Clonal Selection Method CSA	Y (AM)	Y (CSA)	Less computation time	Power losses reduction and improvement of the voltage profile
GA+Real-coded Genetic Algorithm RCGA	Y (GA)	Y (RCGA)	Overall system power losses reduction and improvement of the characteristics of voltage	Power losses reduction and improvement of the voltage profile
Single DG Placement SDGP+PSO	Y (SDGP)	Y (PSO)	Improved convergence characteristics and less computation time	Power losses reduction and improvement of the voltage profile
SDGP+ABC	Y (SDGP)	Y (ABC)	Shorter computation time	Power losses reduction and improvement of the voltage profile
Fuzzy Logic FL+ABC	Y FL)	Y (ABC)	Shorter computation time	Power losses reduction and improvement of the voltage profile

Both in the manual method of connecting PV to the grid and with the execution of the DPL script, mathematical constraints were derived by the various NERSA regulatory policies (NERSA, NRS048-4:2009, NRS097-2-3) and technical codes and standards for DG integration at medium voltage level [37] [38]. By mathematically defining a mechanism of network improvement percentage (%) per amount of DG penetration, critical points and network paths on MV feeders can be identified leading to the quantification of network upgrades and optimal connecting points for feasible DG project outputs.

The conventional method of integrating PV to the MV network was first completed. Thereafter, DIgSILENT Powerfactory Language (DPL) was used to structure the script to assess the entire MV network and clean up any duplicate of problematic PV systems before executing studies. The PSO algorithm was coded into the program (DPL) and with user inputs to the script, several simulations of different iterations and DG units were then executed. The results were then documented systematically. This was be done by changing each PV output by the number of inverters and output power, keeping its mode of operation constant, and location of the connecting plant to the grid. The quantification of the magnitude of DG and location was determined with the results from the script and compared to the results obtained from the conventional modelling. The objective function was then calculated and was presented in Section 4 and summarized in Sections 4 & 4.5. The result file is automatically extracted from the DPL script and is analysed on a simplistic interface designed and built in Microsoft Excel using Visual Basic programming language.

When the DG connects to the grid, the Network Service Provider (NSP) is responsible in ensuring that the quality of supply criteria are met before authorization to connect to the grid can be made. In this case, the NSP will stipulate the operational parameters to which the DG has to adhere to, i.e. the DG has to be operated in power factor control mode as the DG cannot change the voltage on the grid (as per the grid code [38] unless agreed to by the NSP and DG in the operational agreement) by absorbing or injecting reactive power as in the other two modes of voltage and reactive power control [36]. Other compliance assessments include voltage flicker, voltage imbalance and rapid voltage changes (RVC), which is the basis for the studies completed in this research. Typically for PV installations, harmonic currents are generated from inverters but the harmonic current measurements must be completed at the POC by the DG and adhere to the limits specified in the operational agreement derived from standard IEC61727, between the NSP and DG where the Total Harmonic Distortion (THD) < 5%. The assumption that has been made in this thesis is that grid code compliance has to be met in order for the plant to be able to connect to the grid and as such is not touched upon as part of the research. Voltage stability and quality of supply studies as per the grid code are

significant studies to be undertaken once the optimal allocation of the PV system is made to a network. Voltage stability on MV feeders can also be problematic when more than one PV system is connected In close proximity to each other on the same MV network. When a grid fault is not cleared in the critical clearing time period, voltage instability can occur which would disconnect the plant from the grid. Voltage fluctuation can also happen under cloud cover where the inverters switch in and out while operating. When this happens, the protection device on the PV system (DGSL, Chapter 2) may not see the fault on the grid and continue operating, leading to serious equipment damage and safety issues. One of the solutions to maximize PV on the grid and overcome instability is to have a strong fault level at the POC by grid strengthening or if not possible, then the amount of PV is curtailed by the NSP. The control mode and magnitude of the generator are also technical limitations in generating to its full capacity [36] – [38]. The dynamics and assessment of voltage stability studies is beyond the scope of this research but is touched upon in Section 2.7.2. Future work would be to include this in the DPL script for further testing of MV networks with PV integration.

A summary of the following policies and regulations govern the integration of PV to the grid to allow export, self-consumption and wheeling into the utility grid are presented below:

- The generator has to be within the required size limits based on the supply point determined by the NSP.
- Metering should have the ability of measuring bi-directional energy flow to and from the grid.
- For PV type installations, the appropriate and relevant testing and certification must be done by a competent person who is registered as a professional.
- The equipment utilized should be tested against National guidelines in the NRS097-2 series of standards.
- The following standards and documentation are applicable to each installation:
    - NRS 097-2-1 Grid Interconnection of Embedded Generation Part 2: Small-scale embedded generation Section 1: Utility interface [35] – LV/MV connections.
    - NRS 097-2-3 Grid Interconnection of Embedded Generation Part 2: Small-scale embedded generation Section 2: Simplified utility connection criteria for low-voltage connected generators [36]–- LV/MV connections.
    - NERSA–- South African Distribution Code [38] – LV to HV connections
    - SANS 10142-1 & SANS 10142-1-2 standards – LV/MV connections
    - Occupational Health and Safety Act, (Act 85 of 1993) and requirement for a COC

- Operating Guideline for LV networks with Embedded Generation (Unique ID: 240-81732810) and The Dead-Grid Safety lock specification and minimum safety requirements for LV connected PV Embedded Generators (Unique ID: 240-126260252).
- NERSA NRS048 – MV and LV limits [34]–- LV/MV connections.
- NERSA – RPP Grid code ver 3.1 (2022) [37]–- LV to HV connections.
- Eskom Distribution DST 34-1765 – Interconnection Standard–- LV to HV connections
- The latest Electricity Supply Agreement (ESA) with the NSP
- A NERSA registration letter for supplies greater than 100 kW
- A connection and use of system agreement (also called a supplementary agreement to the ESA) between the DG and NSP
- An amendment agreement, if needed, for offset or banking of energy.
    - If a PV plant exports electricity into the grid, a credit is given to the customer as the PV plant requires the grid to operate but cannot offset more than the net energy that has been used per time-of-use category (applicable tariff for peak, standard, off-peak) for that month.
    - For banking of energy – This is the surplus exported energy that is carried over to offset the next month's consumption per TOU period. (Applicable for NSP Eskom customers per financial year)

5.2 Comments on Results

This section comments on how the results obtained in this research correlate with literature. In [100], an allocation strategy for distribution generation (DG) is presented with integration to radial distribution networks under uncertainties of load and generation using Adaptive Genetic Algorithm (GA) where the optimal locations for DG integration and the magnitude of generation are determined by maximum node voltage deviation and minimizing network power loss. The study concludes that DG integration is beneficial only in some specific nodes in a network to obtain significant improvement in power loss and node voltage correlating to the findings as presented in this thesis. Also, the results obtained are very close to that obtained with an exhaustive search and that the optimal location is also dependent on the maximum generation limit [100]. The objective of the study presented in [101] was to minimize the sum of electrical line losses on Distribution lines, the peak power (which incurs additional investment) and the reliability along with the installation cost, operation and maintenance of DGs. Discrete Particle Swarm Optimization (DPSO) algorithm was used to optimize the placement and sizes of DG's

considering all load levels with the initial point of the optimization using the average load level first. It was concluded in [101] that the highest level of DG is related to the peak load and the lowest level is related to 50% loading. This is also clearly seen in Figures 4.79 and 4.80 where in the peak load scenario the highest network capacity improvement was seen with the highest DG penetration level as compared to the light load scenario. Also, in [101] after installation of DGs, the loss and interruption cost decreased which was found to be much more than the total installation cost of DGs. A novel Selective Particle Swarm Optimization (SPSO) technique for optimal placement of Distributed Generation (DG) units in a radial distribution system was presented in [102]. A limitation in this study is that the maximum penetration of DG is considered in a range of 0–50% of the total load. The proposed SPSO algorithm, although minimised the size of DG's within voltage limits but reduced line losses effectively. The effectiveness of the developed DPL script was to maximize DG magnitude with the highest improvement in network capacity mitigating the limitation in [102] mentioned above.

5.3 Contributions and Novelty

The research outputs support the ongoing investigations of connecting and assessing distributed generation facilities to utility-grids but specifically focus on MV networks and inverter-based generation of PV technology. The current problems with existing solutions for un-constraining networks, is that only a certain percentage of improvement in the network's capacity can be achieved. In this research, it was shown that with inverter-based PV generation, the networks capacity (kVA) is increased if the PV installation is optimally located, operated and managed with or without network un-constraining devices. However, the management of the amount of generation added is curtailed in order to prevent line overloading or voltage rise. As mentioned Chapter 2, possible solutions to address line overload would be to:

- Increase feeder impedance by reconductoring with low impedance conductors or splitting the feeder at the substation to reduce the load on the feeder
- Re-template the line to improve sagging conditions under over-load conditions
- Change the control mode of the generator to absorb reactive power
- Add shunt compensation to capacitive loads reducing line loading

It has also been discussed that in the test networks, voltage regulation is the key factor in the objective of this research and the test networks feed actual commercial, agricultural and rural load. How much improvement in the networks' capacity is determined on the location of the PV system, the magnitude of load that the PV can feed (active and reactive power demand),

the network's technical characteristics (impedance and fault level) and whether the assessment is completed during off-peak and peak times which are network load dependent.

Defining a network capacity improvement percentage using DG integration to un-constrain MV networks and using PSO algorithm to achieve this, is the novelty in this research and in addition, its applicability becomes significant in placing microgrids and electric vehicle charging infrastructure. The interface tool would show the maximum distribution of inverter-based generation on the network and network capacity improvement achieved. To optimally integrate PV systems into MV networks, Particle Swarm Optimization Algorithm (PSO) was the proposed search method to determine the most beneficial placement and size due to its simplicity and in its concept and coding implementation compared to other heuristic optimization techniques. Also, its suitability as an optimization technique was less sensitive to the ratio of percentage improvement per MW injected; with less sensitive parameters and is somewhat independent on a set of initial points and generate high-quality function solutions than other stochastic methods.

This software tool in Microsoft Excel and the DPL script developed, would contribute significantly to how utilities and end-users (consumers and project developers) approach the conceptualisation and implementation of DG establishments from a technical and financial perspective. Utilities would be able to use the results to create more capacity on constrained networks thus deferring larger Capital Expenditure (CAPEX). PV alone cannot completely un-constrain MV networks and as such additional generation such as storage (including vehicle to grid capabilities) plays a vital role as power is dispatched during peak times when irradiance levels are low.

The integration of DG is not new but the above methodology of the hybridization of PV and battery storage to create network capacity improvements opens a new paradigm shift of thinking where current conventional practice is not functioning, especially where non-technical losses dominate. Stress on the LV network is reduced by allowing customer load to be fed directly from battery storage under conditions when PV cannot supply the requested demand due to its limited operational functionality of daytime use. This is seen for example during conditions of loadshedding and peak load times which may happen when PV output is low or negligible on a typical MV network. MV networks also benefits from hybridization due to the regulation that battery storage provides when PV output fluctuates due to cloud cover for example thus enabling a constant source of supply to the network feeder (mitigating stability events due to cloud cover) load reducing the stress on the HV network required to provide the demand in the absence of the additional energy that the system provides.

Section 4 of this thesis concluded that the ratio of the improvement in network capacity (%) to the amount of generation added was derived from the analysis on the two networks modelled. There is a constant ratio for every scenario shown in Network 1 and in Network 2 results. Network capacity can then be estimated based on this ratio and within technical and practical means.

5.4 Challenges and Limitations

The main technical challenge faced during the research was implementing the code to the test networks selected. As that the DPL code developed assigned a DG to every medium voltage terminal, the clean-up of the network prior to executing the script had to be correctly done and checked. Also, as that the test networks are actual Distribution networks, the challenge that took some time to overcome was connecting the PV system to the MV terminal of tee-offs with two-phase rather than three-phase medium voltage lines. These conductors were changed to accommodate the script in its limitation of not checking three phase conductors when connecting DG to the MV node However, the code has a clean-up function and LV filtering function. PV systems that were connected incorrectly is removed and LV busbars are also ignored during code execution.

The proposed method of using PSO to improve network capacity using PV has the following limitations summarized below, including future work to address them.

a) Other short term solutions have not been included in the analysis method, for e.g. MV/LV transformer taps based on voltage apportionment limits, changing the control mode of the inverter as discussed above and shunt compensation methods. The future work applicable here would be to include these short term solutions as scenarios in the analysis and compare results to the network feeder base case.
b) The proposed method is only applicable to MV networks of 11 kV and 22 kV and does not apply to HV or LV networks. The proposed method is only designed to accommodate MV networks.
c) The actual limitations of the PSO algorithm as discussed in Section 5.1. Different algorithms and its approach to optimally placing DG in MV networks can be incorporated with a complete re-write of the DPL code but is beyond the scope of this thesis.
d) The proposed method is mostly utilized for loads that have peak times when PV output is high. Future work here would be to analyse a hybrid scenario of PV and BESS to completely address the times of applicability.
e) Results derived from the method analysis does not explicitly take into account voltage stability that can occur due to cloud cover or loss of load (load rejection tests). Future

work in this regard would be to include voltage stability studies in the analysis. This may form step 4 of the analysis approach, i.e. calculating RVC, Voltage, thermal and then stability simulations.

f) Time factor is of great significance to include all possible permutations (which includes the existing short-term solutions) of the derived results and the future work recommend above.

g) The proposed method also assumes that the networks models are built systematically in DIgSILENT Powerfactory with all relevant data such as load, line and cable types and that the model converges with no errors. Future works could include the use of Python programming language and new functionality that Powerfactory may offer, e.g. Graphical representation of results through coding.

5.5 Recommendations for Future work

Future work in this regard would be able to provide an automatic complete report on the feeder capability although this currently can be done by adjusting the script to specific study cases. Also, utilizing PSO in determining the optimal positions proved to be functional in its accuracy when compared to the conventional method initially employed. Grid modernization would propagate an organization into the Smart Grid era where electric vehicles and smart meters provide an extensive range of smart capabilities, provided the necessary infrastructure is installed. One such technology in South Africa is the adoption of electric vehicles and electric vehicle infrastructure. Chapter 2, Section 2.10, describes the role EV's and the relevant charging infrastructure would have on the MV network. To mitigate the negative grid impact when charging, it is best to locate EV chargers near networks that are not constrained. EV charging infrastructure would also offer the capability of power flow via the inverter and power electronics into the grid under a discharging scenario. The developed tool would be able to assess the optimal discharging points required to integrate the charging infrastructure and locate points that would enable charging to take place without constraining the MV network. This opportunity provides forecasting for PV charging hubs to be optimally placed to accommodate this proposal. In the V2G system, the main objective is to realize charging–discharging co-ordination and maintain a charging equilibrium plan to eliminate the problems of stress on the power grid in V2G applications [87,88]. Technical planning assessment offered by the tool should address minimizing active and reactive power losses and the distance to optimal location of charger placement balancing higher EV penetration with fewer grid impacts [89] [85].

6 References

[1] General Microgrids Balance Energy (2023), Microgrids: The Self-Healing Solution [Online]. http://www.generalmicrogrids.com/about-microgrids (last accessed on 20 January 2023).

[2] S. Chowdhury, S.P. Chowdhury and P. Crossley, *Microgrids and Active Distribution Networks*. Stevenage: The Institution of Engineering and Technology, 2009.

[3] C. Marnay and G. Venkataramanan, "Microgrids in the evolving electricity generation and delivery infrastructure," *2006 IEEE Power Engineering Society General Meeting*, Montreal, QC, Canada, 2006, pp.1-5, doi: 10.1109/PES.2006.1709529.

[4] I. Sanchez, “Microgrid Technology: Enabling Energy Reliability and Security – Opportunities in Campus, Commercial & Industrial Communities“, MAYA Smart Energy Consulting. Available: https://docplayer.net/5394686-Microgrid-technology-enabling-energy-reliability-and-security-opportunities-in-campus-commercial-industrial-communities.html (last accessed on 5 February 2022).

[5] A. Baziar, A. Kavoosi-Fard and J. Zare, "A Novel Self Adaptive Modification Approach Based on Bat Algorithm for Optimal Management of Renewable MG," *Journal of Intelligent Learning Systems and Applications*, vol. 5, 2013, pp. 11-18. doi: 10.4236/jilsa.2013.51002.

[6] United states Environmental Protection Agency (2013), *Combined Heat and Power Partnership (CHP)* [Online]. https://www.epa.gov/chp (last accessed on 15 February 2022)

[7] E. Wood (2014, Nov. 25), *The Importance of Heat in the Energy Efficient Microgrid* [Online]. https://www.microgridknowledge.com/infrastructure/article/11433301/the-importance-of-heat-in-the-energy-efficient-microgrid (last accessed on 10 January 2020)

[8] M. Amidpour and M.H.K. Manesh, *Cogeneration and Polygeneration Systems*. Cape Town: Academic Press, 2020.

[9] J. Yang, X. Yuan, J. Li, *Solar Photovoltaic Generation.* Berlin: De Gruyter, 2020.

[10] B. Delfino, "Modeling of the integration of distributed generation into the electrical system," *IEEE Power Engineering Society Summer Meeting*, Chicago, IL, USA, 2002, pp. 170-175 vol.1, doi: 10.1109/PESS.2002.1043206.

[11] International Electrotechnical Commission, “Grid integration of large-capacity renewable energy sources and use of large-capacity electrical energy storage”, October 2012. Available: https://www.iec.ch/basecamp/grid-integration-large-capacity-renewable-energy-sources-and-use-large-capacity-electrical (last accessed on 12 March 2021)

[12] L. Chen and S. Mei, "An integrated control and protection system for photovoltaic microgrids," in *CSEE Journal of Power and Energy Systems*, vol. 1, no. 1, pp. 36-42, 2015, doi: 10.17775/CSEEJPES.2015.00005.

[13] N. Ayai, T. Hisada, T. Shibata, H. MiyosHi, T. Iwasaki and K. Kitayama, “DC Micro Grid System”, SEI Technical Review Number 75, [Online] October 2012. Available: https://global-sei.com/technology/tr/bn75/pdf/75-25.pdf (last accessed on 21 May 2022).

[14] Sentech, Inc. Bethesda, Maryland and University of Hawaii, ”Recommendations for Technologies for Microgrids on the Big Island”, Hawaii Natural Energy Institute School of Ocean and Earth Science and Technology, University of Hawai, Prepared for U.S. Department of Energy Office of Electricity Delivery and Energy Reliability, 2009.

[15] H. R. Pota, M. J. Hossain, M. A. Mahmud and R. Gadh, "Control for microgrids with inverter connected renewable energy resources," *2014 IEEE PES General Meeting | Conference & Exposition*, National Harbor, MD, USA, 2014, pp. 1-5, doi: 10.1109/PESGM.2014.6938911.

[16] A. A. Salam, A. Mohamed and M. A. Hannan, "Technical Challenges on Microgrids" , in *ARPN Journal of Engineering and Applied Sciences*, vol. 3, no. 6, pp.64-69, 2008.

[17] Samia, K.K. Sharma, I. Kaur and B. Singh, "Issues in stability of Micro Grids", in *Indian Journal of Science and Technology*, vol. 9, 2016, pp.1-5, DOI: 10.17485/ijst/2016/v9i38/101474

[18] J. Hu, T. Zhang, S. Du and Y. Zhao, "An Overview on Analysis and Control of Micro-grid System", in *International Journal of Control and Automation*, vol. 8, pp. 65-76, 2015, doi: 10.14257/ijca.2015.8.6.08.

[19] N. Bottrell, M. Prodanovic and T. C. Green, "Dynamic Stability of a Microgrid With an Active Load," in *IEEE Transactions on Power Electronics*, vol. 28, no. 11, pp. 5107-5119, 2013, doi: 10.1109/TPEL.2013.2241455.

[20] E. Rikos, S. Tselepis, C. Hoyer-Klick and M. Schroedter-Homscheidt, "Stability and Power Quality Issues in Microgrids Under Weather Disturbances," in *IEEE Journal of Selected Topics in Applied Earth Observations and Remote Sensing*, vol. 1, no. 3, pp. 170-179, 2008, doi: 10.1109/JSTARS.2008.2010557.

[21] R.M. Kamel, A. Chaouachi and K. Nagasaka, "Detailed Analysis of Micro-Grid Stability during Islanding Mode under Different Load Conditions", in Engineering, vol. 3, pp.508-516, 2011, doi:10.4236/eng.2011.35059.

[22] B. Nitve and R.L. Chakrasali, "Transient Stability Analysis and its Intensification in Microgrid", in *International Journal of Engineering Research and General Science*, vol. 3, pp.1143-1153, 2015.

[23] Y. A. -R. I. Mohamed and E. F. El-Saadany, "Adaptive Decentralized Droop Controller to Preserve Power Sharing Stability of Paralleled Inverters in Distributed Generation Microgrids," in *IEEE Transactions on Power Electronics*, vol. 23, no. 6, pp. 2806-2816, 2008, doi: 10.1109/TPEL.2008.2005100.

[24] K. De Brabandere, B. Bolsens, J. Van den Keybus, A. Woyte, J. Driesen and R. Belmans, "A Voltage and Frequency Droop Control Method for Parallel Inverters," in *IEEE Transactions on Power Electronics*, vol. 22, no. 4, pp. 1107-1115, 2007, doi: 10.1109/TPEL.2007.900456.

[25] X. Wu, Y. Zhang, A. Arulampalam and N. Jenkins, "Electrical Stability of Large Scale Integration of Micro Generation Into Low Voltage Grids", in *International Journal of Electronics*, vol. 1, pp.1-23, 2005.

[26] R.H. Lasseter, "Microgrids and Distributed Generation", in *Journal of Energy Engineering*, American Society of Civil Engineers, Sept. 2007.

[27] E. Demirok, D. Sera, R. Teodorescu, P. Rodriguez and U. Borup, "Clustered PV inverters in LV networks: An overview of impacts and comparison of voltage control strategies," *2009 IEEE Electrical Power & Energy Conference (EPEC)*, Montreal, QC, Canada, 2009, pp. 1-6, doi: 10.1109/EPEC.2009.5420366.

[28] N. Hatziargyriou, N. Jenkins et al., "Microgrids-Large Scale Integration of Microgeneration to Low Voltage Grids", *41st International Conference on Large High Voltage Electric Systems 2006*, CIGRE 2006.

[29] Z. Liu and J. V. Milanović, "Probabilistic Estimation of Voltage Unbalance in MV Distribution Networks With Unbalanced Load," in *IEEE Transactions on Power Delivery*, vol. 30, no. 2, pp. 693-703, April 2015, doi: 10.1109/TPWRD.2014.2322391.

[30] P. Trichakis, P.C. Taylor, P.F. Lyons and R. Hair, “Predicting the technical impacts of high levels of small-scale embedded generators on low-voltage networks”, in *IET renewable Power Generation*, vol. 2, 2008, pp. 249 – 262, DOI: 10.1049/iet-rpg:20080012.

[31] P. -C. Chen, V. Malbasa and M. Kezunovic, "Analysis of voltage stability issues with distributed generation penetration in distribution networks," *2013 North American Power Symposium (NAPS)*, Manhattan, KS, USA, 2013, pp. 1-6, doi: 10.1109/NAPS.2013.6666862.

[32] B. -I. Crăciun, T. Kerekes, D. Séra and R. Teodorescu, "Overview of recent Grid Codes for PV power integration," *2012 13th International Conference on Optimization of Electrical and Electronic Equipment (OPTIM)*, Brasov, Romania, 2012, pp. 959-965, doi: 10.1109/OPTIM.2012.6231767.

[33] *Network and Grid Planning Standard for Generation Grid Connection*, Eskom, DST_34-1946, October 2012.

[34] *Electricity supply-Quality of supply, Part 4: Application practices for licensees*, NERSA, NRS048-4:2009, 2009.

[35] *Grid interconnection of embedded generation, part 2, section 1: Utility Interface*, NERSA, NRS097-2-1:2010, 2010.

[36] *Grid interconnection of embedded generation, part 2, section 3: Simplified utility connection criteria for low-voltage connected generators*, NERSA, NRS097-2-3:2014, 2014.

[37] *Grid connection code for Renewable Power plants (RPPs) connected to the Electricity Transmission system (TS) or the Distribution System (DS) in South Africa*, NERSA, Ver 2.8, 2014.

[38] *The South African Grid code, Network code Rev 7.0*, NERSA, March 2008.

[39] ESRI. (2 March 2021). *ArcGIS 10.2.2 - Spaceman Geographical Information System software reader* [Online]. Available: http://www.esri.com/software/arcgis/arcgis-for-desktop/features.

[40] *DIgSILENT PowerFactory Version 15, User Manual*, DIgSILENT Germany, April 2013.

[41] S. Van Loon, F. Volberda, J. Morren and F. Provoost, “Optimal contribution of distributed generation in medium voltage grids during a fault, now and in the future”, *21st International Conference on Electricity Distribution CIRED*, Frankfurt, Germany, 2011, pp.1-4.

[42] K. Rudion, A. Orths, Z. A. Styczynski and K. Strunz, "Design of benchmark of medium voltage distribution network for investigation of DG integration," *2006 IEEE Power Engineering Society General Meeting*, Montreal, QC, Canada, 2006, pp.1-6, doi: 10.1109/PES.2006.1709447.

[43] J.C. Boemer, K. Burges, et al., “Overview of German Grid Issues and Retrofit of Photovoltaic Power Plants in Germany for the Prevention of Frequency Stability Problems in Abnormal System Conditions of the ENTSO-E Region Continental Europe”, *1st International Workshop on Integration of Solar Power into Power Systems*, Aarhus, Denmark, 2011.

[44] *Eskom Standard DST-34-542, Distribution Voltage Regulation and Apportionment Limits*, Eskom, October 2018.

[45] A. Ramdhin, S. Chowdhury and S.P.Chowdhury, “Grid Interconnection Planning for Embedded Generation: Steady State Distribution Integration”, *Southern African Universities Power Engineering Conference SAUPEC 2011*, Cape Town, South Africa, 2011.

[46] R. Tonkoski, D. Turcotte and T. H. M. EL-Fouly, "Impact of High PV Penetration on Voltage Profiles in Residential Neighborhoods," in *IEEE Transactions on Sustainable Energy*, vol. 3, no. 3, pp. 518-527, 2012, doi: 10.1109/TSTE.2012.2191425.

[47] H. Sadeghian, M. H. Athari and Z. Wang, "Optimized solar photovoltaic generation in a real local distribution network," *2017 IEEE Power & Energy Society Innovative Smart Grid Technologies Conference (ISGT)*, Washington, DC, USA, 2017, pp. 1-5, doi: 10.1109/ISGT.2017.8086067.

[48] E. Ghiani and F. Pilo, "Smart inverter operation in distribution networks with high penetration of photovoltaic systems," in *Journal of Modern Power Systems and Clean Energy*, vol. 3, no. 4, pp. 504-511, December 2015, doi: 10.1007/s40565-015-0165-4.

[49] Y. P. Agalgaonkar, B. C. Pal and R. A. Jabr, "Distribution Voltage Control Considering the Impact of PV Generation on Tap Changers and Autonomous Regulators," in *IEEE Transactions on Power Systems*, vol. 29, no. 1, pp. 182-192, Jan. 2014, doi: 10.1109/TPWRS.2013.2279721.

[50] R. Tonkoski, L. A. C. Lopes and T. H. M. El-Fouly, "Coordinated Active Power Curtailment of Grid Connected PV Inverters for Overvoltage Prevention," in *IEEE Transactions on Sustainable Energy*, vol. 2, no. 2, pp. 139-147, April 2011, doi: 10.1109/TSTE.2010.2098483.

[51] J.M Nye, " Increasing distributed generation penetration when limited by voltage regulation", Master of Engineering Dissertation, Faculty of Engineering, Stellenbosch University, South Africa, 2014.

[52] F.A. Viawan, "Steady State Operation and Control of Power Distribution Systems in the Presence of Distributed Generation", Thesis for the Degree of Licentiate Engineering, Division of Electric Power Engineering, Department of Energy and Environment, Chalmers University of Technology, Göteborg, Sweden, 2006.

[53] T. Lund, "Analysis of distribution systems with a high penetration of distributed generation,", Ph.D. dissertation, Centre for Electric Technology (CET), Technical University of Denmark, Denmark, 2007.

[54] M.N. Ab Wahab, S. Nefti-Meziani and A. Atyabi, "A Comprehensive Review of Swarm Optimization Algorithms", in *PLoS ONE*, vol. 10(5), 2015, e0122827. https://doi.org/10.1371/journal.pone.0122827.

[55] J.J. Jamian, H. Mokhlis, M.W. Mustafa, M.N. Abdullah and M.A. Bahardin, "Comparative learning global particle swarm optimization for optimal distributed generations' output", in *Turkish Journal of Electrical Engineering & Computer Sciences*, vol. 22, no. 5, pp.1323-1337, 2014, DOI: 10.3906/elk-1212-173.

[56] M. R. AlRashidi and M. E. El-Hawary, "A Survey of Particle Swarm Optimization Applications in Electric Power Systems," in *IEEE Transactions on Evolutionary Computation*, vol. 13, no. 4, pp. 913-918, Aug. 2009, doi: 10.1109/TEVC.2006.880326.

[57] T.J. Sahib, M.R. Ab Ghani, Z. Jano, I.H. Mohamed, "Optimum Allocation of Distributed Generation using PSO: IEEE Test Case Studies Evaluation", in *International Journal of Applied Engineering Research*, vol. 12, no. 11, pp. 2900-2906, 2017.

[58] M. Aryanezhad, "Management and coordination of LTC, SVR, shunt capacitor and energy storage with high PV penetration in power distribution system for voltage regulation and power loss minimization", in *International Journal of Electrical Power & Energy Systems*, vol. 100, pp.178-192, 2018, https://doi.org/10.1016/j.ijepes.2018.02.015.

[59] H. Zhao, Q. Wu, S. Hu, H. Xu and C.N. Rasmussen, "Review of energy storage system for wind power integration support", in *Applied Energy*, vol. 137, pp.545–53, 2015, https://doi.org/10.1016/j.apenergy.2014.04.103.

[60] L. Leite, W. Boaventura, L. Errico, E. Cardoso, R. Dutra and B. Lopes, "Integrated voltage regulation in distribution grids with photovoltaic distribution generation assisted by telecommunication infrastructure", in *Electric Power Systems Research*, vol. 136, pp.110-124, 2016, https://doi.org/10.1016/j.epsr.2016.02.016.

[61] K. Zou, A. P. Agalgaonkar, K. M. Muttaqi and S. Perera, "Optimisation of Distributed Generation units and shunt capacitors for economic operation of distribution systems," *2008 Australasian Universities Power Engineering Conference*, Sydney, NSW, Australia, 2008, pp. 1-7.

[62] A. H. Etemadi, M. Fotuhi-Firuzabad, "Distribution System Reliability Enhancement using Optimal Capacitor Placement," in *IET Generation, Transmission & Distribution*, vol. 2, pp. 621-631, September 2008.

[63] Y. P. Agalgaonkar, B. C. Pal and R. A. Jabr, "Distribution Voltage Control Considering the Impact of PV Generation on Tap Changers and Autonomous Regulators," in *IEEE Transactions on Power Systems*, vol. 29, no. 1, pp. 182-192, Jan. 2014, doi: 10.1109/TPWRS.2013.2279721.

[64] M. B. Jannat, “Analysis of Optimal sizing and location of Shunt Capacitors in Active Distribution Networks”, Doctoral Dissertation, University of Belgrade, Belgrade, 2018.

[65] M. Uchendu, “Placement of Distributed Generation and Shunt Capacitor in Distribution Network using Cuckoo Search Algorithm”, in *Nigerian Journal of Technological Development*, vol. 17,no. 2, pp.79-87, June 2020, doi: http://dx.doi.org/10.4314/njtd.v17i2.2.

[66] M. M. Aman, G. B. Jasmon, K. H. Solangi, A. H. A. Bakar and H. Mokhlis, “Optimum Simultaneous DG and Capacitor Placement on the Basis of Minimization of Power Losses”, in International Journal of Computer and Electrical Engineering, vol. 5, no. 5, pp.516-522, October 2013.

[67] F. Bai, R. Yan, T. K. Saha and D. Eghbal, "A New Remote Tap Position Estimation Approach for Open-Delta Step-Voltage Regulator in a Photovoltaic Integrated Distribution Network," in *IEEE Transactions on Power Systems*, vol. 33, no. 4, pp. 4433-4443, July 2018, doi: 10.1109/TPWRS.2017.2776311.

[68] H.R. Esmaeilian, O. Darijany, and M. Mohammadian, “Optimal placement and sizing of DG units and capacitors simultaneously in radial distribution networks based on the voltage stability security margin”, in *Turkish Journal of Electrical Engineering & Computer Science*, pp.1203-1207, 2014.

[69] M. Patsalides, G. E. Georghiou, A. Stavrou and V. Efthymiou, "Voltage regulation via photovoltaic (PV) inverters in distribution grids with high PV penetration levels," *8th Mediterranean Conference on Power Generation, Transmission, Distribution and Energy Conversion (MEDPOWER 2012)*, Cagliari, 2012, pp. 1-6, doi: 10.1049/cp.2012.2051.

[70] J.A. Alberts, “Impact of energy efficiency and renewable energy on electricity master planning and design parameters”, Master of Engineering Dissertation, Electrical and Electronic Engineering Department, North-West University, May 2017.

[71] Electrical Engineering. (20 April 2021). Types of Load – Load Curves – Load Duration Curve [Online]. Available: https://www.electricalengineeringinfo.com/2014/12/variable-load-on-power-stations-load-curve-load-duration-curve-types-of-loads.html

[72] A. Poulin, M. Dostie, M. Fournier and S. Sansregret, “Load duration curve: A tool for technico-economic analysis of energy solutions”, in *Energy and Buildings*, vol. 40, pp.29-35, 2008, https://doi.org/10.1016/j.enbuild.2007.01.020.

[73] S. M. Alizadeh, C. Ozansoy and T. Alpcan, "The impact of X/R ratio on voltage stability in a distribution network penetrated by wind farms," *2016 Australasian Universities Power Engineering Conference (AUPEC)*, Brisbane, QLD, Australia, 2016, pp. 1-6, doi: 10.1109/AUPEC.2016.7749289.

[74] Technavio, “Solar Energy Market in South Africa: Utility Segment to Offer Maximum Business Opportunities, Growth, Trends, Major Companies, and Forecasts (2022 - 2026), 14 Feb 2022.

[75] *Network Planning Guideline for Shunt Capacitors*, Eskom, Eskom Guideline 240-61227331, 2017.

[76] *Network Planning Guideline for MV Voltage Regulators*, Eskom, Eskom Guideline 240-61227343, 2014.

[77] *Determination of Conductor Ratings in Eskom*, Eskom, Eskom Distribution Standard, December 2010.

[78] S. Uski, E. Rinne and J. Sarsama, “Microgrid as a Cost-Effective Alternative to Rural Network Underground Cabling for Adequate Reliability”, in *Energies 11*, no. 8, 1978, 2018, https://doi.org/10.3390/en11081978

[79] H. Lotfi and A. Khodaei, "AC Versus DC Microgrid Planning," in *IEEE Transactions on Smart Grid*, vol. 8, no. 1, pp. 296-304, Jan. 2017, doi: 10.1109/TSG.2015.2457910.

[80] H. Jiayi, J. Chuanwen and X. Rong, “A review on distributed energy resources and microgrid”, in *Renewable and Sustainable Energy Reviews*, vol. 12(9), pp.2472-2483, 2008, https://doi.org/10.1016/j.rser.2007.06.004.

[81] M. Mihaylov, I. Razo-Zapata, R. Rădulescu and A. Nowé A, “Boosting the Renewable Energy Economy with NRGcoin”, *4th International Conference on ICT for Sustainability (ICT4S 2016)*, Amsterdam, The Netherlands, 2016, DOI: 10.2991/ict4s-16.2016.27.

[82] M.T. Yeshalem and B. Khan, “Microgrid Integration”, in Special Topics in Renewable Energy Systems, 1st Edition, Chapter 4, Publisher: IntechOpen, 2018.

[83] D. de la Torre, J. L. Morillo, M. A. Velasquez and N. Quijano, "Technical assessment of microgrids integration into distribution systems," *2014 IEEE PES Transmission & Distribution Conference and Exposition - Latin America (PES T&D-LA)*, Medellin, Colombia, 2014, pp. 1-6, doi: 10.1109/TDC-LA.2014.6955234.

[84] A. J. Collin, S. Z. Djokic, H. F. Thomas and J. Meyer, "Modelling of electric vehicle chargers for power system analysis," *11th International Conference on Electrical Power Quality and Utilisation*, Lisbon, Portugal, 2011, pp. 1-6, doi: 10.1109/EPQU.2011.6128816.

[85] E. Mancini, M. Longo, W. Yaici and D. Zaninelli, “Assessment of the Impact of Electric Vehicles on the Design and Effectiveness of Electric Distribution Grid with Distributed Generation”, in Applied Sciences 10, no. 15, 5125, 2020, https://doi.org/10.3390/app10155125.

[86] S.M. Shariff, D. Iqbal, M.S. Alam and F. Ahmad, “A State of the Art Review of Electric Vehicle to Grid (V2G) technology”, IOP Conference Series: Materials Science and Engineering, vol. 561, 2019, DOI 10.1088/1757-899X/561/1/012103.

[87] Kejun Qian, Chengke Zhou, M. Allan and Yue Yuan, "Load model for prediction of electric vehicle charging demand," *2010 International Conference on Power System Technology*, Zhejiang, China, 2010, pp. 1-6, doi: 10.1109/POWERCON.2010.5666587.

[88] A. M. A. Haidar and K. M. Muttaqi, "Behavioral characterization of electric vehicle charging loads in a distribution power grid through modeling of battery chargers," *2014 IEEE Industry Application Society Annual Meeting*, Vancouver, BC, Canada, 2014, pp. 1-8, doi: 10.1109/IAS.2014.6978412.

[89] P.G.H.C.H. Dharmakeerthi, “Electric Vehicle Integration - Grid Stability Concerns and Countermeasures”, Doctor of Philosophy Thesis, School of Information Technology and Electrical Engineering, University of Queensland, Australia, 2014.

[90] ENTSO-E, “Electric Vehicle Integration into Power Grids”, European Network of Transmission System Operators for Electricity Position Paper [Online], 31 March 2021. Available:https://eepublicdownloads.entsoe.eu/clean-documents/Publications/

Position%20papers%20and%20reports/ 210331_Electric_Vehicles_integration.pdf (last accessed on 20 April 2022).

[91] D. Hall and N. Lutsey, “Emerging Best Practices for Electric Vehicle Charging Infrastructure.”, The International Council on Clean Transportation White Paper [Online], October 2017. Available: https://theicct.org/sites/default/files/publications/EV-charging-best-practices_ICCT-white-paper_04102017_vF.pdf (last accessed on 14 November 2021).

[92] *Network & Grid Planning Standard for Generation Grid Connection – Generators Technology Overview and Effects on Networks*, Eskom, Eskom standard 240-61227305, February 2018.

[93] *Network Planning Guideline for MV Step voltage regulators*, Eskom, Eskom guideline 240-612273432017.

[94] *Network Planning Standard*, Eskom, Eskom guideline 240-75757028, 2019.

[95] Bentley. (2 March 2021). *Microstation* [Online]. Available: https://www.bentley.com/software/microstation/

[96] Inspired Interfaces. (2 March 2021). *Reticmaster power systems analysis tool* [Online]. Available: https://inspiredinterfaces.co.za/ReticMaster.php

[97] *Framework for Design Solutions to connect customer owned SSEG’s*, Eskom, Eskom standard 240-150128782, 2019.

[98] S. Talukder, “Mathematical modelling and Applications of Particle Swarm Optimization”, Master of Science Thesis, School of Engineering, Blekinge Institute of Technology, University in Karlskrona, Sweden, February 2011.

[99] Department of Trade, Industry and Competition, Government of South Africa, “Autogreen Paper on the Advancement of New Energy Vehicles in South Africa”, [Online] 21 May 2021. Available: https://www.gov.za/sites/default/files/gcis_document/202105/44606gen308.pdf (last accessed on 28 January 2022).

[101] S. Ganguly and D. Samajpati, "Distributed Generation Allocation on Radial Distribution Networks Under Uncertainties of Load and Generation Using Genetic Algorithm," in *IEEE Transactions on Sustainable Energy*, vol. 6, no. 3, pp. 688-697, July 2015, doi: 10.1109/TSTE.2015.2406915.

[101] I. Ziari, G. Ledwich, A. Ghosh, D. Cornforth and M. Wishart, "Optimal allocation and sizing of DGs in distribution networks," *IEEE PES General Meeting*, Minneapolis, MN, USA, 2010, pp. 1-8, doi: 10.1109/PES.2010.5588114.

[102] Sarfaraz, A. Bansal and S. Singh, "Optimal allocation and sizing of distributed generation for power loss reduction," *International Conference & Workshop on Electronics & Telecommunication Engineering (ICWET 2016)*, Mumbai, 2016, pp. 15-20, doi: 10.1049/cp.2016.1116.

Appendix A1 – Network Data for All Conductor lines for Network 1

Name	Type	Terminal i	Terminal j	Length	Laying	Type of Phase Conductors	Irated(act.)	Irated	Z1	R1	X1	R0	X0
	TypLne,TypTow,TypGeo,TypCabsys			km		TypCon	kA	kA	Ohm	Ohm	Ohm	Ohm	Ohm
269357291	11 kV 120mm2 Cu PILC 3Core	PointTerm968	PointTerm1001	0.613724	Ground		1	1	0.180	0.094	0.154	1.682	0.061
269357300	MV3 Delta	PointTerm112	PointTerm119	0.01903333	Air	OAK50	0.28	0.28	0.009	0.005	0.007	0.008	0.030
269357313	CHICADEE 3 Delta 11.00	PointTerm15	PointTerm1	0.3853219	Air		0.312	0.312	0.168	0.115	0.122	0.172	0.635
269357323	11 kV 120mm2 Cu XLPE 3Core	PointTerm151	PointTerm125	0.2012384	Ground		1	1	0.044	0.039	0.020	0.195	0.029
269357326	MV3 Delta	PointTerm86	PointTerm71	0.3613751	Air	FOX50	0.148	0.148	0.318	0.284	0.143	0.337	0.571
269357328	MV3 Delta	PointTerm128	PointTerm132	0.01512529	Air	FOX50	0.148	0.148	0.013	0.012	0.006	0.014	0.024
269357330	MV3 Delta	PointTerm112	PointTerm66	1.138612	Air	OAK50	0.28	0.28	0.529	0.324	0.418	0.490	1.766
269357332	MV3 Delta	PointTerm19	PointTerm15	0.1920153	Air	OAK50	0.28	0.28	0.089	0.055	0.071	0.083	0.298
269357340	MV3 Delta	PointTerm32	PointTerm45	0.7463745	Air	OAK50	0.28	0.28	0.347	0.212	0.274	0.321	1.157
269357351	MV3 Delta	PointTerm66	PointTerm74	0.04189635	Air	FOX50	0.148	0.148	0.037	0.033	0.017	0.039	0.066
269357354	MV3 Delta	PointTerm45	PointTerm66	0.1275733	Air	OAK50	0.28	0.28	0.059	0.036	0.047	0.055	0.198
269357357	MV3 Delta	PointTerm80	PointTerm77	0.1522591	Air	FOX50	0.148	0.148	0.134	0.120	0.060	0.142	0.241
269357366	11 kV 120mm2 Cu PILC 3Core	PointTerm1014	PointTerm1011	0.00723285	Ground		1	1	0.002	0.001	0.002	0.020	0.001
269357372	MV3 Delta	PointTerm1106	PointTerm1134	0.2171309	Air	MINK50	0.208	0.208	0.129	0.100	0.082	0.131	0.339
269357376	C3/0.104 3 Delta 11.00	PointTerm1207	PointTerm1271	0.304405	Air		0.1228	0.1228	0.372	0.360	0.096	0.404	0.502
269357379	MV3 Delta	PointTerm1335	PointTerm1326	0.08438697	Air	FOX50	0.148	0.148	0.074	0.066	0.033	0.079	0.133
269357384	MV3 Delta	PointTerm1207	PointTerm1191	0.1332221	Air	FOX50	0.148	0.148	0.117	0.105	0.053	0.124	0.210
269357388	MV3 Delta	PointTerm1145	PointTerm1184	0.09999711	Air	MINK50	0.208	0.208	0.060	0.046	0.038	0.060	0.156
269357391	MV3 Delta	PointTerm1020	PointTerm1059	0.3899242	Air	MINK50	0.208	0.208	0.232	0.179	0.148	0.236	0.609
269357393	MV3 Delta	PointTerm1184	PointTerm1194	0.08657977	Air	MINK50	0.208	0.208	0.052	0.040	0.033	0.052	0.135
269357395	MV3 Delta	PointTerm1083	PointTerm1106	0.04945503	Air	MINK50	0.208	0.208	0.029	0.023	0.019	0.030	0.077
269357397	MV3 Delta	PointTerm1184	PointTerm1188	0.02562014	Air	MINK50	0.208	0.208	0.015	0.012	0.010	0.015	0.040
269357402	MV3 Delta	PointTerm1313	PointTerm1323	0.06648152	Air	FOX50	0.148	0.148	0.059	0.052	0.026	0.062	0.105
269357426	C3/0.104 3 Delta 11.00	PointTerm1027	PointTerm1024	0.01561032	Air		0.1228	0.1228	0.019	0.018	0.005	0.021	0.026
269357432	MV3 Delta	PointTerm1134	PointTerm1145	0.1089959	Air	FOX50	0.148	0.148	0.096	0.086	0.043	0.102	0.172
269357434	MV3 Delta	PointTerm998	PointTerm1020	0.5177391	Air	MINK50	0.208	0.208	0.308	0.238	0.196	0.313	0.809
269357435	MV3 Delta	PointTerm1059	PointTerm1083	0.2264111	Air	MINK50	0.208	0.208	0.135	0.104	0.086	0.137	0.354
269357439	MV3 Delta	PointTerm393	PointTerm384	0.1305469	Air	FOX50	0.148	0.148	0.115	0.103	0.052	0.122	0.206
269357442	MV3 Delta	PointTerm422	PointTerm445	0.2133228	Air	MINK50	0.208	0.208	0.127	0.098	0.081	0.129	0.333
269357447	MV3 Delta	PointTerm327	PointTerm330	0.2797308	Air	MINK50	0.208	0.208	0.167	0.128	0.106	0.169	0.437
269357452	FOX 3 Delta 11.00	PointTerm432	PointTerm439	0.01839894	Ground		0.148	0.148	0.017	0.016	0.006	0.018	0.030
269357455	MV3 Delta	PointTerm377	PointTerm399	0.3636805	Air	MINK50	0.208	0.208	0.217	0.167	0.138	0.220	0.568
269357460	MV3 Delta	PointTerm432	PointTerm429	0.0440571	Air	FOX50	0.148	0.148	0.039	0.035	0.017	0.041	0.070
269357462	MV3 Delta	PointTerm439	PointTerm504	0.4439055	Air	FOX50	0.148	0.148	0.391	0.349	0.176	0.414	0.701
269357467	MV3 Delta	PointTerm370	PointTerm377	0.01697091	Air	FOX50	0.148	0.148	0.015	0.013	0.007	0.016	0.027
269357472	MV3 Delta	PointTerm412	PointTerm422	0.1273348	Air	MINK50	0.208	0.208	0.076	0.058	0.048	0.077	0.199
269357487	MV3 Delta	PointTerm406	PointTerm403	0.1250218	Air	FOX50	0.148	0.148	0.110	0.098	0.050	0.116	0.198
269357495	MV3 Delta	PointTerm422	PointTerm426	0.08846162	Air	MINK50	0.208	0.208	0.053	0.041	0.034	0.053	0.138
269357536	11 kV 120mm2 Cu PILC 3Core	PointTerm1008	PointTerm1033	0.2723207	Ground		1	1	0.080	0.042	0.068	0.746	0.027
269357543	MV3 Delta	PointTerm525	PointTerm592	0.3685911	Air	FOX50	0.148	0.148	0.325	0.290	0.146	0.343	0.582
269357551	MV3 Delta	PointTerm770	PointTerm721	0.2152117	Air	MINK50	0.208	0.208	0.128	0.099	0.082	0.130	0.336
269357557	MV3 Delta	PointTerm786	PointTerm829	0.1846553	Air	MINK50	0.208	0.208	0.110	0.085	0.070	0.112	0.289
269357558	MV3 Delta	PointTerm770	PointTerm783	0.09699957	Air	FOX50	0.148	0.148	0.085	0.076	0.038	0.090	0.153
269357561	MV3 Delta	PointTerm745	PointTerm725	0.04621529	Air	FOX50	0.148	0.148	0.041	0.036	0.018	0.043	0.073
269357567	MV3 Delta	PointTerm451	PointTerm448	0.09800345	Air	MINK50	0.208	0.208	0.058	0.045	0.037	0.059	0.153
269357568	MV3 Delta	PointTerm525	PointTerm491	0.1116158	Air	MINK50	0.208	0.208	0.066	0.051	0.042	0.067	0.174
269357574	C3/0.104 3 Delta 11.00	PointTerm683	PointTerm721	0.06125001	Air		0.1228	0.1228	0.075	0.072	0.019	0.081	0.101
269357578	MV3 Delta	PointTerm562	PointTerm536	0.156169	Air	MINK50	0.208	0.208	0.093	0.072	0.059	0.094	0.244
269357581	MV3 Delta	PointTerm601	PointTerm598	0.00259771	Air	FOX50	0.148	0.148	0.002	0.002	0.001	0.002	0.004
269357586	MV3 Delta	PointTerm579	PointTerm588	0.03098734	Air	FOX50	0.148	0.148	0.027	0.024	0.012	0.029	0.049
269357588	MV3 Delta	PointTerm525	Terminal	0.0579771	Air	FOX50	0.148	0.148	0.051	0.046	0.023	0.054	0.092
269357588_b	MV3 Delta	Terminal(1)	PointTerm536	0.02898855	Air	FOX50	0.148	0.148	0.026	0.023	0.011	0.027	0.046
269357592	11 kV 120mm2 Cu PILC 3Core	PointTerm780	PointTerm819	0.1470592	Ground		1	1	0.043	0.023	0.037	0.403	0.015
269357596	FOX 3 Delta 11.00	PointTerm790	PointTerm796	0.01559711	Ground		0.148	0.148	0.014	0.013	0.005	0.015	0.026
269357600	MV3 Delta	PointTerm829	PointTerm876	0.3050761	Air	MINK50	0.208	0.208	0.182	0.140	0.116	0.184	0.477
269357602	MV3 Delta	PointTerm780	PointTerm751	0.1612447	Air	FOX50	0.148	0.148	0.142	0.127	0.064	0.150	0.255
269357605	MV3 Delta	PointTerm471	PointTerm458	0.1026377	Air	FOX50	0.148	0.148	0.090	0.081	0.041	0.096	0.162
269357612	MV3 Delta	PointTerm540	PointTerm543	0.02276603	Air	FOX50	0.148	0.148	0.020	0.018	0.009	0.021	0.036
269357614	MV3 Delta	PointTerm451	PointTerm455	0.01351139	Air	MINK50	0.208	0.208	0.008	0.006	0.005	0.008	0.021
269357620	MV3 Delta	PointTerm725	PointTerm721	0.06312124	Air	MINK50	0.208	0.208	0.038	0.029	0.024	0.038	0.099
269357626	11 kV 120mm2 Cu PILC 3Core	PointTerm582	PointTerm566	0.06990547	Ground		1	1	0.021	0.011	0.018	0.192	0.007
269357627	MV3 Delta	PointTerm770	PointTerm786	0.1033675	Air	FOX50	0.148	0.148	0.091	0.081	0.041	0.096	0.163
269357633	MV3 Delta	PointTerm971	PointTerm985	0.09605844	Air	MINK50	0.208	0.208	0.057	0.044	0.036	0.058	0.150
269357639	MV3 Delta	PointTerm929	PointTerm926	0.01033083	Air	FOX50	0.148	0.148	0.009	0.008	0.004	0.010	0.016
269357641	MV3 Delta	PointTerm971	PointTerm979	0.01271474	Air	MINK50	0.208	0.208	0.008	0.006	0.005	0.008	0.020
269357644	11 kV 120mm2 Cu PILC 3Core	PointTerm929	PointTerm948	0.1790124	Ground		1	1	0.053	0.027	0.045	0.491	0.018
269357649	MV3 Delta	PointTerm909	PointTerm906	0.01082023	Air	FOX50	0.148	0.148	0.010	0.009	0.004	0.010	0.017
269357652	MV3 Delta	PointTerm915	PointTerm922	0.02126993	Air	MINK50	0.208	0.208	0.013	0.010	0.008	0.013	0.033
269357654	MV3 Delta	PointTerm922	PointTerm932	0.06273779	Air	MINK50	0.208	0.208	0.037	0.029	0.024	0.038	0.098
269357663	MV3 Delta	PointTerm954	PointTerm961	0.017987	Air	MINK50	0.208	0.208	0.011	0.008	0.007	0.011	0.028
269357665	MV3 Delta	PointTerm902	PointTerm889	0.3046213	Air	MINK50	0.208	0.208	0.181	0.140	0.116	0.184	0.476
269357671	MV3 Delta	PointTerm889	PointTerm886	0.02931415	Air	MINK50	0.208	0.208	0.017	0.013	0.011	0.018	0.046
269357676	MV3 Delta	PointTerm961	PointTerm971	0.07120192	Air	MINK50	0.208	0.208	0.042	0.033	0.027	0.043	0.111
269357677	MV3 Delta	PointTerm932	PointTerm954	0.1517681	Air	MINK50	0.208	0.208	0.090	0.070	0.058	0.092	0.237
269357680	11 kV 120mm2 Cu PILC 3Core	PointTerm1069	PointTerm1041	0.2918616	Ground		1	1	0.086	0.045	0.073	0.800	0.029
269357697	MV3 Delta	PointTerm166	PointTerm173	0.01563379	Air	OAK50	0.28	0.28	0.007	0.004	0.006	0.007	0.024
269357700	MV3 Delta	PointTerm180	PointTerm177	0.0407603	Air	FOX50	0.148	0.148	0.036	0.032	0.016	0.038	0.064
269357704	MV3 Delta	PointTerm122	PointTerm141	0.1599134	Air	OAK50	0.28	0.28	0.074	0.045	0.059	0.069	0.248
269357723	MV3 Delta	PointTerm265	PointTerm313	0.09891252	Air	MINK50	0.208	0.208	0.059	0.045	0.038	0.060	0.155
269357734	MV3 Delta	PointTerm248	PointTerm265	0.03747053	Air	MINK50	0.208	0.208	0.022	0.017	0.014	0.023	0.059
269357749	MV3 Delta	PointTerm1168	PointTerm1229	0.2579177	Air	FOX50	0.148	0.148	0.227	0.203	0.102	0.240	0.407
269357752	FOX 3 Delta 11.00	PointTerm1149	PointTerm1134	0.1118625	Air		0.148	0.148	0.101	0.095	0.035	0.111	0.184
269357759	MV3 Delta	PointTerm1142	PointTerm1161	0.09501763	Air	FOX50	0.148	0.148	0.084	0.075	0.038	0.089	0.150
269357762	MV3 Delta	PointTerm1134	PointTerm1139	0.05980182	Air	FOX50	0.148	0.148	0.053	0.047	0.024	0.056	0.094
269357765	MV3 Delta	PointTerm1258	PointTerm1255	0.05181987	Air	FOX50	0.148	0.148	0.046	0.041	0.021	0.048	0.082
269357767	FOX 3 Delta 11.00	PointTerm1175	PointTerm1223	0.2294973	Ground		0.148	0.148	0.207	0.194	0.072	0.228	0.378
269357769	MV3 Delta	PointTerm1229	PointTerm1252	0.1246944	Air	FOX50	0.148	0.148	0.110	0.098	0.049	0.116	0.197
269357771	MV3 Delta	PointTerm1168	PointTerm1155	0.05484748	Air	FOX50	0.148	0.148	0.048	0.043	0.022	0.051	0.087
269357782	MV3 Delta	PointTerm1364	PointTerm1374	0.4419802	Air	MINK50	0.208	0.208	0.263	0.203	0.168	0.267	0.691
269357790	11 kV 120mm2 Cu PILC 3Core	PointTerm1264	PointTerm1197	0.3601477	Ground		1	1	0.106	0.055	0.090	0.987	0.036
269357792	MV3 Delta	PointTerm1297	PointTerm1341	0.2200247	Air	MINK50	0.208	0.208	0.131	0.101	0.083	0.133	0.344
269357795	MV3 Delta	PointTerm1358	PointTerm1355	0.01087391	Air	FOX50	0.148	0.148	0.010	0.009	0.004	0.010	0.017
269357799	MV3 Delta	PointTerm1341	PointTerm1351	0.1751654	Air	MINK50	0.208	0.208	0.104	0.080	0.066	0.106	0.274
269357803	MV3 Delta	PointTerm1351	PointTerm1364	0.2501427	Air	MINK50	0.208	0.208	0.149	0.115	0.095	0.151	0.391
269357811	MV3 Delta	PointTerm1056	PointTerm1072	0.1398443	Air	FOX50	0.148	0.148	0.123	0.110	0.055	0.130	0.221
269357817	11 kV 120mm2 Cu PILC 3Core	PointTerm1050	PointTerm1047	0.01976686	Ground		1	1	0.006	0.003	0.005	0.054	0.002

Name	Type	Terminal i	Terminal j	Length	Laying	Type of Phase Conductors	Irated(act.)	Irated	Z1	R1	X1	R0	X0
269357820	C3/0.104 3 Delta 11.00	PointTerm1093	PointTerm1076	0.2007168	Air		0.1228	0.1228	0.246	0.237	0.063	0.267	0.331
269357822	11 kV 120mm2 Cu PILC 3Core	PointTerm1056	PointTerm1044	0.1648831	Ground		1	1	0.048	0.025	0.041	0.452	0.016
269357825	MV3 Delta	PointTerm1079	PointTerm1072	0.097244	Air	FOX50	0.148	0.148	0.086	0.076	0.039	0.091	0.154
269357830	MV3 Delta	PointTerm1236	PointTerm1240	0.00480801	Air	FOX50	0.148	0.148	0.004	0.004	0.002	0.004	0.008
269357843	MV3 Delta	PointTerm1236	PointTerm1281	0.2561482	Air	FOX50	0.148	0.148	0.226	0.201	0.102	0.239	0.405
269357850	MV3 Delta	PointTerm1096	PointTerm1110	0.00662435	Air	FOX50	0.148	0.148	0.006	0.005	0.003	0.006	0.010
269357852	MV3 Delta	PointTerm1079	PointTerm1100	0.1226548	Air	FOX50	0.148	0.148	0.108	0.096	0.049	0.114	0.194
269357853	MV3 Delta	PointTerm1079	PointTerm1096	0.1222897	Air	FOX50	0.148	0.148	0.108	0.096	0.048	0.114	0.193
269357856	MV3 Delta	PointTerm1281	PointTerm1294	0.105299	Air	FOX50	0.148	0.148	0.093	0.083	0.042	0.098	0.166
270224799	MV3 Delta	PointTerm1271	PointTerm1313	0.1716444	Air	FOX50	0.148	0.148	0.151	0.135	0.068	0.160	0.271
270411021	Internal Line 3 11.00 [kV]	PointTerm510	PointTerm513	0.001	Ground		1000	1000	0.000	0.000	0.000	0.000	0.000
270952227	FOX 3 Delta 11.00	PointTerm198	PointTerm202	0.00311841	Ground		0.148	0.148	0.003	0.003	0.001	0.003	0.005
271024509	MV3 Delta	PointTerm148	PointTerm160	0.1813112	Air	FOX50	0.148	0.148	0.160	0.143	0.072	0.169	0.286
271100113	MV3 Delta	PointTerm141	PointTerm145	0.02465092	Air	HARE50	0.284	0.284	0.011	0.007	0.009	0.010	0.038
271127343	MV3 Delta	PointTerm729	PointTerm761	0.1008844	Air	FOX50	0.148	0.148	0.089	0.079	0.040	0.094	0.159
271127349	MV3 Delta	PointTerm664	PointTerm673	0.08393881	Air	FOX50	0.148	0.148	0.074	0.066	0.033	0.078	0.133
271127367	MV3 Delta	PointTerm657	PointTerm703	0.1626814	Air	FOX50	0.148	0.148	0.143	0.128	0.064	0.152	0.257
271131165	MV3 Delta	PointTerm607	PointTerm657	0.2556968	Air	FOX50	0.148	0.148	0.225	0.201	0.101	0.238	0.404
271131223	MV3 Delta	PointTerm624	PointTerm667	0.2375555	Air	FOX50	0.148	0.148	0.209	0.187	0.094	0.221	0.375
271131225	MV3 Delta	PointTerm617	PointTerm621	0.02336408	Air	FOX50	0.148	0.148	0.021	0.018	0.009	0.022	0.037
271131277	MV3 Delta	PointTerm653	PointTerm696	0.1580893	Air	FOX50	0.148	0.148	0.139	0.124	0.063	0.147	0.250
271131283	MV3 Delta	PointTerm634	PointTerm641	0.02758247	Air	FOX50	0.148	0.148	0.024	0.022	0.011	0.026	0.044
271131295	MV3 Delta	PointTerm644	PointTerm647	0.03782771	Air	FOX50	0.148	0.148	0.033	0.030	0.015	0.035	0.060
271131323	MV3 Delta	PointTerm661	PointTerm693	0.146576	Air	FOX50	0.148	0.148	0.129	0.115	0.058	0.137	0.232
271131375	MV3 Delta	PointTerm758	PointTerm774	0.07656419	Air	FOX50	0.148	0.148	0.067	0.060	0.030	0.071	0.121
271131381	MV3 Delta	PointTerm812	PointTerm816	0.02845001	Air	FOX50	0.148	0.148	0.025	0.022	0.011	0.027	0.045
271131403	MV3 Delta	PointTerm696	PointTerm754	0.1701422	Air	FOX50	0.148	0.148	0.150	0.134	0.067	0.159	0.269
271132027	MV3 Delta	PointTerm839	PointTerm852	0.06365054	Air	FOX50	0.148	0.148	0.056	0.050	0.025	0.059	0.101
271132033	MV3 Delta	PointTerm861	PointTerm864	0.06767247	Air	FOX50	0.148	0.148	0.060	0.053	0.027	0.063	0.107
271132035	MV3 Delta	PointTerm845	PointTerm858	0.09763476	Air	FOX50	0.148	0.148	0.086	0.077	0.039	0.091	0.154
271132073	MV3 Delta	PointTerm849	PointTerm870	0.1863707	Air	FOX50	0.148	0.148	0.164	0.147	0.074	0.174	0.294
271132103	MV3 Delta	PointTerm825	PointTerm833	0.03413478	Air	FOX50	0.148	0.148	0.030	0.027	0.014	0.032	0.054
271133101	MV3 Delta	PointTerm530	PointTerm525	0.0185482	Air	FOX50	0.148	0.148	0.016	0.015	0.007	0.017	0.029
271133121	MV3 Delta	PointTerm627	PointTerm634	0.01618476	Air	FOX50	0.148	0.148	0.014	0.013	0.006	0.015	0.026
271133123	MV3 Delta	PointTerm634	PointTerm653	0.1042287	Air	FOX50	0.148	0.148	0.092	0.082	0.041	0.097	0.165
271133125	MV3 Delta	PointTerm754	PointTerm812	0.225316	Air	FOX50	0.148	0.148	0.198	0.177	0.089	0.210	0.356
271133127	MV3 Delta	PointTerm825	PointTerm845	0.05469098	Air	FOX50	0.148	0.148	0.048	0.043	0.022	0.051	0.086
271133129	MV3 Delta	PointTerm588	PointTerm617	0.107511	Air	FOX50	0.148	0.148	0.095	0.085	0.043	0.100	0.170
271139683	MV3 Delta	PointTerm812	PointTerm825	0.1025958	Air	FOX50	0.148	0.148	0.090	0.081	0.041	0.096	0.162
271174995	11 kV 120mm2 Al XLPE 3Core	PointTerm294	PointTerm301	0.00470304	Ground		1	1	0.002	0.002	0.000	0.005	0.001
271175007	11 kV 120mm2 Al XLPE 3Core	PointTerm215	PointTerm262	0.2527055	Ground		1	1	0.086	0.082	0.025	0.278	0.036
271205497	MV3 Delta	PointTerm360	PointTerm370	0.0591113	Air	MINK50	0.208	0.208	0.035	0.027	0.022	0.036	0.092
271231881	C3/0.104 3 Delta 11.00	PointTerm562	PointTerm683	0.5158659	Air		0.1228	0.1228	0.631	0.610	0.163	0.685	0.851
271265695	MV3 Delta	PointTerm360	PointTerm364	0.02256123	Air	MINK50	0.208	0.208	0.013	0.010	0.009	0.014	0.035
271265697	MV3 Delta	PointTerm350	PointTerm360	0.1441379	Air	FOX50	0.148	0.148	0.127	0.113	0.057	0.134	0.228
271265701	MV3 Delta	PointTerm367	PointTerm387	0.1377723	Air	FOX50	0.148	0.148	0.121	0.108	0.055	0.128	0.218
271547783	MV3 Delta	PointTerm350	PointTerm340	0.5367901	Air	MINK50	0.208	0.208	0.320	0.247	0.204	0.325	0.839
271628925	MV3 Delta	PointTerm340	PointTerm330	0.262253	Air	MINK50	0.208	0.208	0.156	0.120	0.099	0.159	0.410
271670141	MV3 Delta	PointTerm399	PointTerm412	0.2170575	Air	MINK50	0.208	0.208	0.129	0.100	0.082	0.131	0.339
272060055	MV3 Delta	PointTerm553	PointTerm556	0.03041647	Air	FOX50	0.148	0.148	0.027	0.024	0.012	0.028	0.048
272060061	MV3 Delta	PointTerm549	PointTerm533	0.1424566	Air	FOX50	0.148	0.148	0.125	0.112	0.056	0.133	0.225
272149333	MV3 Delta	PointTerm1113	PointTerm1128	0.1753904	Air	FOX50	0.148	0.148	0.154	0.138	0.070	0.163	0.277
272400647	MV3 Delta	PointTerm461	PointTerm451	0.06125275	Air	MINK50	0.208	0.208	0.036	0.028	0.023	0.037	0.096
272400651	MV3 Delta	PointTerm491	PointTerm498	0.01191175	Air	FOX50	0.148	0.148	0.010	0.009	0.005	0.011	0.019
272400667	MV3 Delta	PointTerm507	PointTerm519	0.03313922	Air	FOX50	0.148	0.148	0.029	0.026	0.013	0.031	0.052
272420117	11 kV 120mm2 Cu PILC 3Core	PointTerm170	PointTerm183	0.06403296	Ground		1	1	0.019	0.010	0.016	0.176	0.006
272420125	MV3 Delta	PointTerm141	PointTerm166	0.3179794	Air	OAK50	0.28	0.28	0.148	0.090	0.117	0.137	0.493
272656879	MV3 Delta	PointTerm32	PointTerm36	0.00542333	Air	FOX50	0.148	0.148	0.005	0.004	0.002	0.005	0.009
272673223	MV3 Delta	PointTerm128	PointTerm157	0.2829397	Air	FOX50	0.148	0.148	0.249	0.222	0.112	0.264	0.447
272673245	MV3 Delta	PointTerm93	PointTerm96	0.09216477	Air	FOX50	0.148	0.148	0.081	0.072	0.037	0.086	0.146
272673251	MV3 Delta	PointTerm102	PointTerm86	0.6267222	Air	FOX50	0.148	0.148	0.552	0.493	0.248	0.584	0.990
272673261	MV3 Delta	PointTerm86	PointTerm90	0.02446396	Air	FOX50	0.148	0.148	0.022	0.019	0.010	0.023	0.039
272673329	MV3 Delta	PointTerm102	PointTerm128	0.2357837	Air	FOX50	0.148	0.148	0.208	0.185	0.093	0.220	0.372
272777139	11 kV 120mm2 Cu PILC 3Core	PointTerm4	Internal Node(1)	0.1120345	Ground		1	1	0.033	0.017	0.028	0.307	0.011
272805919	MV3 Delta	PointTerm893	PointTerm896	0.02827505	Air	MINK50	0.208	0.208	0.017	0.013	0.011	0.017	0.044
272805941	MV3 Delta	PointTerm919	PointTerm942	0.1550472	Air	FOX50	0.148	0.148	0.137	0.122	0.061	0.144	0.245
272805947	MV3 Delta	PointTerm902	PointTerm915	0.3029801	Air	MINK50	0.208	0.208	0.180	0.139	0.115	0.183	0.473
272814021	MV3 Delta	PointTerm985	PointTerm995	0.1039597	Air	MINK50	0.208	0.208	0.062	0.048	0.039	0.063	0.162
273091247	MV3 Delta	PointTerm112	PointTerm116	0.00991806	Air	OAK50	0.28	0.28	0.005	0.003	0.004	0.004	0.015
273284111	MV3 Delta	PointTerm1264	PointTerm1297	0.1482516	Air	MINK50	0.208	0.208	0.088	0.068	0.056	0.090	0.232
273622467	MV3 Delta	PointTerm712	PointTerm736	0.1071681	Air	FOX50	0.148	0.148	0.094	0.084	0.042	0.100	0.169
273622471	MV3 Delta	PointTerm673	PointTerm700	0.06211558	Air	FOX50	0.148	0.148	0.055	0.049	0.025	0.058	0.098
273622523	MV3 Delta	PointTerm715	PointTerm729	0.08118746	Air	FOX50	0.148	0.148	0.071	0.064	0.032	0.076	0.128
273622527	MV3 Delta	PointTerm733	PointTerm739	0.01736221	Air	FOX50	0.148	0.148	0.015	0.014	0.007	0.016	0.027
273622579	MV3 Delta	PointTerm617	PointTerm627	0.07698408	Air	FOX50	0.148	0.148	0.068	0.061	0.031	0.072	0.122
273622613	MV3 Delta	PointTerm595	PointTerm607	0.04159116	Air	FOX50	0.148	0.148	0.037	0.033	0.016	0.039	0.066
273688661	MV3 Delta	PointTerm32	PointTerm19	0.1785078	Air	OAK50	0.28	0.28	0.083	0.051	0.066	0.077	0.277
273688665	MV3 Delta	PointTerm19	PointTerm23	0.03783929	Air	OAK50	0.28	0.28	0.018	0.011	0.014	0.016	0.059
273740919	MV3 Delta	PointTerm549	PointTerm569	0.1302984	Air	FOX50	0.148	0.148	0.115	0.102	0.052	0.121	0.206
273856224	MV3 Delta	PointTerm163	PointTerm198	0.3093764	Air	HARE50	0.284	0.284	0.142	0.086	0.112	0.131	0.478
273901449	MV3 Delta	PointTerm1329	PointTerm1291	0.2242852	Air	FOX50	0.148	0.148	0.197	0.176	0.089	0.209	0.354
273901458	MV3 Delta	PointTerm1288	PointTerm1281	0.05863367	Air	FOX50	0.148	0.148	0.052	0.046	0.023	0.055	0.093
273901484	MV3 Delta	PointTerm1096	PointTerm1211	0.6072663	Air	FOX50	0.148	0.148	0.535	0.477	0.241	0.566	0.959
273901490	MV3 Delta	PointTerm1217	PointTerm1236	0.04893677	Air	FOX50	0.148	0.148	0.043	0.038	0.019	0.046	0.077
274006173	MV3 Delta	PointTerm491	PointTerm487	0.00773662	Air	FOX50	0.148	0.148	0.007	0.006	0.003	0.007	0.012
274044964	MV3 Delta	PointTerm487	PointTerm477	0.087712	Air	MINK50	0.208	0.208	0.052	0.040	0.033	0.053	0.137
274044990	MV3 Delta	PointTerm477	PointTerm461	0.1133425	Air	MINK50	0.208	0.208	0.068	0.052	0.043	0.069	0.177
274084462	MV3 Delta	PointTerm248	PointTerm238	0.1319438	Air	HARE50	0.284	0.284	0.060	0.037	0.048	0.056	0.204
274135851	MV3 Delta	PointTerm173	PointTerm192	0.1040302	Air	OAK50	0.28	0.28	0.048	0.030	0.038	0.045	0.161
274142547	MV3 Delta	PointTerm224	PointTerm231	0.03606434	Air	HARE50	0.284	0.284	0.016	0.010	0.013	0.015	0.056
274142556	MV3 Delta	PointTerm224	PointTerm195	0.1442886	Air	HARE50	0.284	0.284	0.066	0.040	0.052	0.061	0.223
274142558	MV3 Delta	PointTerm228	PointTerm224	0.03138505	Air	HARE50	0.284	0.284	0.014	0.009	0.011	0.013	0.049
274142560	MV3 Delta	PointTerm231	PointTerm238	0.01375856	Air	HARE50	0.284	0.284	0.006	0.004	0.005	0.006	0.021
274155879	11 kV 120mm2 Al XLPE 3Core	PointTerm282	PointTerm291	0.00146086	Ground		1	1	0.000	0.000	0.000	0.002	0.000
274350152	MV3 Delta	PointTerm238	PointTerm245	0.01419753	Air	MINK50	0.208	0.208	0.008	0.007	0.005	0.009	0.022
CABLE	Internal Line 3 11.00 [kV]	PointTerm252	PointTerm255	0.001	Ground		1000	1000	0.000	0.000	0.000	0.000	0.000
CRR224	11 kV 120mm2 Cu PILC 3Core	PointTerm49	PointTerm52	0.001	Ground		1	1	0.000	0.000	0.000	0.003	0.000
CRR610 _T	Internal Line 3 11.00 [kV]	PointTerm301	PointTerm307	0.001	Ground		1000	1000	0.000	0.000	0.000	0.000	0.000
CRR90 _T	Internal Line 3 11.00 [kV]	PointTerm513	PointTerm516	0.001	Ground		1000	1000	0.000	0.000	0.000	0.000	0.000
CT VT _T	Internal Line 3 11.00 [kV]	PointTerm57	PointTerm60	0.001	Ground		1000	1000	0.000	0.000	0.000	0.000	0.000
Internal	MV3 Delta	Abattoir 11.0 BB	Internal Node	0.00001	Ground	BULL50	1.15	1.15	0.000	0.000	0.000	0.000	0.000

Appendix A2 – Network Data for Conductor lines > 500m for Network 2

Name	Type	Terminal i	Terminal j	Length	Type of Phase Conductors	Irated(act.)	Irated	Z1	R1	X1	R0	X0
	TypLne,TypTow,TypGeo,TypCabsys			km	TypCor	kA	kA	Ohm	Ohm	Ohm	Ohm	Ohm
269438418	MV3 Delta	PointTerm831	PointTerm1015	1.554158	FOX50	0.148	0.148	1.368	1.222	0.616	1.448	2.455
269438428	MV3 Delta	PointTerm1214	PointTerm1069	1.360552	FOX50	0.148	0.148	1.198	1.070	0.539	1.268	2.149
274385966	MV3 Delta	PointTerm838	PointTerm1107	2.429562	FOX50	0.148	0.148	2.139	1.910	0.963	2.264	3.838
273256721	MV3 Delta	PointTerm1079	PointTerm1121	0.5380088	MINK50	0.208	0.208	0.320	0.247	0.204	0.325	0.841
269425921	MV3 Delta	PointTerm101	PointTerm114	1.091398	FOX50	0.148	0.148	0.961	0.858	0.433	1.017	1.724
273885313	MV3 Delta	PointTerm1153	PointTerm1218	0.6254372	FOX50	0.148	0.148	0.551	0.492	0.248	0.583	0.988
273256807	MV3 Delta	PointTerm1190	PointTerm1235	0.7527433	MINK50	0.208	0.208	0.448	0.346	0.285	0.455	1.176
269438400	MV3 Delta	PointTerm1170	PointTerm1251	0.940576	MINK50	0.208	0.208	0.560	0.432	0.357	0.569	1.470
269438430	MV3 Delta	PointTerm1214	PointTerm1255	0.5272155	FOX50	0.148	0.148	0.464	0.414	0.209	0.491	0.833
274351422	MV3 Delta	PointTerm970	PointTerm1268	2.890356	FOX50	0.148	0.148	2.545	2.272	1.146	2.693	4.566
274385960	MV3 Delta	PointTerm1118	PointTerm1278	1.5102	FOX50	0.148	0.148	1.330	1.187	0.599	1.407	2.386
269438436	MV3 Delta	PointTerm1214	PointTerm1307	0.8380327	FOX50	0.148	0.148	0.738	0.659	0.332	0.781	1.324
269438454	MV3 Delta	PointTerm1388	PointTerm1307	0.6149151	FOX50	0.148	0.148	0.541	0.483	0.244	0.573	0.971
269438438	MV3 Delta	PointTerm1449	PointTerm1311	0.8659157	FOX50	0.148	0.148	0.762	0.681	0.343	0.807	1.368
273885315	MV3 Delta	PointTerm1222	PointTerm1314	0.7563377	FOX50	0.148	0.148	0.666	0.595	0.300	0.705	1.195
273256769	MV3 Delta	PointTerm1248	PointTerm1324	0.5530294	MINK50	0.208	0.208	0.329	0.254	0.210	0.334	0.864
269438434	MV3 Delta	PointTerm1255	PointTerm1336	0.5976337	FOX50	0.148	0.148	0.526	0.470	0.237	0.557	0.944
273846823	MV3 Delta	PointTerm1251	PointTerm1339	0.6131741	MINK50	0.208	0.208	0.365	0.282	0.233	0.371	0.958
272583345	MV3 Delta	PointTerm124	PointTerm134	0.8044176	OAK50	0.28	0.28	0.374	0.229	0.296	0.346	1.248
274351441	MV3 Delta	PointTerm1294	PointTerm1385	0.6939237	FOX50	0.148	0.148	0.611	0.546	0.275	0.647	1.096
274351464	MV3 Delta	PointTerm1290	PointTerm1398	0.7288533	FOX50	0.148	0.148	0.642	0.573	0.289	0.679	1.151
269425925	MV3 Delta	PointTerm134	PointTerm150	1.181059	OAK50	0.28	0.28	0.549	0.336	0.434	0.508	1.832
273885327	MV3 Delta	PointTerm1381	PointTerm1524	0.6817739	FOX50	0.148	0.148	0.600	0.536	0.270	0.635	1.077
273858824	MV3 Delta	PointTerm1333	PointTerm1568	1.305027	MINK50	0.208	0.208	0.777	0.599	0.495	0.789	2.039
274351493	MV3 Delta	PointTerm1398	PointTerm1572	0.8654832	FOX50	0.148	0.148	0.762	0.680	0.343	0.806	1.367
273723688	MV3 Delta	PointTerm1411	PointTerm1576	0.8559288	FOX50	0.148	0.148	0.754	0.673	0.339	0.797	1.352
273256561	MV3 Delta	PointTerm1423	PointTerm1590	0.7276215	MINK50	0.208	0.208	0.433	0.334	0.276	0.440	1.137
269438452	MV3 Delta	PointTerm1873	PointTerm1695	1.545411	FOX50	0.148	0.148	1.361	1.215	0.613	1.440	2.441
273699358	MV3 Delta	PointTerm1548	PointTerm1751	0.6155632	FOX50	0.148	0.148	0.542	0.484	0.244	0.574	0.972
269425937	MV3 Delta	PointTerm239	PointTerm177	2.973463	FOX50	0.148	0.148	2.618	2.338	1.179	2.770	4.697
273723728	MV3 Delta	PointTerm1707	PointTerm1785	0.506278	FOX50	0.148	0.148	0.446	0.398	0.201	0.472	0.800
274351510	MV3 Delta	PointTerm1572	PointTerm1792	0.8724483	FOX50	0.148	0.148	0.768	0.686	0.346	0.813	1.378
272327691	MV3 Delta	PointTerm150	PointTerm180	0.6860783	FOX50	0.148	0.148	0.604	0.539	0.272	0.639	1.084
273256609	MV3 Delta	PointTerm1726	PointTerm1833	0.8306879	MINK50	0.208	0.208	0.495	0.381	0.315	0.502	1.298
273699368	MV3 Delta	PointTerm1798	PointTerm1883	1.273943	FOX50	0.148	0.148	1.122	1.002	0.505	1.187	2.013
269438515	MV3 Delta	PointTerm1981	PointTerm1937	0.5865592	FOX50	0.148	0.148	0.516	0.461	0.233	0.546	0.927
273699372	MV3 Delta	PointTerm1883	PointTerm1971	0.794244	FOX50	0.148	0.148	0.699	0.624	0.315	0.740	1.255
269438389	MV3 Delta	PointTerm1910	PointTerm1993	0.9525275	HARE50	0.284	0.284	0.436	0.265	0.346	0.404	1.473
274365279	MV3 Delta	PointTerm1917	PointTerm2009	0.9825926	FOX50	0.148	0.148	0.865	0.772	0.390	0.915	1.552
269438527	MV3 Delta	PointTerm2018	PointTerm2080	0.5855772	FOX50	0.148	0.148	0.516	0.460	0.232	0.546	0.925
269425899	MV3 Delta	PointTerm4	PointTerm21	0.5534405	OAK50	0.28	0.28	0.257	0.157	0.203	0.238	0.858
273699360	MV3 Delta	PointTerm1971	PointTerm2100	1.028953	FOX50	0.148	0.148	0.906	0.809	0.408	0.959	1.626
269425945	MV3 Delta	PointTerm202	PointTerm218	1.86549	FOX50	0.148	0.148	1.643	1.467	0.740	1.738	2.947
269425947	MV3 Delta	PointTerm246	PointTerm222	0.6716744	FOX50	0.148	0.148	0.591	0.528	0.266	0.626	1.061
269438547	MV3 Delta	PointTerm2623	PointTerm2355	1.078431	FOX50	0.148	0.148	0.950	0.848	0.428	1.005	1.704
269438319	MV3 Delta	PointTerm2527	PointTerm2358	0.6413952	FOX50	0.148	0.148	0.565	0.504	0.254	0.598	1.013
269438541	MV3 Delta	PointTerm2251	PointTerm2428	0.595727	FOX50	0.148	0.148	0.525	0.468	0.236	0.555	0.941
269438852	MV3 Delta	PointTerm2707	PointTerm2500	0.9475345	FOX50	0.148	0.148	0.834	0.745	0.376	0.883	1.497
269438553	MV3 Delta	PointTerm2362	PointTerm2514	0.5355788	FOX50	0.148	0.148	0.472	0.421	0.212	0.499	0.846
269438327	MV3 Delta	PointTerm2419	PointTerm2547	0.5951425	FOX50	0.148	0.148	0.524	0.468	0.236	0.554	0.940
269438283	MV3 Delta	PointTerm2766	PointTerm2619	0.5298811	FOX50	0.148	0.148	0.467	0.417	0.210	0.494	0.837
270284274	MV3 Delta	PointTerm2485	PointTerm2654	0.8580496	FOX50	0.148	0.148	0.755	0.675	0.340	0.799	1.356
269438849	MV3 Delta	PointTerm2947	PointTerm2718	0.7297351	FOX50	0.148	0.148	0.643	0.574	0.289	0.680	1.153
269438477	MV3 Delta	PointTerm232	PointTerm281	0.5885398	FOX50	0.148	0.148	0.518	0.463	0.233	0.548	0.930
269438475	MV3 Delta	PointTerm316	PointTerm281	0.5540851	HARE50	0.284	0.284	0.253	0.154	0.201	0.235	0.857
270428335	MV3 Delta	PointTerm2733	PointTerm2899	0.5490324	FOX50	0.148	0.148	0.483	0.432	0.218	0.512	0.867
269438303	MV3 Delta	PointTerm2691	PointTerm2918	0.6529867	FOX50	0.148	0.148	0.575	0.513	0.259	0.608	1.032
269438307	MV3 Delta	PointTerm3079	PointTerm2937	0.5706046	FOX50	0.148	0.148	0.502	0.449	0.226	0.532	0.901
269437850	MV3 Delta	PointTerm466	PointTerm294	4.909198	FOX50	0.148	0.148	4.322	3.860	1.946	4.574	7.755
269437848	MV3 Delta	PointTerm236	PointTerm294	0.6680529	FOX50	0.148	0.148	0.588	0.525	0.265	0.622	1.055
269438257	MV3 Delta	PointTerm3089	PointTerm2944	0.5381726	FOX50	0.148	0.148	0.474	0.423	0.213	0.501	0.850
271276265	MV3 Delta	PointTerm2776	PointTerm2979	0.6628552	FOX50	0.148	0.148	0.584	0.521	0.263	0.618	1.047
269437841	MV3 Delta	PointTerm262	PointTerm310	0.8618394	FOX50	0.148	0.148	0.759	0.678	0.342	0.803	1.362
269438473	MV3 Delta	PointTerm319	PointTerm328	1.276521	HARE50	0.284	0.284	0.584	0.355	0.463	0.541	1.974
273966785	MV3 Delta	PointTerm3159	PointTerm3376	0.5075229	FOX50	0.148	0.148	0.447	0.399	0.201	0.473	0.802
273723632	MV3 Delta	PointTerm3069	PointTerm3395	1.015642	FOX50	0.148	0.148	0.894	0.798	0.403	0.946	1.604
269438229	MV3 Delta	PointTerm3644	PointTerm3433	0.6025048	FOX50	0.148	0.148	0.530	0.474	0.239	0.561	0.952
274147902	MV3 Delta	PointTerm3216	PointTerm3449	0.6034611	FOX50	0.148	0.148	0.531	0.474	0.239	0.562	0.953
274147923	MV3 Delta	PointTerm3194	PointTerm3527	0.8653082	FOX50	0.148	0.148	0.762	0.680	0.343	0.806	1.367
269438577	MV3 Delta	PointTerm3366	PointTerm3591	0.6517244	FOX50	0.148	0.148	0.574	0.512	0.258	0.607	1.030

Name	Type	Terminal i	Terminal j	Length	Type of Phase Conductors	Irated(act.)	Irated	Z1	R1	X1	R0	X0
269438217	MV3 Delta	PointTerm3754	PointTerm3598	0.6103535	FOX50	0.148	0.148	0.537	0.480	0.242	0.569	0.964
274385867	MV3 Delta	PointTerm3853	PointTerm3620	0.8804048	FOX50	0.148	0.148	0.775	0.692	0.349	0.820	1.391
273723662	MV3 Delta	PointTerm3362	PointTerm3638	0.8317867	FOX50	0.148	0.148	0.732	0.654	0.330	0.775	1.314
273762677	MV3 Delta	PointTerm3497	PointTerm3698	0.6569549	FOX50	0.148	0.148	0.578	0.516	0.260	0.612	1.038
273762513	MV3 Delta	PointTerm3608	PointTerm3733	0.5136103	FOX50	0.148	0.148	0.452	0.404	0.204	0.479	0.811
273672636	MV3 Delta	PointTerm250	PointTerm378	2.835385	FOX50	0.148	0.148	2.497	2.229	1.124	2.642	4.479
274147980	MV3 Delta	PointTerm3634	PointTerm3817	0.7327556	FOX50	0.148	0.148	0.645	0.576	0.291	0.683	1.158
273723636	MV3 Delta	PointTerm3395	PointTerm3857	1.524378	FOX50	0.148	0.148	1.342	1.198	0.604	1.420	2.408
274385897	MV3 Delta	PointTerm3711	PointTerm3864	0.5610309	FOX50	0.148	0.148	0.494	0.441	0.222	0.523	0.886
269438583	MV3 Delta	PointTerm3737	PointTerm3902	0.5661253	FOX50	0.148	0.148	0.498	0.445	0.224	0.527	0.894
274219594	MV3 Delta	PointTerm3751	PointTerm3914	0.5682557	FOX50	0.148	0.148	0.500	0.447	0.225	0.529	0.898
272655691	MV3 Delta	PointTerm3747	PointTerm3921	0.583431	FOX50	0.148	0.148	0.514	0.459	0.231	0.544	0.922
272752265	MV3 Delta	PointTerm416	PointTerm400	0.5943206	MINK50	0.208	0.208	0.354	0.273	0.225	0.359	0.929
271712231	MV3 Delta	PointTerm3837	PointTerm4060	0.673418	FOX50	0.148	0.148	0.593	0.529	0.267	0.627	1.064
274147982	MV3 Delta	PointTerm3841	PointTerm4075	0.7946595	FOX50	0.148	0.148	0.700	0.625	0.315	0.740	1.255
273723634	MV3 Delta	PointTerm3857	PointTerm4081	0.751063	FOX50	0.148	0.148	0.661	0.590	0.298	0.700	1.187
273762750	MV3 Delta	PointTerm3946	PointTerm4084	0.5167584	FOX50	0.148	0.148	0.455	0.406	0.205	0.481	0.816
274219607	MV3 Delta	PointTerm3914	PointTerm4115	0.6247083	FOX50	0.148	0.148	0.550	0.491	0.248	0.582	0.987
270081965	MV3 Delta	PointTerm4291	PointTerm4128	0.662067	FOX50	0.148	0.148	0.583	0.521	0.262	0.617	1.046
273739984	MV3 Delta	PointTerm3853	PointTerm4151	0.925616	FOX50	0.148	0.148	0.815	0.728	0.367	0.862	1.462
269438177	MV3 Delta	PointTerm3976	PointTerm4185	0.749512	FOX50	0.148	0.148	0.660	0.589	0.297	0.698	1.184
273739971	MV3 Delta	PointTerm3938	PointTerm4189	0.9130943	FOX50	0.148	0.148	0.804	0.718	0.362	0.851	1.442
269438894	MV3 Delta	PointTerm416	PointTerm420	0.8076933	FOX50	0.148	0.148	0.711	0.635	0.320	0.753	1.276
269438209	MV3 Delta	PointTerm4101	PointTerm4219	0.5347496	FOX50	0.148	0.148	0.471	0.420	0.212	0.498	0.845
273966829	MV3 Delta	PointTerm4095	PointTerm4223	0.5486272	FOX50	0.148	0.148	0.483	0.431	0.218	0.511	0.867
269438479	MV3 Delta	PointTerm416	PointTerm424	0.8155741	FOX50	0.148	0.148	0.718	0.641	0.323	0.760	1.288
273966858	MV3 Delta	PointTerm4088	PointTerm4264	0.6923859	FOX50	0.148	0.148	0.610	0.544	0.274	0.645	1.094
274219620	MV3 Delta	PointTerm4115	PointTerm4268	0.6365538	FOX50	0.148	0.148	0.560	0.500	0.252	0.593	1.006
273966882	MV3 Delta	PointTerm4105	PointTerm4274	0.6935515	FOX50	0.148	0.148	0.611	0.545	0.275	0.646	1.096
273762762	MV3 Delta	PointTerm4144	PointTerm4503	1.066585	FOX50	0.148	0.148	0.939	0.839	0.423	0.994	1.685
273966884	MV3 Delta	PointTerm4295	PointTerm4551	0.5267888	FOX50	0.148	0.148	0.464	0.414	0.209	0.491	0.832
273067051	MV3 Delta	PointTerm4444	PointTerm4660	0.5087602	FOX50	0.148	0.148	0.448	0.400	0.202	0.474	0.804
273762870	MV3 Delta	PointTerm4278	PointTerm4666	0.8681617	FOX50	0.148	0.148	0.764	0.683	0.344	0.809	1.371
273470625	MV3 Delta	PointTerm420	PointTerm472	0.9723159	FOX50	0.148	0.148	0.856	0.764	0.385	0.906	1.536
274037527	MV3 Delta	PointTerm4352	PointTerm4738	0.9997721	FOX50	0.148	0.148	0.880	0.786	0.396	0.931	1.579
273762363	MV3 Delta	PointTerm4589	PointTerm4745	0.5059199	FOX50	0.148	0.148	0.445	0.398	0.201	0.471	0.799
273740830	MV3 Delta	PointTerm4400	PointTerm4817	1.110514	FOX50	0.148	0.148	0.978	0.873	0.440	1.035	1.754
273762407	MV3 Delta	PointTerm4657	PointTerm4856	0.6340289	FOX50	0.148	0.148	0.558	0.498	0.251	0.591	1.002
274003712	MV3 Delta	PointTerm4599	PointTerm4872	0.7950645	FOX50	0.148	0.148	0.700	0.625	0.315	0.741	1.256
273745063	MV3 Delta	PointTerm4721	PointTerm4896	0.5326248	FOX50	0.148	0.148	0.469	0.419	0.211	0.496	0.841
273723520	MV3 Delta	PointTerm4688	PointTerm4923	0.7392777	FOX50	0.148	0.148	0.651	0.581	0.293	0.689	1.168
274003669	MV3 Delta	PointTerm4749	PointTerm4947	0.6048344	FOX50	0.148	0.148	0.533	0.476	0.240	0.564	0.955
273762366	MV3 Delta	PointTerm4745	PointTerm4960	0.6944655	FOX50	0.148	0.148	0.611	0.546	0.275	0.647	1.097
273762765	MV3 Delta	PointTerm4503	PointTerm4975	1.430499	FOX50	0.148	0.148	1.260	1.125	0.567	1.333	2.260
269438489	MV3 Delta	PointTerm459	PointTerm498	0.8484436	FOX50	0.148	0.148	0.747	0.667	0.336	0.790	1.340
274162062	MV3 Delta	PointTerm4830	PointTerm4997	0.603238	FOX50	0.148	0.148	0.531	0.474	0.239	0.562	0.953
269438458	MV3 Delta	PointTerm478	PointTerm504	0.6772635	MINK50	0.208	0.208	0.403	0.311	0.257	0.410	1.058
269438410	MV3 Delta	PointTerm621	PointTerm508	1.14765	FOX50	0.148	0.148	1.010	0.902	0.455	1.069	1.813
273771129	MV3 Delta	PointTerm4888	PointTerm5085	0.6275559	FOX50	0.148	0.148	0.553	0.493	0.249	0.585	0.991
271310261	MV3 Delta	PointTerm4650	PointTerm5089	1.403599	FOX50	0.148	0.148	1.236	1.103	0.556	1.308	2.217
273740824	MV3 Delta	PointTerm4817	PointTerm5097	0.9045888	FOX50	0.148	0.148	0.796	0.711	0.359	0.843	1.429
269437852	MV3 Delta	PointTerm488	PointTerm511	0.5305464	FOX50	0.148	0.148	0.467	0.417	0.210	0.494	0.838
273762419	MV3 Delta	PointTerm4936	PointTerm5185	0.7070418	FOX50	0.148	0.148	0.623	0.556	0.280	0.659	1.117
269437860	MV3 Delta	PointTerm559	PointTerm524	0.6535575	HARE50	0.284	0.284	0.299	0.182	0.237	0.277	1.011
273723576	MV3 Delta	PointTerm4923	PointTerm5255	0.989275	FOX50	0.148	0.148	0.871	0.778	0.392	0.922	1.563
274148002	MV3 Delta	PointTerm4947	PointTerm5268	0.9255376	FOX50	0.148	0.148	0.815	0.728	0.367	0.862	1.462
269425907	MV3 Delta	PointTerm37	PointTerm53	0.8533463	OAK50	0.28	0.28	0.397	0.243	0.314	0.367	1.323
269438497	MV3 Delta	PointTerm598	PointTerm531	0.7980711	FOX50	0.148	0.148	0.703	0.627	0.316	0.744	1.261
273851062	MV3 Delta	PointTerm5072	PointTerm5337	0.7225592	FOX50	0.148	0.148	0.636	0.568	0.286	0.673	1.141
269438104	MV3 Delta	PointTerm5156	PointTerm5356	0.5090153	FOX50	0.148	0.148	0.448	0.400	0.202	0.474	0.804
270149060	MV3 Delta	PointTerm611	PointTerm538	0.7815256	FOX50	0.148	0.148	0.688	0.614	0.310	0.728	1.235
273762830	MV3 Delta	PointTerm4975	PointTerm5401	1.099175	FOX50	0.148	0.148	0.968	0.864	0.436	1.024	1.736
273880145	MV3 Delta	PointTerm5040	PointTerm5446	1.157254	FOX50	0.148	0.148	1.019	0.910	0.459	1.078	1.828
269438408	MV3 Delta	PointTerm504	PointTerm547	0.7363925	MINK50	0.208	0.208	0.439	0.338	0.279	0.445	1.151
273319257	MV3 Delta	PointTerm5360	PointTerm5497	0.548435	FOX50	0.148	0.148	0.483	0.431	0.217	0.511	0.866
273762770	MV3 Delta	PointTerm5401	PointTerm5520	0.501196	FOX50	0.148	0.148	0.441	0.394	0.199	0.467	0.792
274148015	MV3 Delta	PointTerm5321	PointTerm5523	0.6623988	FOX50	0.148	0.148	0.583	0.521	0.263	0.617	1.046
269438460	MV3 Delta	PointTerm478	PointTerm553	1.46649	MINK50	0.208	0.208	0.873	0.673	0.556	0.887	2.291
273762767	MV3 Delta	PointTerm5401	PointTerm5545	0.6137012	FOX50	0.148	0.148	0.540	0.482	0.243	0.572	0.970
273723522	MV3 Delta	PointTerm5255	PointTerm5582	1.091456	FOX50	0.148	0.148	0.961	0.858	0.433	1.017	1.724
271320855	MV3 Delta	PointTerm5446	PointTerm5609	0.6928383	FOX50	0.148	0.148	0.610	0.545	0.275	0.646	1.095
273851076	MV3 Delta	PointTerm5538	PointTerm5657	0.522116	FOX50	0.148	0.148	0.460	0.410	0.207	0.486	0.825

Name	Type	Terminal i	Terminal j	Length	Type of Phase Conductors	Irated(act.)	Irated	Z1	R1	X1	R0	X0
273762467	MV3 Delta	PointTerm5557	PointTerm5737	0.82583	FOX50	0.148	0.148	0.727	0.649	0.327	0.769	1.305
273918579	MV3 Delta	PointTerm5622	PointTerm5756	0.6020631	FOX50	0.148	0.148	0.530	0.473	0.239	0.561	0.951
273723524	MV3 Delta	PointTerm5582	PointTerm5766	0.8368857	FOX50	0.148	0.148	0.737	0.658	0.332	0.780	1.322
273851080	MV3 Delta	PointTerm5657	PointTerm5785	0.725295	FOX50	0.148	0.148	0.639	0.570	0.288	0.676	1.146
273851086	MV3 Delta	PointTerm5785	PointTerm5857	0.6594075	FOX50	0.148	0.148	0.581	0.518	0.261	0.614	1.042
273055285	MV3 Delta	PointTerm5789	PointTerm5861	0.6646086	FOX50	0.148	0.148	0.585	0.523	0.263	0.619	1.050
273424595	MV3 Delta	PointTerm5430	PointTerm5886	2.572945	FOX50	0.148	0.148	2.265	2.023	1.020	2.397	4.065
274037488	MV3 Delta	PointTerm5839	PointTerm5905	0.5949028	FOX50	0.148	0.148	0.524	0.468	0.236	0.554	0.940
273918531	MV3 Delta	PointTerm5799	PointTerm5911	1.193863	FOX50	0.148	0.148	1.051	0.939	0.473	1.112	1.886
273055287	MV3 Delta	PointTerm5861	PointTerm5921	0.6699864	FOX50	0.148	0.148	0.590	0.527	0.266	0.624	1.058
269438693	MV3 Delta	PointTerm6002	PointTerm5931	0.667036	FOX50	0.148	0.148	0.587	0.524	0.264	0.621	1.054
274037419	MV3 Delta	PointTerm5809	PointTerm5942	1.355426	FOX50	0.148	0.148	1.193	1.066	0.537	1.263	2.141
274037407	MV3 Delta	PointTerm5968	PointTerm6012	0.6492189	FOX50	0.148	0.148	0.572	0.510	0.257	0.605	1.026
273918487	MV3 Delta	PointTerm6035	PointTerm6062	0.5680914	FOX50	0.148	0.148	0.500	0.447	0.225	0.529	0.897
274159159	MV3 Delta	PointTerm6101	PointTerm6146	0.8103412	FOX50	0.148	0.148	0.713	0.637	0.321	0.755	1.280
274159139	MV3 Delta	PointTerm6098	PointTerm6156	0.9440438	FOX50	0.148	0.148	0.831	0.742	0.374	0.880	1.491
269438095	MV3 Delta	PointTerm5956	PointTerm6162	3.126234	FOX50	0.148	0.148	2.753	2.458	1.239	2.913	4.939
269438719	MV3 Delta	PointTerm6115	PointTerm6203	1.62465	FOX50	0.148	0.148	1.430	1.277	0.644	1.514	2.567
274181223	MV3 Delta	PointTerm6219	PointTerm6259	0.8846712	FOX50	0.148	0.148	0.779	0.696	0.351	0.824	1.398
274181235	MV3 Delta	PointTerm6269	PointTerm6288	0.5087926	FOX50	0.148	0.148	0.448	0.400	0.202	0.474	0.804
274181296	MV3 Delta	PointTerm6288	PointTerm6295	1.234743	FOX50	0.148	0.148	1.087	0.971	0.490	1.150	1.951
274181316	MV3 Delta	PointTerm6295	PointTerm6308	0.5989391	FOX50	0.148	0.148	0.527	0.471	0.237	0.558	0.946
274026706	MV3 Delta	PointTerm6292	PointTerm6340	2.210073	FOX50	0.148	0.148	1.946	1.738	0.876	2.059	3.491
274026712	MV3 Delta	PointTerm6340	PointTerm6414	0.7722438	FOX50	0.148	0.148	0.680	0.607	0.306	0.719	1.220
274026750	MV3 Delta	PointTerm6414	PointTerm6430	1.497974	FOX50	0.148	0.148	1.319	1.178	0.594	1.396	2.366
274181358	MV3 Delta	PointTerm6404	PointTerm6440	1.748909	FOX50	0.148	0.148	1.540	1.375	0.693	1.629	2.763
274181352	MV3 Delta	PointTerm6379	PointTerm6449	2.207817	FOX50	0.148	0.148	1.944	1.736	0.875	2.057	3.488
274026756	MV3 Delta	PointTerm6430	PointTerm6490	1.129638	FOX50	0.148	0.148	0.995	0.888	0.448	1.052	1.785
274181348	MV3 Delta	PointTerm6469	PointTerm6500	0.8037797	FOX50	0.148	0.148	0.708	0.632	0.319	0.749	1.270
274026762	MV3 Delta	PointTerm6497	PointTerm6519	0.8593451	FOX50	0.148	0.148	0.757	0.676	0.341	0.801	1.358
274026766	MV3 Delta	PointTerm6506	PointTerm6529	0.9153183	FOX50	0.148	0.148	0.806	0.720	0.363	0.853	1.446
274171765	MV3 Delta	PointTerm6529	PointTerm6539	0.6438105	FOX50	0.148	0.148	0.567	0.506	0.255	0.600	1.017
274026768	MV3 Delta	PointTerm6536	PointTerm6552	0.9111133	FOX50	0.148	0.148	0.802	0.716	0.361	0.849	1.439
274026760	MV3 Delta	PointTerm6519	PointTerm6558	1.317876	FOX50	0.148	0.148	1.160	1.036	0.522	1.228	2.082
270432249	MV3 Delta	PointTerm53	PointTerm66	1.004368	OAK50	0.28	0.28	0.467	0.286	0.369	0.432	1.558
274026792	MV3 Delta	PointTerm6580	PointTerm6602	0.5700725	FOX50	0.148	0.148	0.502	0.448	0.226	0.531	0.901
274026788	MV3 Delta	PointTerm6602	PointTerm6615	1.36285	FOX50	0.148	0.148	1.200	1.071	0.540	1.270	2.153
272273623	MV3 Delta	PointTerm582	PointTerm662	0.5827082	MINK50	0.208	0.208	0.347	0.268	0.221	0.352	0.911
274405255	MV3 Delta	PointTerm6615	PointTerm6628	1.794668	FOX50	0.148	0.148	1.580	1.411	0.711	1.672	2.835
274392973	MV3 Delta	PointTerm6635	PointTerm6654	0.5545706	FOX50	0.148	0.148	0.488	0.436	0.220	0.517	0.876
274405270	MV3 Delta	PointTerm6654	PointTerm6658	0.5871517	FOX50	0.148	0.148	0.517	0.462	0.233	0.547	0.928
274405288	MV3 Delta	PointTerm6654	PointTerm6664	0.6406348	FOX50	0.148	0.148	0.564	0.504	0.254	0.597	1.012
274026776	MV3 Delta	PointTerm6638	PointTerm6670	1.08999	FOX50	0.148	0.148	0.960	0.857	0.432	1.016	1.722
274026774	MV3 Delta	PointTerm6670	PointTerm6698	0.5448353	FOX50	0.148	0.148	0.480	0.428	0.216	0.508	0.861
269438412	MV3 Delta	PointTerm621	PointTerm701	0.5347405	FOX50	0.148	0.148	0.471	0.420	0.212	0.498	0.845
273259749	MV3 Delta	PointTerm594	PointTerm704	0.7001834	MINK50	0.208	0.208	0.417	0.322	0.266	0.423	1.094
270439527	MV3 Delta	PointTerm83	PointTerm73	0.8843305	FOX50	0.148	0.148	0.779	0.695	0.351	0.824	1.397
269438501	MV3 Delta	PointTerm598	PointTerm737	0.7788672	FOX50	0.148	0.148	0.686	0.612	0.309	0.726	1.230
269438503	MV3 Delta	PointTerm841	PointTerm743	0.6734245	MINK50	0.208	0.208	0.401	0.309	0.255	0.407	1.052
269425911	MV3 Delta	PointTerm66	PointTerm76	0.627129	OAK50	0.28	0.28	0.291	0.178	0.230	0.270	0.973
274351377	MV3 Delta	PointTerm605	PointTerm812	1.096194	FOX50	0.148	0.148	0.965	0.862	0.435	1.021	1.732
274385939	MV3 Delta	PointTerm682	PointTerm825	0.7867098	FOX50	0.148	0.148	0.693	0.618	0.312	0.733	1.243
272752297	MV3 Delta	PointTerm675	PointTerm831	0.8379334	FOX50	0.148	0.148	0.738	0.659	0.332	0.781	1.324
273741528	MV3 Delta	PointTerm717	PointTerm848	0.8948241	FOX50	0.148	0.148	0.788	0.703	0.355	0.834	1.414
273858729	MV3 Delta	PointTerm749	PointTerm858	0.7957066	FOX50	0.148	0.148	0.701	0.626	0.315	0.741	1.257
274351378	MV3 Delta	PointTerm812	PointTerm925	1.167279	FOX50	0.148	0.148	1.028	0.918	0.463	1.088	1.844
269425915	MV3 Delta	PointTerm76	PointTerm95	1.049526	OAK50	0.28	0.28	0.488	0.299	0.386	0.451	1.628
274365365	MV3 Delta	PointTerm848	PointTerm951	0.7938688	FOX50	0.148	0.148	0.699	0.624	0.315	0.740	1.254
269425917	MV3 Delta	PointTerm101	PointTerm98	1.652911	OAK50	0.28	0.28	0.768	0.470	0.607	0.711	2.563
269438395	MV3 Delta	PointTerm1751	Terminal(3)	0.8522295	FOX50	0.148	0.148	0.750	0.670	0.338	0.794	1.346

Appendix A2: Single Line Diagram for Network 2

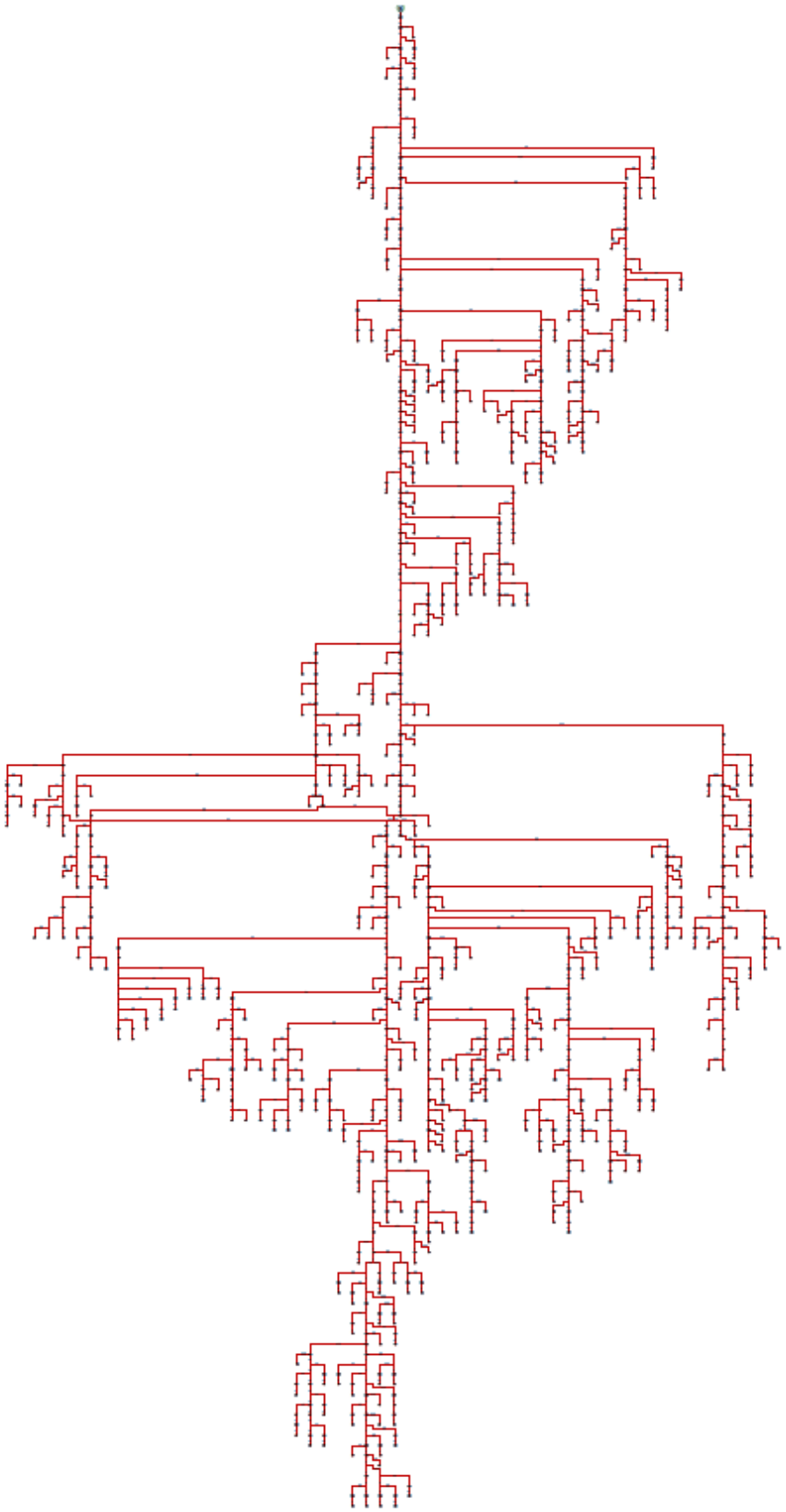

Appendix B – Lookup table for MV bus-position to bus-index mapping for Network 1

Position	Bus-index	Position	Bus-index	Position	Bus-index	Position	Bus-index	Position	Bus-index	Position	Bus-index	Position	Bus-index	Position	Bus-index
1	0	44	178	87	304	130	381	173	559	216	710	259	818	302	991
2	3	45	178	88	307	131	384	174	562	217	710	260	818	303	994
3	3	46	185	89	310	132	387	175	562	218	717	261	821	304	997
4	6	47	190	90	313	133	390	176	565	219	724	262	824	305	1000
5	9	48	190	91	313	134	393	177	568	220	731	263	831	306	1003
6	16	49	195	92	313	135	393	178	571	221	731	264	836	307	1006
7	19	50	202	93	313	136	396	179	574	222	738	265	839	308	1009
8	24	51	209	94	313	137	399	180	577	223	738	266	846	309	1012
9	31	52	209	95	316	138	402	181	580	224	745	267	846	310	1015
10	38	53	212	96	316	139	405	182	583	225	745	268	853	311	1018
11	45	54	212	97	316	140	408	183	583	226	752	269	860	312	1021
12	52	55	212	98	316	141	411	184	583	227	752	270	863	313	1024
13	52	56	219	99	319	142	414	185	586	228	759	271	870	314	1027
14	55	57	219	100	319	143	417	186	589	229	759	272	870	315	1030
15	55	58	226	101	319	144	420	187	592	230	766	273	875	316	1033
16	58	59	226	102	319	145	423	188	592	231	769	274	882	317	1036
17	65	60	226	103	324	146	430	189	592	232	776	275	885	318	1039
18	72	61	233	104	324	147	437	190	592	233	776	276	890	319	1042
19	75	62	236	105	324	148	444	191	595	234	779	277	890	320	1045
20	82	63	239	106	324	149	447	192	598	235	779	278	890	321	1048
21	87	64	242	107	327	150	454	193	601	236	782	279	897	322	1051
22	90	65	245	108	327	151	457	194	608	237	782	280	904	323	1054
23	97	66	251	109	330	152	464	195	611	238	785	281	907	324	1057
24	104	67	254	110	330	153	467	196	617	239	785	282	914	325	1060
25	107	68	261	111	333	154	474	197	617	240	788	283	917	326	1063
26	112	69	261	112	336	155	477	198	624	241	788	284	922	327	1066
27	112	70	261	113	339	156	482	199	627	242	791	285	925	328	1069
28	119	71	268	114	342	157	489	200	627	243	791	286	930	329	1072
29	122	72	268	115	345	158	496	201	630	244	794	287	930	330	1075
30	129	73	275	116	345	159	499	202	630	245	794	288	937	331	1078
31	129	74	280	117	348	160	506	203	633	246	797	289	940	332	1081
32	136	75	280	118	348	161	513	204	640	247	797	290	943	333	1084
33	141	76	283	119	351	162	516	205	640	248	800	291	950	334	1087
34	148	77	286	120	351	163	523	206	647	249	800	292	953	335	1090
35	148	78	286	121	354	164	530	207	647	250	803	293	960	336	1093
36	148	79	289	122	357	165	530	208	654	251	803	294	963	337	1096
37	148	80	289	123	360	166	537	209	661	252	806	295	970		
38	155	81	292	124	363	167	544	210	668	253	806	296	973		
39	158	82	292	125	366	168	547	211	675	254	809	297	976		
40	165	83	295	126	369	169	547	212	682	255	812	298	979		
41	168	84	298	127	372	170	550	213	689	256	812	299	982		
42	171	85	298	128	375	171	553	214	696	257	815	300	985		
43	171	86	301	129	378	172	556	215	703	258	815	301	988		

Appendix C – Lookup table for MV bus-position to bus-index mapping for Network 2

Bus position	Bus-index	Bus position	Bus-index	Bus position	Bus-index	Bus position	Bus-index	Bus position	Bus-index	Bus position	Bus-index	Bus position	Bus-index	Bus position	Bus-index	Bus position	Bus-index	Bus position	Bus-index	Bus position	Bus-index
1	0	51	205	101	330	151	508	201	657	251	730	301	809	351	1010	401	1221	451	1421	501	1670
2	6	52	210	102	330	152	513	202	657	252	733	302	816	352	1017	402	1226	452	1428	502	1670
3	12	53	210	103	333	153	513	203	657	253	733	303	816	353	1017	403	1226	453	1435	503	1673
4	18	54	216	104	333	154	518	204	662	254	736	304	823	354	1022	404	1231	454	1435	504	1673
5	18	55	216	105	336	155	518	205	662	255	736	305	823	355	1027	405	1231	455	1442	505	1676
6	24	56	222	106	336	156	525	206	665	256	739	306	830	356	1027	406	1236	456	1442	506	1676
7	24	57	227	107	339	157	525	207	665	257	739	307	830	357	1032	407	1236	457	1449	507	1679
8	30	58	227	108	339	158	532	208	668	258	742	308	837	358	1039	408	1241	458	1456	508	1679
9	30	59	234	109	342	159	537	209	668	259	742	309	837	359	1039	409	1248	459	1463	509	1682
10	36	60	240	110	342	160	537	210	671	260	745	310	844	360	1044	410	1248	460	1470	510	1682
11	42	61	240	111	345	161	544	211	671	261	745	311	851	361	1044	411	1255	461	1470	511	1685
12	42	62	246	112	345	162	551	212	674	262	748	312	851	362	1049	412	1255	462	1477	512	1685
13	49	63	246	113	348	163	556	213	674	263	748	313	858	363	1054	413	1262	463	1477	513	1688
14	49	64	252	114	348	164	556	214	676	264	751	314	858	364	1054	414	1269	464	1484	514	1688
15	56	65	258	115	351	165	563	215	676	265	751	315	865	365	1061	415	1269	465	1491	515	1691
16	56	66	264	116	351	166	570	216	679	266	754	316	865	366	1068	416	1274	466	1498	516	1694
17	61	67	270	117	354	167	575	217	679	267	754	317	872	367	1068	417	1274	467	1498	517	1697
18	61	68	276	118	354	168	575	218	682	268	757	318	879	368	1073	418	1281	468	1505	518	1700
19	67	69	282	119	357	169	582	219	682	269	757	319	879	369	1080	419	1286	469	1512	519	1700
20	73	70	282	120	357	170	586	220	685	270	760	320	886	370	1087	420	1286	470	1512	520	1703
21	73	71	285	121	360	171	593	221	685	271	760	321	891	371	1094	421	1291	471	1519	521	1703
22	79	72	285	122	360	172	600	222	688	272	763	322	891	372	1099	422	1291	472	1526	522	1706
23	85	73	288	123	363	173	607	223	688	273	763	323	898	373	1104	423	1298	473	1533	523	1706
24	91	74	288	124	363	174	607	224	691	274	766	324	898	374	1104	424	1305	474	1538	524	1709
25	97	75	291	125	370	175	614	225	691	275	766	325	905	375	1109	425	1310	475	1545	525	1709
26	97	76	291	126	377	176	621	226	694	276	769	326	905	376	1116	426	1310	476	1552	526	1712
27	103	77	294	127	377	177	621	227	694	277	769	327	912	377	1116	427	1315	477	1552	527	1712
28	103	78	294	128	384	178	624	228	697	278	772	328	919	378	1121	428	1315	478	1559	528	1715
29	110	79	297	129	391	179	624	229	697	279	772	329	919	379	1121	429	1320	479	1559	529	1715
30	116	80	297	130	398	180	627	230	700	280	775	330	926	380	1128	430	1320	480	1566	530	1718
31	122	81	300	131	405	181	627	231	700	281	775	331	926	381	1128	431	1327	481	1573	531	1718
32	128	82	300	132	412	182	630	232	703	282	778	332	931	382	1135	432	1334	482	1580	532	1721
33	128	83	303	133	412	183	630	233	703	283	778	333	931	383	1135	433	1341	483	1587	533	1721
34	134	84	303	134	419	184	633	234	706	284	778	334	936	384	1142	434	1341	484	1594	534	1724
35	140	85	306	135	426	185	633	235	706	285	781	335	943	385	1149	435	1348	485	1601	535	1727
36	146	86	306	136	433	186	636	236	709	286	781	336	950	386	1154	436	1348	486	1601	536	1730
37	146	87	309	137	440	187	636	237	709	287	784	337	957	387	1161	437	1355	487	1608	537	1730
38	152	88	309	138	447	188	639	238	712	288	784	338	957	388	1168	438	1355	488	1615	538	1733
39	152	89	312	139	454	189	639	239	712	289	787	339	962	389	1175	439	1362	489	1622	539	1733
40	158	90	312	140	461	190	642	240	715	290	787	340	962	390	1175	440	1362	490	1622	540	1736
41	164	91	315	141	468	191	642	241	715	291	790	341	967	391	1180	441	1369	491	1629	541	1736
42	164	92	315	142	468	192	645	242	718	292	793	342	967	392	1185	442	1376	492	1636	542	1739
43	170	93	318	143	475	193	645	243	718	293	793	343	972	393	1185	443	1381	493	1636	543	1739
44	176	94	318	144	475	194	648	244	721	294	793	344	979	394	1190	444	1386	494	1643	544	1742
45	181	95	321	145	482	195	648	245	721	295	790	345	984	395	1197	445	1393	495	1643	545	1742
46	181	96	321	146	482	196	651	246	724	296	796	346	984	396	1197	446	1400	496	1650	546	1745
47	187	97	324	147	487	197	651	247	724	297	799	347	989	397	1202	447	1400	497	1650	547	1745
48	193	98	324	148	494	198	654	248	727	298	799	348	989	398	1209	448	1407	498	1656	548	1748
49	199	99	327	149	501	199	654	249	727	299	802	349	996	399	1209	449	1414	499	1656	549	1748
50	205	100	327	150	508	200	657	250	730	300	802	350	1003	400	1214	450	1421	500	1663	550	1751

Bus position	Bus-index	Bus position	Bus-index	Bus position	Bus-index	Bus position	Bus-index	Bus position	Bus-index	Bus position	Bus-index	Bus position	Bus-index	Bus position	Bus-index	Bus position	Bus-index	Bus position	Bus-index	Bus position	Bus-index
551	1751	601	1823	651	1898	701	1973	751	2048	801	2195	851	2317	901	2413	951	2548	1001	2719	1051	2918
552	1754	602	1826	652	1901	702	1976	752	2051	802	2200	852	2317	902	2413	952	2554	1002	2725	1052	2918
553	1754	603	1826	653	1901	703	1976	753	2051	803	2200	853	2320	903	2416	953	2554	1003	2732	1053	2923
554	1757	604	1829	654	1904	704	1979	754	2054	804	2205	854	2320	904	2422	954	2559	1004	2738	1054	2928
555	1757	605	1829	655	1904	705	1979	755	2054	805	2211	855	2323	905	2422	955	2559	1005	2744	1055	2928
556	1760	606	1832	656	1907	706	1982	756	2057	806	2216	856	2323	906	2427	956	2565	1006	2750	1056	2934
557	1760	607	1832	657	1907	707	1982	757	2057	807	2216	857	2326	907	2427	957	2565	1007	2756	1057	2934
558	1760	608	1835	658	1910	708	1985	758	2060	808	2221	858	2326	908	2433	958	2570	1008	2762	1058	2939
559	1760	609	1835	659	1910	709	1985	759	2060	809	2227	859	2329	909	2433	959	2570	1009	2767	1059	2939
560	1765	610	1838	660	1913	710	1988	760	2063	810	2233	860	2329	910	2439	960	2575	1010	2772	1060	2944
561	1765	611	1838	661	1913	711	1988	761	2063	811	2238	861	2332	911	2439	961	2575	1011	2778	1061	2944
562	1765	612	1841	662	1916	712	1991	762	2066	812	2243	862	2332	912	2445	962	2580	1012	2778	1062	2950
563	1765	613	1841	663	1916	713	1991	763	2066	813	2248	863	2335	913	2445	963	2580	1013	2783	1063	2956
564	1770	614	1844	664	1919	714	1994	764	2069	814	2254	864	2335	914	2451	964	2585	1014	2789	1064	2962
565	1770	615	1844	665	1919	715	1994	765	2069	815	2260	865	2338	915	2451	965	2585	1015	2789	1065	2962
566	1770	616	1847	666	1922	716	1997	766	2072	816	2266	866	2338	916	2457	966	2592	1016	2795	1066	2967
567	1770	617	1847	667	1922	717	1997	767	2072	817	2266	867	2341	917	2462	967	2592	1017	2795	1067	2967
568	1775	618	1850	668	1925	718	2000	768	2075	818	2269	868	2341	918	2467	968	2598	1018	2802	1068	2973
569	1775	619	1850	669	1925	719	2000	769	2075	819	2269	869	2344	919	2472	969	2604	1019	2802	1069	2973
570	1778	620	1853	670	1928	720	2003	770	2078	820	2272	870	2344	920	2478	970	2604	1020	2809	1070	2979
571	1778	621	1853	671	1928	721	2003	771	2078	821	2272	871	2347	921	2478	971	2609	1021	2809	1071	2979
572	1781	622	1856	672	1931	722	2006	772	2081	822	2275	872	2347	922	2483	972	2609	1022	2815	1072	2985
573	1781	623	1856	673	1931	723	2006	773	2081	823	2275	873	2350	923	2483	973	2615	1023	2815	1073	2985
574	1784	624	1859	674	1934	724	2009	774	2084	824	2278	874	2350	924	2490	974	2615	1024	2821	1074	2991
575	1784	625	1859	675	1934	725	2009	775	2084	825	2278	875	2353	925	2490	975	2621	1025	2821	1075	2997
576	1787	626	1862	676	1937	726	2012	776	2087	826	2281	876	2353	926	2497	976	2621	1026	2827	1076	3003
577	1787	627	1862	677	1937	727	2012	777	2087	827	2281	877	2356	927	2497	977	2626	1027	2827	1077	3003
578	1790	628	1865	678	1940	728	2015	778	2090	828	2284	878	2356	928	2503	978	2626	1028	2833	1078	3009
579	1790	629	1865	679	1940	729	2015	779	2090	829	2284	879	2359	929	2503	979	2631	1029	2839	1079	3015
580	1793	630	1868	680	1943	730	2018	780	2093	830	2284	880	2359	930	2509	980	2636	1030	2845	1080	3015
581	1793	631	1868	681	1943	731	2018	781	2099	831	2287	881	2362	931	2509	981	2636	1031	2845	1081	3021
582	1796	632	1871	682	1946	732	2021	782	2104	832	2287	882	2362	932	2514	982	2641	1032	2851	1082	3021
583	1796	633	1871	683	1946	733	2021	783	2109	833	2290	883	2365	933	2514	983	2641	1033	2851	1083	3026
584	1799	634	1874	684	1949	734	2024	784	2114	834	2290	884	2365	934	2520	984	2647	1034	2857	1084	3026
585	1799	635	1874	685	1949	735	2024	785	2114	835	2293	885	2368	935	2520	985	2654	1035	2857	1085	3032
586	1802	636	1877	686	1952	736	2027	786	2119	836	2293	886	2368	936	2527	986	2660	1036	2863	1086	3037
587	1802	637	1877	687	1952	737	2027	787	2124	837	2296	887	2371	937	2527	987	2660	1037	2863	1087	3037
588	1805	638	1880	688	1955	738	2030	788	2129	838	2296	888	2371	938	2530	988	2666	1038	2869	1088	3040
589	1805	639	1880	689	1955	739	2030	789	2135	839	2299	889	2374	939	2530	989	2672	1039	2869	1089	3040
590	1808	640	1883	690	1958	740	2033	790	2140	840	2299	890	2374	940	2533	990	2677	1040	2874	1090	3043
591	1808	641	1883	691	1958	741	2033	791	2145	841	2302	891	2377	941	2533	991	2683	1041	2879	1091	3043
592	1811	642	1886	692	1961	742	2036	792	2150	842	2302	892	2384	942	2536	992	2689	1042	2884	1092	3046
593	1811	643	1886	693	1961	743	2036	793	2155	843	2305	893	2391	943	2536	993	2695	1043	2884	1093	3046
594	1814	644	1889	694	1964	744	2039	794	2160	844	2305	894	2397	944	2539	994	2695	1044	2889	1094	3049
595	1814	645	1889	695	1964	745	2039	795	2165	845	2308	895	2404	945	2539	995	2701	1045	2889	1095	3049
596	1817	646	1892	696	1967	746	2042	796	2170	846	2308	896	2404	946	2542	996	2701	1046	2894	1096	3052
597	1817	647	1892	697	1967	747	2042	797	2175	847	2311	897	2407	947	2542	997	2707	1047	2900	1097	3052
598	1820	648	1895	698	1970	748	2045	798	2180	848	2311	898	2407	948	2545	998	2707	1048	2906	1098	3055
599	1820	649	1895	699	1970	749	2045	799	2185	849	2314	899	2410	949	2545	999	2713	1049	2912	1099	3055
600	1823	650	1898	700	1973	750	2048	800	2190	850	2314	900	2410	950	2548	1000	2719	1050	2912	1100	3058

Bus position	Bus-index	Bus position	Bus-index	Bus position	Bus-index	Bus position	Bus-index	Bus position	Bus-index	Bus position	Bus-index	Bus position	Bus-index	Bus position	Bus-index	Bus position	Bus-index	Bus position	Bus-index	Bus position	Bus-index
1101	3058	1151	3133	1201	3250	1251	3387	1301	3579	1351	3753	1401	3828	1451	3939	1501	4089	1551	4239	1601	4389
1102	3061	1152	3136	1202	3253	1252	3387	1302	3585	1352	3753	1402	3828	1452	3942	1502	4092	1552	4242	1602	4392
1103	3061	1153	3136	1203	3253	1253	3392	1303	3585	1353	3756	1403	3831	1453	3945	1503	4095	1553	4245	1603	4395
1104	3064	1154	3139	1204	3256	1254	3392	1304	3590	1354	3756	1404	3831	1454	3948	1504	4098	1554	4248	1604	4398
1105	3064	1155	3139	1205	3256	1255	3395	1305	3590	1355	3759	1405	3834	1455	3951	1505	4101	1555	4251	1605	4401
1106	3067	1156	3142	1206	3259	1256	3395	1306	3596	1356	3759	1406	3834	1456	3954	1506	4104	1556	4254	1606	4404
1107	3067	1157	3142	1207	3259	1257	3398	1307	3596	1357	3762	1407	3837	1457	3957	1507	4107	1557	4257	1607	4407
1108	3070	1158	3145	1208	3262	1258	3398	1308	3603	1358	3762	1408	3837	1458	3960	1508	4110	1558	4260	1608	4410
1109	3070	1159	3145	1209	3262	1259	3401	1309	3609	1359	3765	1409	3840	1459	3963	1509	4113	1559	4263	1609	4413
1110	3073	1160	3148	1210	3268	1260	3401	1310	3609	1360	3765	1410	3840	1460	3966	1510	4116	1560	4266	1610	4416
1111	3073	1161	3148	1211	3268	1261	3408	1311	3614	1361	3768	1411	3843	1461	3969	1511	4119	1561	4269	1611	4419
1112	3076	1162	3151	1212	3274	1262	3408	1312	3614	1362	3768	1412	3843	1462	3972	1512	4122	1562	4272	1612	4422
1113	3076	1163	3151	1213	3274	1263	3415	1313	3619	1363	3771	1413	3846	1463	3975	1513	4125	1563	4275	1613	4425
1114	3079	1164	3154	1214	3281	1264	3422	1314	3624	1364	3771	1414	3846	1464	3978	1514	4128	1564	4278	1614	4428
1115	3079	1165	3154	1215	3281	1265	3427	1315	3624	1365	3774	1415	3849	1465	3981	1515	4131	1565	4281	1615	4431
1116	3082	1166	3157	1216	3287	1266	3433	1316	3630	1366	3774	1416	3849	1466	3984	1516	4134	1566	4284	1616	4434
1117	3082	1167	3157	1217	3287	1267	3440	1317	3635	1367	3777	1417	3852	1467	3987	1517	4137	1567	4287	1617	4437
1118	3085	1168	3160	1218	3294	1268	3440	1318	3641	1368	3777	1418	3852	1468	3990	1518	4140	1568	4290	1618	4440
1119	3085	1169	3160	1219	3294	1269	3445	1319	3646	1369	3780	1419	3855	1469	3993	1519	4143	1569	4293	1619	4443
1120	3088	1170	3163	1220	3300	1270	3452	1320	3652	1370	3780	1420	3855	1470	3996	1520	4146	1570	4296	1620	4446
1121	3088	1171	3163	1221	3304	1271	3459	1321	3652	1371	3783	1421	3858	1471	3999	1521	4149	1571	4299	1621	4449
1122	3091	1172	3166	1222	3309	1272	3459	1322	3659	1372	3783	1422	3858	1472	4002	1522	4152	1572	4302	1622	4452
1123	3091	1173	3166	1223	3309	1273	3465	1323	3665	1373	3786	1423	3861	1473	4005	1523	4155	1573	4305	1623	4455
1124	3094	1174	3169	1224	3316	1274	3465	1324	3670	1374	3786	1424	3861	1474	4008	1524	4158	1574	4308	1624	4458
1125	3094	1175	3175	1225	3316	1275	3470	1325	3676	1375	3789	1425	3864	1475	4011	1525	4161	1575	4311	1625	4461
1126	3097	1176	3180	1226	3319	1276	3470	1326	3681	1376	3789	1426	3864	1476	4014	1526	4164	1576	4314	1626	4464
1127	3097	1177	3186	1227	3319	1277	3477	1327	3687	1377	3792	1427	3867	1477	4017	1527	4167	1577	4317	1627	4467
1128	3100	1178	3193	1228	3322	1278	3477	1328	3692	1378	3792	1428	3870	1478	4020	1528	4170	1578	4320	1628	4470
1129	3100	1179	3199	1229	3322	1279	3482	1329	3698	1379	3795	1429	3873	1479	4023	1529	4173	1579	4323	1629	4473
1130	3103	1180	3204	1230	3325	1280	3487	1330	3703	1380	3795	1430	3876	1480	4026	1530	4176	1580	4326	1630	4476
1131	3103	1181	3209	1231	3325	1281	3493	1331	3708	1381	3798	1431	3879	1481	4029	1531	4179	1581	4329	1631	4479
1132	3106	1182	3214	1232	3327	1282	3498	1332	3715	1382	3798	1432	3882	1482	4032	1532	4182	1582	4332	1632	4482
1133	3106	1183	3219	1233	3330	1283	3503	1333	3715	1383	3801	1433	3885	1483	4035	1533	4185	1583	4335	1633	4485
1134	3109	1184	3226	1234	3332	1284	3510	1334	3722	1384	3801	1434	3888	1484	4038	1534	4188	1584	4338	1634	4488
1135	3109	1185	3226	1235	3332	1285	3510	1335	3729	1385	3804	1435	3891	1485	4041	1535	4191	1585	4341	1635	4491
1136	3112	1186	3229	1236	3338	1286	3517	1336	3729	1386	3804	1436	3894	1486	4044	1536	4194	1586	4344		
1137	3112	1187	3229	1237	3338	1287	3517	1337	3732	1387	3807	1437	3897	1487	4047	1537	4197	1587	4347		
1138	3115	1188	3232	1238	3345	1288	3522	1338	3732	1388	3807	1438	3900	1488	4050	1538	4200	1588	4350		
1139	3115	1189	3232	1239	3345	1289	3527	1339	3735	1389	3810	1439	3903	1489	4053	1539	4203	1589	4353		
1140	3118	1190	3235	1240	3351	1290	3532	1340	3735	1390	3810	1440	3906	1490	4056	1540	4206	1590	4356		
1141	3118	1191	3235	1241	3351	1291	3538	1341	3738	1391	3813	1441	3909	1491	4059	1541	4209	1591	4359		
1142	3121	1192	3238	1242	3358	1292	3543	1342	3738	1392	3813	1442	3912	1492	4062	1542	4212	1592	4362		
1143	3121	1193	3238	1243	3358	1293	3549	1343	3741	1393	3816	1443	3915	1493	4065	1543	4215	1593	4365		
1144	3124	1194	3241	1244	3363	1294	3555	1344	3741	1394	3816	1444	3918	1494	4068	1544	4218	1594	4368		
1145	3124	1195	3241	1245	3368	1295	3555	1345	3744	1395	3819	1445	3921	1495	4071	1545	4221	1595	4371		
1146	3127	1196	3244	1246	3368	1296	3560	1346	3744	1396	3819	1446	3924	1496	4074	1546	4224	1596	4374		
1147	3127	1197	3244	1247	3374	1297	3560	1347	3747	1397	3822	1447	3927	1497	4077	1547	4227	1597	4377		
1148	3130	1198	3247	1248	3374	1298	3566	1348	3747	1398	3822	1448	3930	1498	4080	1548	4230	1598	4380		
1149	3130	1199	3247	1249	3381	1299	3566	1349	3750	1399	3825	1449	3933	1499	4083	1549	4233	1599	4383		
1150	3133	1200	3250	1250	3381	1300	3572	1350	3750	1400	3825	1450	3936	1500	4086	1550	4236	1600	4386		

Appendix-D

Current publications based on PhD work:

[1] A. Ramdhin and S. Chowdhury, "Estimation of Inverter-Based Solar PV Penetration on Medium Voltage Networks Using Grid Impedance," 2018 IEEE PES/IAS Power Africa, Cape Town, South Africa, 2018, pp. 480-484, doi: 10.1109/PowerAfrica.2018.8521068.

[2] A. Ramdhin and S. Chowdhury, "A study of technical and regulatory issues for integration of distributed generation to medium voltage networks," 2017 IEEE AFRICON, Cape Town, South Africa, 2017, pp. 1101-1106, doi: 10.1109/AFRCON.2017.8095636

[3] A. Ramdhin and S. Chowdhury, "A network planning perspective for grid integration of renewable distributed generation in South Africa," 2015 50th International Universities Power Engineering Conference (UPEC), Stoke on Trent, UK, 2015, pp. 1-6, doi: 10.1109/UPEC.2015.7339902

Planned journal paper:

Topic: Estimating Network Capacity Improvement with PV integration on Constrained Medium Voltage Networks using PSO optimization algorithm

Abstract:

Medium voltage (MV) networks are designed for forward power flow and unidirectionally distribute power to various types of electrical loads. Incremental load growth through economic driven factors or non-technical losses such as theft, can result in the network feeder having unacceptable voltage regulation and/or thermal limitations where no new load or increase of existing load can be connected. Defined as constrained networks, short-term and long-term mitigation solutions are implemented to create more electrical capacity to meet the rising load demand. These solutions may include the installation of voltage regulators, shunt compensation, new substations and/or various other network strengthening solutions. Due to the fixed and limited output of these devices, an alternate, additional un-constraining mechanism is required. This journal documents the utilization and integration of DG, specifically solar photovoltaic (PV) installations, as an alternate approach to improve the capacity of constrained electricity MV networks. Using power system analysis software, DIgSILENT Powerfactory, a coded DPL script and data analyzer interface built in

Microsoft Excel is developed for network analysis. This analysis optimally places PV to the network to maximize network capacity and is quantified by defining an objective function that relates network capacity improvement to DG power generation. Particle Swarm Optimization (PSO) was found to be best suited for this research due to its efficiency to solving non-linear optimization problems and is proposed as the appropriate method of optimally integrating DG to un-constrain MV networks.